Cohesin and maintenance of genome integrity at DNA double-strand breaks

Jamie Phipps

THÈSE DE DOCTORAT

NNT : 2024UPASL005

université PARIS-SACLAY

Cohesin and maintenance of genome integrity at DNA double-strand breaks

Cohésines et maintien de l'intégrité des chromosomes aux cassures double brin

Thèse de doctorat de l'université Paris-Saclay

École doctorale n°577 : Structure et Dynamique des Systèmes Vivants (SDSV)
Spécialité de doctorat : Biologie moléculaire et cellulaire
Graduate School : Life Sciences and Health. Référent : Faculté des sciences d'Orsay

Thèse préparée dans l'unité de recherche **Stabilité génétique, Cellules Souches et Radiations (Université Paris-Saclay, Inserm, CEA)**, sous la direction de **Karine DUBRANA**, directrice de recherche

Thèse soutenue à Paris-Saclay, le 22 Janvier 2024, par

Jamie PHIPPS

Composition du Jury

Membres du jury avec voix délibérative

Jean-Baptiste CHARBONNIER DR, CEA / I2BC, Gif-sur-Yvette, France	Président
Frederic BECKOUET CR HDR, CNRS / CBI, Toulouse, France	Rapporteur & Examinateur
Gaëlle LEGUBE DR, CNRS / CBI, Toulouse, France	Rapporteur & Examinatrice
Stephan GRUBER Professeur, DMF, Université de Lausanne, Suisse	Examinateur
Angela TADDEI DR, CNRS / Institut Curie, Paris, France	Examinatrice

université PARIS-SACLAY

ÉCOLE DOCTORALE
Structure et dynamique des systèmes vivants (SDSV)

Titre : Cohesin and maintenance of genome integrity at DNA double-strand breaks

Mots clés : Cohesin, DNA repair, Homologous recombination

Résumé : DNA double-strand breaks (DSB) must be repaired to ensure genome stability. Crucially, DSB ends must be kept together for timely repair. In Saccharomyces cerevisiae, two poorly understood pathways mediate DSB end-tethering. One employs the Mre11-Rad50-Xrs2 (MRX) complex to physically bridge DSB ends. Another requires the conversion of DSB ends into single-strand DNA (ssDNA) by Exo1, but the bridging proteins are unknown. We uncover that cohesin, its loader and Smc5/6 act with Exo1 to tether DSB ends. Remarkably, cohesin specifically impaired in oligomerization fails to tether DSB ends, revealing a new function for cohesin oligomerization.

In addition to the known importance of sister chromatid cohesion, microscopy-based microfluidic experiments unveil a new role for cohesin in repair by ensuring DSB end-tethering. Altogether, our findings demonstrate that oligomerization of cohesin prevents DSB end separation and promotes DSB repair, revealing a novel mode of action and role for cohesin in safeguarding genome integrity.

Title : Cohésines et maintien de l'intégrité des chromosomes aux cassures double brin

Keywords : Cohésine, réparation de l'ADN, recombinaison homologue

Abstract : Il est essentiel que les extrémités du DSB soient maintenues ensemble pour une réparation rapide. Chez Saccharomyces cerevisiae, deux voies mal comprises interviennent dans l'attache finale du DSB. L'un utilise le complexe Mre11-Rad50-Xrs2 (MRX) pour relier physiquement les extrémités DSB. Un autre nécessite la conversion des extrémités DSB en ADN simple brin (ssDNA) par Exo1, mais les protéines de pontage sont inconnues. Nous découvrons que la cohésine, son chargeur et Smc5/6 agissent avec Exo1 pour attacher les extrémités du DSB. Remarquablement, la cohésine spécifiquement altérée lors de l'oligomérisation ne parvient pas à attacher les extrémités du DSB, révélant une nouvelle fonction pour l'oligomérisation de la cohésine.

En plus de l'importance connue de la cohésion des chromatides sœurs, des expériences microfluidiques basées sur la microscopie dévoilent un nouveau rôle de la cohésine dans la réparation en garantissant l'attache des extrémités du DSB. Globalement, nos résultats démontrent que l'oligomérisation de la cohésine empêche la séparation des extrémités du DSB et favorise la réparation du DSB, révélant ainsi un nouveau mode d'action et un nouveau rôle pour la cohésine dans la sauvegarde de l'intégrité du génome.

Contents

List of figures

List of abbreviations

DSB – Double-strand break

NHEJ – Non homologous end-joining

HR – Homologous recombination

a-EJ – Alternative end-joing

MMEJ – Microhomology mediated end-joining

SSA – Single strand annealing

SMC – Structural maintenance of chromosomes

HAWK – HEAT repeat protein associated with kleisin

CC – coiled-coils

NPF – Nucleoprotein filament

TAD – Topologically associated domain

CAR – Cohesin associated region

smFRET – Single molecule FRET

Cryo-EM – Cryo electron microscopy

AFM – Atomic force microscopy

ROS – Reactive oxygen species

3C – Chromosome conformation capture

ssDNA – single-strand DNA

dsDNA – double-strand DNA

WT – Wild-type

KD – Knockdown

Preface

Each cell is subject to many assaults against its genome each day. These assaults arise from both endogenous and exogenous sources and can lead to aberrations in the DNA at the site of attack. The formation of single-strand DNA breaks, double-strand DNA breaks, or the chemical alteration of a nucleotide base can all lead to mutagenesis of the DNA code. The downstream consequences of mutagenesis can lead to cell death, or diseases such as cancer in multicellular organisms. Thus, DNA damage is both highly sensed and highly regulated in all organisms, in a robust and generally conserved manner.

Single cell eukaryotes such as the budding yeast *Saccharomyces cerevisiae* represent ideal organisms to probe the complex molecular mechanisms of DNA repair. The long-standing genetic and molecular tools, ease of manipulating, and relatively cheap cost of working with these organisms has been essential in understanding biological processes. Without this option, the time, technical constraints and expense required to achieve this explorative work in mammalian cells alone would have hindered scientific progress. Despite the remarkable conservation of DNA repair processes, it is important to consider the millions of years of divergence between organisms such as yeast and humans when interpreting results for the human context.

Much progress has been made in understanding how the cell adapts to DNA double strand-breaks (DSBs). In budding yeast, we now know much about the factors recruited to DSB sites, local chromatin modifications, cell cycle regulation, and repair pathways used in pursuit of ensuring genome integrity. Two main repair pathways are favoured - non-homologous end joining (NHEJ) that directly re-ligates DSB ends with little to no DNA processing, and homologous recombination (HR) that uses a homologous donor sequence to reconstitute the damaged site. Homologous recombination is typically restricted to S-M phases of the cell cycle, when a homologous donor is present in the form of the replicated sister chromatid. Yeast observations have proven remarkably translatable to the human context, lacking only a few factors, or changing in scale of response due to its smaller genome and Rabl configuration.

An important requirement for DNA repair following DSB is the assurance that the two ends of the broken chromosome are kept together. This prevents separation of the two ends and facilitates timely and faithful repair with the correct partner. As a result, DSB end-tethering represents one of the initial steps in the DNA damage response. In yeast, DSB end-tethering is

partially achieved by one of the first DSB binding factors, the protein complex Mre11-Rad50-Xrs2^{Nbs1} (MRX). MRX plays a complex role in regulating DNA repair in response to DSBs. Beyond end-tethering, MRX initiates DNA damage signalling, facilitates repair as an essential member of the NHEJ complex, and initiates the ssDNA formation required for repair by homologous recombination.

Once DNA ends are resected, a second DSB end-tethering pathway has been identified, which requires the ssDNA forming activity of the exonuclease Exo1. Herein lies the focus of the work presented in this thesis. Despite the observation of this Exo1 pathway, the bridging proteins responsible for holding two resected DNA ends together remain unknown. Using genetics and a microscopy-based assay, I was able to demonstrate that the structural maintenance of chromosomes (SMC) complex, cohesin, and another SMC complex, Smc5/6, act with Exo1 to tether DSB ends. With a modified microscopy-based approach, I was able to show that two cohesin populations act at DNA DSBs. The first population compacts DSB adjacent chromatin, and does not depend on the cohesin regulator Pds5. The second population tethers DSB ends in a Pds5 and cohesin oligomerization dependent manner. Our work therefore identifies a new role for cohesin in DSB repair, as well as for its poorly understood oligomerization capability.

Furthermore, microfluidic experiments allowed us to follow the real-time repair kinetics and frequency of inducible DSBs. In addition to the known importance of sister chromatid cohesion, we unveiled a specific role for cohesin intra-chromosomal end-tethering in repair. Together, our findings demonstrate that oligomerization of cohesin prevents DSB end separation and promotes DSB repair, revealing a novel mode of action and role for cohesin in safeguarding genome integrity (https://doi.org/10.1101/2023.11.08.566226). Our findings correlate with a growing body of research that implicates cohesin in DNA repair processes, as reviewed in 2022 by Karine and me (https://doi.org/10.3390/genes13020198), and developed further in this thesis.

Beyond this, I was also fortunate enough to make minor contributions to two other DNA repair and genome integrity related projects. The first investigated the role of the Rad51 paralogs Rad55 and Rad57 in promoting HR repair of UV induced ssDNA damage (https://doi.org/10.1371/journal.pgen.1010639). The second demonstrated stalling of loop extrusion by telomere protein arrays (https://doi.org/10.1101/2023.10.29.564563).

Acknowledgements

To my family, for putting up with my absence and supporting me through all of these years.

To my supervisor Karine, for advice and guidance throughout this exciting project.

To Stéphane and all other lab members for creating an intellectually stimulating environment.

To Xhaf, Sara, Jenny and Constance, for keeping me smiling through tough CEA days.

To Alessandra, for providing an escape from work and keeping my feet on the trails.

To my friends in Paris, for making these past three years of living in a shoebox bearable.

To French administrative procedures, for teaching me the true meaning of patience.

And to five wonderful years in Paris.

Chapter 1: Introduction

1) DNA repair – dealing with DNA double-strand breaks

DNA DSBs are surprisingly frequent, and predicted to occur at each cell cycle (Vilenchik and Knudson, 2003). Endogenous sources of DSB include stresses received during DNA related processes such as replication. However, extrinsic sources including ionising radiation and genotoxic agents also generate DSBs (Vignard et al., 2013). If unrepaired, DSBs can result in chromosome loss, and if repaired incorrectly can lead to point mutations, loss of heterozygosity, and chromosomal rearrangements (Jackson and Bartek, 2009). All of which could lead to oncogenesis or cell death (Tubbs and Nussenzweig, 2017).

In eukaryotes, including yeast and humans, DSBs are predominantly repaired by two mechanisms: Non-Homologous End Joining (NHEJ), and Homologous Recombination (HR; Figure 1). NHEJ ligates two DSB ends in a homology independent manner (Emerson and Bertuch, 2016). Although accurate when re-ligation takes place without DNA processing, NHEJ can lead to genome alteration by the loss or addition of nucleotides (Tseng et al., 2008), or chromosomal translocations (Yu and Gabriel, 2004). In contrast, HR uses an intact homologous donor sequence to reconstitute broken DNA. Typically, use of the homologous sister chromatid during HR results in faithful DSB repair (Wright et al., 2018). However, transfer of mutation or loss of heterozygosity can occur if HR is performed between alleles or heterologous sequences. Although NHEJ and HR are the predominant pathways used for DSB repair, other less faithful mechanisms are observed. If NHEJ is compromised, repair by Alternative End Joining (a-EJ) pathways can take place. For example, repair by Microhomology-Mediated End Joining (MMEJ) is dependent on the annealing of roughly 4-20bp of microhomology close to both ends of the DSB, which are exposed after limited end resection, and generates small deletions (Figure 1; Sallmyr and Tomkinson, 2018). Alternatively, Single Strand Annealing (SSA) can be used for repair if resection unmasks longer direct homologous repeats, in a process which also removes the genomic sequence which separated them (Figure1; Sallmyr and Tomkinson, 2018).

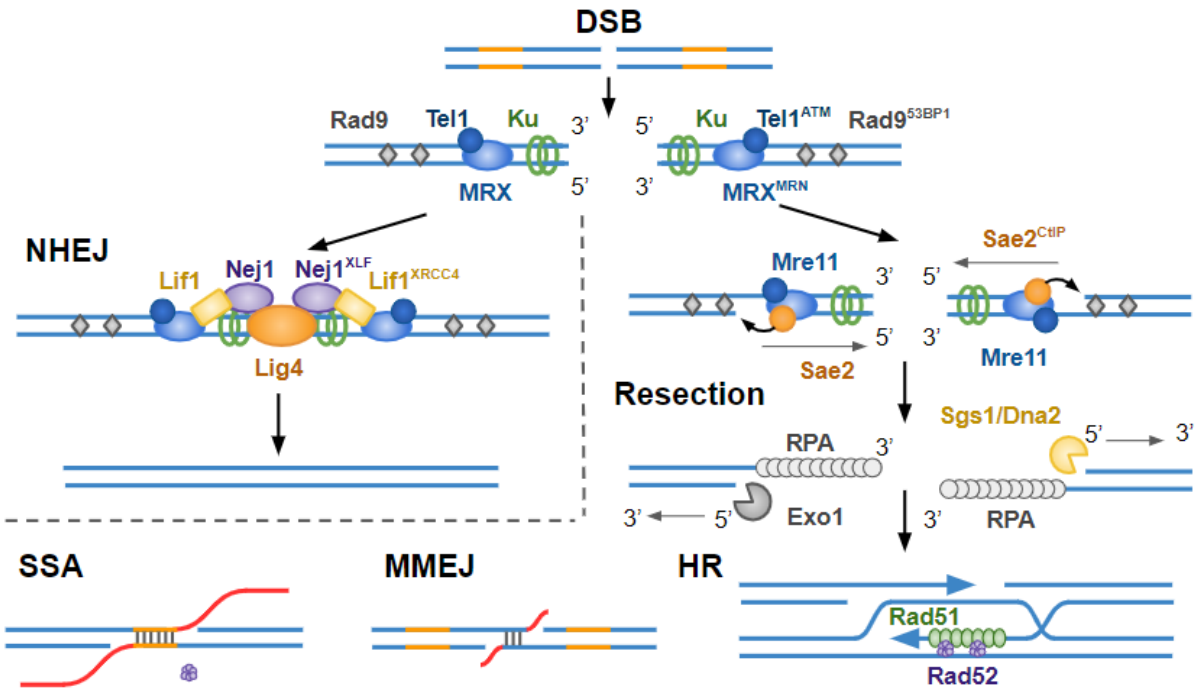

Figure 1. DNA double-strand break repair pathways. DNA double-strand breaks (DSBs) can be repaired by direct re-ligation of broken ends (non-homologous end joining, NHEJ), or through using a homologous template (homology-directed repair, HDR). Upon DSB, DNA damage response factors Ku, MRX, Tel1 and Rad9 are recruited to the damaged site. For NHEJ, Lif1, Nej1 and Lig4 are recruited, and broken DNA is re-ligated. HDR requires formation of 3' single-strand-DNA (ssDNA) overhangs at the DSB site in a process known as resection. Resection is initiated by the endonuclease activity of Mre11 upon stimulation by Sae2. Mre11 exonuclease activity then generates a small ssDNA overhang. Long-range resection proceeds due to the activity of the redundant exonucleases Exo1 and Sgs1/Dna2. The 3' ssDNA overhangs are stabilised by replication protein A (RPA). Rad52 mediates replacement of RPA for Rad51. Typically, resected Rad51-bound DSB ends undergo repair by homologous recombination (HR). The resultant nucleoprotein filament invades the DNA duplex of the replicated sister chromatid for use as a template for faithful repair. Although NHEJ and HR are the canonical DSB repair pathways, other mechanisms are also observed. Repair by microhomology-mediated end joining (MMEJ) is dependent on short ~2–20 bp homologous sequences situated close to the DSB on either side of the break. These short homologous sequences can anneal with one another, sealing the DSB, but generating small deletions (in red). Alternatively, unmasking of longer direct homologous repeats (in orange) can lead to repair by single-strand annealing (SSA), a process that also sees the loss of the genomic sequence that once separated them (in red; Phipps and Dubrana, 2022).

1A) DNA repair prior to resection

NHEJ

Repair by NHEJ is homology independent, and is achieved through assembly of a large protein complex, which senses, bridges and re-ligates free DNA ends. In yeast and humans, the Ku70/80 heterodimer is the first protein complex to bind DSBs (Zhang et al., 2007; Wu et al., 2008). This forms a ring complex and engages DNA in a sequence independent manner (Mimori and Hardin 1986; Walker et al. 2001). Ku acts both to protect DNA ends from degradation (Mimitou and Symington, 2010; Shao et al., 2012), and as a landing platform for recruiting other members of the NHEJ complex (Ma et al., 2004). The structural maintenance of chromosome (SMC) complex Mre11-Rad50-Xrs2^{Nbs1} (MRX^{MRN}) also senses and binds DSB ends shortly after but independently of Ku (Wu et al., 2008).

The NHEJ complex

Other factors responsible for forming the NHEJ synaptic complex and driving the re-ligation process in yeast are Dnl4^{LIG4}-Lif1^{XRCC4} and Nej1^{XLF}, while the recruitment of Tel1^{ATM} and Rad9^{53BP1} to the DSB site is important for signalling and chromatin modification (Lisby et al., 2004). MRX is also an essential NHEJ factor in yeast (Chen et al., 2001). Dnl4 contains the ligase activity for the complex, and is active primarily in canonical NHEJ (cNHEJ; Wilson et al.,1997; Zhang et al., 2007). Dnl4 interacts with Lif1, which is crucial for stabilisation of Dnl4 (Herrmann et al., 1998). Interaction between Ku and Dnl4-Lif1 is essential for Dnl4 recruitment and NHEJ at DSBs (Palmbos et al., 2008). Lif1 and Xrs2 of MRX interact, which is also important for Dnl4 stabilisation at DSBs (Matsuzaki et al., 2008). To achieve ligation, ATP binds Dnl4, leading to auto-adenylation of its active site. Consequently, activated AMP is transferred to the available 5’ phosphate on DNA, and the adjacent 3’ hydroxyl group attacks the bond created by this to re-ligate the DNA (Ellenberger and Tomkinson, 2008).

Nej1 does not interact directly with Dnl4, but instead with Lif1 and Ku70 (Deshpande and Wilson, 2007; Chen and Tomkinson, 2011). It is important for stabilising the NHEJ complex, and promoting reactivation of Dnl4 following ligation by enhancing deadenylation of the Dnl4 active site (Chen and Tomkinson, 2011). Beyond NHEJ, Nej1 also plays a role in regulating end-processing factors by inhibiting the interaction between Mre11 and Sae2, and Sae2 dependent recruitment of the Dna2 nuclease (Mojumdar et al., 2019; Mojumdar et al., 2022).

The yeast NHEJ complex does not include other mammalian NHEJ factors such as Paralogue of XRCC4 and XLF (PAXX), MRI, Cyren and DNA-PKcs, which in conjunction with Ku forms an active protein kinase (Tang et al., 2022). Among these, DNA-PKcs appears to play particularly important roles, including DSB end synapsis (DeFazzio et al., 2002; Chen et al., 2021; Buehl et al., 2023), and recruiting other factors such as the NHEJ DSB end processing nuclease, Artemis (Leiber et al., 2003). However, many of these proteins appear to play redundant roles, with their loss not abolishing the cells ability to perform cNHEJ at some breaks (Gao et al., 1998; Zhang et al., 2011).

The MRX complex

Structural work from *S. pombe* MRN originally lead to the conclusion that MRX stoichiometry consists of two copies of each of the three subunits ($M_2R_2X_2$; Schiller et al., 2014; Tisi et al., 2020; Figure 2A). However, recent Cryo-EM maps of *Chaetomium thermophilum* (Ct) and human MRN revealed a stoichiometry of $M_2R_2N_1$, complicating this prediction (Rotheneder et al., 2023). Rad50 contains long coiled coil (CC) arms, which separate a globular Walker ATPase head domain and a hinge-like zinc hook at the apex of the CCs (Hopfner et al., 2002). Rad50 dimerization through the zinc hook, and association between the globular head domains, generates a large closed ring of approximately 50nm in length (Hopfner et al., 2002). Mre11 and Xrs2 sit near the globular ATPase head domain of Rad50 (Schiller et al., 2014; Rotheneder et al., 2023). Whereas the Mre11-Rad50 complex exists in most organisms, the $Xrs2^{Nbs1}$ subunit is exclusive to eukaryotes. Mre11 provides both 5' endonuclease and 3' exonuclease activity to the MRX complex (Paull and Gellert, 1998). In its resting state, the catalytic domain of the Mre11 dimer makes many contacts with the Rad50 globular domain, preventing the nuclease from accessing DNA for cleavage (Kashammer et al., 2019).

Xrs2 is a key regulator of MRX in eukaryotes, and is essential for MRXs import into the nucleus (Desai-Mehta et al., 2001; Tsukamoto et al., 2005). In its N-terminus, it contains two key domains, an FHA domain and a BRCT domain, both important for interactions with phosphorylated proteins (Becker et al., 2006; Callebaut and Mornon, 1997; Sun et al., 1998; Yu et al., 2003). The Xrs2 C-terminus contains important motifs for its interaction with Mre11 (Schiller et al., 2014; Tsukamoto et al., 2005), and other factors such as the DNA damage signalling kinase $Tel1^{ATM}$ (Nakada et al., 2003). The FHA domain promotes interaction with

other MRX partners including Lif1^{Xrcc4} (Zhang et al., 2007), and Sae2^{CtIP} (Oh et al., 2016), important for activation of Mre11 nuclease activity.

Stable binding of DNA by MRX is dependent on its ability to hydrolyse ATP, with recent structural work of *Escherichia coli* MR showing DNA clamped between Rad50 heads and the base of the CCs (Figure 2B-C; Kashammer et al., 2019). However, MRX can translocate along DNA molecules in which DNA ends are blocked, suggesting that alternative binding between MRX and DNA might be possible (Myler et al., 2017). Alternatively, MRX might assemble as a complex on DNA itself, circumventing the requirement for unblocked DNA ends.

MRX in NHEJ

In yeast and humans, MRX is important for repair by both cNHEJ and homologous recombination, through distinct activities and mechanisms. As a cNHEJ factor, MRX modifies the DSB adjacent chromatin and coordinates the DSB response (Casari et al., 2019). Furthermore, MRX stabilises the NHEJ complex and tethers DSB ends by physically bridging either side of the DNA break (Chen et al., 2001; Lobachev et al., 2004). MRX promotes accurate NHEJ in yeast (Iwasaki et al., 2016), and its absence abolishes NHEJ (Chen et al., 2001). In mammals, the role of MRN in cNHEJ is less clear. Most MRN literature focuses on its role in DNA damage signalling, through both recruitment of ATM, and the initiation of resection through its nuclease Mre11 (Anand et al., 2016; Uziel et al., 2003). However, a role in both cNHEJ and a-EJ has been described (Dinklemann et al., 2009; Rass et al., 2009; Xie et al., 2009). In line with a role in bridging DNA ends, structural studies have demonstrated the ability of two Rad50 dimers to oligomerize through their apices in both yeast and humans (Kissling et al., 2022; Rotheneder et al., 2023). Fittingly, human Mre11-Rad50 was shown to tether short DNA oligos by atomic force microscopy (AFM; Moreno Herrero et al., 2005); as was also demonstrated by Cryo-EM in yeast (Kissling et al., 2022).

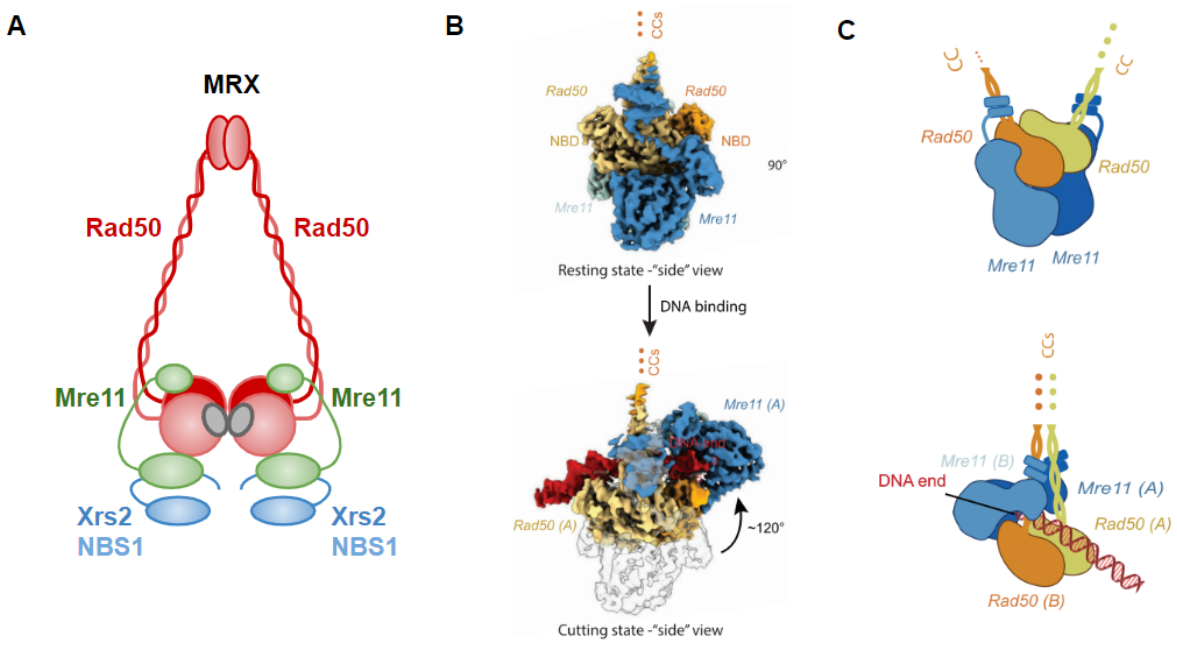

Figure 2. MRX Structure and different MR states. A) Schematic representation of the Mre11-Rad50-Xrs2 (MRX^{MRN}) complex. Rad50 homodimers assemble through interactions in its Walker ATPase head and Zn hook domains, generating a ring compartment. Two ATP binding sites are located in the Rad50 heads (grey). Mre11 binds Rad50, and Xrs2 binds Mre11 through domains in its C terminus, completing the complex. B) Structural representation of *Escherichia coli* Mre11-Rad50 globular domain in its resting state (absence of DNA) and cutting state (presence of DNA). Of note, DNA binding stimulates rotation of the Mre11 subunit towards DNA, whilst liberating the nuclease site for cutting. C) Schematic representation of Mre11-Rad50 in its resting state with coiled coils separated, and DNA bound state with coiled coils closed. (Adapted from Kashammer et al., 2019).

1B) Cell cycle arrest and pathway choice

In yeast and humans, MRX^{MRN} remains essential for proper DNA damage response through Tel1^{ATM} activation (D'Amours and Jackson, 2001). DSB dependent recruitment of the PI3 kinase Tel1 leads to phosphorylation of the local histone population to form γH2Ax (Shroff et al., 2004; Jackson and Bartek, 2009). This identifies the chromatin domain as damaged to downstream factors, and recruits the adaptor protein Rad9 (Hammet et al., 2007). Tel1 phosphorylates Rad9, which negatively regulates DNA resection by inhibiting Dna2/Sgs1 activity (Bonetti et al., 2015). Rad9 also acts as a scaffold for recruitment of effector checkpoint kinases such as Rad53^{CHK2} and Chk1^{CHK1}, leading to their phosphorylation (Sanchez et al., 1999; Schwartz et al., 2002; Vialard et al., 1998). DNA damage signalling is handed over to the PI3 kinase Mec1^{ATR} following resection. Formation of ssDNA recruits Mec1-Ddc2^{ATRIP} to DNA damage through interaction with the ssDNA binding RPA (Deshpande et al., 2017; Paciotti et al., 2000). As such, Mec1 is also important for checkpoint activation at stalled replication forks, and other ssDNA lesions (Friedel et al., 2009). Mec1 also targets many of the same targets as Tel1, including H2A, Chk1, Rad9 and Rad53 (Sanchez et al., 1996; Sanchez et al., 1999; Sweeney et al., 2005). Whereas Tel1 dependent phosphorylation is proposed to occur in *cis*, Mec1 is able to phosphorylate target proteins in *trans* and has been proposed to reach its target by 3D diffusion (Li et al., 2020). This assists in the extensive spreading of γH2Ax in the surrounding 50kb in yeast (Shroff et al., 2004), and 1Mb in humans (Rogakou et al., 1999). Mec1 mediated activation of Rad53 plays an important role in limiting resection, through phosphorylation and inactivation of Exo1 (Chappidi et al., 2019), which ultimately prevents gross chromosomal rearrangements (Xie et al., 2023). Thus, the Tel1 and Mec1 dependent DNA damage response arrests the cell cycle and is crucial for mediating DNA repair.

In humans, DSBs are also detected by PARP, which is important for PARsylation of the surrounding histones, further promoting the recruitment of PAR sensing repair factors (Chaudhuri and Nussenzweig, 2019). Ultimately, DDR, through the action of effector kinases, is highly regulated to ensure cell cycle arrest until damage is resolved. Subsequent repair pathway choice is largely defined by the cell cycle stage upon DSB, the condition of the DNA ends, and the chromatin context of the DSB (below).

Resection and its initiation

A key determinant of repair pathway choice is the process of resection. Resection involves the nucleolytic degradation of one of the dsDNA strands, to form a ssDNA 3' overhang (Cjeka and Symington, 2021). Once ssDNA is generated, DNA ends are no longer competent for NHEJ and overhangs are instead used for homology directed repair mechanisms, through pairing with a homologous sequence (Wright et al., 2018). During HR, the ssDNA overhang forms a nucleoprotein filament that is used as a guiding sensor to search for and identify a homologous donor sequence, eventually leading to faithful restoration of chromosome integrity (Wright et al., 2018). However, if cNHEJ and HR fail, mechanisms such as MMEJ and SSA can be used to restore genome integrity through simple annealing with other ssDNA direct homologous repeats (Sfeir and Symington, 2015; Sallmyr and Tomkinson, 2018). Although these pathways save the chromosome, they are known as error prone due to the deletions that they incur.

Many checks and balances exist to regulate the decision to resect DNA or not. Crucially, the activity of cell cycle dependent kinases ensure HR is generally restricted to S-G2 phase cells, ensuring an undamaged donor sequence is present (the recently replicated sister chromatid). Furthermore, DSB ends produced by ionising radiation cannot be re-ligated without some level of resection, demonstrating that the condition of DNA ends is important for pathway choice (Vogt et al., 2023).

Resection initiation at the DSB site is due to the activity of an already present actor at the NHEJ step, MRX^{MRN}. As a HDR factor, MRX^{MRN} initiates resection upon interaction with $Sae2^{CtIP}$ (Cannavo and Cjeka 2014; Cannavo et al., 2018; Clerici et al., 2005). Short-range resection removes end protection by Ku, allowing exonucleases access to generate long ssDNA tracts (Mimitou and Symington, 2010). To do this, Mre11 endonuclease forms a ssDNA nick typically 60-70bp from a DSB site, which is then processed from 5' to 3' towards the DNA end by its exonuclease activity (Bazzano et al., 2021). Interaction between Mre11 and $Sae2^{CtIP}$ rotates Mre11 within the complex, allowing it to cleave DNA (Kashammer et al 2019). Sae2 activity is negatively regulated in G1 by the absence of Cdk1, which activates Sae2 through phosphorylation (Yu et al., 2019). This in turn promotes NHEJ and protects heterochromatin from unscheduled HR (Bordelet et al., 2022). Ultimately, this means that NHEJ is promoted in G1, and HDR inhibited. Following initial short range resection, the task of unmasking long

tracts of single-strand DNA is undertaken by the exonucleases Exo1 and the flap endonuclease Dna2 with assistance from the helicase Sgs1 (Zhu et al., 2008).

Chromatin context and pathway choice

Breaks induced in different chromatin contexts lead to varied responses to DSBs, supporting a role of pre-established chromatin marks in DSB repair choice. Indeed, DSB repair pathway usage and efficiency in various chromatin environments has been addressed. These studies employ genome-wide analysis of repair in euchromatic DSB sites (Aymard et al., 2014), or the repair of specific heterochromatic sites (Bordelet et al., 2022; Chiolo et al., 2011; Goodarzi et al., 2008; Peng and Carpen, 2009; Noon et al., 2010; Lemaitre et al., 2014; Ryu et al., 2015; Janssen et al., 2016; Tsouroula et al., 2016). The various forms of chromatin interfere with the recruitment of DSB repair proteins, thus contributing to DSB processing and DNA repair pathway choice. HR was shown to be the prevalent repair mechanism for endonuclease induced DSB sites in transcriptionally active genes in human cell lines, while noncoding or silent euchromatic sequences exhibit a preference for NHEJ (Aymard et al., 2014; Clouaire et al., 2018). The H3K36me3 histone mark, typical of actively transcribed euchromatin, promotes HR through the recruitment of the protein LEDGF, which mediates the recruitment of CtIP, triggering ssDNA formation, Rad51 loading and HR initiation (Aymard et al., 2014; Clouaire et al., 2015; Pfister et al., 2014). In parallel, the active chromatin mark H4K16-Ac, catalysed by the TIP60 acetyltransferase, inhibits binding of the anti-resection and pro-NHEJ factor 53BP1, favouring resection and HR commitment (Tang et al., 2013). In contrast, H3K27me3-associated heterochromatin and chromatin targeted to the repressive nuclear lamina was shown to favour NHEJ or alt-NHEJ through an undefined mechanism (Lemaitre et al., 2014).

In *S. cerevisiae*, Sir3, the mammalian HP1 functional ortholog, suppresses resection initiation through direct interaction and inhibition of the MRX^{MRN} activator $Sae2^{CtIP}$ (Bordelet et al., 2022). The compacted chromatin structure of heterochromatin modulates long-range resection through a still unknown mechanism (Batté et al., 2017; Bordelet and Dubrana, 2019). Notably, although delayed by resection inhibition, HR repair is proficient in yeast heterochromatin. Resection is limited at subtelomeric DSBs (which are heterochromatic), which avoids loss of chromosome end sequences and favours repair by conservative HR (Batté et al., 2017).

1C) DNA repair after resection

MMEJ

If DNA resection is initiated at the break site by the Mre11-Sae2^{CtIP} complex, homologies present as direct repeats in DSB flanking DNA can be used in multiple ways for repair. Some of these mechanisms, unlike classical homologous recombination, lead to unfaithful repair, often presented as deletions. The extent of deletions depends largely on the extent of DNA resection and the position of the homologies used to seal the break.

In the case of MMEJ, short 3'-ssDNA overhangs of 60-70 bp may unmask short direct repeats that can be used for repair (Bazzano et al., 2021; Tisi et al., 2020; Cejka and Symington 2021). MMEJ was first identified in Ku deficient cells and requires >6bp in budding yeast and as little as 2bp in mammalian cells (Lee and Lee 2007; Koole et al., 2014; He and Yang 2018; Villarreal et al., 2012). Once direct repeats anneal, the Rad1-Rad10 complex removes the 3' non-homologous tail generated by this ectopic alignment (Ma et al., 2003). Flap removal is followed by DNA synthesis by DNA polymerases Polδ and Pol4 in budding yeast (Pol θ in mammals; Sallmyr and Tomkinson, 2018). In mammals, ligation then takes place in a primarily Lig3 dependent manner, however Lig1 is also sufficient for some MMEJ reactions (Simsek et al., 2011). Interestingly, a Lig3 ortholog does not exist in yeast. Therefore, it should be assessed if Lig1 is responsible.

HR

If resection proceeds further, longer 3'-ssDNA overhangs are generated that can engage in HR. Long 3'-ssDNA overhangs are rapidly stabilised by Replication Protein A (RPA), which in turn is replaced by the Rad51 recombinase via the Rad52 recombinase mediator (Andriuskevicius et al., 2018). The resulting right-handed helical filament is used for repair by searching for and invading the homologous donor DNA duplex. This ultimately leads to DNA synthesis and sealing of the DSB, followed by resolution of intermediate recombination structures (Wright et al., 2018). As the homologous donor is typically the sister chromatid, this leads to faithful repair of the damaged site.

Despite work describing the exchange and dynamics of the proteins involved in nucleoprotein filament (NPF) formation *in vitro* (Roy et al., 2021), the dynamics and regulation of homology

search *in vivo* has traditionally been difficult to follow. However, various groups have now successfully begun investigating these properties in a range of bacterial and eukaryotic systems (Wiktor et al., 2021; Horikoshi et al., 2021; Liu et al., 2023; Chimthanawala et al., 2022).

A recent budding yeast study used a functional fluorescent Rad51 tag to provide important insights into the characteristics and behaviour of the Rad51 NPF *in vivo* (Liu et al., 2023). After as little as two hours, induction of a single DSB frequently resulted in the formation of strikingly long Rad51 filaments, sometimes exceeding the diameter of the yeast G1 nucleus (2µm; Hozé et al., 2013). Rad51 enrichment around DSBs correlated with the level of resection, indicating that a 1µm filament corresponds to roughly 2kb of ssDNA (Liu et al., 2023). Crucially, only one filament per DSB was described, demonstrating that the ssDNA from either side of the DSB remains aligned. These filaments were able to go through cycles of contraction and elongation, in multiple directions, allowing the Rad51 filament to explore vast areas of the nucleus in search of a homologous donor sequence.

Ultimately, this work demonstrates that homology search in yeast is an active process, and does not exclusively rely on passive diffusion of the NPF through the nuclear space. Interestingly, DSB dependent increase in mobility of homologous donor sequences has also been demonstrated, coupled with reduced nucleosome occupancy and chromosome decompaction through INO80 dependent remodelling (Cheblal et al., 2020; Hauer et al., 2017). If this represents a mechanism for homology identification or facilitates strand invasion remains to be deciphered.

Beyond the NPF, an increasing number of studies have highlighted the contribution of higher-order chromosome organization to DNA damage signalling and repair. The successive layers of genome folding—from topologically associated domains (TADs), TAD cliques, compartments and whole chromosome territories, as well as chromosome positioning within the nucleus—each constrain contacts between genomic sequences. These structures also regulate HR, which is highly dependent on contact between the damaged DNA and the homologous template (Bordelet and Dubrana; 2019; Dumont et al., 2023).

SSA

Long-range resection on either side of the DSB may also unmask longer direct repeats that, unlike MMEJ, anneal in a Rad52 dependent manner to mediate repair by SSA (Mortensen et al., 1996; Reddy et al., 1997; Ivanov et al., 1996). Resolution of SSA intermediates is also achieved by Rad1-Rad10 cleavage of 3' non-homologous tails (Ma et al., 2003; Decottignies et al., 2007), before ligation by unknown ligases. This pathway does not require the invasion of a donor DNA duplex, and is therefore Rad51 independent.

2) DNA DSB end-tethering – Keeping two DNA ends together

Bringing two DNA ends together for DSB repair is one of the first and most crucial steps in the DSB repair process. If the ends fail to find each other, genome integrity cannot be restored, and harmful events such as chromosome translocations may occur. As such, ends must be kept together for both NHEJ and HR.

This is particularly important when considering the dynamic nature of chromatin. A number of studies have described changes in chromatin motion in response to DNA damage. In *S. cerevisiae*, both the damaged DNA site and the whole undamaged genome increase mobility (Figure 3A; (Dion et al., 2012; Miné-Hattab et al., 2012), with increased DSB motion also described in Drosophila and mammalian cells (Chiolo et al., 2011; Krawczyk et al., 2012). Enhanced chromatin movement was first proposed to increase the probability that separated DSB ends find each other prior to NHEJ (Dimitrova et al., 2008). However, in the absence of efficient end-tethering, increased movement could drive ectopic repair events between multiple DSBs.

Numerous studies using *in vitro* and *in vivo* assays have tried to decipher how DSB end-tethering takes place. Recent theoretical work demonstrated that this task is unlikely achieved through passive diffusion (Yang et al., 2023). Instead, active DSB end tethering mechanisms have been identified. These studies implicate members of the NHEJ complex using *Xenopus* and human proteins (Graham et al., 2016; Zhao et al., 2019), as well as MRX and pathways involving Exo1 and ssDNA formation in yeast (Lobachev et al., 2004; Nakai et al., 2011). Generally, the techniques used highlight DSB end tethering on two levels. The first concentrates on the synapsis that takes place prior to re-ligation during NHEJ, which tethers DNA ends on an Angstrom scale (Vogt and He, 2023). The second follows DSB ends *in vivo*, demonstrating DSB end-tethering in the nuclear context, and as such represent a larger scale (Lobachev et al., 2004; Lee et al., 2008; Nakai et al., 2011).

2A) Tethering by the NHEJ synaptic complex

In yeast and humans, MRX^{MRN} and Ku are two of the factors most rapidly drawn to broken DNA ends, and both are implicated in DNA DSB end-tethering and cNHEJ. Ku plays a key role in forming the cNHEJ structure necessary for bridging broken ends and re-ligating DNA (Vogt and He, 2023). The mammalian and *Xenopus* NHEJ synaptic complex has been extensively studied, using both intricate single molecule FRET (smFRET), biochemical assays, and structural approaches. Using *Xenopus* egg extracts, an initial long-range complex between two DNA ends, followed by a short-range synaptic complex was identified (Graham et al., 2016). Since then, this has been described using human proteins, and various compositions of the NHEJ complex (Zhao et al., 2019).

The first smFRET assays performed using *Xenopus* egg extracts described a long range complex which forms in the presence of Ku, DNA-PKcs, XLF, XRCC4, and LIG4 (Graham et al., 2016). This transitions to a short-range synaptic complex in which DNA-PKcs is evicted and re-ligation of DSB ends occurs (Chen et al., 2021). Cryo-EM structures confirmed this, with the distance between ends defined as 115Å, in accordance with the >100Å observed by smFRET (Graham et al., 2016; Chen et al., 2021; Chaplin et al., 2021). LIG4, XRCC4, XLF, were all found alongside DNA-PKcs in such structures. Other interactions within the complex generate a complex scaffold across the DSB and include XRCC4-XLF, XRCC4-LIG4 (complex dubbed X4L4, the flexibility of which allows LIG4 access to DNA ends), and LIG4-Ku70 (Chaplin et al., 2021; Chen et al., 2021; Hammel et al., 2011; Ropars et al., 2011; Wu et al., 2009). Interestingly PAXX, generally considered as an accessory factor for NHEJ, stabilises synaptic complex formation and improves the efficiency of end joining (Tadi et al., 2016; Yano et al., 2011). PAXX overlaps with the position/role of XLF in the synaptic complex to some degree. Both contain the same Ku binding motifs, and structures indicate that they interact similarly (Chen et al., 2023; Seif-El-Dahan et al., 2023). Further evidence they may be redundant for synapsis comes from XLF deficient *Xenopus* egg extracts, which form synapsis (Graham et al., 2016). Despite this, PAXX alone in the absence of XLF does not form a ligation competent complex (Chen et al., 2023).

Interestingly, a structure of DNA-PKcs dimers holding two DNA ends has also been solved, indicating that the NHEJ scaffolding proteins are non-essential for synapsis (Chaplin et al., 2021). In addition, although DNA-PKcs is frequently described in these structures, it is not essential, with X4L4-XLF interactions sufficient for tethering DNA molecules *in vitro* (Brouwer

et al., 2016; Graham et al., 2018). Furthermore, DNA-PKcs was not required for synapsis in smFRET experiments with human proteins (Zhao et al., 2019). These results imply that the NHEJ proteins facilitate multiple redundant ways in which it can hold DSBs together. Each might demonstrate steps along the path to re-ligation, or that different complexes are required depending on the nature of the DSB.

In summary, the current literature points towards the formation of a long range complex containing only Ku and DNA-PKcs, which transitions to a long range complex containing XRCC4, LIG4 and is mediated by XLF or PAXX (Figure 3; Chaplin et al., 2021; Chen et al., 2023; Seif-El-Dahan et al., 2023). This complex transitions to a short-range synaptic complex without DNA-PKcs, which is capable of ligation (Figure 3; Chen et al., 2021). How such conformational and compositional changes are mediated has to be deciphered. Ultimately, *in vivo* work using separation of function mutants will be essential for understanding the contribution and necessity of DNA-PKcs and other NHEJ factors to efficient DSB end tethering and repair.

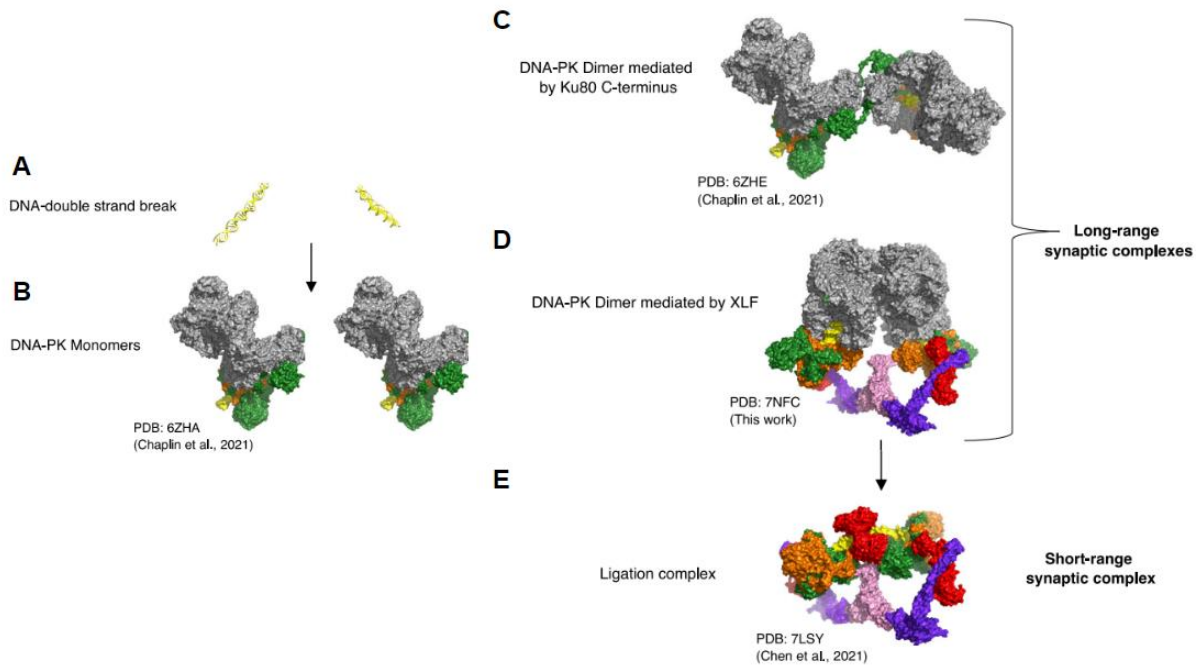

Figure 3. Mammalian NHEJ synapsis and re-ligation. A-B) Upon DNA DSB, KU rapidly binds DNA ends. DNA-PKcs is then recruited to the KU bound DNA ends and forms the DNA-PK complex with KU. C) Together, DNA-PK dimers form an initial long-range synaptic complex, bridging the broken DNA molecule. D) Next, XLF, XRCC4 and LIG4 join the long-range synaptic complex. E) The short-range synaptic complex is formed following autophosphorylation and ejection of DNA-PKcs, leaving the complex competent for ligation. (Adapted from Chaplin et al., 2021).

2B) Tethering by MRX

Strikingly, DNA-PKcs, which has been the focus of many studies in human NHEJ synapsis, is not present in budding yeast. DNA-PKcs is dispensable for repair of nuclease induced DSBs in mammals (Gao et al.,1998), but essential for cell survival upon irradiation, which necessitate processing of DSB ends (Rooney et al., 2002; Riballo et al., 2004). As DNA-PKcs is dispensable for some end-joining structures, it might be essential for transitioning the synaptic complex to provide access for processing factors (Buehl et al., 2023). As such, the lack of DNA-PKcs in yeast might be explained by compensation through other yeast NHEJ factors which can facilitate these functions. One candidate is the MRX complex, which is a core NHEJ factor in yeast. Although the same is less clear in humans, MRN's ability to maintain DNA ends in proximity has not been tested by smFRET. However, the MRX complex has been shown to play an early and important role in budding yeast DSB end-tethering (Figure 5; Lobachev et al., 2004; Lee et al., 2008). In contrast, yeast NHEJ factors Ku and Nej1 play moderate roles in DSB end-tethering (Rinaldi et al., 2023; Mojumunder et al., 2019), and Dnl4 is not required (Lobachev et al., 2004).

The mechanisms that facilitate the tethering of DSB ends have been characterized in *Saccharomyces cerevisiae* using a live-cell fluorescence microscopy approach (Lee et al., 2008; Lobachev et al., 2004; Kaye et al., 2004; Nakai et al., 2011; Mojumdar et al., 2019). Arrays of the ectopic LacI transcription factor binding sequence (LacO) and/or TetR transcription factor binding sequence (TetO) are positioned either side of an inducible DSB. Using this assay, some cNHEJ factors have been demonstrated to affect separation of DSB ends. However, the core members of the synaptic complex as observed in mammalian cells and *Xenopus* extracts, do not have the strongest phenotypes. This indicates that *in vivo* something else keeps DSB ends in proximity beyond the synaptic complex, potentially facilitating synaptic complex formation by keeping broken ends in proximity.

These studies demonstrate that MRX is particularly important for early time point end-tethering, independently of its nuclease activity (Lobachev et al., 2004), and that Exo1 is important for late time point end-tethering, through its nuclease activity (Nakai et al., 2011). Double knockout of these two genes leads to increased separation of DSB ends at late time points, but not at early time points where Exo1 deficiency has no effect (Nakai et al., 2011). As such, these two factors appear to act through separate mechanisms to hold DSB ends

together. Tel1^{ATM} is also important for DSB end-tethering, acting in the same pathway as MRX likely by stabilising MRX at DSBs (Cassini et al., 2016; Lee et al., 2008).

These observations imply that MRX might play a larger scale role than the NHEJ synaptic complex in DSB end-tethering. Through grabbing adjacent dsDNA around DSBs, MRX could keep the two sides of the chromosome in proximity so that the NHEJ synaptic complex can form. This hypothesis is supported further by observations that MRX is enriched away from DSBs by ChIP (Cassani et al., 2016; Zhang et al., 2007), the formation of Mre11 foci at DSB sites (Lisby et al., 2004), and bridging structures seen between dsDNA and MRX^{MRN} complexes by electron microscopy (Kissling et al., 2022; Rotheneder et al., 2023).

MRX nuclease activity is dispensable for *in vivo* DSB end-tethering (Lobachev et al., 2004). Instead, the ZN-hook domain and ATPase activity of Rad50 are essential, suggesting a physical bridging mechanism by stably bound MRX dimers (Lobachev et al., 2004). Fittingly, MRX^{MRN} is able to oligomerize through interactions between head domains, or the CC/zinc hook region (Figure 4; Kissling et al., 2022; Rotheneder et al., 2023). Dimerization events have been observed in the presence or absence of DNA using electron microscopy *in vitro* with yeast MRX, and *Chaetomium thermophilum* (Ct) MRN (Kissling et al. 2022; Rotheneder et al., 2023). The same structures have yet to be solved using human MRN, but would provide insights into the possibility of the complex playing a similar end-tethering role in humans

Multiple MRX complexes can also oligomerize through Rad50 heads in vitro (Kissling et al., 2022), with disruption of a Rad50 beta sheet abolishing this property (Kissling et al., 2022). Loss of Rad50 head oligomerization prevents MRX foci formation following DSB in vivo, and disrupts the complexes endonuclease activity. In contrast, exonuclease activity is unaffected in vitro (Kissling et al., 2022). This suggests that clustering of MRX at DSBs may be important for endonuclease activity. Although this mutant was deficient for repair after Camptothecin and hydroxyurea DNA damage, its ability to perform DSB end-tethering or NHEJ was not determined.

Zinc-hook tetramerization is essential for repair of ROS-mediated DNA damage in human cells, which increases DSBs formed by replication stress (Rotheneder et al., 2023). This indicates that oligomerization through both Rad50 heads and the zinc hook are required for effective DNA repair (Kissling et al., 2022; Rotheneder et al., 2023). In line with this, the MR subunits of

Ct MRN form Velcro like structures with many MR molecules forming large assemblies with CC-CC and head-head interactions. This correlates with observations that the zinc hook is required for DSB end tethering in yeast (Lobachev et al., 2004). Interestingly, disrupting CC-CC dimerization in human cells had less of an effect on HR efficiency than it did on repair of ROS mediated damage using a comet assay (Rotheneder et al., 2023). This may be due to the apex mutant still being able to drive resection and downstream repair by HR, despite losing its DSB end-tethering and NHEJ capacity.

With all of these mutants it is important to consider the effects of such mutations on functions beyond the targeted disruption. Structural changes may not only affect the dimerization ability of the complex, but also the stability of the protein, the DNA binding affinity, or the ability to initiate endonuclease and exonuclease activity. For example, the human Rad50 zinc hook has now been shown to be important for MRN-DNA binding (He et al., 2012), meaning loss of end-tethering in this mutant might be due to lack of recruitment to DSBs. As such, these results should be treated with caution, and appropriate controls for DNA binding, and nuclease activity should be performed where not previously described.

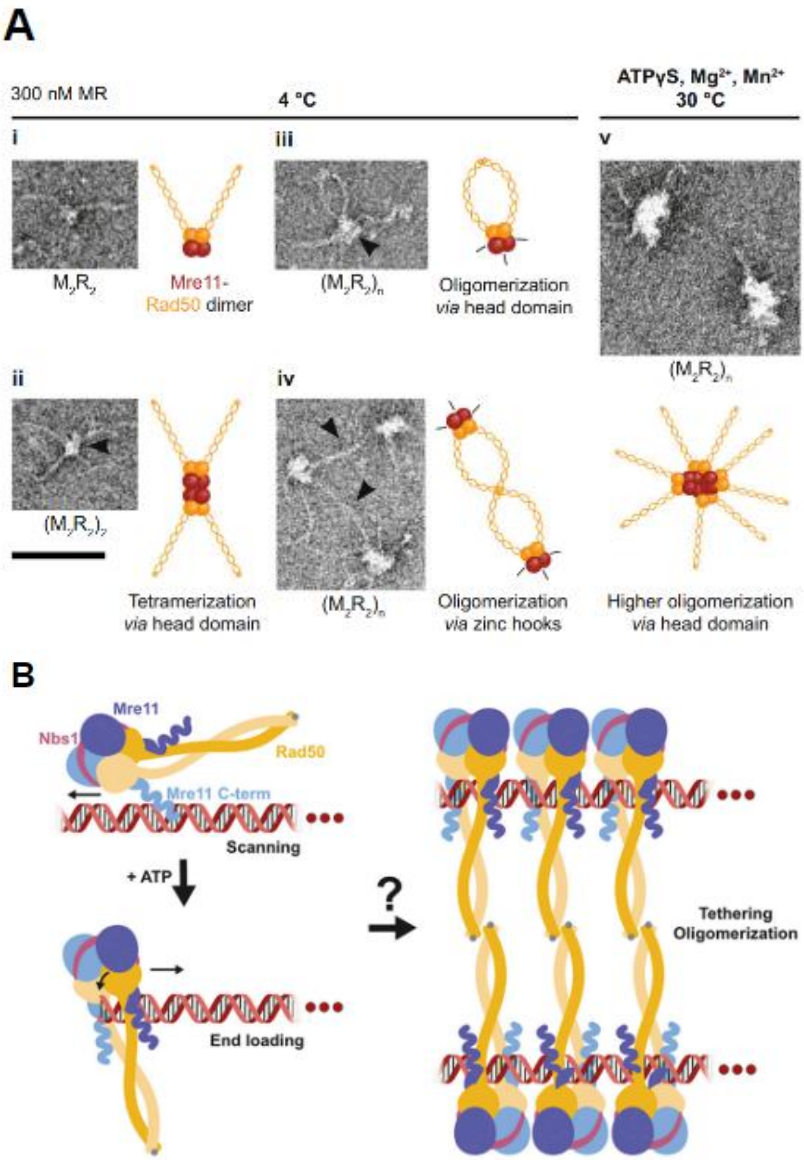

Figure 4. *in vitro* tethering by MRX/N. A) Transmission electron microscopy images and associated schemes demonstrating ways in which MRX can oligomerize. B) Schematic representation of Velcro like structures formed between CtMRN complexes. Two DNA molecules are tethered by direct interactions between MRN head domains, and coiled-coil apices. (Adapted from Kissling et al., 2022; Rotheneder et al., 2023).

2C) Exo1 dependent tethering

Loss of MRX does not completely abolish DSB end tethering in yeast, suggesting multiple mechanisms or a redundancy between factors (Lobachev et al., 2004). Indeed, tethering of persistent DSBs also requires Exo1 and specifically its exonuclease activity (Figure 5; Nakai et al., 2011). How end-tethering works following end resection is poorly understood. However, *in vivo* microscopy based assays in yeast demonstrate that ends remain tethered even as resection proceeds. This is in agreement with single RPA and Rad52 focus formed per single DSB (Lisby et al., 2004), and the single Rad51 NPF observed during coordinated homology search by both sides of an inducible DSB (Liu et al., 2023; Dumont et al., 2023). How alignment of ssDNA filaments is achieved, and how the adjacent DNA is maintained together in this context remains to be deciphered.

Rad52 has been proposed as a tethering factor (Kaye et al., 2004), in a different pathway to MRX, and interestingly presents phase separation properties (Miné-Hattab et al., 2021). Oligmerization or phase separation of Rad52 could therefore tether Rad52 coated ssDNA. Of note, Nakai et al. did not look at the effect of RAD52 deletion in the presence or absence of Exo1. If EXO1 deletion in cells lacking Rad52 does not increase end-separation further, it is likely that these proteins act in the same end-tethering pathway. Lee et al. did not see a dependence on Rad52 for end tethering, however these experiments were performed in G1 cells in which resection is inhibited.

Interestingly, Sae2 also plays a role in end-tethering, with increased end-separation upon double deletion with RAD50 (of MRX; Nakai et al., 2011). This provides further evidence that ssDNA tracts, and not Exo1 protein interactions per se, are important for DSB end-tethering. Although Rad52 may play a role in this process, it is unknown if Rad51 shares these same phase separation properties, and RPA does not (Miné-Hattab et al., 2021), indicating that tethering of ssDNA ends may require other factors. Furthermore, the 9-1-1 clamp, which sits at the junction between ssDNA and dsDNA, was recently proposed to tether resected DSB ends in budding yeast, using chromosome conformation capture techniques (3C; Piazza et al., 2021).

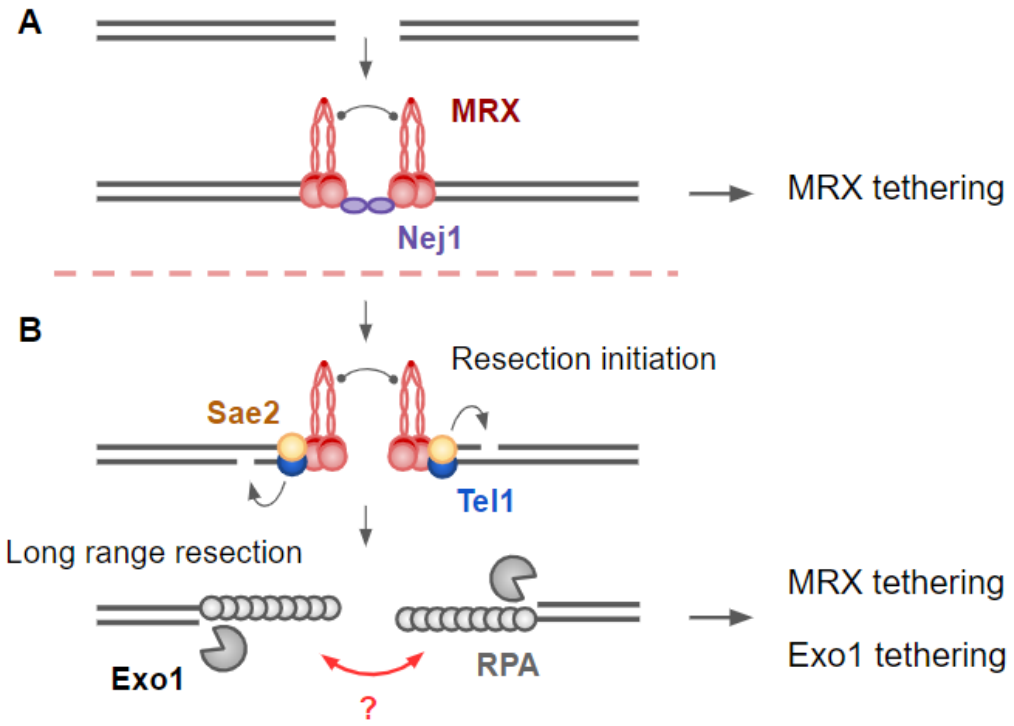

Figure 5. Schematic representation of DSB end-tethering pathways in *S. cerevisiae*. A) Upon DSB MRX is rapidly bound to DNA ends. In conjunction with Nej1, MRX tether DSB ends, preventing separation. B) If resection is initiated, a second DSB end-tethering pathway holds DSB ends together. This depends on Exo1 and its ability to form ssDNA tracts. However, the proteins involved in holding ends together in this pathway are unknown.

2D) Other potential tethering mechanisms

Recent theoretical research has proposed a role for DNA loop extrusion DSB end-tethering (Yang et al., 2023). Loop extrusion, a property associated with SMC family complexes, has recently emerged as a conserved mechanism for folding the genome into loops (Yatskevich et al., 2019). Among SMC complexes, cohesin (comprising Smc1, Smc3, Mcd1^{SCC1} and Scc3$^{STAG1/2}$) and the Smc5/6 complex are recruited to DNA damage sites in both yeast and mammals (Sjögren and Nasmyth, 2001; Kim et al., 2002; Ström et al., 2004; De Piccoli et al., 2006; Betts et al., 2006). In yeast, the loading of cohesin to DSBs involves various factors, including the cohesin loader Scc2/Scc4, DNA damage factors like MRX, γH2A, Tel1^{ATM}, Mec1^{ATR}, and Smc5/6 (Ström et al., 2004, Ünal et al., 2004, Lindroos et al., 2006, De Piccolo et al., 2006, McAleenan et al., 2012). Interestingly, Smc5/6 contains ssDNA binding domains which are important for DNA repair (Alt et al., 2017), and could explain the importance of ssDNA in DSB end-tethering.

Cohesin is enriched at DSB sites, but also throughout the entire genome. This tightens sister chromatid cohesion (Ström et al., 2007; Unal et al., 2007; Heidinger-Pauli et al., 2009; Dodson 2009; Kim 2010), locally restricts homology search (Piazza et al., 2021), and aids in DNA damage checkpoint establishment (Arnould et al., 2021). Given the involvement of cohesin in DSB response, including restricting translocations (Gelot et al., 2016), the motion of DSB ends *in vivo* (Gelot et al., 2018), and its ability to bridge DNA molecules *in vitro* (Gutierrez-Escribano et al., 2019), cohesin presents a possible candidate for DSB end-tethering. Of note, cohesin oligomerization, like seen for MRX, has also been demonstrated, which could provide an alternative tethering mechanism than cohesin's ability to form DNA loops (Ryu et al., 2021; Xiang and Koshland et al., 2021). Cohesin and its roles at DSBs will be explained in detail in sections 3 and 4.

Other less obvious questions also remain. For example, it is unknown if there is a transient separation of DNA ends following DSB, or if they somehow constantly stay in proximity. If they do separate, the time for the ends to come back together, and the mechanism that drives the attraction are unknown. It is also important to consider DSB in the context of the chromatin fibre, if a DSB occurs whilst contained within a nucleosome, can the nucleosome assume a tethering role? Nucleosomes in the proximity of DSBs are actively remodelled (Karl et al., 2022), however is this facilitates recruitment of tethering factors is unclear. These questions

will be technically difficult to answer, but are critical to understanding the *in vivo* context of DSB end-tethering.

3) Cohesin – A genome organising complex

Cohesin is a multiprotein, ring-shaped SMC complex, initially identified in budding yeast, and conserved in almost all eukaryotes. The complex was first described to hold sister chromatids together from S-phase to anaphase, entrapping them to ensure equal division of chromosomes (Figure 6B; Marston, 2014). However, cohesin has increasingly been implicated in novel functions, including the 3D organization of chromatin by the formation of long-range intra-chromatid loops (Figure 6C; Zuin et al., 2014; Dauban et al., 2020).

3A) Structure

Various forms of SMC complexes exist in viruses, bacteria and eukaryotes, sharing similar architecture and DNA related activities (Yatskevich et al., 2019). Each of these share the same characteristic shape. In *S. cerevisiae*, cohesin consists of four core and essential subunits. The SMC proteins Smc1^{SMC1} and Smc3^{SMC3} generate the cohesin ring with the kleisin Scc1 ^{SCC1} (also known as Mcd1), and Scc3^{SCC3} is constitutively associated to the kleisin (Figure 6A; Haering et al., 2002; Gruber et al., 2003; Gligoris and Lowe 2016; Yatskevich et al., 2019). SMC proteins consist of “head” and “hinge” domains, separated by 50nm long antiparallel coiled-coil arms (Haering et al., 2002). The coiled coils contain two key features. The elbow is 16nm from the hinge, and facilitates folding of aligned coiled coils (Burmann et al., 2019). A disruption near the globular ATPase domain is known as the joint (Diebold-Durand et al., 2017). The head comprises the N and C terminal domains that respectively provide the A and B motifs of a Walker ATPase (Hopfner et al., 2000). The hinge is generated where the coiled-coil, which separates the two halves of the head domain, reverse direction. Smc1 and Smc3 heterodimerize through their hinge domains, as well as making contacts through their head domains, which are essential for ATPase activity (Gligoris and Lowe 2016; Weitzer et al., 2003). The Scc1 subunit binds Smc3 at its N terminal and Smc1 at its C terminal, generating separate SMC (S) and kleisin (K) compartments when ATPase heads are engaged upon binding of two ATP molecules (Figure 6D). The Scc3 subunit binds to the central domain of Scc1, completing the cohesin complex (Gligoris and Lowe 2016, Roig et al., 2014).

Various conformations of the human cohesin complex have been identified by advanced microscopy techniques, which provide insight into how it facilitates both its sister chromatid cohesion and loop extrusion functions. These *in vitro* studies indicate that the Smc1/3 heads

can either be engaged, separated or juxtaposed, in a dynamic manner which is regulated by ATP binding (engaged) and hydrolysis (separated/juxtaposed) (Figure 6D; Yatskevic et al., 2019; Bauer et al., 2021; Davidson and Peterson, 2021). Engagement of the ATPase heads upon ATP binding confers a conformation with coiled coil arms separated, generating distinct S and K compartments (Figure 6A). In the ATP unbound state, ATPase heads can be separated or juxtaposed. When separated, the coiled coil arms do not align, generating one open SMC-kleisin (SK) compartment (Figure 6D). In the juxtaposed state, the SMC coiled coils align, generating a rod shaped complex, in which only a juxtaposed-kleisin compartment is present (Figure 6D). Alignment of the coiled coil is permissive to bending at an elbow region within the arms, which can bring the hinge domain into close contact with the Smc3 head domain (Figure 2D; Bauer et al., 2021).

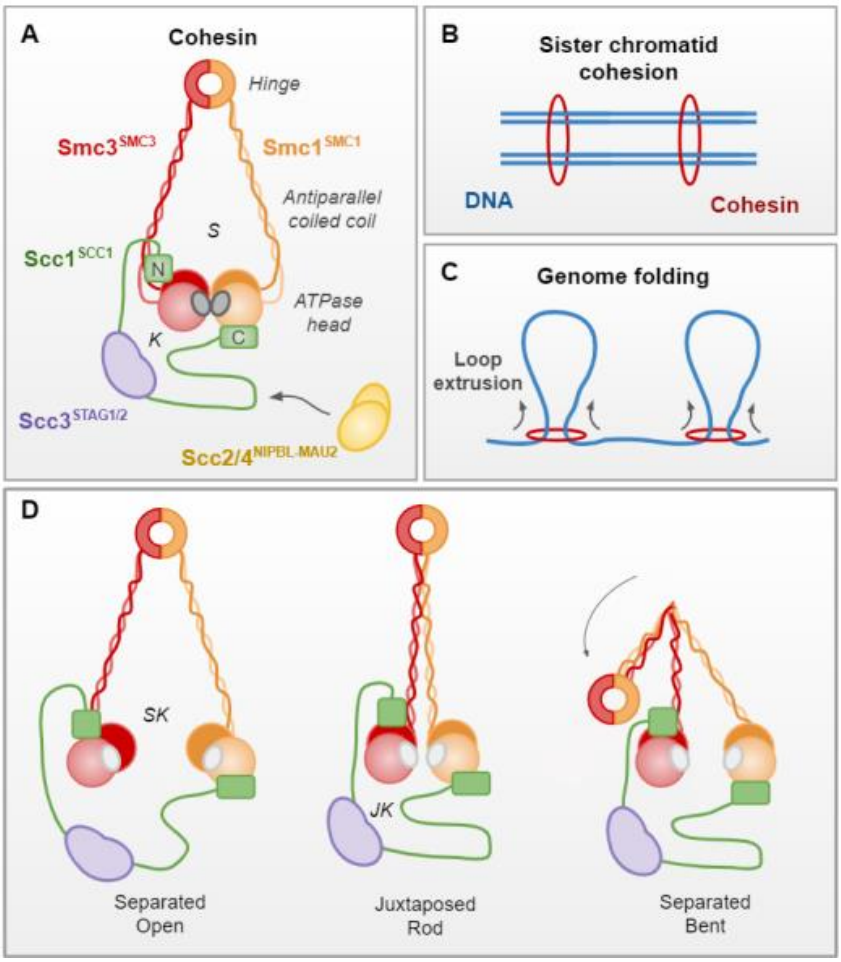

Figure 6. Cohesin structure and molecular functions. (A) The cohesin complex, shown in the ATP-bound state, has four core subunits: the structural maintenance of chromosomes proteins, Smc1 and Smc3, the kleisin Scc1 and the kleisin-associating Scc3$^{STAG1/2}$. The loading complex Scc2/4$^{NIPBLA/NIPBLB–Mau2}$ interacts with cohesin through Scc1. SMC proteins consist of ATPase head and hinge domains, and a long antiparallel coiled-coil arm. In the ATP-bound state, closed SMC (S) and kleisin (K) compartments are observed. (B) Cohesin holds sister chromatids together from S phase to anaphase. (C) Cohesin forms long-range intrachromatid loops, likely by a symmetrical extrusion process. (D) Cohesin can exist in multiple conformations determined by ATP binding (Smc heads engaged) and hydrolysis (Smc heads juxtaposed/separated). When separated, the coiled-coil arms generate one open SMC–kleisin (SK) compartment. In the juxtaposed state, the Smc coiled coils align, generating a rod-shaped complex, with a juxtaposed kleisin (JK) compartment. Alignment of the coiled coil is permissive to bending at an elbow region within the arms, bringing the hinge domain into close contact with the Smc3 head domain (Phipps and Dubrana, 2022).

3B) Auxiliary factors

Associating proteins Scc2/Scc4$^{NIPBLA/NIPBLB\text{-}Mau2}$, Pds5$^{PDS5A/PDS5B}$ and Wpl1^{WAPL} also bind to the complex through the Scc1 recruitment platform (Figure 7; Kikuchi et al., 2016; Lee et al., 2016; Hara et al., 2014). Dynamic interactions with these proteins facilitate cohesin loading and translocation (Scc2/4), releasing (Wpl1), or in the case of Pds5, counteracts loop expansion and has a dual role in the establishment and maintenance of sister chromatid cohesion, as well as releasing through recruiting Wpl1 (Ciosk et al., 2000; Murayama and Uhlmann 2015). Scc2 and Pds5 have a characteristic hook-like shape and HEAT repeats that are also found in the constitutively kleisin associated Scc3. As such, all three are known as HEAT repeat proteins Associated with Kleisin (HAWKs). It is described that only two HAWKs can associate to the kleisin at any one point (Scc3 and Scc2 or Pds5), and that this composition plays a key role in regulating cohesin function (Figure 7). Crucially, Scc2 containing complexes are active as ATPase's, whereas those containing Pds5 are not (Petela et al., 2018). As such, multiple different populations of cohesin can exist on chromosomes at any one time.

In both yeast and humans, cohesin ATPase activity is negatively regulated by Eco1$^{ESCO1/ESCO2}$ dependent acetylation of Smc3. Eco1 is recruited to cohesin through interactions with Pds5 (Chan et al., 2013; Minamino et al., 2015; Noble et al., 2006). Sororin is another cohesin associated factor, although it is not present in budding yeast. Sororin is common in multicellular eukaryotes, and is necessary for preventing WAPL mediated releasing of the cohesin complex (Nishiyama et al., 2010). Sororin is recruited to the cohesin complex through direct interaction with Pds5, and competes for the same binding site as WAPL (Ouyang et al., 2016).

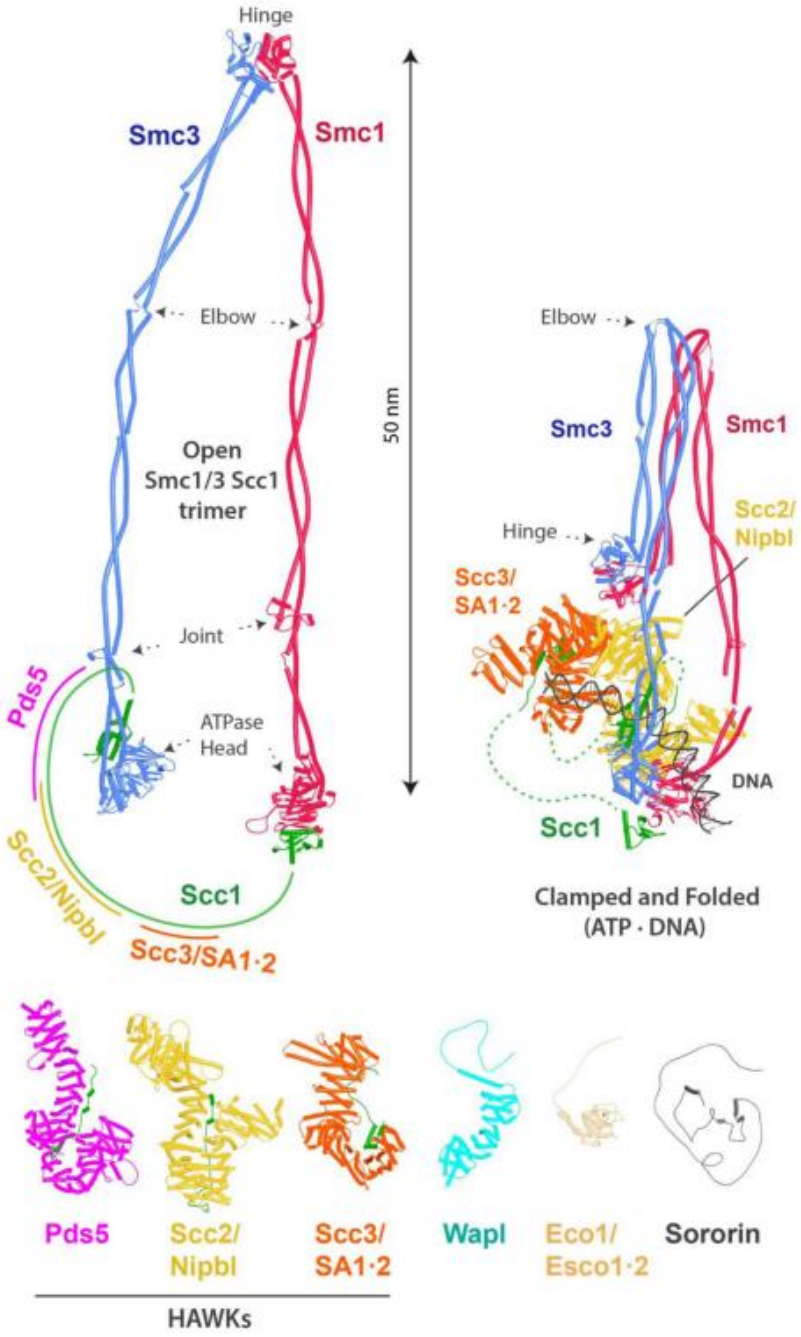

Figure 7. Cohesin and its HAWKs as predicted by Alphafold. In the Absence of ATP, Smc3 and Smc3 heads are not engaged. The kleisin Scc3$^{SA1/SA2}$ binds to Smc3 through its N-terminus, and Smc1 through its C-terminus. The regions in which cohesin's HAWKs associate to the kleisin are highlighted. In the presence of ATP and Scc2, cohesin assumes a folded state in which it clamps DNA to the Smc3 head. (Adapted from Nasmyth et al., 2023).

3C) Sister chromatid cohesion - overview

Cohesin is loaded onto chromosomes prior to S phase by Scc2/4 (Ciosk et al., 2000), which causes a conformational change in the cohesin complex and stimulates its ATPase activity (Petela et al., 2018). When the replication machinery encounters cohesin, it is used to topologically entrap the newly replicated sister chromatid, in a process known as cohesion establishment (Figure 8; Srinivasin et al., 2020). This can also be achieved through *de novo* loading of cohesin to capture both of the replicating strands (Srinivasin et al., 2020; Minamino et al., 2023; Murayama et al., 2018). This entrapment keeps sister chromatids together until cell division, and is protected by Smc3 acetylation (and Sororin in humans; cohesion maintenance). Cohesin is then completely removed from chromosomes prior to anaphase for equal division of the replication products between the dividing and daughter cells (dissociation; Uhlmann et al., 2000; Haering et al., 2008; Ivanov and Nasmyth, 2005).

In humans, cohesin release is regulated by two waves of cohesin dissociation from chromosomes. In the first wave, cohesin becomes sensitive to WAPL releasing activity due to inactivation and dissociation of Sororin from Pds5 (Marston, 2014; Peters and Nishiyama 2012). Centromeric cohesin is protected during this initial wave, and is only removed prior to chromosome segregation and cell division. Cohesin is removed in the second wave through Scc1 cleavage by a cysteine protease, Separase (Marston, 2014; Peters and Nishiyama 2012). In yeast, cohesive cohesin's are removed only at the onset of anaphase, through Scc1 cleavage by Esp1 (Separase; Marston, 2014; Peters and Nishiyama 2012).

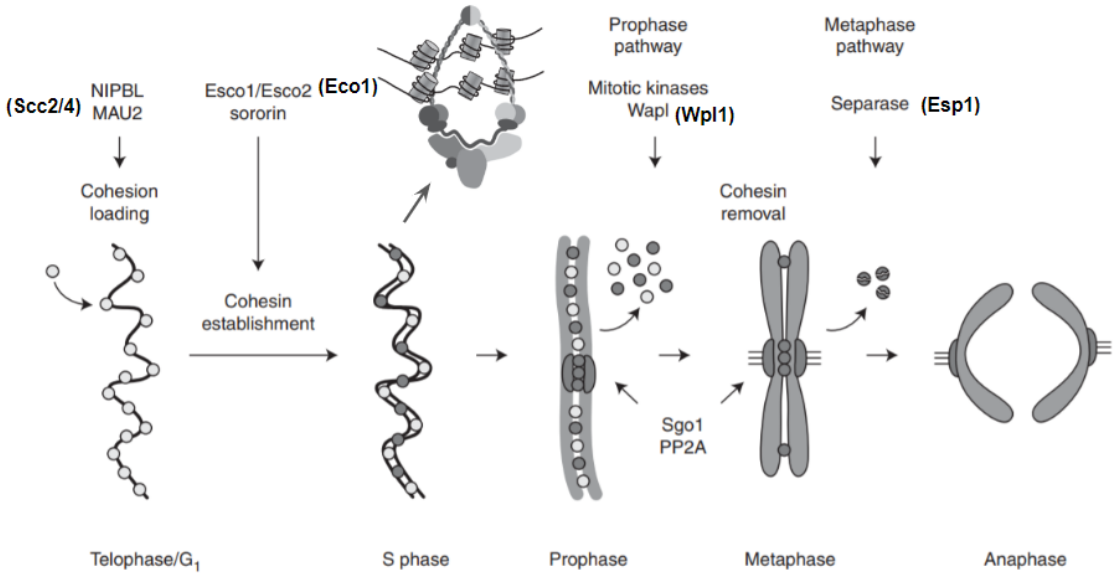

Figure 8. Schematic representation of cohesin establishment, maintenance and releasing to facilitate timely sister chromatid cohesion in humans. Cohesin is loaded on to individual chromosomes during G1 phase by NIPBL-MAU2. In a replication coupled process, cohesin entraps the replicating sister chromatid. The acetyltransferases Esco1/2 acetylate cohesin, preventing its releasing by WAPL. In a first prophase wave of cohesin releasing, chromosome arm cohesin's are sensitized to releasing by WAPL. In a second metaphase wave of cohesin releasing, remaining cohesin complexes are removed from chromosomes following cleavage by the protease Separase. *S. cerevisiae* protein names are given in parenthesis. Of note, the prophase pathway is not present in budding yeast, and cohesin is removed only via the metaphase pathway. (Adapted from Peters and Nishiyama 2012).

Sister chromatid cohesion – establishment and maintenance

Two redundant pathways can achieve entrapment of DNA by cohesin (Xu et al., 2007; Srinivasin et al., 2020). The first establishes cohesion by conversion of preloaded cohesin as replication passes through the cohesin ring (Lengronne et al., 2006; Srinivasin et al., 2020). Alternatively, cohesin newly captures both the dsDNA synthesized by leading strand replication, and the ssDNA generated by the lagging strand (*de novo* capture; Minamino et al., 2023; Murayama et al., 2018; Srinivasin et al., 2020). These two pathways are not mutually exclusive, and are genetically separable (Xu et al., 2007). Cohesion by the conversion pathway requires the replisome associating proteins Chl1, Ctf4, Csm3 and Tof1 (Xu et al., 2007). The *de novo* capture pathway requires the replisome associating Ctf18-RFC complex, which loads the DNA clamp PCNA (Bermudez et al., 2003; Xu et al., 2007). Ablation of either mechanism results in sister chromatid cohesion defects, which become severe if both pathway are lost (Rolef Ben-Shahar et al., 2008; Unal et al., 2008; Xu et al., 2007).

Much progress has been made in understanding replication coupled sister chromatid cohesion (Figure 9). In this instance, a replication coupled process opens the cohesin ring and allows it to embrace both replication products (Gruber et al., 2006; Collier and Nasmyth 2022; Minamino et al., 2023). Scc2 and NIPBL are recruited to the replicating chromosome through a direct interaction with PCNA (Psakhye et al., 2023). $Scc2^{NIPBL}$ dependent loading depends on cohesin ATP hydrolysis, which opens the cohesin ring at the hinge interface (Muryama and Uhlmann, 2014; Petela et al., 2018; Muryama et al., 2018; Srinivasan et al., 2018; Gruber et al., 2006; Collier and Nasmyth, 2022), although entry though the kleisin-Smc3 interface has also been reported (Muryama and Uhlman 2015; Higashi et al., 2020). This allows *de novo* loading of cohesin on to chromosomes, capturing both replicating strands (Minamino et al., 2023).

Once loaded, Pds5 bound cohesin stimulates acetylation of Smc3 by the acetyltransferase $Eco1^{ESCO1/ESCO2}$ (Noble et al., 2006; Chan et al., 2013). Smc3 acetylation promotes cohesion maintenance through antagonizing cohesin releasing by $Wpl1^{WAPL}$ (K112 and K113 in yeast, K105 and K106 in humans; Heidinger-Pauli et al., 2009; Ladurner et al., 2016). Structural insights have demonstrated that Scc2 binds these two key lysines near the Smc3 ATPase domain to generate an ATP bound state that grips DNA during cohesin loading (Collier et al., 2020; Higashi et al., 2020; Shi et al., 2020; Kaushik et al., 2023). Therefore, loading and

releasing is negatively regulated by acetylation of Smc3, which is recruited to cohesin by Pds5 (Noble et al., 2006; Chan et al., 2013; Kaushik et al., 2023).

As such, the timing of Smc3 acetylation is imperative for ensuring timely opening of the cohesin ring for establishment of sister chromatid cohesion, and to prevent early cohesin releasing and sister chromatid separation. Recent work demonstrated that replication coupled acetylation is not regulated by Eco1 post-translational modification or activity of the Smc3 deacetylase (Minamino et al., 2023). Instead, an *in vitro* reconstitution of DNA replication and cohesion establishment demonstrated that Eco1 interacts with PCNA, through a domain which is also found in the human ESCO2 (Minamino et al., 2023). Smc3 acetylation was dependent on active replication, PCNA and Eco1 (Minamino et al., 2023). In this case, cohesin acetylation is not complete immediately after replication, but instead continues to increase following DNA synthesis (Minamino et al., 2023).

In contrast, the cohesion by conversion pathway establishes cohesion by replication passing through acetylated Smc3 stabilised cohesins in the absence of Scc2 (Srinivasan et al., 2020). This was demonstrated in budding yeast using separase resistant cohesin's loaded onto mini chromosomes during G2 phase, and following a round of re-replication (Srinivasan et al., 2020). Converting cohesin associated with un-replicated DNA into cohesive structures requires Chl1, Ctf4, and Csm3/Tof1 (Srinivasan et al., 2020). Further evidence for this pathway comes from Smc3 acetylation in humans, where both Esco1 and Esco2 share roles in cohesion establishment. Esco1 acetylates cohesin in a Pds5 dependent but replisome independent manner, and therefore prior to replication (Minamino et al., 2015). Esco2 on the other hand requires both PCNA and the MCM helicase of the replication machinery (Ivanov et al., 2018; Yoshimura et al., 2021). Although the yeast observations by Minamino et al. might explain the role of PCNA for Esco2 dependent cohesion**,** the importance of the MCM interaction for acetylation remains less clear.

The chamber within which sister chromatids sit once inside the cohesin complex remains of debate, with recent evidence suggesting DNA resides in a kleisin sub compartment (Gruber et al., 2003; Li et al., 2018; Murayama and Uhlmann, 2015; Chappard et al.,2019; Collier and Nasmyth et al.,2022). Whether the DNA is actively engaged with DNA binding domains within these compartments is unknown. Many have been shown as essential for loop extrusion (Bauer et al., 2021), however their role in sister chromatid cohesion remains unclear. A recent

study demonstrated that disruption of two of these patches inhibited *in vitro* loop extrusion activity whilst having little effect of sister chromatid cohesion (Guerin et al., 2023). Therefore, not all cohesin-DNA interaction are required for establishment and maintenance of sister chromatid cohesion. Although certain patches are required for cohesion establishment (Srinivasan et al., 2018), it is possible that these interactions are not required for cohesion maintenance, or that a redundancy exists.

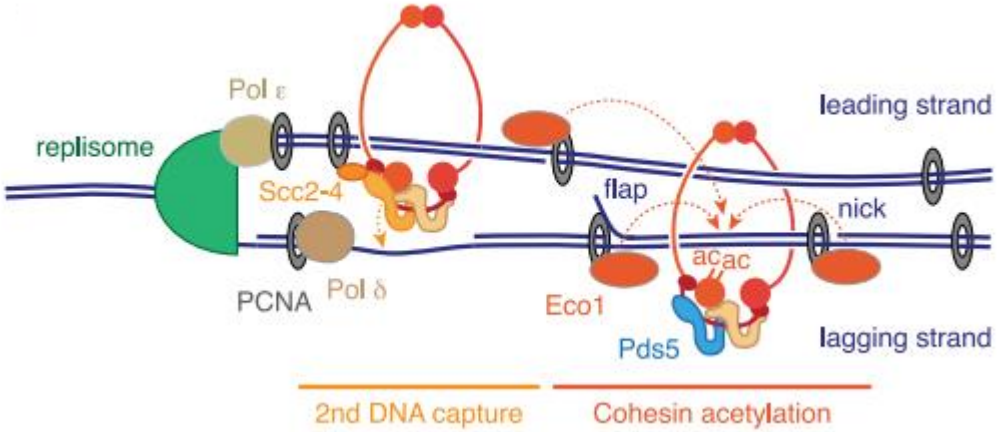

Figure 9. Replication coupled establishment of sister chromatid cohesion. Schematic representation of sister chromatid cohesion establishment at the DNA replication fork in *S. cerevisiae*. Cohesin on the double-stranded leading strand captures the adjacent single-stranded lagging strand DNA. PCNA at flap and nick structures promote Eco1 dependent acetylation of Pds5 containing cohesin, stabilizing sister chromatid cohesion. (Adapted from Minamino et al., 2023).

Resolving sister chromatid cohesion

In yeast, protection of cohesive cohesin from Wpl1 releasing is dependent solely on Smc3 acetylation. Once Smc3 is acetylated, this Pds5 bound cohesin population is resistant to Wpl1^{WAPL} dependent opening of the cohesin ring. Pds5 protects Smc3 from deacetylation by Hos1^{HDAC8} through G2 phase of the cell cycle, before cohesin is cleaved by Separase at the onset of anaphase (Beckouet et al., 2010; Borges et al., 2010; Xiong et al., 2010; Chan et al., 2013; Deardorff, et al., 2012). Cleavage of Scc1 by Separase occurs following cell cycle dependent activation of Cdc5 and the APC complex. This results in phosphorylation of Scc1 by Cdc5, and degradation of the Separase inhibitor Securin by the APC complex (activated by Cdk1). This removes cohesin from chromosomes, allowing full segregation of sister chromatids. Smc3 from cleaved cohesin's is deacetylated by Hos1, while the N and C terminal fragments of Scc1 are degraded (Rao et al., 2001; Beckouet et al., 2016).

In humans, both Smc3 acetylation and Sororin are required for protection from releasing. Sororin occupies WAPL's binding site with Pds5, preventing WAPL association with the cohesin complex (Nishiyama et al., 2010). In contrast to yeast, cohesin is removed from chromosomes in two waves. In the first prophase wave, Sororin is deactivated by Cdk1 dependent phosphorylation. This acts along chromosome arms, but not at centromeres where Sororin is protected by Shugoshin (Rankin et al., 2005; Nishiyama et al., 2010; Garcia-Nieto et al., 2023). WAPL binds cohesin in the absence of Sororin, and facilitates releasing through an Scc1-Smc3 interface, leaving only the centromeres connected (Gandhi et al., 2006; Chan et al., 2012). The second wave, like in yeast, is mediated by Separase dependent cleavage of Scc1, which removes all remaining cohesin from chromosomes.

Mechanistic insights to Wpl1 dependent releasing

Opening of the Scc1-Smc3 interface was recently described, and requires ATP binding and Smc1-Smc3 ATPase engagement (Muir et al., 2020). This results in a conformational change that remodels the coiled-coil domain of Smc3 and disrupts the binding surface for Scc1, opening the cohesin ring (Muir et al., 2020). The mechanism through which Wpl1 mediates cohesin releasing remains unclear. A recent study using AlphaFold structural modeling provides interesting insights into how this might work. AlphaFold predicts the formation of a tripartite complex of Wpl1^{WAPL}, Scc3^{STAG} and Pds5 that positions Wpl1^{WAPL} such that it

sequesters Scc1's N-terminal helices (Figure 10A; Nasmyth et al., 2023). This would prevent the Scc1 N-terminal helices from reengaging with the Smc3 head, resulting in a stable opening between the Scc1-Smc3 interface, through which DNA could exit the cohesin complex.

Another mechanism by which Pds5 and Wpl1^{WAPL} could mediate the transition between cohesive and non-cohesive cohesins was proposed in a recent review (Figure 10B; Rowland and Oldenkamp, 2022). Here the authors consider recent structural data that demonstrate an interaction between the Pds5 N-terminus and SMC hinge domain, and the Pds5 C-terminus and Smc3 head domain at the key acetylable lysines (Petela et al., 2021). The authors propose that maintaining both of these interactions at once would require the cohesin complex to be in its folded conformation with the elbow bent. In this state, Smc1-Smc3 heads cannot engage (Bauer et al., 2021). Therefore, ATP binding and head engagement required for opening of the cohesin ring would not be able to take place (Muir et al., 2020). As Wpl1^{WAPL} interacts with the Pds5 N-terminus (Chan et al., 2012; Ouyang et al., 2016), it could displace the Pds5-hinge interaction in the absence of Sororin, allowing the SMC arms to elongate, the heads to engage and the Scc1-Smc3 interface to open. This model provides a satisfactory preliminary step to Wpl1^{WAPL} mediated ring opening, and it remains feasible that both Wpl1^{WAPL} mediated arm elongation/head engagement could present a first step in cohesin releasing before the opening is stabilised by a Wpl1^{WAPL}-Scc1 interaction. However, it should be considered if the Pds5-hinge interaction is compatible with the presence of Sororin.

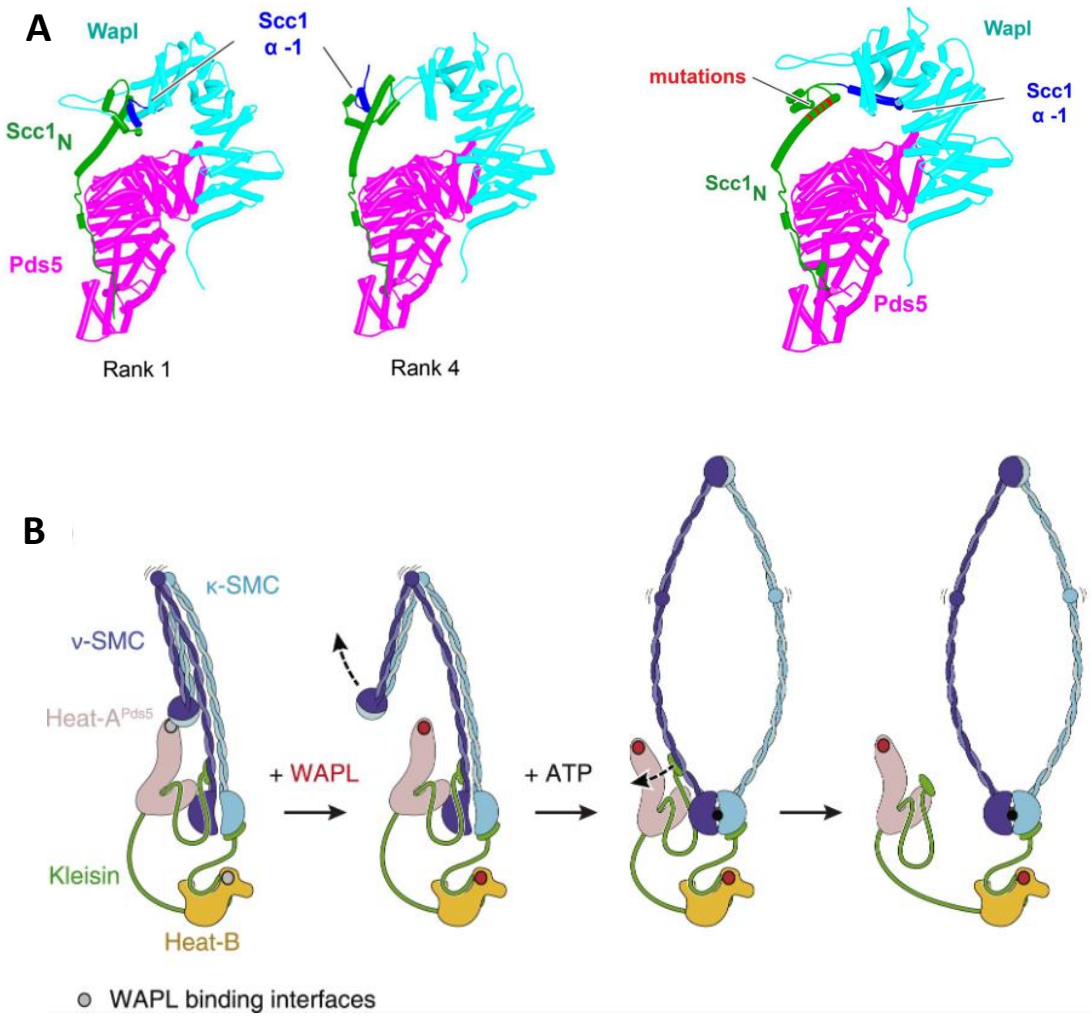

Figure 10. Potential mechanisms for WAPL mediated cohesin releasing. A) Alphafold predicitions for how WAPL might sequester alpha helices in Scc1's N-terminus, preventing its association with Smc3. Holding the Scc1 N-terminus would stabilise the opening of the Scc1-Smc3 interface. Mutations were introduced into the Scc1 N-terminus to demonstrate a potential unfolded form in which alpha helix 1 can embed in WAPL. B) Schematic representation of how WAPL might disrupt a Pds5 interaction with the cohesin hinge domain. Disrupting this interaction would allow the coiled-coils to elongate and the Scc1-Smc3 interface to open. (Adapted from Nasmyth et al., 2023; Rowland and Oldenkamp, 2022)

Protection without Sororin

How budding yeast prevent Wpl1 dependent releasing in the absence of Sororin has not yet been demonstrated. However, AlphaFold predicts an interaction between Scc3's N-terminus and the surface of Smc3 in which its acetylable residues sit (Nasmyth et al., 2023). Fittingly, amino acid switches in the same Scc3 surface at D189 and E202 abolish releasing activity by Wpl1 *in vivo* (Rowland et al., 2009). Therefore, if Smc3 is acetylated at residues K112 and K113, and Scc3 interaction with Smc3 at this position is essential for Wpl1 dependent releasing of cohesin, Smc3 acetylation alone would be sufficient to block interaction with Scc3 and prevent Wpl1 releasing activity. In humans, Smc3 acetylation alone is not sufficient to protect cohesin from WAPL induced releasing, instead, acetylation is necessary for Sororin recruitment, and hence protection from releasing. AlphaFold predicts that Sororin may interact with the Smc3-Scc1 interface to stablise the closed cohesin ring further (Nasmyth et al., 2023). In summary, acetylation of human Smc3 promotes Sororin-Pds5 interaction, which excludes WAPL and AlphaFold predicts to stabilise the Scc1-Smc3 interface. In contrast, acetylation of Smc3 in yeast might protect against Wpl1 releasing activity by inhibiting an interaction between Scc3 and Smc3, which is essential for opening the cohesin ring at the interface between Scc1s N-terminus and Smc3.

Regulating cohesin releasing by complex composition

Scc2/4 containing cohesin complexes are protected from $Wpl1^{WAPL}$ by displacing Pds5, which facilitates $Wpl1^{WAPL}$ mediated ring opening (Kueng et al. 2006; Sutani et al., 2009; Murayama and Uhlmann 2015). However, yeast studies have demonstrated that sister chromatid cohesion is also defective in absence of Pds5. This is partially because Pds5 is required, through recruitment of Eco1 to cohesin and protecting the resultant Smc3 acetylation, for both establishment and maintenance (Chan et al., 2013). This acetylation is important for counteracting Wpl1, which can also interact with cohesin independently of Pds5 both *in vitro* and *in vivo* (Kueng et al. 2006; Sutani et al., 2009). Despite this, WPL1 deletion in cells containing a temperature sensitive Pds5 allele (pds5-1) is not sufficient to rescue sister chromatid cohesion, as is also the case for Wpl1 deletion in cells lacking Eco1 (Sutani et al. 2009; Guacci and Koshland 2012). Although it is important to note that Wpl1 deficient cells presents a modest cohesion defect, it is significantly more severe in pds5-1 cells (Tong and

Skibbens, 2015). This could be due to opening of the cohesin ring during the ATPase cycle, or alternative mechanisms for regulating sister chromatid cohesion.

Alternative mechanisms for regulating sister chromatid cohesion

In contrast to WPL1 deletion, ELG1 deletion (which increase PCNA residency on chromosomes), is able to rescue cohesion in *pds5-1* cells, or cells lacking Eco1 (Skibbens et al., 1999; Tong and Skibbens, 2015). As previously described, acetylation of Smc3 stabilises the closure of the Scc1-Smc3 interface by preventing Scc2/4 binding and opening of the cohesin ring by ATP hydrolysis (Arumugam et al., 2003; Murayama and Uhlmann, 2015; Beckouet et al., 2016; Boardman et al., 2023). In addition, this prevents the proposed Scc3-Smc3 interaction required for cohesin releasing (Nasmyth et al., 2023; Rowland et al., 2009). It is possible that increased PCNA localization (which recruits Eco1 to the replicating chromosome; Minamino et al., 2022) during cohesion establishment in *pds5-1* cells rescues Smc3 acetylation by Eco1. Indeed, Eco1 overexpression can rescue survival in *pds5-1* cells (Noble et al., 2006), and Smc3 acetylation is still present, albeit severely reduced, in Pds5 depleted cells (Chan et al., 2013; Psakhye and Branzei 2021). However, Smc3 acetylation remained low in *pds5 elg1 wpl1* triple null cells (Psakhye and Branzei 2021), and this cannot explain how rescue occurs in Eco1 deficient cells.

The ability of ELG1 deletion to rescue survival of cells lacking either Pds5 or Eco1 exposes a pathway that is independent of Smc3 acetylation and Wpl1. Indeed, Scc2 is also recruited to replicating chromosomes through a PCNA interacting domain (Psakhye et al., 2023). This interaction is essential for sister chromatid cohesion in the absence of the Chl1 helicase, which is required for cohesion by the conversion pathway (Srinivasan et al., 2020; Psakhye et al., 2023). In contrast, Scc2-PCNA interaction is not required for cohesion when only the PCNA loader Ctf18-RFC is lost, clearly separating these two pathways (Psakhye et al., 2023). By increasing the replication coupled loading of cohesin on chromosomes, PCNA retention on DNA may rescue cell viability in Pds5 and Eco1 cells, which are sensitive to Wpl1 dependent releasing. Crucially, the PCNA-Scc2 interaction is conserved for human PCNA-NIPBL (Psakhye et al., 2023). Increased PCNA retention also increases recruitment of the Srs2 helicase to replication forks, which evicts Rad51 from ssDNA. This was demonstrated to further elevate

levels of cohesin loading (Choudhary et al., 2022), likely due to the increased availability of ssDNA, which is required for this process (Minamino et al., 2023).

Increased releasing in cells lacking Pds5 could also be explained by its role in preventing polySUMOlation of the kleisin subunit, which it achieves in partnership with the SUMO protease Ulp2 (D'Ambrosio and Lavoie, 2014; Psakhye and Branzei 2021). This would maintain cohesive cohesin's on chromosomes through protection from proteasome degradation. The SUMOligase responsible for Scc1 SUMOlylation in this pathway remains to be identified.

3D) Organising the genome with loops - overview

Eukaryotic genomes are organised at multiple levels, and ultimately exist in a highly folded state. The first level of chromatin folding consists of the periodic wrapping of the DNA double helix around a core of histone octamers to form nucleosomal chromatin fibres. These fibres are further organised into topologically associated domains (TADs), which have defined boundaries and exhibit increased local interactions within them and decreased interactions between them (Davidson and Peters, 2021; Sexton et al., 2012). The mammalian genome is partitioned into a succession of TADs, which range in size from tens of kilobases to 1–2 Mb of DNA, whereas in yeast, smaller TAD-like structures have been described (50–100 kb in S. pombe and 5 kb in *S. cerevisiae*).

Current models propose that cohesin forms TADs by loop extrusion between boundary proteins such as CTCF in mammals, or CARs (cohesin-associated regions) in yeast (Dauban et al., 2020; Costatino et al., 2020; Rao et al., 2017; Schwarzer et al., 2017; Wutz et al., 2017). Cohesin also contributes to the higher-order organisation of TADs, into TAD cliques, in which increased interactions are observed between distant TADs, in a constitutive or dynamic manner (Paulsen et al., 2019). The contribution of cohesin to the individualisation of chromosome domains imposes a constraint on the distance between sequences in the nucleus. This has explained cohesin's importance for a broad range of DNA related processes, which go beyond its role in sister chromatid cohesion. These include regulation of gene transcription, and significantly, the DNA damage response in both yeast and mammals (Phipps and Dubrana, 2022). Crucially, this constraint could favour or disfavour contacts between DNA sequences during DNA repair and modulate both the DNA damage response and outcome (see Section 4).

Various DNA binding domains throughout the cohesin complex, as well as the loading partner $Scc2^{NIPBL}$, have been shown to be essential for *in vitro* loop extrusion activity by human cohesin (Davidson et al., 2019; Bauer et al., 2021). Conformation changes within the cohesin complex facilitate the passing over of the DNA molecule between DNA binding sites. Although consensus is building, the full sequence and order of these events remains unclear, with multiple models being proposed (Bauer et al., 2021; Davidson and Peters, 2021; Dekker et al., 2023; Shaltiel et al., 2022; Yatskevic et al., 2019).

Despite this, evidence exists to suggest that cohesin does not form intra-chromosomal DNA contacts exclusively through loop extrusion, with mutant complexes unable to loop extrude *in vitro* still forming cohesin dependent loops *in vivo* (Guerin et al., 2023). The different ways in which cohesin may form loops is explored throughout this section, and with strong evidence for each mechanism, it is reasonable to assume that they are not mutually exclusive.

Other loop extruding SMC complexes

Whereas cohesin primarily organises interphase chromosomes, other loop forming SMC complexes with distinct functions exist. Notably in eukaryotes, the condensin complex condenses mitotic chromosomes to facilitate correct segregation upon cell division (Gibcus et al., 2018; Hirano et al., 2012). Like cohesin, the condensin ring is formed of two SMC proteins (Smc2 and Smc4), and a kleisin (Brn1; Lee et al., 2020). Unlike cohesin, condensin contains only two kleisin associating HAWKs (Ycs4 and Ycg1; Lee et al., 2020). Like cohesin, condensin is capable of topologically entrapping DNA within its SMC compartment (Tang et al., 2023).

Yeast and humans also contain another loop extruding SMC complex, Smc5/6. The ring is composed of the SMC proteins Smc5 and Smc6, and the kleisin Nse4 (Taschner et al., 2021). The Smc5/6 holocomplex is an octamer, with Nse1 and Nse3 interacting with the kleisin (Taschner et al., 2021). Smc5/6 varies from cohesin and condensin in that its associating factors (kleisin-interacting tandem winged-helix element; Kites) are structurally distinct from HAWKs. Instead, Smc5/6 and its associating Kites are closer in composition and structure to bacterial SMC complexes (Palecek and Gruber, 2015). As such, cohesin and condensin are likely derived from an ancestral Smc5/6 like complex. Of these three complexes, only Smc5/6 contains enzymatic activity. Its Nse1 subunit is a ubiquitin-ligase, and its Nse2/Mms21 subunit, which interacts with Smc5 CC's, is a SUMO-ligase (Andrews et al., 2005; Pebernard et al., 2008; Potts and Yu 2005). Finally, the Nse5 and Nse6 subcomplex appears to modulate ATP hydrolysis and DNA binding through regulating ATPase activity (Taschner et al., 2021). Dimerised Smc5/6 hexamers (without Nse5/6) loop extrude symmetrically *in vitro*, which is strictly inhibited by Nse5/6 binding (Pradhan et al., 2023). Nse5/6 instead favours translocation of individual Smc5/6 complexes (Pradhan et al., 2023).

Smc5/6 plays various roles in DNA related processes. However, compared to cohesin and condensin, its functions remain relatively elusive. To date, it has been implicated in resolving topological constraints on the genome (Jeppson et al., 2023), and assists in DNA replication and repair (Agashe et al., 2021; De Piccoli et al., 2006; Tanasie et al., 2022). Bacterial SMC complexes also form loops as dimers (Liu, Roisné-Hamelin et al., 2022). These organise their circular genomes and also play important roles in restriction of circular viral DNA, a feature shared with Smc5/6 (Lioy et al., 2018; Lioy et al., 2021; Liu, Roisné-Hamelin et al., 2022; Murphy et al., 2016; Yiu et al., 2021).

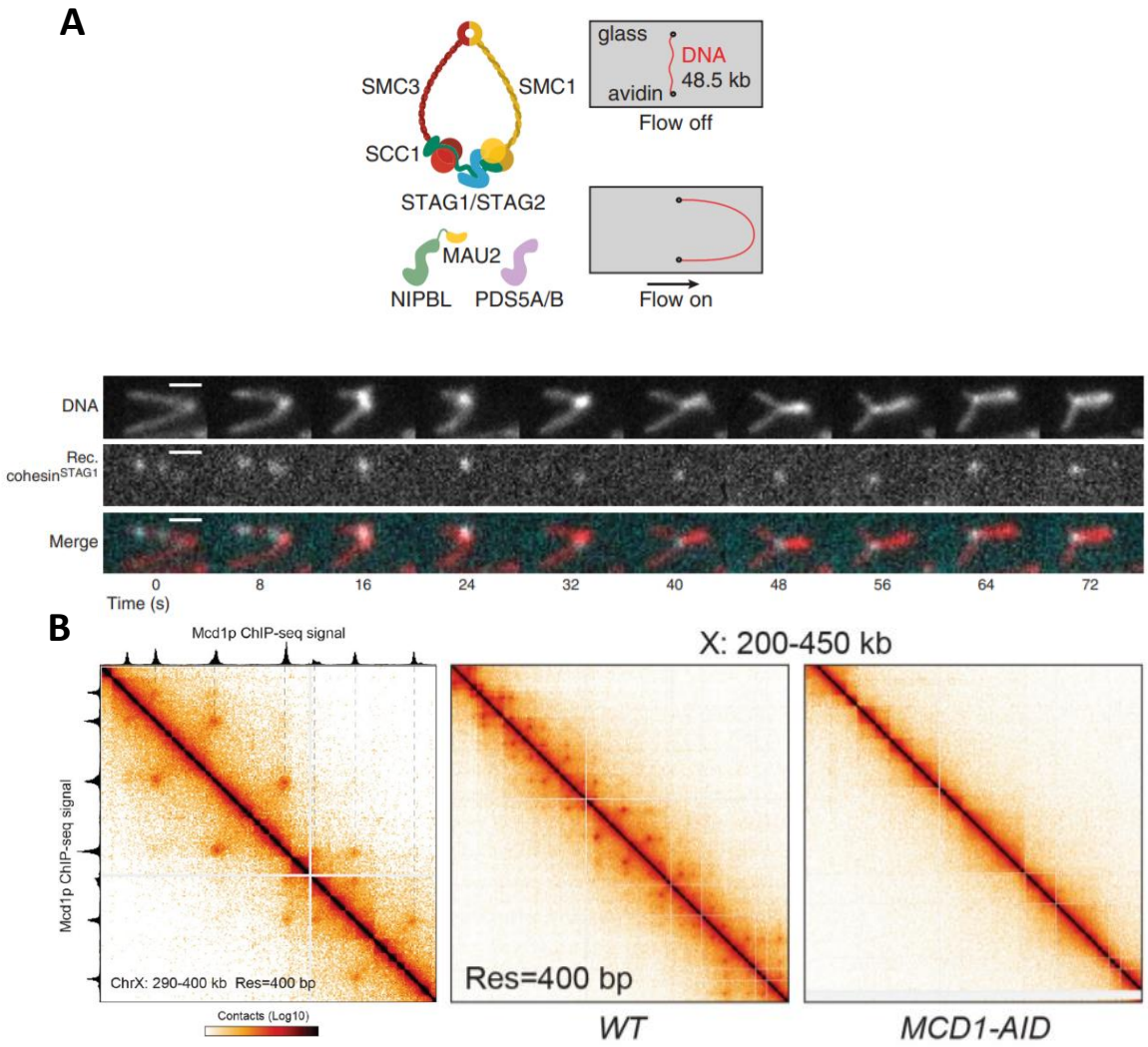

Figure 11. Loop extrusion *in vitro* and cohesin dependent chromosome contacts *in vivo*. A) Typical assay demonstrating loop extrusion by human cohesin. DNA attached to a glass slide, cohesin and its loader are incubated together. A directional flow is applied, and the expansion of loops in the presence of ATP are observed. Cohesin complexes sit at the base of loops as they form. B) Chromosome contact maps from Micro-C experiments and the associated enrichment of Mcd1^{Scc1} in *S. cerevisiae*. Hotspots of interaction correlate with cohesin ChIP peaks, and are abolished upon depletion of cohesin complex proteins. (Adapted from Davidson et al., 2019; Costatino et al., 2020).

Loop formation by extrusion

Loop extrusion by both the budding yeast and human cohesin complex has been demonstrated *in vitro* (Figure 11A; Davidson et al., 2019; Guerin et al., 2023). In these assays, DNA is attached to a glass slide, incubated with cohesin, ATP and $Scc2^{NIPBL}$, and the expansion of a DNA loop is visualized by microscopy techniques. Before this, conclusions on cohesin's ability to form loops were drawn from observations that WAPL depleted human cells generated super condensed interphase chromosomes (Tedeschi et al., 2013). Hi-C contact maps then demonstrated long range intra-chromosome contacts, the boundaries of which correlated with cohesin ChIP peaks, and were lost upon cohesin depletion (Figure 11B; Rao et al., 2017; Schwarzer et al., 2017; Wutz et al., 2017; Dauban et al., 2020; Costatino et al., 2020). *In vivo* evidence for loop extrusion itself then came from the observation that cohesin dependent loops expand when cohesin residency time is increased or barriers are removed, by $Wpl1^{WAPL}$ and Pds5 depletion (at centromeres; Dauban et al., 2020; Costatino et al., 2020).

A Perspective in Science synthesizes many of the experimental observations for loop extrusion by SMC complexes (Figure 12A; Dekker et al., 2023). Loop extrusion has been extensively studied using cohesin and condensin. The authors propose SMC complexes, which share similar architecture, use a conserved mechanism. Cohesin and condensin both require ATP hydrolysis and two HAWKs for loop extrusion, generating loops at a similar rate of 1kb per second in a directional manner (Davidson et al., 2019; Ganji et al., 2018). Each round of ATP hydrolysis induces a step of around 100bp (Ryu et al., 2022), correlating with the ~50nm length of the SMC complexes themselves. Here, the authors define a new model named reel and seal.

In this model, DNA is not topologically entrapped inside the cohesin ring, based on observations that a covalently linked cohesin ring can perform loop extrusion (Davidson 2019; Pradhan et al., 2022). Instead, the HAWK subunits engage the DNA in collaboration with the kleisin subunit, leading to pseudo-topological entrapment of the DNA inside two newly formed chambers (Shaltiel et al., 2022). This is coupled with direct DNA-protein interactions with known DNA binding sites, which are essential for loop extrusion (Shatiel et al., 2022; Bauer et al., 2021; Guerin et al., 2023). The HAWK closest to the kleisin C-terminus acts as an anchor, holding onto the DNA as the loop is increased in size during the loop extrusion process. Upon ATP binding/SMC head engagement, a second contact with the HAWK closest to the kleisin N terminus clamps DNA onto the SMC ATPase head (Kaushik et al., 2023). ATP binding

simultaneously elongates the SMC arms, generating an open space inside the SMC ring (Bauer et al., 2021; Shaltiel et al., 2022; Vazquez Nunez et al., 2021). The force of this conformational change is believed to induce a power stroke motion that drives DNA into the lumen (Shatiel et al., 2022), although, if the force of the power-stroke is sufficient to achieve this remains to be formally demonstrated. Here, DNA still passes into the cohesin ring lumen, despite interfaces of the ring not opening, by performing a double passage in which the DNA comes back out in the same direction.

Based on Cryo-EM structures and dynamic AFM imaging of SMC complexes, it is then proposed that from this elongated position, the hinge grabs a new distal DNA section. ATP hydrolysis causes the SMC heads to disengage, the non-anchoring kleisin to release from the SMC head, and the SMC arms to realign (Bauer et al., 2021; Shaltiel et al., 2022; Vazquez Nunez et al., 2021). This releases the original non-anchored DNA section from the complex, becoming part of the growing DNA loop. Realignment of the coiled coils simultaneously results in bending at the elbow, bringing the hinge back towards the SMC heads (Bauer et al., 2021; Bürmann et al., 2019). The DNA is then passed from the hinge to the non-anchored HAWK and kleisin, which following ATP binding and head reengagement results in the clamping of the new DNA section on to the SMC head as the cycle restarts.

Importantly, Shaltiel et al. did not observe the hinge-head interaction (Figure 12B). Instead they propose that the power-stroke, alongside realignment of the coiled-coils following ATP hydrolysis, drives the new DNA section into contact with the non-anchoring HAWK and kleisin in a zipper-like action. Interestingly, a folded structure of Smc5/6 has not yet been identified (Serrano et al., 2020; Taschner et al., 2021; Yu et al., 2021). If this conformation truly does not exist, this may favour the zippering model for all SMC complexes, unless different classes of SMCs use a non-conserved mechanism.

Furthermore, Shaltiel et al. demonstrate that although loading of DNA within the S compartment is not essential for loop extrusion *in vitro*, preventing the condensin kleisin-Smc2 interface from opening *in vivo* drastically reduces cell viability. As such, it remains possible that entry of DNA into the S compartment is an important step for condensin function. However, it remains unclear if this is for loop formation, either through loop extrusion or another mechanism such as second-DNA capture (Gerguri et al., 2021; Higashi et al., 2021; Guerin et al., 2023).

Further discrepancies not explained by this global model for loop extrusion include the bidirectional nature of cohesin loop extrusion compared to the unidirectional activity of condensin (Davidson et al., 2019; Ganji et al., 2018). Ultimately, how SMC complexes perform loop extrusion remains to be fully understood, despite much progress having been made. It is also possible that loop extrusion by SMC complexes differ slightly in mechanism, with more work needed to clarify this.

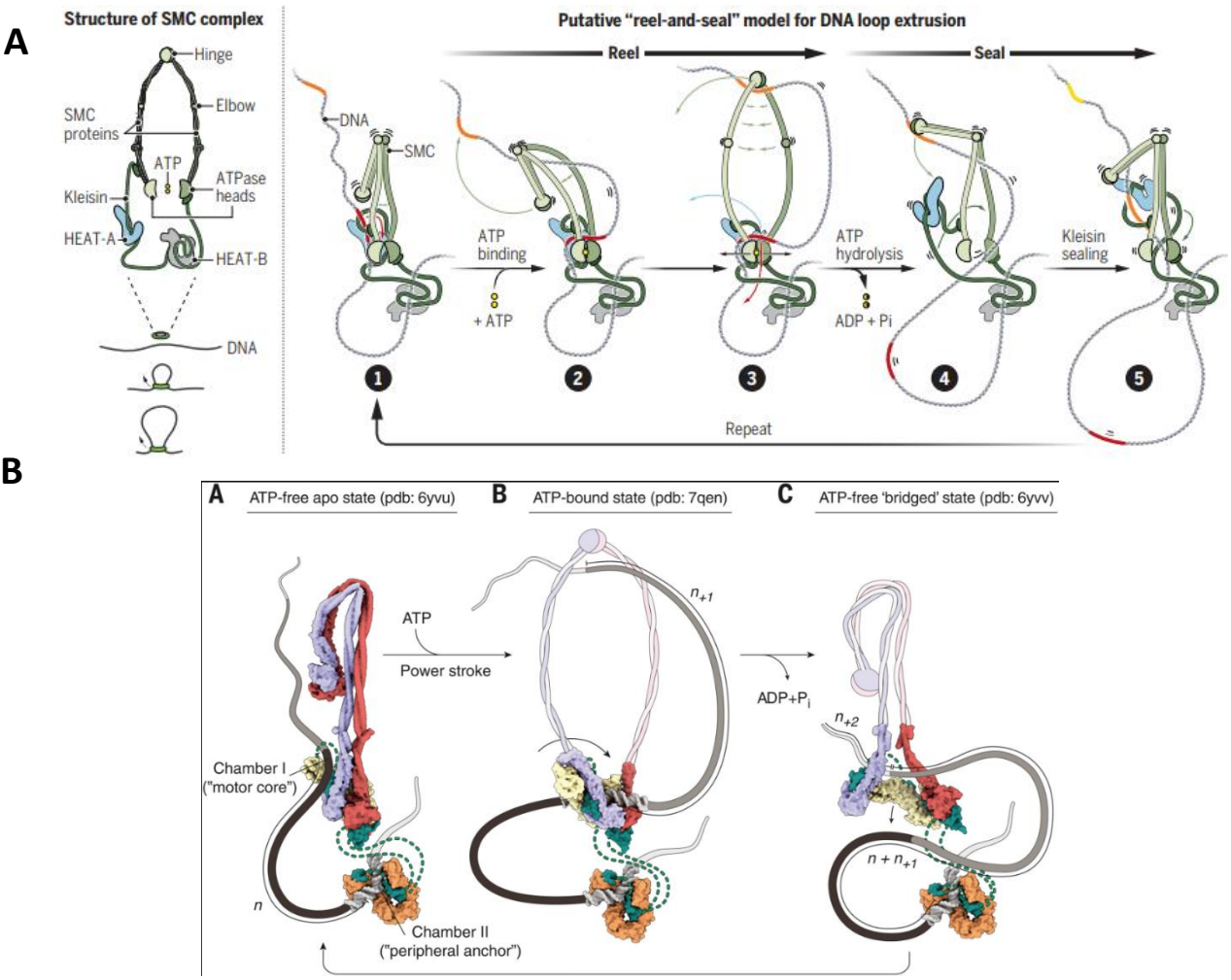

Figure 12. Proposed models for loop extrusion by SMC complexes. A) The HAWK subunits engage DNA in collaboration with the kleisin subunit, pseudotopoligcally entraping DNA inside two chambers. The HAWK closest to the kleisin C-terminus anchors the complex to DNA. The HAWK closest to the kleisin N-terminus clamps DNA onto the SMC head upon ATP binding and head engagement. The SMC arms elongate, generating an open SMC ring. This conformational change induces a power-stroke motion, driving DNA into the lumen. The hinge grabs a new distal DNA section, ATP hydrolysis causes the SMC heads to disengage. The non-anchoring kleisin is released from the SMC head, and the arms realign. The non-anchored DNA is released, becoming part of the growing DNA loop. Realignment of the coiled-coils results in elbow folding, bringing the hinge towards the SMC heads. DNA is passed from the hinge to the non-anchored HAWK and kleisin. ATP binding and head reengagement clamps the new DNA section to the SMC head as the cycle restarts. B) A model without the hinge-head interaction. Instead, the power-stroke and coiled-coil realignment is sufficient for bringing the new DNA section into contact with the non-anchored HAWK and kleisin, in a zipper-like action (Adapted from Dekker et al., 2023 and Shaltiel et al., 2022).

Loop extrusion in the chromatin context

To date, *in vitro* assays have interrogated loop extrusion in the context of naked DNA (Davidson et al., 2019; Ganji et al., 2018; Pradhan et al., 2023), or individual nucleosomes (Kim et al., 2019). However, it is clear from Hi-C experiments that complex chromatin regions are organised in an SMC dependent manner *in vivo* (Gassler et al., 2017; Rao et al., 2017; Sanborn et al., 2015; Schwarzer et al., 2017; Wutz et al., 2017; Dauban et al., 2020; Costatino et al., 2020). Much progress is required to understand how loop extrusion proceeds in the chromatin context of the nucleus. If technically feasible, *in vitro* loop extrusion assays should be modified to include more complex DNA-protein substrates. This would provide insight into how SMCs extrude through nucleosomes in the context of euchromatin and heterochromatin. It should be determined if permissibility to loop extrusion requires the activity of chromatin remodelling factors. Other biologically relevant questions include how loop extrusion responds to encountering DNA processing factors such as polymerases.

Loop extrusion through barriers such as nucleosomes, which are relatively small (roughly 11nm diameter) and dynamically remodelled, is easily explained by the model proposed in the above section. It is harder to reconcile experiments demonstrating that large gold particles of 200nm did not present a barrier to loop extrusion by condensin (Pradhan et al., 2022), as a double passage of the DNA in and then out of the SMC lumen is still required.

This observation may be explained by the use of Cas9 in tethering the particle to DNA, which may associate and dissociate with the DNA long enough for the DNA to enter the lumen. Alternatively, this could be due to the linker between Cas9 and the particle, which could leave the large particle outside of the SMC ring during this power stroke motion. Incidentally, loop extrusion by the *Escherichia coli* SMC complex, WadJET, was shown to be strictly halted by the covalent linking of large 2.6µm particles, but not of those in the 10nm range (Liu, Roisné-Hamelin et al., 2023). This confirms that some level of passage through the SMC ring likely takes place during loop extrusion. It will be important to test the ability of covalently linked particles to stall loop extrusion by condensin, as well as cohesin and Smc5/6. Of note, WadJET is slightly different to cohesin and condensin, but similar to Smc5/6, in that its kleisin associating proteins, Kites, vary in structure to HAWKs (Paleck and Gruber, 2015; Wells et al., 2017). HAWK containing cohesin and condensin complexes could behave differently in the

presence of covalently linked particles compared to the Kite containing WadJET and eukaryotic Smc5/6. This would provide important mechanistic and regulatory insights.

Regulating loop extrusion

Loop extrusion activity is dependent on ATPase activity and as such the composition of the cohesin complex. In yeast, Scc2, Pds5, Wpl1, and Eco1, all play key roles in regulating loop expansion and accumulation at boundaries (Figure 13; Dauban et al., 2020; Costatino et al., 2020). Scc2 positively regulates loop expansion by promoting ATPase activity (Davidson et al., 2019). In contrast, Pds5 negatively regulates loop formation, with its absence expanding loops compared to wild-type cells, and only the centromere presenting a barrier (Dauban et al., 2020; Costatino et al., 2020). Genetic analysis demonstrated that this is dependent on both inhibiting Wpl1-mediated releasing activity, and a different Eco1-dependent protection mechanism (Dauban et al., 2020). Eco1 also inhibits loop expansion and mediates loop positioning. Wpl1 deletion results in strengthening of wild-type cohesin boundaries, indicating it also negatively regulates cohesin dependent loops, but does not alter cohesin susceptibility to boundaries (or that cohesin dependent boundaries are not lost; Dauban et al., 2020; Costatino et al., 2020; Bastié, Chaphard et al., 2023).

Stalling of cohesin at boundaries depends on Smc3 acetylation in yeast (Bastié et al., 2022), and humans (van Ruiten et al., 2022; Wutz et al., 2020). Fittingly, Smc3 acetylated cohesive cohesin act as a non-permissive barrier to loop extrusion in yeast (Bastié, Chappel et al., 2023). Furthermore, in yeast and humans transcriptional activity is proposed to position cohesin at convergent genes, defining loop boundaries (Busslinger et al., 2017; Glynn et al., 2004; Guerin et al., 2023; Jeppsson et al., 2022; Lengronne et al., 2004; Ocampo-Hafalla et al., 2016). Transcription perhaps does this by driving cohesin's into hotspots (CARs).

In yeast, a Scc1V137K mutation has a super extruding phenotype, similar to that of Pds5 deficiency (Bastié, Chapard et al., 2023). Indeed, this mutant has lost Pds5 binding ability, whilst maintaining interaction with Scc2 (Chan et al., 2013; Bastié, Chapard et al., 2023; van Ruiten 2022). As such, this mutant is deficient for Smc3 acetylation and sister chromatid cohesion, with loops expanding through loss of barriers formed by cohesive cohesin, and hyperactivity of Scc2 (Bastié et al 2022; Bastié, Chapard et al., 2023). Despite this, Cdc45

depleted cells, which lack both Smc3 acetylation and a sister chromatid, still form positioned wild-type like loops (Duaban et al., 2020), confirming that sister chromatid cohesion is not the only defining factor in loop positioning. This provides further evidence for transcription being a driving factor in defining loop boundaries in yeast (Jeppsson et al., 2022; Guerin et al., 2023).

In humans, loop formation facilitates interaction between distant enhancers and promoters, and is stalled by the DNA binding boundary protein CTCF (Hansen, 2020). Interestingly, the boundary effect of CTCF is dependent on the directionality of the CTCF cohesin interaction (Fudenberg et al., 2016), indicating that this is the result of a direct interaction between the two. Indeed, human Shugoshin was recently shown to interact with the same surface of the Scc1-STAG2 interface as CTCF, indicating an important site for regulating cohesin activity (Garcia-Nieto et al., 2023).

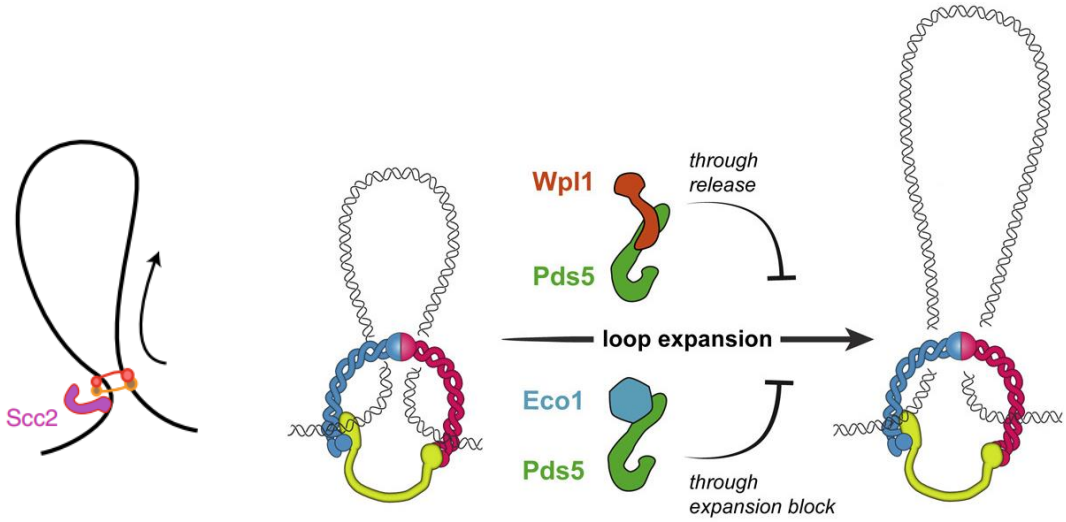

Figure 13. Cohesin complex composition regulates loop extrusion activity. Cohesin performs loop extrusion in the presence of ATP and Scc2. In contrast, loop expansion is prevented by Pds5-Wpl1 mediated cohesin releasing, or Pds5-Eco1 mediated acetylation of Smc3. Loops expand in the absence of Wpl1, Pds5, and Eco1. (Adapted from Dauban et al., 2020; Bastié et al., 2022).

Other models for loop formation

Although loop extrusion by cohesin has been thoroughly demonstrated and is relatively well characterized, questions remain. These include the *in vivo* consequences of this mechanism, if cohesin dependent chromosome contacts are entirely dependent on it, and if cohesin can work as multimers *in vivo*. Initial observations that cohesin loop extrusion is bidirectional *in vitro* was explained by extrusion through cohesin dimers, each acting in opposite directions (Davidson et al., 2019; Golfier et al., 2020; Kim et al., 2019). However, directional switching of cohesin monomers whilst extruding has also been observed (Davidson et al., 2023). These results suggest that cohesin might be able to switch the DNA anchor point between the two HAWKs, in order to change direction (Dekker et al., 2023).

Another possible explanation for bidirectional loop expansion could be based on a different mechanism for loop formation. One such model predicts expansion by Brownian motion and cycles of SMC-DNA capture (Gerguri et al.,2021; Higashi et al., 2021; Guerin et al., 2023). In this model, the mobile chromosome moves into proximity at two distant DNA loci, and SMC complexes already present at one of these loci captures the other DNA section (Guerin et al., 2023). The DNA loop could then be held by a gripping state in which the SMC complex is bent at the elbow (Higashi et al. 2021). Cycles of cohesin capture and release, and DNA related process such as transcription, would result in expansion of the loop.

Direct evidence that cohesin-DNA capture and loop extrusion might co-exist came recently (Guerin et al., 2023). This study characterized cohesin mutants that are unable to extrude DNA loops *in vitro*, but are sufficient for sister chromatid cohesion and maintain cohesin dependent intra-chromosomal contacts *in vivo* (Guerin et al., 2023). Indeed both mechanisms might be physiologically relevant for chromosome conformation, with tight regulation depending on the required result. For example, a condensin loop capture mechanism could present a challenge to dividing cells during anaphase. If condensin does form loops through such a mechanism, one may imagine that erroneous capture of the sister chromatid during chromosome condensation would re-establish some level of sister cohesion and hinder correct chromosome segregation.

Another possibility instead of capturing a distant DNA section is that cohesin's bound at two distinct loci bridge the DNA sections through cohesin-cohesin interactions (Xiang and

Koshland et al., 2021; Ryu et al., 2021). Ultimately, loop expansion does not have to be exclusive to any of these models, and indeed, evidence for each exists.

3E) Cohesin oligomerization

Beyond loop extrusion, *in vitro* studies have demonstrated the ability of budding yeast cohesin to bridge and compact DNA molecules through cohesin-cohesin interactions (Gutierrez et al., 2019; Xiang and Koshland, 2021; Ryu et al., 2021). Although not yet observed for human cohesin, yeast cohesin forms molecular condensates *in vitro* upon interactions with DNA, leading to pronounced clustering (Figure 14; Ryu et al., 2021). Furthermore, recent work using budding yeast has also demonstrated the formation of cohesin clusters *in vivo*, through a proximity ligation assay (Xiand and Koshland, 2021). The biological significance of these observations remains to be demonstrated. However, recent Cryo-EM observations of budding yeast MRX revealed it shares an ability to form condensates, which are proposed to be important for its role in DSB end-tethering and DNA damage signalling. Crucially responsible protein motifs were identified (Kissling et al., 2021). Whether these motifs in Rad50 are conserved in cohesin and are relevant for their clustering activity remains to be determined.

Despite evidence for cohesin working as a monomer, cohesin dimerization/oligomerization has been proposed as a potential method for sister chromatid cohesion and other cohesin processes (Zhang and Pati, 2009; Xiang and Koshland, 2021). The evidence for cohesin working as oligomers is mounting. Early evidence came with regards to sister chromatid cohesion. TEM analysis of minichromosomes purified from M phase yeast cells revealed rod like structures that appeared to tether chromosomes through tetrameric coiled coil structures (Surcel et al., 2008). Furthermore, two studies noted interaction between Smc1-Smc3-Scc1 and $STAG^{Scc3}$ from different complexes (Zhang et al., 2008; Zhang and Pati, 2009). Dimerization between $STAG^{Scc3}$ is important for Scc1-Scc1 interactions in humans by Co-IP, yeast two hybrid and FRET, with STAG binding motif mutations reducing this interaction (Zhang et al., 2013). This led to the handcuff model of sister chromatid cohesion being proposed, through two cohesin's individually loaded on to each sister chromatid interacting.

Evidence for cohesin oligomerization developed further recently, in a yeast study monitoring proximity ligation of biotin to differentially tagged domains of the Smc3 protein (Xiang and

Koshland 2021). To do this, the authors expressed two copies of Smc3, each containing either an Avi-tag or the biotinylating BirA on different Smc3 domains. Biotinylation of the tag occurred from S-M phase, and demonstrated Smc3 head-head or head-hinge contacts. This peaked in the S phase, and was also present in G2/M, but crucially, not in G1 when Scc1 is not expressed. This study identified a dependence on Pds5 and Scc1, but not Eco1, indicating Smc3 acetylation is non-essential. Importantly, all of the interactions are detected *in vivo*.

Another recent study described budding yeast cohesin oligomerization *in vitro* using AFM, demonstrating bridging induced phase separation of cohesin (Ryu et al., 2021). Cohesin and DNA incubated together created large clusters with physical properties similar to droplets, including the way they form, and their exchange with the environment. Whilst interactions between a few cohesin's were observed, droplets containing many cohesin's (700-1500), were also common. How relevant these observations are for the *in vivo* context remains to be determined, but this demonstrates that the physical properties exist. Treatment of yeast cells with hexanediol, which disrupts weak hydrophobic protein-protein interactions and cohesin oligomerization, decreased cohesin enrichment on chromosomes (Ryu et al., 2021). Crucially, this did not fully abolish cohesin residency on chromosomes. This could be explained by presence of a hexanediol resistant population of topologically loaded cohesin's, alongside a hexanediol sensitive population of non-topologically loaded cohesin's.

Interestingly, a body of literature is also accumulating for clustering of condensin. A theoretical study proposed that condensin loop extrusion alone is not sufficient to reproduce observed levels of mitotic chromosome condensation (Sakai et al., 2018; Gerguri et al., 2021; Forte et al., 2024). Furthermore, the authors demonstrate that with bridging condensin's such as those observed for cohesin by Ryu et al., and Xiang and Koshland, these characteristics can be reproduced. Strikingly, condensin clusters have also been visualized on budding yeast and *Xenopus* mitotic chromosomes *in vivo* (Gerguri et al., 2021; Kinoshita et al., 2022).

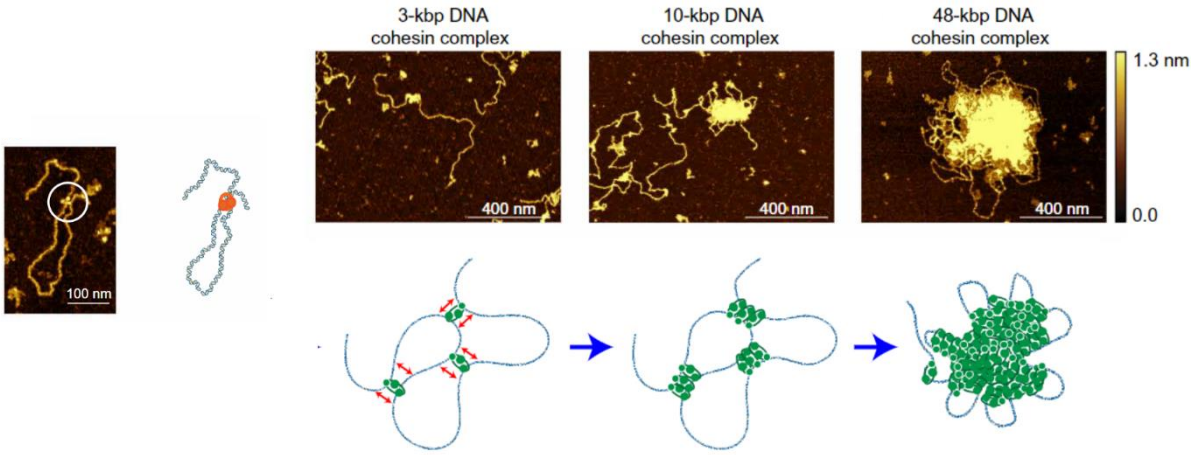

Figure 14. *In vitro* cohesin oligomerization forms pronounced DNA-cohesin clusters. Representative AFM images of S. cerevisiae cohesin bridging-induced phase separation in the presence of different length DNA. Images include representation of DNA bridging by a single cohesin, to pronounced clustering by many cohesin's. Schematic representation of bridging induced phase separation below. As the local concentration of DNA increase, more cohesin complexes bind this region, leading to the formation of a large DNA/cohesin droplet. (Adapted from Ryu et al., 2021).

4A) Cohesin and repair

With the emerging importance of cohesin in shaping the genome by loop formation, new aspects of cohesin contribution to DNA damage signalling and repair are appearing. A role for cohesin in DNA repair was in fact discovered before its well described role in sister chromatid cohesion, with the S. pombe Rad21^{Scc1} gene providing resistance to ionizing radiation (Birkenbihl and Subramani, 1992). Since then, cohesin is increasingly implicated in DNA damage repair. Its function in repair was first linked to its capacity to maintain sister chromatid cohesion at the DSB site to facilitate HR. Cohesin has also been proposed to regulate NHEJ in both yeast and human cells (Schar et al., 2004; Gelot et al., 2016). However, loop formation by cohesin also regulates the DNA damage response and constrains homology search during HR (Arnould et al., 2021; Piazza et al., 2021).

Studies in yeast and mammals have demonstrated that cohesin is recruited to DSB sites (Caron et al., 2012; Unal et al., 2004; Strom et al., 2004; Potts et al., 2006), but how cohesin is enriched and regulated at DSBs remains to be fully described. In yeast and humans, the cohesin loading complex Scc2/4$^{NIPBL\text{-}Mau2}$ is essential for the enrichment of cohesin at DSBs. However, as Scc2/4$^{NIPBL\text{-}Mau2}$ is required for loop extrusion and cohesion establishment (Davidson et al., 2019; Guerin et al., 2023; Minamino et al., 2015), it is not clear if de novo cohesin loading or rearrangement of pre-loaded cohesin's through loop extrusion is responsible (Arnould et al., 2021; Strom et al., 2004; Unal et al., 2004). Strikingly, key components of the DNA damage checkpoint are important for recruitment of cohesin to DSBs. MRX^{MRN} and the Tel1^{ATM} kinase are required both in yeast and humans (Unal et al., 2004, Arnould et al., 2021), and γH2AX, the Mec1^{ATR}, and Chk1 kinases are also important for cohesin enrichment at DSB in yeast (Unal et al., 2004). SUMOylation of the cohesin subunit Scc1 by the SUMO ligase Mms21 (Mms21/Nse2 in humans) also assists the recruitment of cohesin at yeast DSBs (McAleenan et al., 2012). Cohesin binding at DSBs is kept in check by the SUMO-dependent ubiquitin ligase Uls1, whose absence increases MRX and cohesin levels at DSB (Cheblal et al., 2020).

4B) Smc5/6 at DNA DSBs

The Mms21 SUMO ligase is itself recruited to DSBs by the Smc5/6 complex (Andrews et al., 2005). Smc5/6 was originally identified in S. pombe in genetic screens probing for increased radiation sensitivity (Fousteri and Lehmann, 2000). Smc5/6 monomers and the holistic complex including Mms21 have ssDNA binding affinity, through novel and unique hub and latch domains not found in the other SMC family proteins (Alt et al., 2017). Like cohesin, Smc5/6 is enriched in the 50kb region flanking the DSB (DePiccoli et al., 2006; Betts Lindros et al., 2006). Furthermore, knockdown (KD) of the Smc5/6 complex was shown to reduce cohesin loading at DSB (Potts et al., 2006). Crucially, KD of cohesin alone, or together with Smc5/6, resulted in the same reduction in HR events by sister chromatid exchange, indicating that these two complexes act in the same DNA repair pathway (Potts et al., 2006). These observations may suggest that the Smc5/6 complex acts as a sensor for DSB ends, leading to the recruitment of the cohesin complex to the DSB.

How Smc5/6 senses DSB ends is unknown. One hypothesis is that ssDNA formed by resection is detected through the Smc5/6 ssDNA binding motifs (Alt et al., 2017). Another mechanism could be linked to the deposition of γH2AX in the DSB adjacent chromatin. Indeed, Rtt107, a γH2AX binding protein with which Smc5/6 can interact, is necessary for its enrichment at DSBs (Leung et al., 2011; Leung et al., 2016). The full functional role Smc5/6 plays in DNA repair remains unclear, including the mechanism by which it leads to cohesin recruitment. Furthermore, it is possible that Smc5/6 plays roles beyond cohesin recruitment, as demonstrated by the importance of the SUMOylation activity of its Nse2 subunit for relocation of heterochromatic DSBs in Drosophila (Ryu et al., 2015), and DSB interaction with the nuclear periphery in yeast (Horigome et al., 2016). Whether cohesin is also relevant to these responses remains to be tested.

Smc5/6 is also a loop extruding complex *in vitro*, with important functions in correcting topological stress on the chromosome (Pradhan et al., 2023; Jeppsson et al., 2023). If this function could somehow play a role in DSB repair remains to be investigated. However, cohesin depletion alone abolishes γH2Ax spreading in mammalian cells, demonstrating that Smc5/6 and its loop extrusion capacities are not sufficient for this function (Arnould et al., 2021).

4C) Cohesin loop extrusion and repair

Multiple observations demonstrate that sister chromatid cohesion is not cohesin's exclusive role in DSB repair. For example, Scc2 dependent cohesin enrichment is required for efficient repair of DSBs formed in G2/M blocked cells in which sister chromatid cohesion is maintained by S phase cohesin (as well as an MRX dependent mechanism; Strom et al., 2004; Potts et al., 2006; Seeber et al., 2016).

More recently, cohesin dependent loop extrusion has been implicated in DSB signalling and repair. One of the first signalling events following DSB induction is the phosphorylation of H2A (γH2AX in mammals) by the PI3-kinases Tel1^{ATM}, Mec1^{ATR} and DNA-PK (in mammals) (Jackson and Bartek, 2009; Shroff et al., 2004). γH2AX can spread over 50-100kb in yeast (Lee et al., 2014; Shroff et al., 2004), and 1-2 Mb of the adjacent chromatin in mammals (Berkovich et al., 2007; Iacovoni et al., 2010), while the kinases appear to be bound close to the DSB ends. Recent studies in human cells have demonstrated that cohesin dependent TADs are functional units of the DNA damage response, through γH2AX spreading (Arnould et al., 2021; Collins et al., 2020). Hi-C and ChIP-seq data have demonstrated that contacts between the DSB site and distant *cis* chromosome loci are important for establishing γH2AX domains, with the interactome of the break site correlating strongly with the density and spread of γH2AX (Collins et al., 2020). These domains are largely defined to TADs, with TAD disruption extending γH2AX spreading (Collins et al., 2020). Furthermore, DSB sites act as a cohesin translocation roadblock in yeast and humans (Arnould et al., 2021; Piazza et al., 2021), with cohesin extruding loops away from DSB sites. Therefore, a role for cohesin loop extrusion activity in γH2AX spreading could be imagined, beyond its role in defining TADs (Arnould et al., 2021). These observations support a model in which cohesin complexes, anchored at DSB ends where the kinase is located, facilitate phosphorylation of H2Ax as chromatin passes through the cohesin ring during loop extrusion (Figure 15B). Interestingly, γH2Ax spreading was not exclusively correlated with individual TADs, with *trans* spreading in yeast occurring in a cohesin dependent manner, in this context, a cohesin-DNA capture mechanism may come into play (Lee et al., 2014).

Cohesin loops also favours repair with proximal DNA sequences by restricting chromosome interactions and possibly DSB motion. Indeed, the interactome around a DSB is altered in absence of cohesin, resulting in increased genome wide contacts (Figure 15C; Piazza et al.,

2021). Furthermore, cohesin depletion increases DSB movement beyond the heightened movement observed at DSB sites in wid-type (WT) yeast cells (Figure 15A; Cheblal et al., 2020). Together this data highlights the contribution of DSB bound cohesin. Cohesin drives contacts between DSB ends and proximal sequences through loop extrusion, participating in DNA damage signalling by γH2AX spreading and promoting intra-chromosomal repair. Cohesin also restrains DSB motion, restricting *trans* interactions, further favouring repair with proximal sequences. Of note, loss of both loops and sister chromatid cohesion could contribute to increased motion and inter-chromosomal interactions.

4D) DDR and movement of DSBs into domains

Interestingly, in mammalian cells, cohesin has been shown to play a key role in driving DSBs into DNA damage domains. Recent literature has demonstrated how DSB dependent localisation of ATM to DSBs stimulates cohesin dependent loop extrusion at DSB sites, which act as a barrier to loop extrusion, and that this loop extrusion activity drives further ATM dependent spreading of γH2Ax (Arnould 2021). This leads to clustering of damaged TADs in humans, in a 53BP1 dependent manner (Arnould et al., 2023)**,** which has phase separation properties and forms condensates (Kilic et al., 2019). In this pathway, phosphorylation of the acetyltransferase ESCO2 by ATM results in recruitment of the MDC1 scaffold to DSB sites, which in turn acetylates SMC3 and stabilises cohesin at DSBs (Fu et al., 2023). This ultimately leading to 53BP1 recruitment and the formation of the 53BP1 DNA damage micro domains (Fu et al., 2023). Such domains might be important for increasing repair efficiency by concentrating DNA repair factors. However, moving DSB ends into specific DNA damage domains could also have deleterious side effects. For example, this could facilitate illegitimate joining of DNA ends from different DSBs by NHEJ, resulting in harmful translocations (Arnould et al., 2023; Gelot et al., 2016). In yeast, DSBs are known to localise to the nuclear periphery in a SUMO dependent manner (Nagai et al., 2008). Whether cohesin activity is also an important factor in driving the required chromatin modification for nuclear periphery localisation should be studied.

4E) V(D)J recombination

Loop extrusion by the cohesin complex has also been implicated in the random rearrangement of antibody gene segments of the mouse immune system through a repair process named V(D)J (for a detailed review see (Peters, 2021). V(D)J recombination is triggered by the programmed formation of DSBs by the RAG endonuclease, and results in repair between distant sequences arranged in tandem. Segments destined for rearrangement are interspersed by CTCF sites, which Hi-C data has revealed act as loop anchors and boundaries, limiting contacts and repair between more distant segments (Ba et al., 2020, Dai et al., 2021). Further supporting a functional role for loop extrusion, depletion of cohesin reduces long-range interactions and recombination between distal segments (Ba et al., 2020), whereas down regulation of WAPL, and thus increasing the size of cohesin-mediated loops, favours repair between more distant segments (Hill et al., 2020). Indeed, loop extrusion by cohesin appears to favour intra-chromosomal DNA repair between proximal sequences (Piazza et al., 2021; Dumont et al., 2023).

4F) Chromosome individualization

In addition, enhanced genome wide loading of cohesin could mediate the individualization of chromosomes, therefore disfavouring ectopic repair events (Piazza et al., 2021). Indeed, Hi-C experiments upon HO induced DSB in *S. cerevisiae* demonstrated that HR repair occurs in a chromatin context spatially shaped at the global level by cohesin (Piazza et al., 2021). Whether this relies on pre-existing or de novo loaded cohesin remains to be determined. Cohesin appears to mediate chromosome individualization, reducing overall inter-chromosomal interactions which may also restrain the homology search process and promote *cis* dsDNA sampling (Figure 15C; Piazza et al., 2021). Accordingly, cohesin depletion increases DSB contacts and favours recombination with the rest of the genome (Piazza et al., 2021). Importantly, biasing the homology search in *cis* may safeguard the genome against genome instability by preventing gross chromosomal rearrangements. However, this may also have the negative effect of biasing ectopic repair events such as SSA.

4G) Sister chromatid cohesion and repair

Cohesin enrichment is also enhanced genome-wide in response to DSB induction (Strom et al., 2007; Unal et al., 2007). In yeast, this enrichment at undamaged sites globally tightens

sister chromatid cohesion (Heidinger-Pauli et al., 2009; Unal et al., 2007). Like establishment of S phase cohesion, DSB induced global cohesin loading relies on Scc2/4, Eco1 mediated Smc3 acetylation and cohesin SUMOylation (McAleenan et al., 2012; Almedawar et al., 2012). Additionally, DSB induced phosphorylation of Scc1 by the Chk1 checkpoint kinase is required to allow subsequent Smc3 acetylation by Eco1 (Heidinger-Pauli et al., 2009; Heidinger-Pauli et al., 2008). DSB induced cohesin stabilisation may act redundantly with the Chk1 mediated phosphorylation and stabilization of Pds5, antagonizing the activity of the Esp1 Separase to delay the metaphase-anaphase transition. In line with this, cohesin accumulates on chromatin upon formation of DSBs (Arnould et al., 2021; Potts et al., 2006; Bekker-Jensen et al., 2006), and is involved in the DNA damage-induced intra-S and G2/M checkpoint activation in human cells (Watrin and Peters, 2009).

4H) Cohesin in meiosis

Cohesin is also required for another fundamental cellular process – meiosis (Borner et al., 2023). In this context a meiosis specific cohesin complex is formed, which replaces the kleisin Scc1 with Rec8 (Watanabe and Nurse, 1999). During meiosis, cohesin is essential for axial element formation (Klein et al., 1999). With cohesin enriched at meiosis specific loop boundaries (Schalbetter et al., 2019). This process is essential for proper meiotic recombination, in a process that involves controlled DSB formation and recombination (Borner et al., 2023). Importantly, cohesin promotes inter homolog recombination, as opposed to inter sister recombination, promoting crossing over between homolog pairs (Borner et al., 2023). In contrast, the Smc5/6 complex is important for resolving crossover products (Copsey et al., 2013; Lilienthal et al., 2013; Xaver et al., 2013).

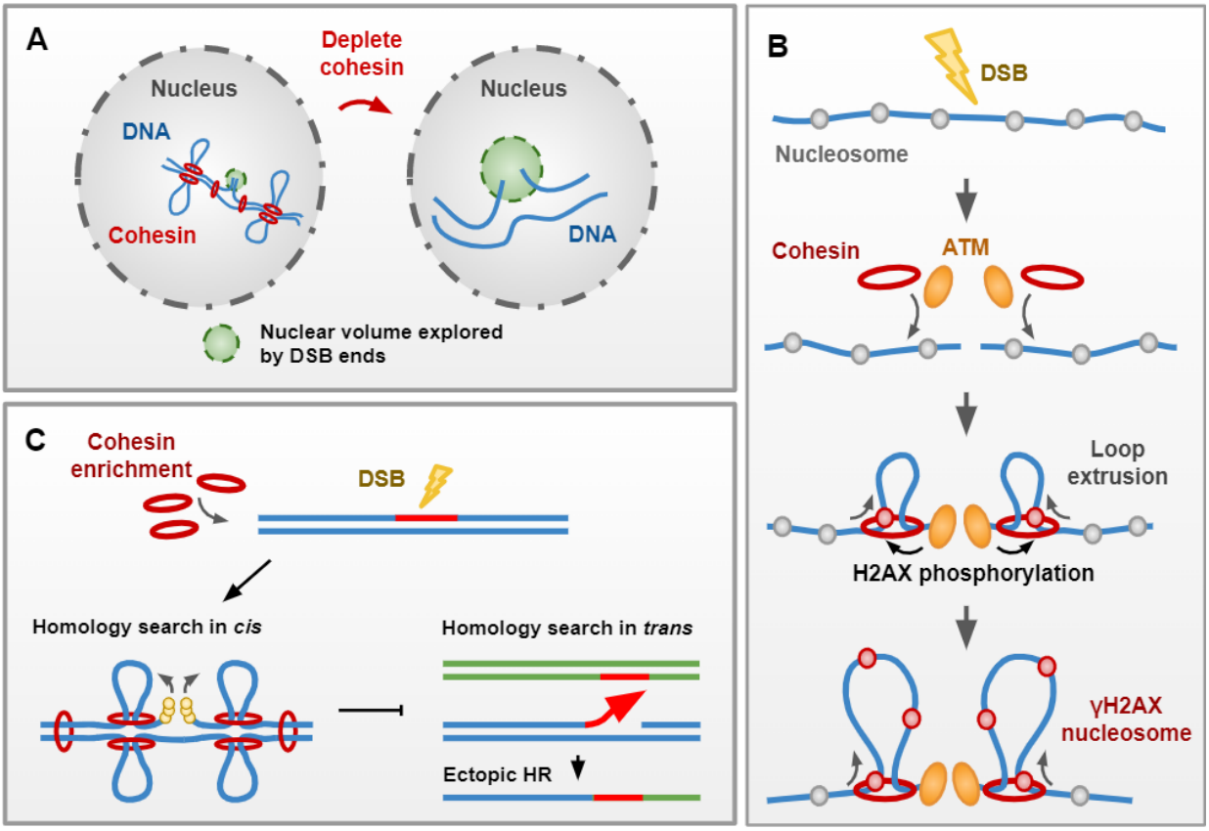

Figure 15. Cohesin contributes to DNA damage signaling and repair. (A) Cohesion of sister chromatids restricts chromatin mobility. Cohesin also restricts chromatin mobility in response to DNA damage, with the nuclear volume explored by DSB ends increasing upon cohesin disruption. (B) Cohesin dependent TADs are functional units of the DNA damage response, through γH2Ax spreading. Loop-extrusion activity away from a DSB site drives γH2Ax spreading by the PI3 kinase ATM, allowing the establishment of γH2Ax domains. (C) Genome-wide loading of cohesin upon DSB leads to the individualization of chromosomes. Loss of cohesin leads to an increase in interchromosomal interactions and decrease in *cis* dsDNA sampling. Individualization of chromosomes may disfavour ectopic repair events by restraining the homology search process. Preventing interchromosome recombination demonstrates a key role for cohesin in safeguarding the genome against genome instability. (Phipps and Dubrana, 2022).

4I) Cohesin in disease

Ultimately, the importance of cohesin in DNA damage repair can be seen in the human population through disease. Cohesin mutations present in individuals with Cornelia de Lange syndrome have been extensively characterized in human cell-lines and budding yeast. These demonstrated a sensitivity to irradiation, which correlates with errors in sister chromatid cohesion and loop extrusion (Vrouwe et al. 2007; Revenkova et al. 2009; Bauer et al., 2021; Kaur et al., 2023).

In most cases, cohesin mutations in cancer are progression rather than initiation events (Konink and Losada, 2016). Of those that occur, mutations in the kleisin STAG2 effect most of the cases (Konink and Losada, 2016). Often, these result in loss of STAG2 or presence of a non-functional protein. In this case, STAG1, which is normally developmentally specific, takes over (Adane et al., 2021). STAG2 KO cells present longer DNA loops, loss of E-P contacts, and gene expression misregulation (Adane et al., 2021; Tothova et al., 2021). Replication fork stalling was also observed, leading to increased R loops and persistence of gH2Ax (Tothova et al., 2021). Interestingly, changes in expression levels of DNA damage response genes was observed, and attributed to splicing defects (Wheeler et al., 2022). These DNA damage response genes were proposed to be particularly sensitive to increased splicing defects due to their longer than average length. This is interesting, as it demonstrates that cohesin mutations may also have indirect impacts on the ability of cells to repair DNA damage and cancer progression.

Chapter 2: Results

Results

The results from my doctoral work will be divided into two sections. The first contains my primary work, in which we identify cohesin as a key player in DNA double-strand break end-tethering. This finding is particularly important as we detect a mechanism for DSB end-tethering prior to HDR events that was previously missed. This is in the form of an article, which was recently published on BioRxiv and is currently out for review at Nature Cell Biology (https://doi.org/10.1101/2023.11.08.566226).

Some results that did not make it into the final article on cohesin's role in DSB end-tethering, but provide important insights into the DSB response in budding yeast, are included after the article.

Next is a project to which I contributed in collaboration with Stéphane Marcand's group, which describes how telomere protein arrays stall loop extrusion by the condensin complex. This is important due to condensin's canonical function in condensing mitotic chromosomes. The absence of a barrier to loop extrusion at telomeres could hinder condensation, with downstream consequences on chromosome segregation. This article is also published on BioRxiv, and is currently out for review at Cell (https://doi.org/10.1101/2023.10.29.564563). My contribution to this project included the construction of the base strain used for the microscopy experiments in Figure 4, establishment of the pipeline used for the analysis of these experiments, as well as undertaking and analysing microscopy experiments to finalise the figure. I also had the pleasure of sharing lab meetings with Stéphane's group, which led to many fruitful conversations on this topic and others, to which I am extremely grateful.

I also contributed to the planning of experiments and analysis of microscopy experiments in another article from Eric Coic's group, in collaboration with Laurent Maloisel, which were critical for the revision process. This article, published in PLOS Genetics (https://doi.org/10.1371/journal.pgen.1010639), describes the key roles of the Rad51 paralogs Rad55 and Rad57 in stabilising the Rad51 filament. Rad55 and Rad57 are thus important for counteracting error-prone translesion polymerase synthesis at ssDNA gaps and promoting repair by homologous recombination. This paper is included in the annex of this thesis.

Article 1 – Cohesin complex oligomerization maintains end-tethering at DNA double-strand breaks

PAPER

Title: Cohesin complex oligomerization maintains end-tethering at DNA double-strand breaks

Authors: Jamie Phipps[1,2], Mathias Toulouze[1,2], Cécile Ducrot[1,2], Rafaël Costa[1,2], Clémentine Brocas[1,2] and Karine Dubrana[1,2]*

Affiliations:

[1] Université Paris Cité, Inserm, CEA, Stabilité Génétique Cellules Souches et Radiations, F-92260 Fontenay-aux-Roses, France

[2] Université Paris-Saclay, Inserm, CEA, Stabilité Génétique Cellules Souches et Radiations, F-92260 Fontenay-aux-Roses, France

* Corresponding author. E-mail: karine.dubrana@cea.fr

Abstract: DNA double-strand breaks (DSB) must be repaired to ensure genome stability. Crucially, DSB ends must be kept together for timely repair. In *Saccharomyces cerevisiae*, two pathways mediate DSB end-tethering. One employs the Mre11-Rad50-Xrs2 (MRX) complex to physically bridge DSB ends. Another requires the conversion of DSB ends into single-strand DNA (ssDNA) by Exo1, but the bridging proteins are unknown. We uncover that cohesin, its loader and Smc5/6 act with Exo1 to tether DSB ends. Remarkably, cohesin specifically impaired in oligomerization fails to tether DSB ends, revealing a new function for cohesin oligomerization. In addition to the known importance of sister chromatid cohesion, microscopy-based microfluidic experiments unveil a new role for cohesin in repair by ensuring DSB end-tethering. Altogether, our findings demonstrate that oligomerization of cohesin prevents DSB end separation and promotes DSB repair, revealing a novel mode of action and role for cohesin in safeguarding genome integrity.

Main Text:

Introduction

DNA double strand breaks (DSBs) pose a significant threat to genome stability as they disrupt chromosome integrity. Repair mechanisms, such as NHEJ and homologous recombination are essential for restoring chromosome continuity by directly rejoining DSB ends or using a donor homologous template (*1*). However, before these repair processes can occur, it is imperative to bring DSB ends together, a task unlikely achieved through passive diffusion (*2*). Instead, active DSB end-tethering mechanisms have been identified, and represent a critical step in preventing joining or recombination events between unrelated chromosome loci, which could lead to harmful translocations.

The mechanisms that facilitate the tethering of DSB ends were initially characterized in the budding yeast *Saccharomyces cerevisiae* (*3*–*5*). The MRX^{MRN} complex (Mre11-Rad50-Xrs2^{NBS1}) is rapidly recruited to DSB ends and plays an early role in end-tethering (*3*, *5*, *6*). MRN has been proposed to serve a similar tethering function, thus preventing translocations in humans (*7*–*9*). In yeast, MRX nuclease activity is dispensable for DSB end-tethering. Instead, the ZN-hook domain and ATPase activity of Rad50 are essential, suggesting a physical bridging mechanism by MRX dimers (*3*). In contrast, during later stages of repair, DSB end-tethering requires Exo1 exonuclease activity to reveal single stranded DNA (ssDNA) (*4*). However, the proteins responsible for physical bridging of DSB ends during these late stages of repair remain unidentified.

Recent theoretical research has proposed a role for DNA loops in the tethering of DSB ends (*2*). Loop extrusion, a property associated with SMC family complexes, has emerged as a conserved mechanism for folding the genome (*10*). Among these SMC complexes, cohesin (comprising Smc1, Smc3, Mcd1^{Scc1} and Scc3$^{STAG1/2}$) and the Smc5/6 complex are recruited to DNA damage sites in both yeast and mammals (*11*–*14*). In yeast, the loading of cohesin to DSBs involves various factors, including the cohesin loader Scc2/Scc4, DNA damage factors like MRX, γH2A, Tel1^{ATM}, Mec1^{ATR}, and Smc5/6 (*13*–*17*). Cohesin is not only enriched at DSB sites, but also throughout the entire genome (*18*–*20*), contributing to tightening of sister chromatid cohesion (*18*, *19*, *21*–*23*), locally restricting homology search (*24*), and aiding in DNA damage checkpoint establishment (*20*).

Given the involvement of cohesin in DSB response (*25*), its demonstrated ability to bridge DNA molecules *in vitro* (*26*), and the observed gross chromosomal rearrangements and translocations in cohesin mutants (*27*), we hypothesized that cohesin and/or Smc5/6 play a critical role in DSB repair by maintaining proximity between DSB ends.

In this study, we combine genetic and live microscopy-based approaches to demonstrate a cohesin dependent DSB end-tethering mechanism, involving Exo1 and Smc5/6. Furthermore, we show that cohesin compacts DSB adjacent chromatin, beyond compaction observed in G2/M cells. We expose oligomerization as a key mechanism for both MRX- and cohesin-dependent tethering through both disruption of protein-protein interactions in response to hexanediol treatment, and genetic loss of function mutants. Specifically, disruption of cohesin oligomerization through mutation in the $Mcd1^{SCC1}$ subunit, maintains compaction at the vicinity of DSB, but prevents the ability to tether DSB ends. Disruption of oligomerization between Rad50 heads also leads to loss of MRX dependent DSB end-tethering. Finally, our real-time microfluidic assay demonstrates that cohesin is essential for efficient repair of DSBs, through its end-tethering capacity.

Results

Cohesin Tethers DSB ends

To assess the requirement of cohesin in tethering DSB ends, we developed a microscopy-based assay in which LacO and TetO repeats were positioned either side of the endogenous HO endonuclease cleavage site at the *MAT* locus of *Saccharomyces cerevisiae* (Fig. 1A; (*28*)). Targeted by LacI-mCherry and TetR-GFP fusion proteins, these arrays allow for visualization of the regions flanking the DSB site as red and green spots. DSBs were induced by galactose treatment, which triggers the Gal promoter-controlled expression of the HO endonuclease (fig. S1A). In individual cells, we distinguished tethering or separation of DSB ends based on the distance between the spot centers being less than or greater than 400 nm (Fig. 1B). This threshold was established by quantifying spot separation in the absence of DNA DSB, where less than 5% of WT cells exhibited spots exceeding 400nm separation (fig. S1B). We confirmed the assay's sensitivity to detect the previously described, early MRX-, and late Exo1-dependent end-tethering pathways by imaging at 2 hours and 4 hours post-DSB induction. At 2 hours post-DSB, WT and *exo1Δ* cells showed less than 10% untethering, while cells lacking Mre11 displayed 31% separation (Fig. 1C). At 4 hours post-DSB, separation remained unchanged in WT cells but increased to 23% in *exo1Δ* cells. Importantly, double deletion of *EXO1* and *MRE11* led to a significant increase in end separation compared to either single mutation, highlighting the presence of two pathways of DSB end-tethering (Fig. 1D).

To investigate the role of cohesin in DSB end-tethering, we employed the auxin-induced degron (AID) system to deplete the cohesin subunit Smc1 (*29*). Following a 1-hour auxin incubation, Smc1 protein levels were substantially reduced and maintained at near undetectable levels for over 4 hours (fig. S2A). Depletion of Smc1 resulted in the appearance of cells with separated sister chromatids (Fig. 1E) and impaired cell growth (fig. S2E), consistent with the essential role of the cohesin complex in sister chromatid cohesion. At 2 hours post-DSB, a non-significant increase in end separation was observed upon cohesin depletion (Fig. 1E). However, at 4 hours post-DSB, approximately 30% of DSB ends were untethered (Fig. 1F). To ensure that the increase in spot separation above 400 nm was due to the lack of DSB end-tethering and not due to the loss of cohesin-mediated chromatin folding, we quantified the percentage of cells with spots exceeding 400 nm upon Smc1 depletion in the absence of DSB. No significant increase in spot separation was observed when Smc1 was

depleted in absence of DSB (Fig. 1F), excluding an involvement of cohesin-mediated chromatin folding. Overall, these results reveal the requirement of cohesin for DSB end-tethering.

Cohesin tethers DSB ends in the Exo1 pathway

To determine the specific pathway in which cohesin tethers DSB ends, we quantified the extent of DSB end separation upon depletion of cohesin in cells lacking Mre11 and Exo1. In contrast to depletion of Smc1 alone, loss of Smc1 in *mre11Δ* cells significantly increased end separation at 2 hours post-DSB (fig. S1C). This early Smc1-dependent end-tethering separation is not seen in *mre11Δ exo1Δ* double mutants, or *exo1Δ* cells depleted for Smc1 (fig. S1D), suggesting that, at 2 hours, cohesin acts in parallel to MRX, independently of Exo1, to maintain end-tethering. Strikingly, at 4 hours post-DSB, depleting cohesin in *mre11Δ* cells significantly increased end separation (Fig. 1G), recapitulating the separation observed in *mre11Δ exo1Δ* cells (Fig. 1D). In contrast, depletion of Smc1 in *exo1Δ* cells did not further increase end separation compared to *exo1Δ* cells (Fig. 1H). These findings suggest that cohesin functions with Exo1 to tether DSB ends at 4 hours post-DSB.

Cohesin DSB end-tethering requires *de novo* cohesin loading

Next, we wondered if the presence of cohesin on chromosomes prior to DSB induction is sufficient for maintaining DSB end-tethering, or if the DSB-induced *de novo* loaded population of cohesin is required for this function. To address this, we arrested cells in G2/M phase using nocodazole, depleted Scc2 for 1 hour to prevent *de novo* cohesin loading while maintaining pre-existing loops (*30*) and induced DSB (Fig. 2A, and fig. S2B). We observed an increase in separated ends after 4 hours DSB induction upon Scc2 depletion (Fig. 2B), reaching a similar level as that observed in Smc1-depleted and *exo1Δ* cells under the same experimental settings. These results indicate that preformed cohesin loops are not sufficient and that *de novo* loading of cohesin is necessary for DSB end-tethering.

Previous studies have shown the importance of Smc5/6 in enriching cohesin at DSBs (*14*). To further explore this, we depleted Smc5 in our DSB end-tethering assay (fig. S2C). At 4 hours post-DSB induction, Smc5 depletion resulted in a significant increase in DSB end separation (Fig. 2C). Simultaneous depletion of Smc5 and Smc1 did not increase end separation beyond that observed upon Smc1 depletion alone (Fig. 2C), indicating that cohesin and Smc5/6 function in the same DSB end-tethering pathway. In conclusion, at 4 hours post-DSB, *de novo*

cohesin loading at DNA DSB sites, mediated by Scc2/4 and Smc5/6, is necessary for DSB end-tethering.

Cohesin DSB end-tethering does not require sister chromatid cohesion

Despite efficient cleavage of both sister chromatids in our assay (fig. S1A), which makes tethering of a cleaved chromatid by its sister unlikely, we aimed to confirm that DSB end-tethering was independent of sister chromatid cohesion. In absence of Cdc45, G1 cells progress to G2/M phase and load cohesin on chromosomes without firing replication origins and synthesizing sister chromatids (*31*), enabling us to assess the role of cohesin in DSB end-tethering in the absence of sister chromatid cohesion (Fig. 2D, and fig. S2D and S3A). Depletion of Cdc45 did not disrupt DSB end-tethering at 4 hours post-DSB induction (Fig. 2E), indicating that the presence of a sister chromatid is not essential for DSB end-tethering. Additional depletion of Smc1 resulted in increased DSB end separation, reaching levels similar to those observed in cells depleted of Smc1 alone. This indicates that cohesin can tether DSB ends even in the absence of DNA replication and a sister chromatid.

Together, these findings unveil a series of events that ultimately result in cohesin-dependent DSB end-tethering (Fig. 2F). Initially, the MRX complex binds and tethers DSB ends. Later, an Exo1-dependent pathway comes into play with the recruitment and *de novo* loading of cohesin at DSBs, facilitated by Scc2/4 and Smc5/6, actively participating in the tethering of DSB ends within individual chromatids.

Cohesin orchestrates compaction of DSB flanking chromatin

Cohesin has been shown to form DNA loops and we hypothesized this activity could contribute to DSB end-tethering. To gain insights into the behavior of cohesin in the chromatin surrounding DSB, we modified our DSB end-tethering system to investigate chromatin compaction in a 48 kb region flanked by LacO-LacI-mCherry and TetO-TetR-GFP arrays, located 7 kb upstream of the DSB site (Fig. 3A). We measured the distance between these two signals in the presence or absence of DSB, to evaluate DSB-induced chromatin compaction (Fig. 3B). As the occurrence of a DSB triggers the DNA damage checkpoint and a G2/M cell cycle arrest, we treated all cells with nocodazole to ensure a fair comparison between DSB and no-DSB conditions.

We first examined the impact of cohesin on chromatin folding in G2/M-arrested cells with no DSB. We observed a significant increase in the distribution of the distances upon cohesin depletion (fig. S4, A and B), showing that our assay enables detection of the previously reported cohesin-dependent compaction of chromatin (*32*, *33*). Following 4 hours of DSB induction, we detected a significant reduction in distances between the two signals compared to the no-DSB condition, indicative of a compaction of the DSB-flanking chromatin (Fig. 3C; black versus red). This DSB-induced compaction was abolished upon depletion of Smc1, demonstrating that cohesin is responsible for the compaction of DSB flanking sequences (Fig. 3C; orange, and fig. S4C).

Pds5 is required for DSB end-tethering but not DSB-induced genome compaction

If loop formation were at the basis of DSB end-tethering, the latter should be challenged by modulating loop expansion and turn over. To explore this, we tested the role of Pds5, a key factor responsible for cohesin loop regulation. Pds5 depletion weakens loop boundaries, reduces defined chromosome contacts/loops, and generate much longer loops in regions such as those near centromeres (*34*, *35*). We found that DSB induced chromatin compaction still occurs in absence of Pds5 (Fig. 3D, and fig. S4, D-F). In contrast, Pds5 depletion increased end separation at 4 hours post-DSB, mimicking the effects of cohesin depletion (Fig. 3E). These results imply that either the loops formed in absence of Pds5 were not sufficient to support the function of cohesin in DSB end-tethering, or that cohesin tethers DSB ends independently of loop formation, through another mechanism requiring Pds5. A recent study has revealed an essential role of Pds5 in the oligomerization of multiple cohesin complexes (*36*), opening the door for a role of Pds5-dependent cohesin oligomerization in DSB end-tethering.

Cohesin and MRX tethering rely on weak hydrophobic interactions

To investigate if protein-protein interactions and the oligomerization of cohesin complexes participates in DSB end-tethering, we used the aliphatic alcohol 1,6-hexanediol. Hexanediol has been instrumental in studying the liquid phase separation and oligomerization properties of various proteins, including cohesin and proteins involved in the DNA damage response (such as Rad52 and RPA; fig. S5, A and D-E; (*37*, *38*)).

The treatment of cells with hexanediol 10 minutes prior to imaging at 2 hours post-DSB, when tethering mostly relies on MRX, increased end separation independently of Smc1 presence

(Fig. 3F). Moreover, end separation was not increased by hexanediol in the absence of Mre11 alone. These results suggest a role for weak hydrophobic interactions in MRX-dependent tethering. In addition, hexanediol had no effect in cells depleted for both Mre11 and Smc1, suggesting that no other weak hydrophobic interactions intervene in DSB end-tethering at this early stage. Strikingly, hexanediol-treated *mre11Δ* cells do not exhibit the separation levels observed in Smc1 depleted *mre11Δ* cells (Fig. 3F, and fig. S1C), with or without hexanediol treatment (Fig. 3F). This finding aligns with a recent *in vivo* study in *S. cerevisiae* that demonstrated the resistance of a subset of topologically important cohesins to hexanediol treatment (*37*). As hexanediol is known to disrupt protein-protein interactions, this further supports our early finding that an Exo1-independent population of cohesin can tether DSB ends that are formed within a cohesin loop (fig. S1, C and D, and fig. S5F).

At 4 hours post-DSB, hexanediol-treated control cells also exhibited untethering (Figure 3G). In line with our observation at 2 hours that hexanediol disrupts MRX-dependent tethering, hexanediol and Smc1-depletion have additive effects at 4 hours. Hexanediol also increases end separation in absence of Mre11 suggesting that it also disrupts cohesin-dependent DSB end-tethering. Strikingly, in contrast to the 2-hour time point, hexanediol increased end separation in *mre11Δ* cells to levels comparable to cells depleted for both Smc1 and Mre11 (Fig. 3G). These results indicate that protein-protein interactions play a key role in DSB end-tethering by both MRX and cohesin (Fig. 3J).

MRX has been shown to form oligomers *in vitro* and disruption of these oligomers by a mutation of the hydrophobic interaction patch within the Rad50 head domain (*rad50lo* mutant, (*39*)) led to the disappearance of DSB-dependent Mre11 foci *in vivo*. Since hexanediol also disrupts Mre11-GFP foci formation in our strain background (fig. S5, B and C), we introduced this mutation in our tethering system. Strikingly, complementation of *rad50Δ* cells with *rad50lo*, was unable to restore end-separation to WT levels at 2 hours post-DSB, unlike wild-type *RAD50* (Fig. 3H). Therefore, disrupting Rad50 head oligomerization impairs DSB end-tethering.

The cohesin subunit Mcd1 has been identified as a mediator of cohesin oligomerization, and a 5 amino-acid insertion at Q266 in its regulation of cohesion and condensation (ROCC) domain has been shown to abolish cohesin oligomerization potential *in vivo* (*36*, *40*). To test the role of cohesin oligomerization in DSB end-tethering, we complemented *MCD1-AID* cells

with the *mcd1-Q266* mutant in both our compaction and end-tethering strains (fig. S6, A and B). Critically, *mcd1Q266* mutants exhibited strong DSB-dependent genome compaction (fig. S6, C-H), indicating cohesin is recruited to DSB sites and able to form chromatin loops. However, unlike complementation with *MCD1*, *mcd1Q266* failed to restore DSB end-tethering to WT-like levels (Fig. 3I), further strengthening our hypothesis that cohesin oligomerization tethers DSB ends. Taken together, these results indicate that both MRX and cohesin employ an oligomerization-dependent mechanism to tether DSB ends (Fig. 3J).

Cohesin is required for efficient DNA DSB repair by homology directed mechanisms

Having identified a role for cohesin in tethering DSB ends, we questioned its significance for repair. We took advantage of our tethering system, which contains direct homologous repeats flanking the inserted LacO and TetO arrays (Fig. 4A). Following DSB induction and resection initiation, progressive formation of ssDNA away from the DSB causes loss of the dsDNA substrate which is necessary for the binding of the LacI-mCherry and TetR-GFP fusion proteins, and gradually leads to the disappearance of the fluorescent signals. Resection also unmasks the direct homologous repeats, which can anneal and be used to resynthesize the broken DNA strand. This restores chromosome continuity but results in loss of the genetic material that previously separated the homologous repeats used for repair. Following resynthesis, either the red or the green signal reappears, depending on the repeats used for repair (Fig. 4, A and B). After completion of the repair process, cells are released from the DNA damage checkpoint and proceed through cell division (Fig. 4B).

To assess repair events, we employed a microfluidics system to follow individual cells and image each fluorescent signal over a 12-hour period after DSB induction. To validate our assay, we imaged cells lacking *RAD52*, which is essential for all homology directed repair (HDR) events. In the absence of Rad52, no instances of spot reappearance were observed (Fig. 4C, and fig. S7A). Conversely, the loss of Rad51, which impedes gene conversion and promotes single-strand annealing (SSA), led to an increase in repair events compared to WT-like condition (SMC1-AID without auxin, Fig. 4, C and E, and fig. S7B), as previously reported (*41*, *42*). This result suggests that inhibiting gene conversion, and favouring repair by SSA, leads to more detectable repair events in this assay, with unaltered repair kinetics compared to the WT-like condition (Fig. 4D). In contrast, upon Smc1 depletion, we observed a significant reduction in the frequency of repair events associated with a noticeable delay in repair kinetics

(Fig. 4, C, D, E and F). This decrease in repair frequency was not caused by a resection defect (fig. S7C). To separate the dependence of repair events on sister chromatid cohesion from DSB end-tethering, we employed Cdc45 depletion. Strikingly, despite repair events still taking place upon Cdc45 depletion, simultaneous depletion with Smc1 resulted in a severe decrease in both the frequency of repair events and their kinetics compared to cells depleted of Cdc45 alone (Fig. 4, G, H and fig. S7, D-F). This indicates that the specific function of cohesin in DSB end-tethering is essential for efficient repair between DSB ends.

Discussion

Cohesin enrichment at DSBs has long been known (*11*–*13*) with early studies also highlighting the importance of cohesin for survival after DNA damage inducing radiation (*11*, *13*, *43*). Recent observations have suggested that loop extrusion at DNA DSBs helps establish DNA damage response related chromatin modifications (*20*), which ultimately organize DSBs into microdomains (*44*). Moreover, sister chromatid cohesion, which is increased in response to DSB (*18*, *19*, *21*–*23*), prevents promiscuous repair events with far loci (*24*, *27*).

In addition to these functions, we reveal a new cohesin role in tethering DSB ends. Cohesin's first contribution, early after DSB formation is independent of MRX and Exo1 and likely relies on cohesin-dependent genome looping, as predicted by recent theoretical work (*2*). Later, cohesin-dependent DSB end-tethering requires *de novo* cohesin loading, acts in cooperation with Exo1 and Smc5/6, is independent of sister chromatid cohesion and loop formation, and relies on cohesin oligomerization. Importantly, our data provide a biological function to the recently described cohesin oligomerization mechanism (*36*, *37*) that is independent of cohesin's canonical roles in sister chromatid cohesion and loop extrusion.

Strikingly, our results support the existence of two populations of DSB-bound cohesin with separable functions, namely chromatin compaction and DSB end-tethering, and different modes of action, namely loop formation and oligomerization. One population of cohesin acts in a Pds5- and oligomerization-independent manner and compacts DSB adjacent chromatin. This cohesin-dependent compaction may participate in DSB signaling though a loop extrusion-mediated spreading of histone H2AX phosphorylation, as previously suggested (*20*). A second population requires Pds5 and cohesin oligomerization, and tethers DSB ends. What distinguishes loop-forming cohesin from DSB end-tethering cohesin, beyond the capacity to

form oligomers, is unknown. However the fact that the DSB end-tethering cohesin population acts independently of MRX, which has been implicated in cohesin enrichment at DSBs (*12*, *15*), suggests a new mode of recruitment of these cohesin to DSB ends.

Our data supports a role for Scc2, Smc5/6 and Exo1 mediated ssDNA formation in recruiting or stabilizing DSB end-tethering cohesin. Whereas Scc2 and Smc5/6 were previously implicated in the recruitment of cohesin to DSB, the formation of ssDNA by Exo1 is specifically required for cohesin-dependent DSB end-tethering. Since dsDNA bound cohesin can capture ssDNA (*45*), formation of ss-DNA may directly intervene in cohesin recruitment. Bridging dsDNA with ssDNA could also be sufficient to account for DSB end tethering. Otherwise, cohesin recruitment could be mediated by Smc5/6, which interacts with ssDNA through its hinge domain (*46*, *47*), and stably associates with ss-dsDNA junctions (*47*, *48*). Smc5/6, that bears both ubiquitin and SUMO ligase activity, could then locally modify a pool of cohesin, promoting cohesin oligomerization and DSB end-tethering.

Our results, which reveal cohesin's role in DSB end-tethering, contrast with a previous report suggesting that cohesin is dispensable for contacts between both sides of a DSB as captured by a Hi-C approach (*24*). One plausible explanation for this discrepancy is rooted in the technologies used to make such observations. Single-cell live-microscopy is more sensitive at this scale considering we detect DSB-induced compaction beyond G2/M and cohesin-dependent loss of end tethering, both appearing below the detection threshold of the population-wide Hi-C approach (*24*).

We also show that Rad50 (MRX^{MRN}) head oligomerization is required for MRX dependent DSB end-tethering. MRX oligomerization via both the Rad50 heads and coiled coils has been described in both yeast and humans (*39*, *49*). Our data demonstrates that Rad50 head oligomerization observed *in vitro*, is significant for MRX end-tethering *in vivo*. Alongside the necessity of the Rad50 Zn-hook for DSB end-tethering demonstrated *in vivo* (*3*), our data supports the Velcro model recently proposed based on structures frequently observed by electron microscopy for MRX-driven DSB end-tethering (*49*).

Together, our results suggest that oligomerization of SMC complexes is a conserved and functionally relevant mechanism for maintaining genome integrity in response to DNA damage. Interestingly, hexanediol treatment disrupted MRX foci in response to DSB,

suggesting MRX at DSBs may form condensates. Although, cohesin does not form detectable foci in response to DSB in yeast, it has been shown to form phase separation condensates *in vitro* (*37*). These observations question the relevance of phase separation in DSB end-tethering, which should be investigated using single molecule microscopy in the future.

Given the prevalence of chromosome translocations in cancer, and the role of DSB induction in cohesin sensitive developmental processes such as V(D)J recombination (*50*) our study gives further insights into how SMC complex dysregulation may lead to disease in the human population.

References and Notes

1. H. Bordelet, K. Dubrana, Keep moving and stay in a good shape to find your homologous recombination partner. *Curr. Genet.* **65**, 29–39 (2019).
2. J. H. Yang, H. B. Brandão, A. S. Hansen, DNA double-strand break end synapsis by DNA loop extrusion. *Nat. Commun.* **14**, 1913 (2023).
3. K. Lobachev, E. Vitriol, J. Stemple, M. A. Resnick, K. Bloom, Chromosome Fragmentation after Induction of a Double-Strand Break Is an Active Process Prevented by the RMX Repair Complex. *Curr. Biol.* **14**, 2107–2112 (2004).
4. W. Nakai, J. Westmoreland, E. Yeh, K. Bloom, M. A. Resnick, Chromosome integrity at a double-strand break requires exonuclease 1 and MRX. *DNA Repair* **10**, 102–110 (2011).
5. K. Lee, Y. Zhang, S. E. Lee, Saccharomyces cerevisiae ATM orthologue suppresses break-induced chromosome translocations. *Nature* **454**, 543–546 (2008).
6. J. Oh, S. J. Lee, R. Rothstein, L. S. Symington, Xrs2 and Tel1 Independently Contribute to MR-Mediated DNA Tethering and Replisome Stability. *Cell Rep.* **25**, 1681-1692.e4 (2018).
7. M. De Jager, J. Van Noort, D. C. Van Gent, C. Dekker, R. Kanaar, C. Wyman, Human Rad50/Mre11 Is a Flexible Complex that Can Tether DNA Ends. *Mol. Cell* **8**, 1129–1135 (2001).
8. E. van der Linden, H. Sanchez, E. Kinoshita, R. Kanaar, C. Wyman, RAD50 and NBS1 form a stable complex functional in DNA binding and tethering. *Nucleic Acids Res.* **37**, 1580–1588 (2009).

9. V. Roukos, T. C. Voss, C. K. Schmidt, S. Lee, D. Wangsa, T. Misteli, Spatial Dynamics of Chromosome Translocations in Living Cells. *Science* **341**, 660–664 (2013).

10. I. F. Davidson, J.-M. Peters, Genome folding through loop extrusion by SMC complexes. *Nat. Rev. Mol. Cell Biol.* **22**, 445–464 (2021).

11. C. Sjögren, K. Nasmyth, Sister chromatid cohesion is required for postreplicative double-strand break repair in Saccharomyces cerevisiae. *Curr. Biol.* **11**, 991–995 (2001).

12. J.-S. Kim, T. B. Krasieva, V. LaMorte, A. M. R. Taylor, K. Yokomori, Specific recruitment of human cohesin to laser-induced DNA damage. *J. Biol. Chem.* **277**, 45149–45153 (2002).

13. L. Ström, H. B. Lindroos, K. Shirahige, C. Sjögren, Postreplicative Recruitment of Cohesin to Double-Strand Breaks Is Required for DNA Repair. *Mol. Cell* **16**, 1003–1015 (2004).

14. G. De Piccoli, F. Cortes-Ledesma, G. Ira, J. Torres-Rosell, S. Uhle, S. Farmer, J.-Y. Hwang, F. Machin, A. Ceschia, A. McAleenan, V. Cordon-Preciado, A. Clemente-Blanco, F. Vilella-Mitjana, P. Ullal, A. Jarmuz, B. Leitao, D. Bressan, F. Dotiwala, A. Papusha, X. Zhao, K. Myung, J. E. Haber, A. Aguilera, L. Aragón, Smc5–Smc6 mediate DNA double-strand-break repair by promoting sister-chromatid recombination. *Nat. Cell Biol.* **8**, 1032–1034 (2006).

15. E. Ünal, A. Arbel-Eden, U. Sattler, R. Shroff, M. Lichten, J. E. Haber, D. Koshland, DNA Damage Response Pathway Uses Histone Modification to Assemble a Double-Strand Break-Specific Cohesin Domain. *Mol. Cell* **16**, 991–1002 (2004).

16. B. H. Lindroos, L. Ström, T. Itoh, Y. Katou, K. Shirahige, C. Sjögren, Chromosomal Association of the Smc5/6 Complex Reveals that It Functions in Differently Regulated Pathways. *Mol. Cell* **22**, 755–767 (2006).

17. A. McAleenan, V. Cordon-Preciado, A. Clemente-Blanco, I.-C. Liu, N. Sen, J. Leonard, A. Jarmuz, L. Aragón, SUMOylation of the α-Kleisin Subunit of Cohesin Is Required for DNA Damage-Induced Cohesion. *Curr. Biol.* **22**, 1564–1575 (2012).

18. L. Ström, C. Karlsson, H. B. Lindroos, S. Wedahl, Y. Katou, K. Shirahige, C. Sjögren, Postreplicative Formation of Cohesion Is Required for Repair and Induced by a Single DNA Break. *Science* **317**, 242–245 (2007).

19. E. Ünal, J. M. Heidinger-Pauli, D. Koshland, DNA Double-Strand Breaks Trigger Genome-Wide Sister-Chromatid Cohesion Through Eco1 (Ctf7). *Science* **317**, 245–248 (2007).

20. C. Arnould, V. Rocher, A.-L. Finoux, T. Clouaire, K. Li, F. Zhou, P. Caron, P. E. Mangeot, E. P. Ricci, R. Mourad, J. E. Haber, D. Noordermeer, G. Legube, Loop extrusion as a mechanism for formation of DNA damage repair foci. *Nature* **590**, 660–665 (2021).

21. J. M. Heidinger-Pauli, E. Ünal, D. Koshland, Distinct Targets of the Eco1 Acetyltransferase Modulate Cohesion in S Phase and in Response to DNA Damage. *Mol. Cell* **34**, 311–321 (2009).

22. H. Dodson, C. G. Morrison, Increased sister chromatid cohesion and DNA damage response factor localization at an enzyme-induced DNA double-strand break in vertebrate cells. *Nucleic Acids Res.* **37**, 6054–6063 (2009).

23. B.-J. Kim, Y. Li, J. Zhang, Y. Xi, Y. Li, T. Yang, S. Y. Jung, X. Pan, R. Chen, W. Li, Y. Wang, J. Qin, Genome-wide Reinforcement of Cohesin Binding at Pre-existing Cohesin Sites in Response to Ionizing Radiation in Human Cells*. *J. Biol. Chem.* **285**, 22784–22792 (2010).

24. A. Piazza, H. Bordelet, A. Dumont, A. Thierry, J. Savocco, F. Girard, R. Koszul, Cohesin regulates homology search during recombinational DNA repair. *Nat. Cell Biol.* **23**, 1176–1186 (2021).

25. J. Phipps, K. Dubrana, DNA Repair in Space and Time: Safeguarding the Genome with the Cohesin Complex. *Genes* **13**, 198 (2022).

26. P. Gutierrez-Escribano, M. D. Newton, A. Llauró, J. Huber, L. Tanasie, J. Davy, I. Aly, R. Aramayo, A. Montoya, H. Kramer, J. Stigler, D. S. Rueda, L. Aragon, A conserved ATP- and Scc2/4-dependent activity for cohesin in tethering DNA molecules. *Sci. Adv.* **5**, eaay6804 (2019).

27. C. Gelot, J. Guirouilh-Barbat, T. Le Guen, E. Dardillac, C. Chailleux, Y. Canitrot, B. S. Lopez, The Cohesin Complex Prevents the End Joining of Distant DNA Double-Strand Ends. *Mol. Cell* **61**, 15–26 (2016).

28. A. Mojumdar, K. Sorenson, M. Hohl, M. Toulouze, S. P. Lees-Miller, K. Dubrana, J. H. J. Petrini, J. A. Cobb, Nej1 Interacts with Mre11 to Regulate Tethering and Dna2 Binding at DNA Double-Strand Breaks. *Cell Rep.* **28**, 1564-1573.e3 (2019).

29. C. Brocas, C. Ducrot, K. Dubrana, Degradation of S. cerevisiae Cohesin with the Auxin-Inducible Degron System. *Methods Mol. Biol. Clifton NJ* **2004**, 17–24 (2019).

30. N. Bastié, C. Chapard, L. Dauban, O. Gadal, F. Beckouët, R. Koszul, Smc3 acetylation, Pds5 and Scc2 control the translocase activity that establishes cohesin-dependent chromatin loops. *Nat. Struct. Mol. Biol.* **29**, 575–585 (2022).

31. J. A. Tercero, K. Labib, J. F. Diffley, DNA synthesis at individual replication forks requires the essential initiation factor Cdc45p. *EMBO J.* **19**, 2082–2093 (2000).

32. S. A. Schalbetter, A. Goloborodko, G. Fudenberg, J.-M. Belton, C. Miles, M. Yu, J. Dekker, L. Mirny, J. Baxter, SMC complexes differentially compact mitotic chromosomes according to genomic context. *Nat. Cell Biol.* **19**, 1071–1080 (2017).

33. L. Lazar-Stefanita, V. F. Scolari, G. Mercy, H. Muller, T. M. Guérin, A. Thierry, J. Mozziconacci, R. Koszul, Cohesins and condensins orchestrate the 4D dynamics of yeast chromosomes during the cell cycle. *EMBO J.* **36**, 2684–2697 (2017).

34. L. Costantino, T.-H. S. Hsieh, R. Lamothe, X. Darzacq, D. Koshland, Cohesin residency determines chromatin loop patterns. *eLife* **9**, e59889 (2020).

35. L. Dauban, R. Montagne, A. Thierry, L. Lazar-Stefanita, N. Bastié, O. Gadal, A. Cournac, R. Koszul, F. Beckouët, Regulation of Cohesin-Mediated Chromosome Folding by Eco1 and Other Partners. *Mol. Cell* **77**, 1279-1293.e4 (2020).

36. S. Xiang, D. Koshland, Cohesin architecture and clustering in vivo. *eLife* **10**, e62243 (2021).

37. J.-K. Ryu, C. Bouchoux, H. W. Liu, E. Kim, M. Minamino, R. De Groot, A. J. Katan, A. Bonato, D. Marenduzzo, D. Michieletto, F. Uhlmann, C. Dekker, Bridging-induced phase separation induced by cohesin SMC protein complexes. *Sci. Adv.* **7**, eabe5905 (2021).

38. J. Miné-Hattab, M. Heltberg, M. Villemeur, C. Guedj, T. Mora, A. M. Walczak, M. Dahan, A. Taddei, Single molecule microscopy reveals key physical features of repair foci in living cells. *eLife* **10**, e60577 (2021).

39. V. M. Kissling, G. Reginato, E. Bianco, K. Kasaciunaite, J. Tilma, G. Cereghetti, N. Schindler, S. S. Lee, R. Guérois, B. Luke, R. Seidel, P. Cejka, M. Peter, Mre11-Rad50 oligomerization promotes DNA double-strand break repair. *Nat. Commun.* **13**, 2374 (2022).

40. T. Eng, V. Guacci, D. Koshland, ROCC, a conserved region in cohesin's Mcd1 subunit, is essential for the proper regulation of the maintenance of cohesion and establishment of condensation. *Mol. Biol. Cell* **25**, 2351–2364 (2014).

41. P. G. Cerqueira, D. Meyer, L. Zhang, B. Mallory, J. Liu, B. X. Hua Fu, X. Zhang, W.-D. Heyer, Saccharomyces cerevisiae DNA polymerase IV overcomes Rad51 inhibition of DNA polymerase δ in Rad52-mediated direct-repeat recombination. *Nucleic Acids Res.*, gkad281 (2023).

42. G. M. Manthey, A. M. Bailis, Rad51 inhibits translocation formation by non-conservative homologous recombination in Saccharomyces cerevisiae. *PloS One* **5**, e11889 (2010).

43. X. Kong, A. R. Ball, H. X. Pham, W. Zeng, H.-Y. Chen, J. A. Schmiesing, J.-S. Kim, M. Berns, K. Yokomori, Distinct Functions of Human Cohesin-SA1 and Cohesin-SA2 in Double-Strand Break Repair. *Mol. Cell. Biol.* **34**, 685–698 (2014).

44. J. Fu, S. Zhou, H. Xu, L. Liao, H. Shen, P. Du, X. Zheng, ATM–ESCO2–SMC3 axis promotes 53BP1 recruitment in response to DNA damage and safeguards genome integrity by stabilizing cohesin complex. *Nucleic Acids Res.*, gkad533 (2023).

45. Y. Murayama, C. P. Samora, Y. Kurokawa, H. Iwasaki, F. Uhlmann, Establishment of DNA-DNA Interactions by the Cohesin Ring. *Cell* **172**, 465-477.e15 (2018).

46. M.-A. Roy, D. D'Amours, DNA-binding properties of Smc6, a core component of the Smc5–6 DNA repair complex. *Biochem. Biophys. Res. Commun.* **416**, 80–85 (2011).

47. N.-L. Tanasie, P. Gutiérrez-Escribano, S. Jaklin, L. Aragon, J. Stigler, Stabilization of DNA fork junctions by Smc5/6 complexes revealed by single-molecule imaging. *Cell Rep.* **41**, 111778 (2022).

48. J. T.-H. Chang, S. Li, E. C. Beckwitt, T. Than, C. Haluska, J. Chandanani, M. E. O'Donnell, X. Zhao, S. Liu, Smc5/6's multifaceted DNA binding capacities stabilize branched DNA structures. *Nat. Commun.* **13**, 1–11 (2022).

49. M. Rotheneder, K. Stakyte, E. van de Logt, J. D. Bartho, K. Lammens, Y. Fan, A. Alt, B. Kessler, C. Jung, W. P. Roos, B. Steigenberger, K.-P. Hopfner, Cryo-EM structure of the

Mre11-Rad50-Nbs1 complex reveals the molecular mechanism of scaffolding functions. *Mol. Cell* **83**, 167-185.e9 (2023).

50. J.-M. Peters, How DNA loop extrusion mediated by cohesin enables V(D)J recombination. *Curr. Opin. Cell Biol.* **70**, 75–83 (2021).

51. S. E. Lee, J. K. Moore, A. Holmes, K. Umezu, R. D. Kolodner, J. E. Haber, Saccharomyces Ku70, mre11/rad50 and RPA proteins regulate adaptation to G2/M arrest after DNA damage. *Cell* **94**, 399–409 (1998).

52. H. Bordelet, R. Costa, C. Brocas, J. Dépagne, X. Veaute, D. Busso, A. Batté, R. Guérois, S. Marcand, K. Dubrana, Sir3 heterochromatin protein promotes non-homologous end joining by direct inhibition of Sae2. *EMBO J.* **41** (2022).

53. A. Batté, C. Brocas, H. Bordelet, A. Hocher, M. Ruault, A. Adjiri, A. Taddei, K. Dubrana, Recombination at subtelomeres is regulated by physical distance, double-strand break resection and chromatin status. *EMBO J.* **36**, 2609–2625 (2017).

54. K. J. Livak, T. D. Schmittgen, Analysis of relative gene expression data using real-time quantitative PCR and the 2(-Delta Delta C(T)) Method. *Methods San Diego Calif* **25**, 402–408 (2001).

Acknowledgments: We thank F. Ulhman, S. Marcand, A. Quinet, A. Campalans, P. Radicella and P. Bertrand for critical reading of this manuscript and members of the Dubrana and Marcand laboratories for stimulating discussions. We thank Douglas Koshland and Matthias Peter for sharing plasmids and strains.

Funding: This research was supported by the European Research Council under the European Community's Seventh Framework Program (FP7/2007 2013/European Research Council Grant Agreement 281287), Fondation ARC pour la Recherche sur le Cancer (PJA-), CEA Radiation biology and Impulsion programs, EDF. JP was supported by a fellowship from the CEA.

Author contributions: JP, MT, CD, CB and RC performed experiments. KD designed and supervised the entire project with the help of MT and JP. KD and JP analyzed the data, assembled the figures and wrote the manuscript with critical input of the other authors.

Competing interests: The authors declare no competing interests

Supplementary Materials

Material and Methods

Fig. S1-S7

Tables S1-S3

References 28-29, 51-54

Movie S1-S4

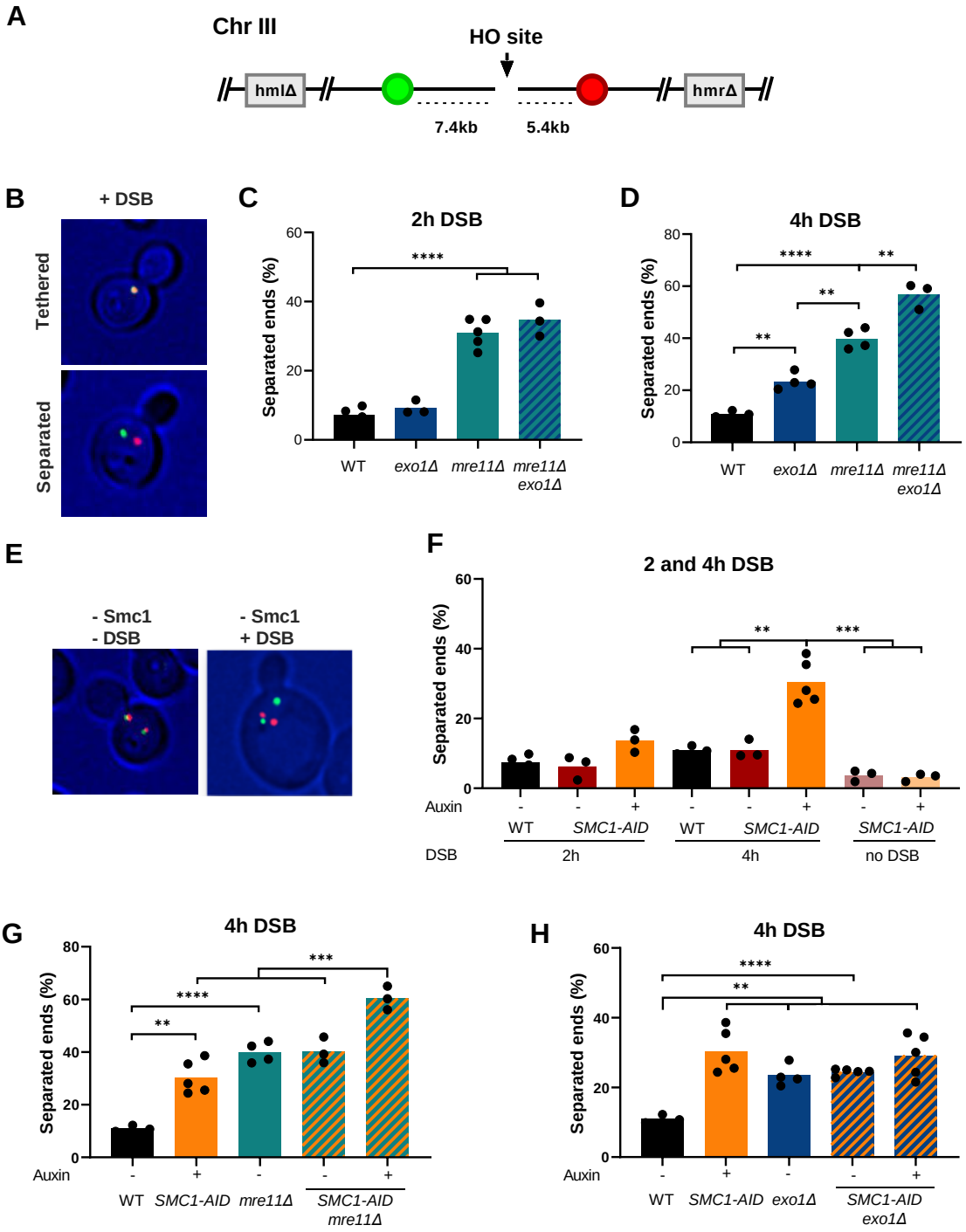

Fig. 1. Cohesin Tethers DSB ends in the Exo1 pathway

(**A**) LacO/LacI-mCherry tag and a TetO/TetR-GFP tag were inserted at 5 and 7 kb from the HO DSB site at the MAT locus respectively.

(B) Example of cells with tethered or separated ends. Signals are considered as separated when the distance between centers is more than 400nm.

(C-D) Percentage of cells with separated ends in the indicated strains after 2 hours (B) or 4 hours (D) DSB induction.

(E) Examples of cells showing sister chromatid separation and DSB end separation upon Smc1-AID auxin mediated degradation in absence or in presence of DSB induction.

(F) Percentage of cells with separated ends in WT and SMC1-AID strains in absence (-) or presence (+) of auxin after 2 hours, 4 hours or no DSB induction as indicated.

(G-H) Percentage of cells with separated ends in the indicated strains after 4h DSB induction.

Black stars indicate statistical differences (* = $p<0,05$; ** = $p<0,01$; *** = $p<0,005$; **** = $p<0,001$).

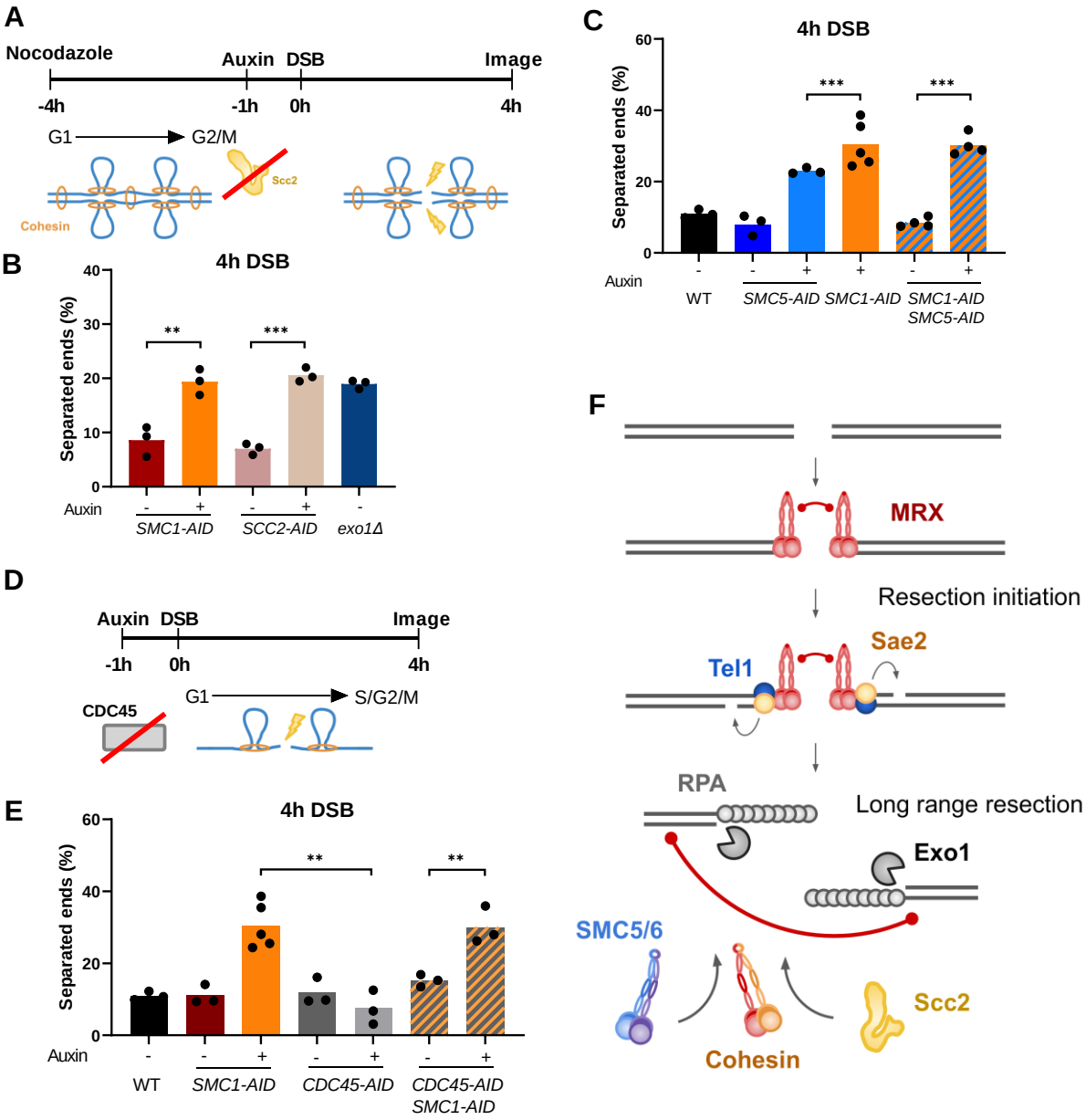

Fig. 2: Cohesin DSB end-tethering requires de novo cohesin loading but not sister chromatid cohesion

(**A**) Schematic representation of assay to determine DSB end-tethering in absence of *de novo* cohesin loading. DSB was induced after cells were blocked in G2/M with nocodazole for 3 hours, and incubated with auxin or ethanol for a further 1 hour.

(B) Percentage of G2/M blocked cells with separated ends in the indicated strains after 4 hours DSB induction.

(C) Percentage of cells with separated ends in the indicated strains after 4 hours DSB induction.

(D) Schematic representation of assay to determine DSB end-tethering in absence of replication. Cultures were incubated with auxin or ethanol for 1 hour. In the absence of Cdc45, cells advance through the cell cycle upon DSB induction, and load cohesin onto chromosomes without undergoing replication.

(E) Percentage of cells with separated ends in the indicated strains after 4 hours DSB induction.

(F) Schematic representation of DSB end-tethering pathways.

Black stars indicate statistical differences (* = p<0,05; ** = p<0,01; *** = p<0,005; **** = p<0,001).

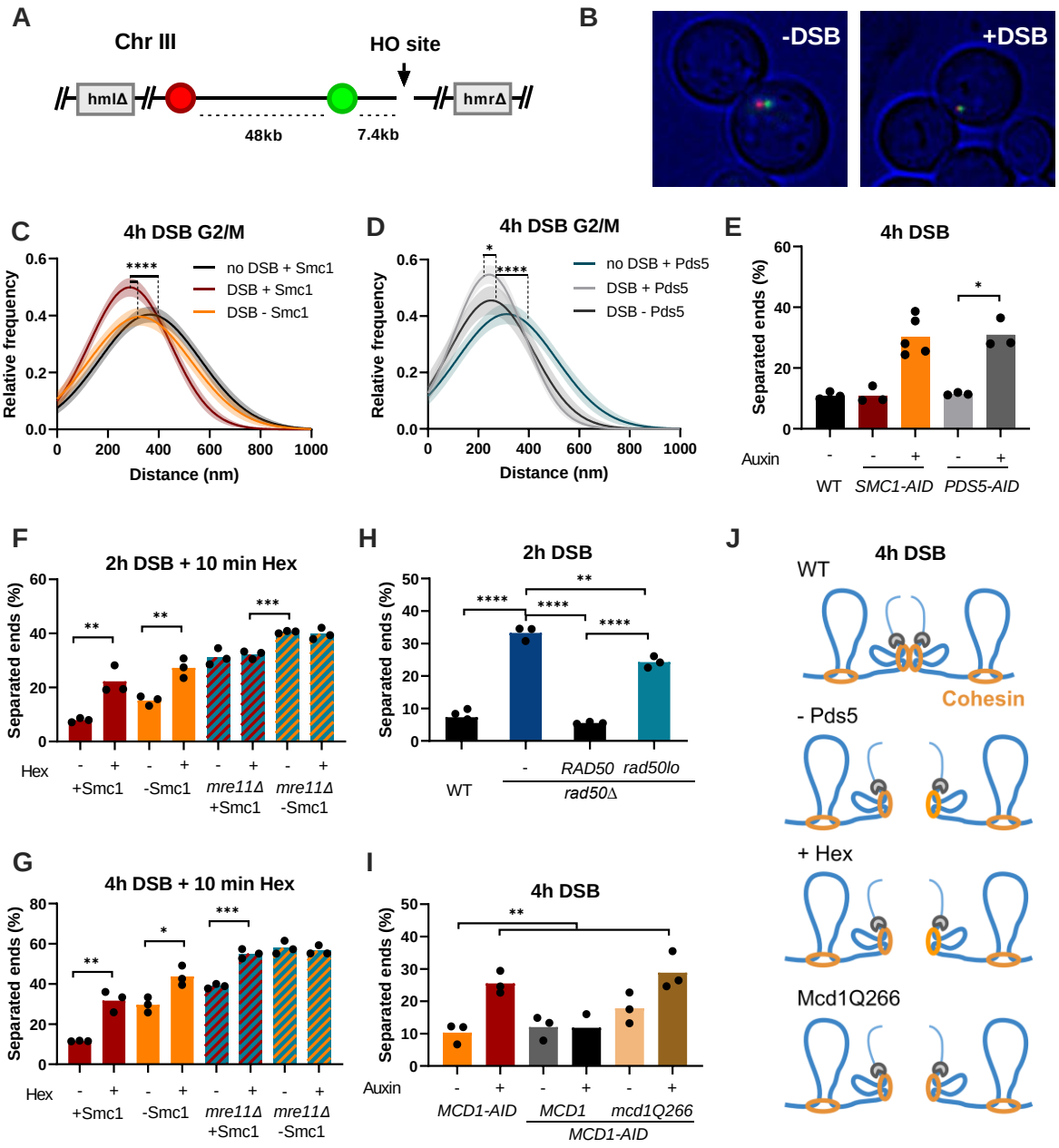

Fig. 3: Cohesin compacts DSB flanking chromatin and DSB-ends are tethered by MRX- or cohesin-oligomerization

(**A**) LacO/LacI-mCherry tags and a TetO/TetR-GFP tag inserted at 7 and 55 kb from the HO DSB site at the MAT locus respectively.

(B) Representative images in presence and absence of DSB.

(C) Relative frequency of distances between the two tags in nocodazole arrested *SMC1-AID* tagged cells treated with ethanol (+Smc1) or auxin (-Smc1) after 4 hours and no DSB.

(D) Relative frequency of distances measured between the two tags in nocodazole arrested *PDS5-AID* tagged cells treated with ethanol (+Pds5) or auxin (-Pds5) in after 4 hours or no DSB induction.

(E) Percentage of cells with separated ends in the indicated strains after 4 hours DSB induction.

(F-G) Percentage of cells with separated ends in the indicated strains treated with auxin or ethanol, and for 10 minutes with digitonin (-) or digitonin and 1,6-hexanediol (+), after 2 hours (F) or 4 hours (G) DSB induction.

(H) Percentage of cells with separated ends in WT, rad50Δ, and rad50Δ cells complemented with *RAD50* or *rad50-lo*, after 2 hours DSB induction.

(I) Percentage of cells with separated ends in MCD1-AID, and MCD1-AID strains complemented with *MCD1* or *mcd1-Q266*, in absence (-) or presence (+) of auxin, after 4 hours DSB induction.

(J) Schematic representation of how loss of oligomerization disrupts DSB end-tethering.

Black stars indicate statistical differences (*= p<0,05; **= p<0,01; ***= p<0,005; ****= p<0,001). Shaded area indicates the 95% confidence interval of the fitting of 3 experiments per data set.

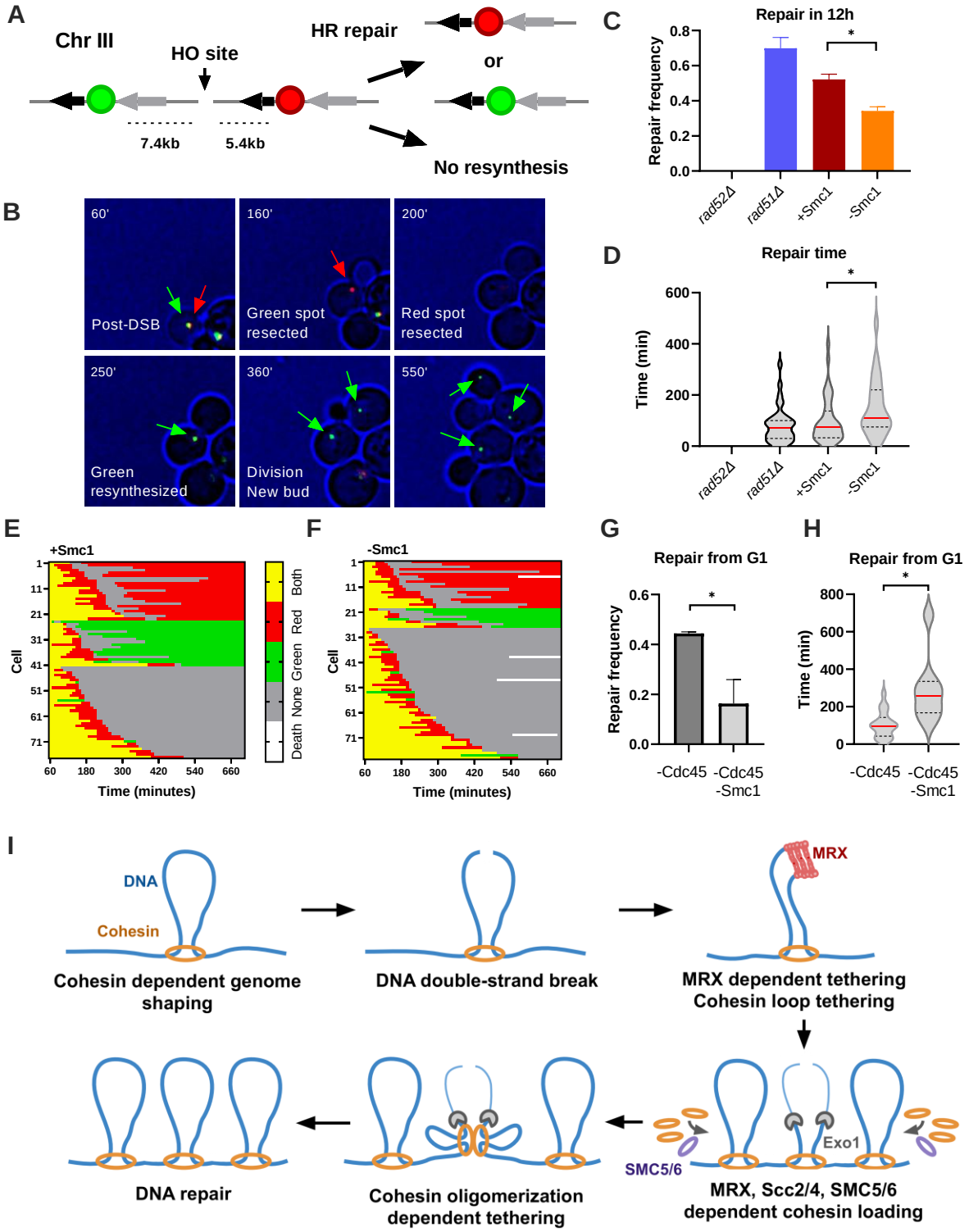

Fig. 4: Cohesin is required for efficient DNA DSB repair by homology directed mechanisms

(**A**) Schematic representation of repair events after resection and disappearance of the spots followed by resynthesis of one spot. Black and grey triangles show direct repeats used for homologous recombination.

(B) Sequence of images showing disappearance of both spots upon resection and reappearance of a green spot that is propagated to daughter cells at each division. Time post DSB is indicated on each frame.

(C) Relative frequency of repair events corresponding to the resynthesis of a spot in *rad52Δ*, *rad51Δ* and *SMC1-AID* strains treated with ethanol (+Smc1) or auxin (-Smc1).

(D) Time taken for a spot to reappear, in *rad52Δ*, *rad51Δ* and *SMC1-AID* strains treated with ethanol (+Smc1) or Auxin (-Smc1).

(E-F) Spot characteristics of + Smc1 (C), and - Smc1 (D) individual cells imaged every 10 minutes during 12 hours after DNA DSB induction. Lines represent individual cell lineages, and each segment a time point. Colors indicate presence of both spots (yellow), a red spot only (red), a green spot only (green), or no spots (grey).

(G) Relative frequency of repair events corresponding to the resynthesis of a spot in the indicated strains treated with auxin. Cells in G1 phase upon induction were imaged.

(H) Time for a spot to reappear in the indicated strains treated with auxin. Cells in G1 phase upon induction were imaged.

(I) Schematic representation of MRX and cohesin tethering DSB ends. MRX requires oligomerization through Rad50 head domains, and interaction between Rad50 coiled coils. Exo1 drives long-range DNA resection, leads to the recruitment of cohesin that mediates DSB end-tethering by oligomerization.

Black stars indicate statistical differences (*= p<0,05; **= p<0,01; ***= p<0,005; ****= p<0,001).

Materials and Methods

Strains and plasmids

Yeast strains used in this study are derivative of JKM179, JKM139 (*51*) or yKD809 (*28*), and were generated by PCR gene targeting, plasmid transformation or cross (Table S1-S2).

Media and growth conditions

Yeast strains were grown at 30°C in glucose rich yeast extract-peptone-dextrose (YPD) medium, with appropriate antibiotic, or in synthetic medium (SD) lacking the appropriate amino acid. YPLGg medium containing 2% lactate, 3% glycerol and 0.05% glucose was used for DNA DSB induction, by addition of galactose (f.c. 2%), to ON cultures of OD600 0.4 - 0.8 as in (*52*). Conditional protein knockdown was achieved in AID tagged strains by addition of IAA in EtOH to a f.c. of 2Mm (*29*) 1,6-hexanediol treatment (f.c. 10%) was performed for 10 minutes, with 10µg/ml digitonin.

Microscopy

Live-cell images were acquired using a wide-field inverted micro-scope (Leica DMI-6000B) equipped with Adaptive Focus Control to eliminate Z drift, a 100×/1.4 NA immersion objective with a PriorNanoScanZ Nanopositioning Piezo Z Stage System, a CMOS camera(ORCA-Flash4.0; Hamamatsu) and a solid-state light source (Spec-traX, Lumencore). The system is piloted by MetaMorph software(Molecular Device). Images were acquired at indicated time points after DSB induction. 19 focal steps of 0.20µm were acquired sequentially for GFP and mCherry with an exposure time of 50ms using solid-state 475- and 575-nm diodes and appropriate filters (GFP-mCherry filter; excitation: double BP, 450–490/550–590 nm and dichroic double BP 500–550/600–665 nm; Chroma Technology Corp.). Images were processed using ImageJ software (National Institutes of Health). 3D images were converted to 2D projections, from which XY coordinates of the most intense pixels were extracted. Distance analysis between proximal fluorescent signals in mCherry and GFP channels was performed using an Rstudio script. All images shown are z projections of z-stack images.

Quantifications and statistical analysis

Quantifications and statistical analysis were done using PRISM (GraphPad). For the end-tethering assay, at least 3 independent experiments analysing more than 100 cells were performed for each genotype and statistical significance was determined by a two-tailed Student's t test. ns=not significant p>0,005, * = p<0,05; ** = p<0,01; *** = p<0,005; **** = p<0,001. For the compaction measurements, distance data of at least 100 cells was sorted into 200 nm bins, and the bins of 3 independent experiments were fitted with a gaussian curve using Prism software, with shaded areas representing an interval of confidence of 95%. Statistical significance was determined by a Kolmogorov-Smirnov test. ns=not significant p>0,005, * = p<0,05; ** = p<0,01; *** = p<0,005; **** = p<0,001.

Microscopy in microfluidic plates

CellASIC ONIX microfluidic plates (Y04C-02; MilliporeSigma) were used for long duration movies. HO was induced in YPLGg cultures of OD600nm 0.5 by addition of galactose to a f.c. of 2%, and incubation at 30°C for 30 minutes. After break induction, cultures were loaded into the microfluidic plate. The remaining culture was centrifuged at 3000rpm for 3 minutes, and the conditioned media was loaded into the microfluidic plate for flow over the cells for the duration of the experiment. After loading the plate, cell positions were defined, and images were acquired every 10 minutes for up to 24 hours. 19 focal steps of 0.20µm were acquired sequentially for GFP and mCherry with an exposure time of 30ms using solid-state 475- and 575-nm diodes and appropriate filters (GFP-mCherry filter; excitation: double BP, 450–490/550–590 nm and dichroic double BP 500–550/600–665 nm; Chroma Technology Corp.). A single bright-field image on one focal plane was acquired at each time point with an exposure of 10ms. For Cdc45 depleted strains, cells were loaded into the microfluidic plate immediately following galactose addition, and cells that were in G1 prior DSB induction were imaged.

Monitoring DSB efficiency

Cells were grown in 2ml of YPD ON. Cultures were then diluted in YPLGg, and grown to an OD600nm of 0.5-0.8, and incubated with 2mM IAA or EtOH for 1 hour. HO expression was

induced by addition of galactose to a final concentration of 2%. At 0, 1, 2, 4 and 6 hours post DSB induction, approximately 4 x 10^7 cells were collected by 3000rpm centrifugation for 5 min. DNA was extracted from cell pellets by Winston preparation. Samples were analyzed by qPCR with primers 1kb upstream of the HO site to analyze resection (200nM), flanking the HO site to determine DSB efficiency (450nM) or targeting the OGG1 reference gene (200nM). See Table 3 for primer sequences. Reactions were performed as in (*53*). Each sample and no template controls were run in triplicate, and reaction specificity determined by melt curve analysis. Relative quantitation of resection and DSB efficiency reactions was achieved using the comparative Ct method (*54*).

Western blot

Auxin induced protein degradation of AID containing strains was confirmed by Western blot analysis (Brocas et al., 2019). Cells were grown in 2ml of YPD ON. Cultures were then diluted in YPLGg, and grown to an OD600nm of 0.5-0.8, and incubated with 2mM IAA or EtOH for 1, 2, and 4 hours (hrs). Approximately 4 OD600nm of cells were collected by centrifugation at 3000rpm for 5 min. Cells were washed in dH2O, and collected by centrifugation at 3000rpm for 5 min. Supernatant was removed, and cell pellets frozen at -80°C. Whole cell extracts were prepared from cell pellets using a standard Trichloroacetic acid (TCA) extraction protocol and suspended in Laemmli buffer. Protein concentrations were determined by Bradford assay, and samples prepared for SDS PAGE by 5 min incubation at 90°C. 20µg of sample was migrated at 100v for 1 hr on 10% SDS polyacrylamide gels in standard running buffer. Nitrocellulose membrane transfer was performed using the iBlot transfer apparatus as per manufacturers guidelines (Thermo Fisher). Membranes were washed with TBS-T, revealed by ponceau staining, and blocked with 5% milk TBS-T for 1hr. Membranes were then incubated at room temperature with mouse primary anti-myc (1:1000), and anti-mouse secondary antibodies (1:1000) in 5% milk TBS-T for 1hr each. Membranes were developed by fluorescence using the Odyssey Clx (LI-COR).

Flow cytometry

0.5 OD600nm of cells were fixed in ethanol 70% and stored at -20°C. Cells were pelleted, washed, and then incubated in Sodium Citrate pH7.4 50mM with 0.25mg/ml RNAseA for 1

hour at 50°C. Proteinase K was then added, to a final concentration of 2mg/ml, and incubated for further 1 hour at 50°C. Cells were pelleted, and then stained in a pH7.4 50mM Sodium Citrate solution containing 1µM SYTOX Green Nucleic Acid Stain (Invitrogen – S7020). Cells were sonicated, and flow cytometry was performed on a Novocyte cytometer (ACEA bioscience.Inc) machine. Data was analyzed using FlowJo software.

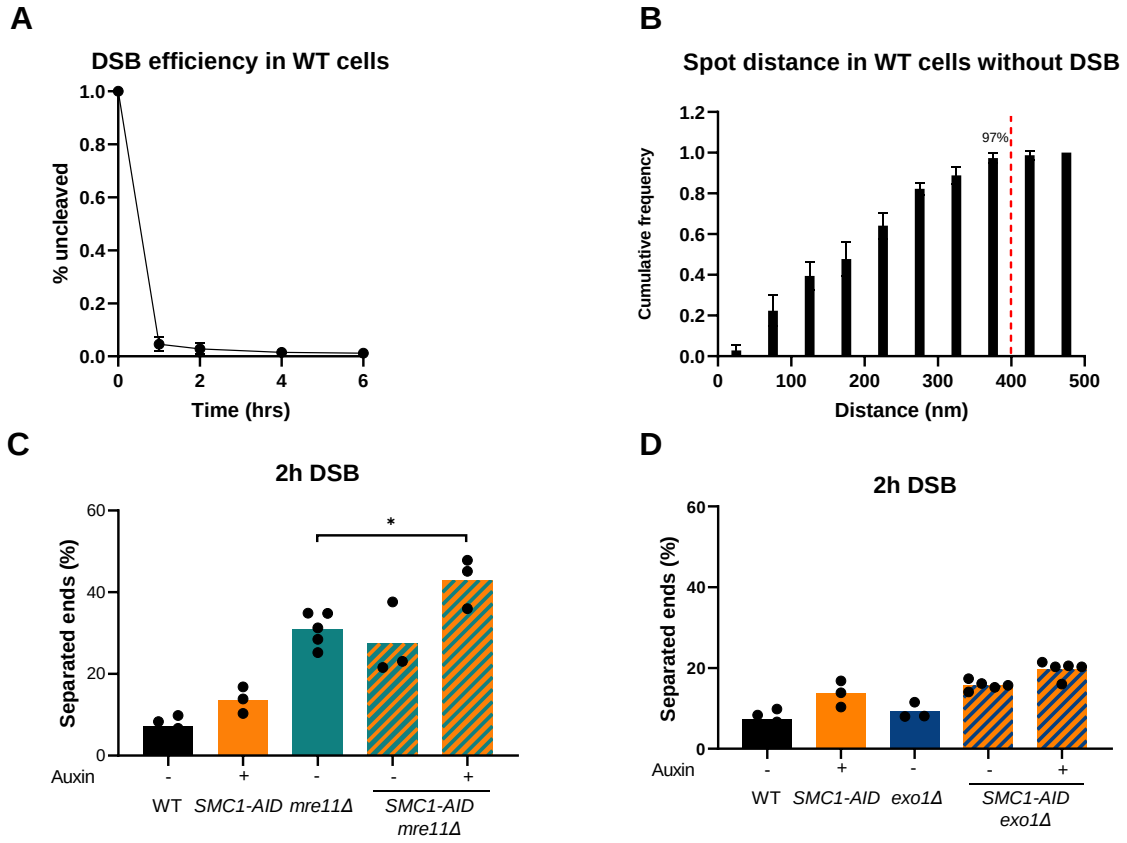

Fig. S1. LacI-mCherry and TetR-GFP spot distance rarely exceed 400nm, and HO induced DSB is fast and efficient. Cohesin contributes to DSB end tethering at 2 hours post-DSB in absence of MRX.

(A) qPCR detection of the HO cleavage site in WT cells at 0, 1, 2, 4 and 6 hours after DSB induction. (B) Cumulative distance between LacI-mCherry and TetR-GFP signals in exponential WT cells without DNA DSB induction. Red line indicates 400nm threshold, which 97% of distances are under. (C) Percentage of cells with separated ends in WT, SMC1-AID, mre11Δ, mre11Δ SMC1-AID strains after 2h DSB induction. (D) Percentage of cells with separated ends in WT, SMC1-AID, exo1Δ, exo1Δ SMC1-AID strains after 2h DSB induction.

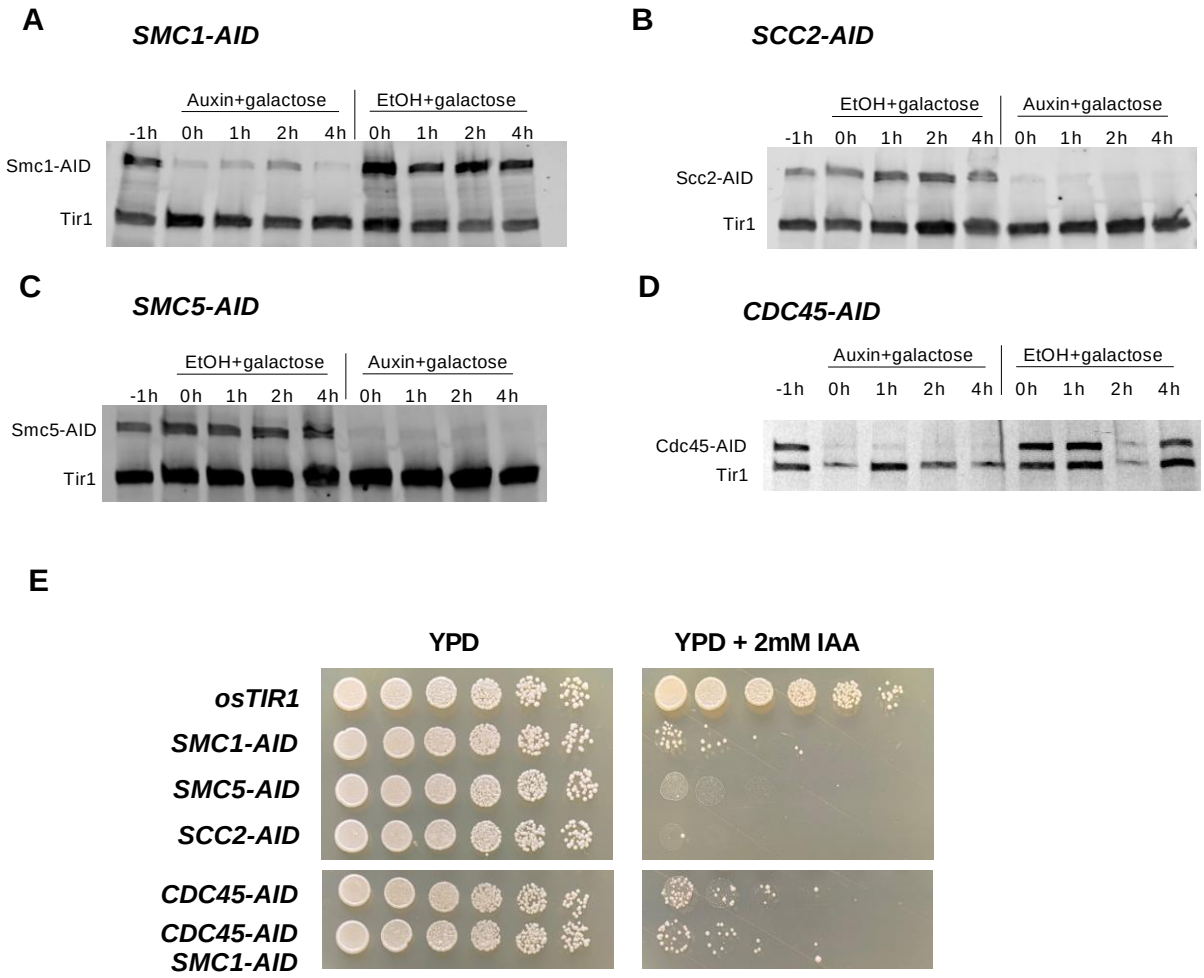

Fig. S2. Auxin induced degradation of target proteins leads to efficient depletion.

(A-D) anti-myc Western blots demonstrating protein levels of 9myc-AID tagged proteins treated with auxin or ethanol throughout microscopy DSB end tethering assays. t-1 (before IAA/EtOH addition), t0 (1 hour IAA/EtOH), t1 (2 hour IAA/EtOH + 1h galactose), t2 (3 hour IAA/EtOH +2h galactose) and t4 (5 hours IAA/EtOH + 4h galactose). (E) Drop assay of all tethering strains on YPD and YPD + auxin, incubated for 48 hours at 30°C.Type or paste caption here.

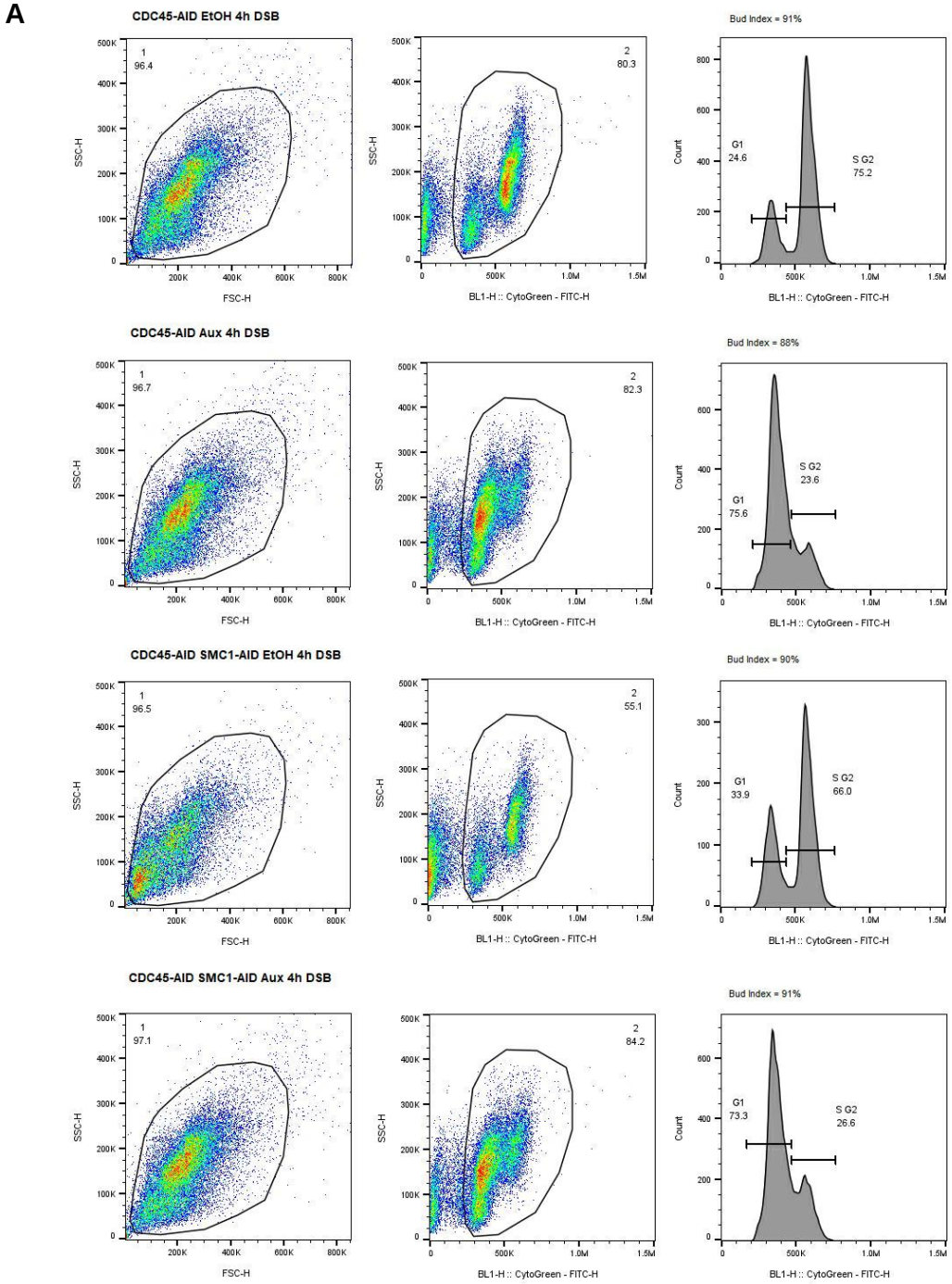

Fig. S3. Cdc45 degradation prevents genome duplication whilst allowing cells to proceed to G2/M.

(A) Gating and fluorescent intensity profiles, determind by flowcytometry, of CDC45-AID and CDC45-AID SMC1-AID strains treated with IAA or EtOH after 4h DSB induction. Percentage of cells with large buds is indicated above intensity profiles as bud index.

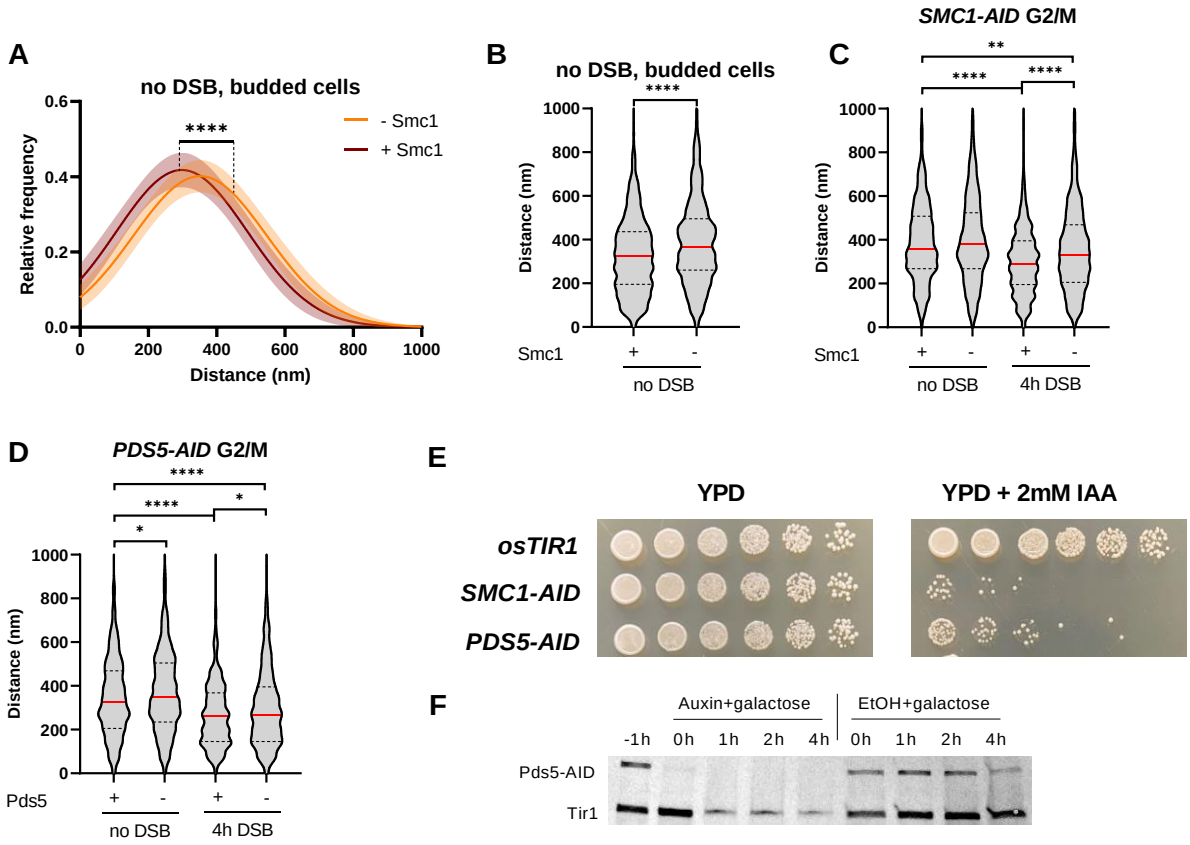

Fig. S4. Smc1 depletion reveals cohesin dependent genome compaction in S-M phase cells. Pds5 is not required for DSB dependent genome compaction.

(A) Relative frequency of distances measured between two tags separated by 45kb in a SMC1-AID tagged strain treated with ethanol (+SMC1) or auxin (-SMC1) in cycling cells in which a bud is present. (B) Distances between 45kb separated tags from three individual replicas for SMC1-AID tagged strain treated with ethanol (+Smc1) or auxin (-Smc1), represented as a violin plot. Red line at median, quartiles represented by dashed line. (C-D) Distances between 45kb separated tags from three individual replicas for SMC1-AID and PDS5-AID tagged strains treated with noodazole and following 4 hours DSB, treated with ethanol or auxin, represented as a violin plot. Red line at median, quartiles represented by dashed line. (E) Drop assay of compaction strains plated on YPD and YPD + auxin, incubated for 48 hours at 30°C. (F) anti-myc Western blot demonstrating protein levels of PDS5-AID strains treated with auxin or ethanol throughout microscopy DSB end tethering assay timecourse. t-1 (before IAA/EtOH addition), t0 (1 hour IAA/EtOH), t1 (2 hour IAA/EtOH + 1 hour galactose), t2 (3 hours IAA/EtOH +2 hours galactose) and t4 (5 hours IAA/EtOH + 4 hours galactose).

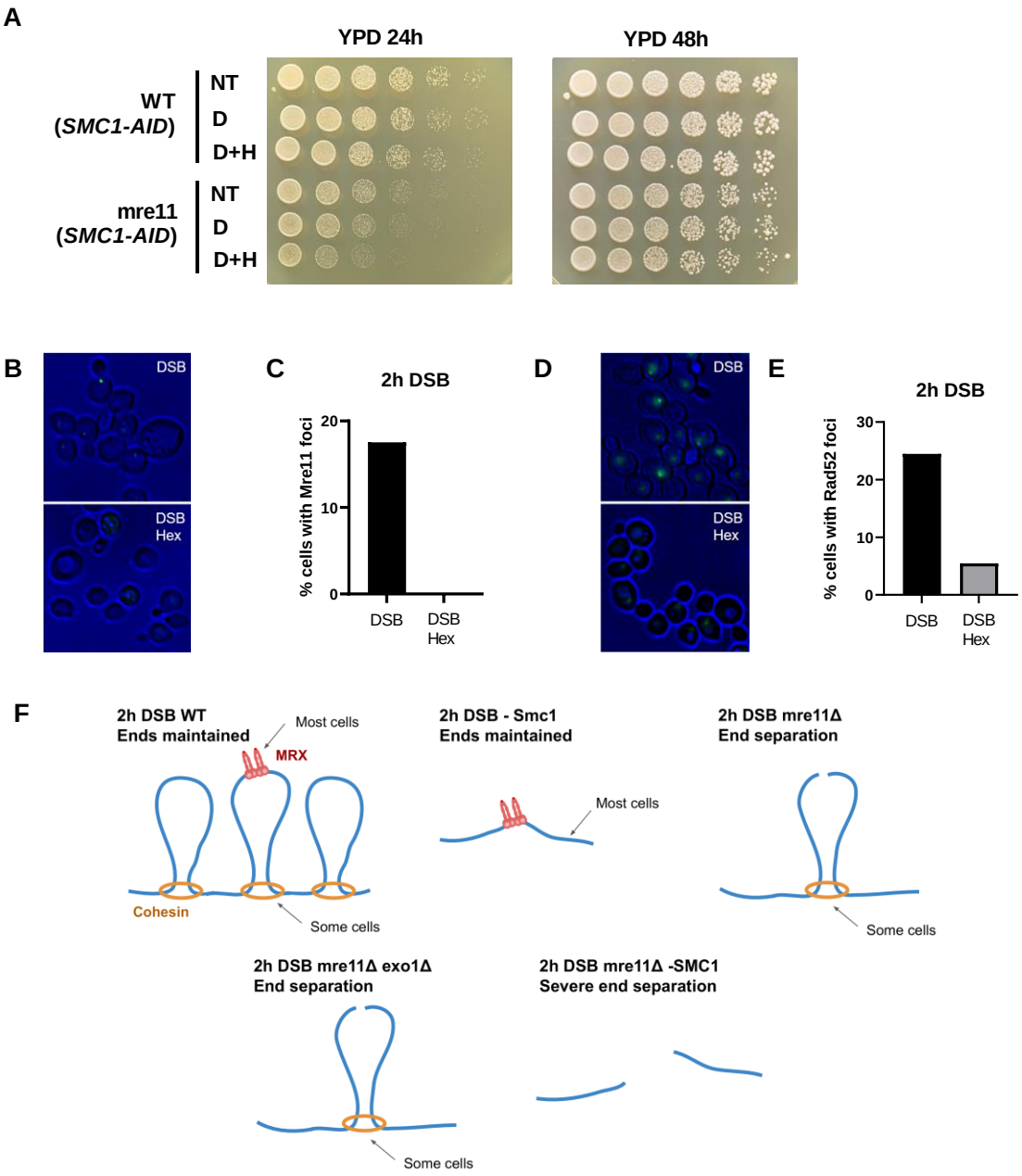

Fig. S5. Cells recover following hexanediol treatment without growth defect, and Mre11-GFP foci are abolished by hexanediol treatment. A hexanediol resistant cohesin population reduces end separation in the absence of MRX at 2 hour DSB.

(A) Drop assay of strains plated on YPD after no treatment (NT), 10 minutes digitonin (D), or 10 minutes digitonin + hexanediol (D+H) treatment, incubated for 24 and 48 hours at 30°C. (B) Representative images of Mre11-GFP foci at 2 hour DSB with no treatment (DSB), or 30 minutes digitonin + hexanediol (DSB Hex) treatment. (C) Quantification of cells with Mre11-GFP foci at 2 hour DSB with no treatment (DSB), or 30 minutes digitonin + hexanediol (DSB Hex) treatment. (D) Representative images of Rad52-YFP foci at 2 hour DSB with no treatment (DSB), or 30 minutes digitonin + hexanediol (DSB Hex) treatment. (E) Quantification of cells

with Rad52-YFP foci at 2 hour DSB with no treatment (DSB), or 30 minutes digitonin + hexanediol (DSB Hex) treatment. (F) Schematic representation of cohesin dependent end tethering in a looping dependent manner. In WT cells, MRX tethers early DSB ends, and the DSB might be in a cohesin loop. Cohesin depletion following 2 hour DSB doesn't increase end separation due to MRX compensation. In the absence of MRX, DSB ends that occured within a cohesin loop rescues some loss of DSB end tethering. In contrast, loss of both MRX and cohesin leads to increased end separation as both the cohesin and MRX dependent mechanisms are lost.

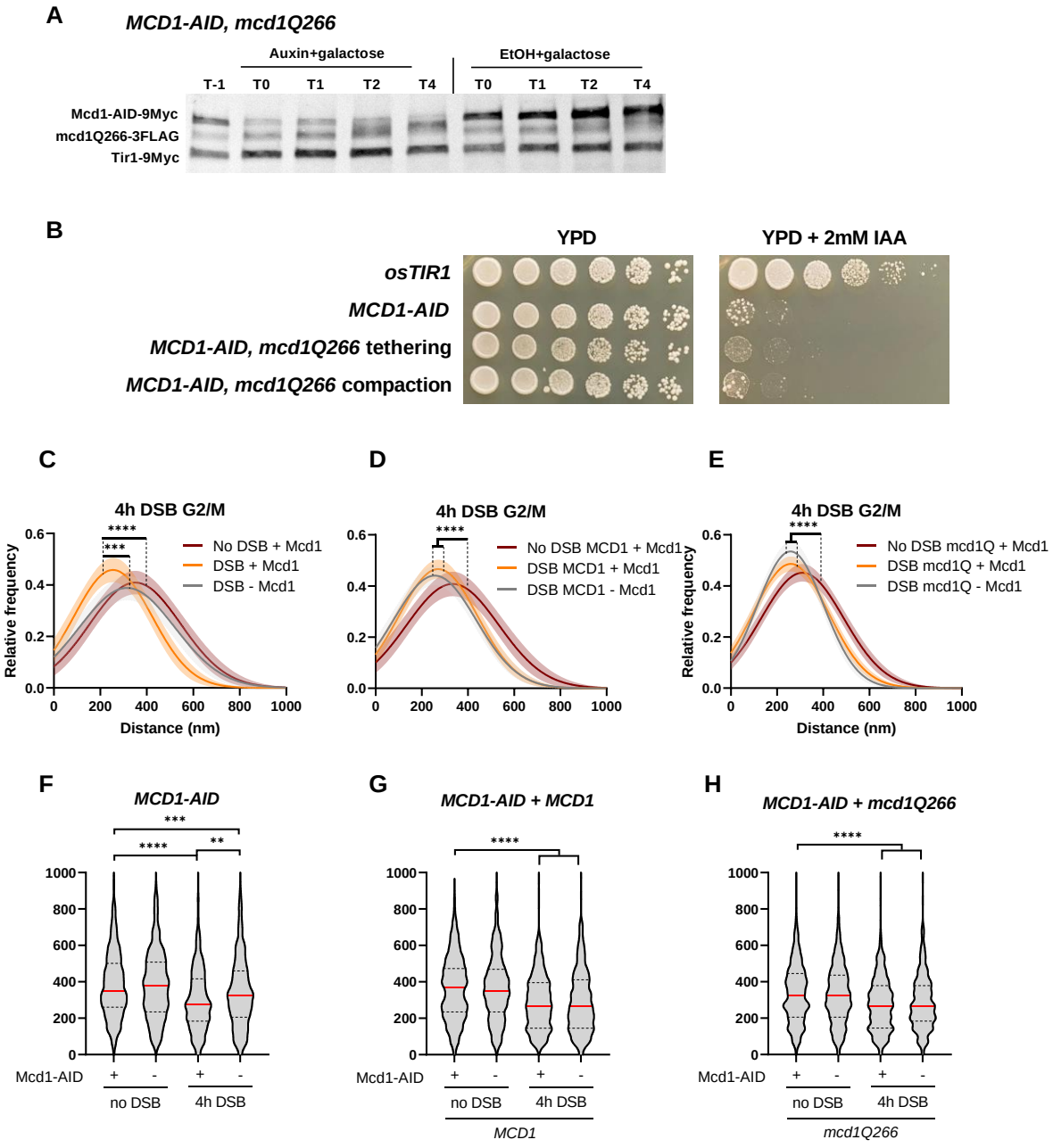

Fig. S6. mcd1Q266 rescues DSB dependent genome compaction in the absence of Mcd1.

(A) anti-myc/anti-flag Western blots demonstrating protein levels of AID-myc and mcd1Q266-FLAG tagged proteins treated with auxin or ethanol throughout microscopy DSB end tethering assays. t-1 (before IAA/EtOH addition), t0 (1 hour IAA/EtOH), t1 (2 hours IAA/EtOH + 1 hours galactose), t2 (3 hours IAA/EtOH +2 hours galactose) and t4 (5 hours IAA/EtOH + 4 hours galactose). (B) Drop assay of MCD1 strains on YPD and YPD + auxin, incubated for 72 hours at 23°C. (C-E) Relative frequency of distances measured between two tags separated by 45kb in MCD11-AID tagged strains complemented with nothing, MCD1, or mcd1Q266, treated with ethanol or auxin and nocodazole after 4h DSB. (F-H) Distances between 45kb separated

tags from three individual replicas for *MCD1-AID* tagged strains complemented with nothing, *MCD1*, or *mcd1Q266*, treated with ethanol or auxin and nocodazole after 4 hour DSB, represented as a violin plot. Red line at median, quartiles represented by dashed line.

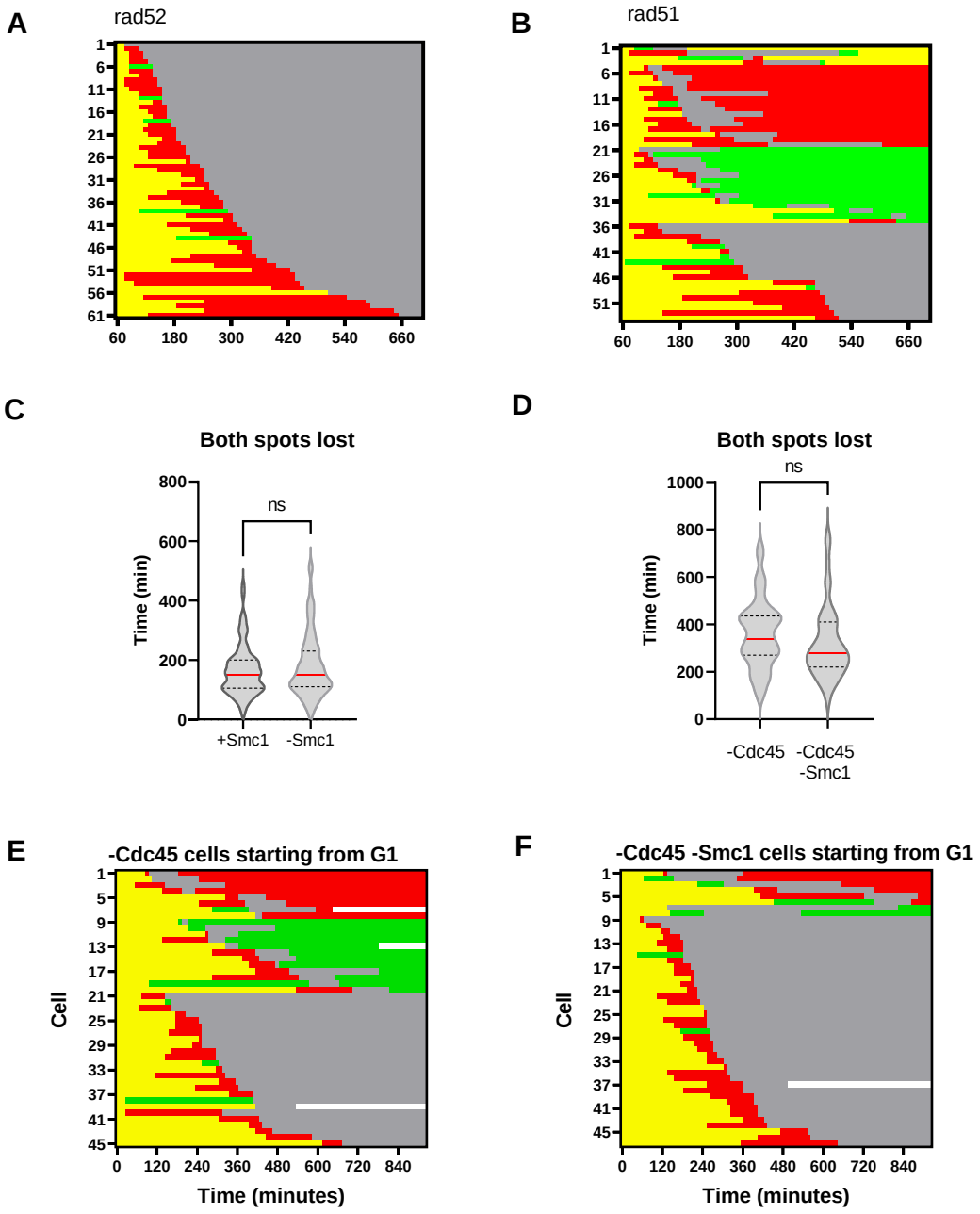

Fig. S7. Cohesin depletion does not alter rate of resection following DSB.

(A-B) Spot characteristics of individual cells in *rad52* and *rad51* cells during a 12 hour period after DNA DSB induction (C) Time taken for loss of both spots after DSB induction in microfluidic experiments for *SMC1-AID* strains. (D) Time taken for loss of both spots after DSB induction in microfluidic experiments for auxin exposed *CDC45-AID* and *CDC45-AID SMC1-AID* strains. (E-F) Spot characteristics of individual cells in *CDC45-AID*, *CDC45-AID SMC1-AID* cells during a 15.5 hour period after DNA DSB induction. DSB was induced in the microfluidic plate.

Strain	Strain genotype	Strain type	Reference	Figure ID
JKM139	*MATa hml::ADE1 hmr::ADE1 ade3::pGal-HO ade1 leu2-3,112 lys5 trp1::hisG ura3-52*	Galactose-inducible HO cleavage	Lee et al., 1998	
JKM179	*MATα hml::ADE1 hmr::ADE1 ade3::pGal-HO ade1 leu2-3,112 lys5 trp1::hisG ura3-52*	Galactose-inducible HO cleavage	Lee et al., 1998	
yKD809	JKM139, *ura3-52Δ::LacI-mCherry-URA3, leu2-3Δ::TetR-GFP-LEU2, TAF2-LacOpFx-TRP1, 4.4kb MATa-TetO-LEU2*	Tethering	Mojumdar et al. , 2019	1B-D, 1F-H, 2C, 2E, 3E, 3H, S1A, S1C-D
yKD1107	yKD809*, exo1Δ::HPH*	Tethering	This study	1C-D, 1H, 2B, S1D
yKD925	yKD809, *mre11Δ::HPH*	Tethering	Mojumdar et al. , 2019	1C-D, 1G, S1C
yKD2365	yKD809, *exo1Δ::HPH mre11Δ::Nat*	Tethering	This study	1C-D
yKD1175	yKD809, *ura3-52Δ:: OsTIR1-9myc-URA3-LacI-mCherry-KanMx*	Tethering	This study	S1B, S2E, S6B
yKD1177	yKD1175, *SMC1-AID-9myc-HPH*	Tethering	This study	1E-H, 2B-C, 2E, 3E-G, 4B-F, S1C-D, S2A, S2E, S5A, S7C
yKD2318	yKD1175, *SMC1-AID-9myc-HPH mata-inc*	Tethering	This study	1F
yKD1483	yKD1175, *SMC1-AID-9myc-HPH mre11Δ::Nat*	Tethering	This study	1G, 3F-G, S1C, S5A
yKD1486	yKD1175, *SMC1-AID-9myc-HPH* exo1Δ::Nat	Tethering	This study	1H, S1D
yKD1488	yKD1175, *SCC2-AID-9myc-HPH*	Tethering	This study	2B, S2B, S2E
yKD1178	yKD1175, *SMC5-AID-9myc-HPH*	Tethering	This study	2C, S2C, S2E

yKD2436	yKD1175, *SMC1-AID-9myc-Nat SMC5-AID-9myc-HPH*	Tethering	This study	2C
yKD2496	*yKD1175, CDC45-AID-9myc-Nat*	Tethering	This study	2E, 4G-H, S2D-E, S3A, S7D-E
yKD2497	*yKD1175, CDC45-AID-9myc-Nat SMC1-AID-9myc-HPH*	Tethering	This study	2E, 4G-H, S2E, S3A, S7D, S7F
yKD2285	*4.4kb MATa-TetO-LEU2 0.5kb-CWH43::lacOpFX-TRP1 ura3Δ::OsTIR1-URA3-LacI-mCherry-KanMx leu2-3Δ::TetR-GFP-LEU2*	Compaction	This study	S4E
yKD2289	yKD2285, *SMC1-AID-9myc-HPH*	Compaction	This study	3B-C, S4A-C, S4E
yKD2438	yKD2285, *PDS5-AID-9myc-HPH*	Compaction	This study	3D, S4D-F
yKD2439	yKD1175, *PDS5-AID-9myc-HPH*	Tethering	This study	3E
yKD2484	yKD809, *ura3-52Δ::LacI-mCherry-KanMX rad50Δ::Nat*	Tethering	This study	3H
yKD2549	yKD2484, *ura3-52Δ::LacI-mCherry-RAD50-URA3*	Tethering	This study	3H
yKD2550	yKD2484, *ura3-52Δ::LacI-mCherry-rad50L116A/I119A/T127A/L128A-URA3*	Tethering	This study	3H
yKD2485	yKD1175, *ura3Δ::OsTIR1-Nat-LacI-mCherry-KanMx MCD1-AID-9myc-HPH*	Tethering	This study	3I, S6B
yKD2491	yKD2485, *mcd1-Q266-3FLAG-URA3*	Tethering	This study	3I, S6B
yKD2492	yKD2485, *MCD1-3FLAG-URA3*	Tethering	This study	3I, S6B
yKD1172	yKD809, *rad52Δ::KanMx*	Tethering	This study	4C-D, S7A
yKD2366	yKD809, *rad51Δ::Nat*	Tethering	This study	4C-D, S7B
yKD2552	yKD2285, *ura3Δ::OsTIR1-Nat-LacI-mCherry-KanMx*	Compaction	This study	S6B

yKD2553	yKD2552, *MCD1-AID-9myc-HPH*	Compaction	This study	S6C, S6F
yKD2554	yKD2553, *mcd1-Q266-3FLAG-URA3*	Compaction	This study	S6E, S6H
yKD2555	yKD2553, *MCD1-3FLAG-URA3*	Compaction	This study	S6D, S6G
yKD1598	JKM139, *NUP49::NUP49-mCherry-URA3 MRE11-yEGFP-HPH, sae2::NAT*	DDR foci	This study	S5B-C
yKD282	JKM179, *RAD52-YFP*	DDR foci	This study	S5D-E

Table S1.

Saccharomyces cerivisae strains used in this study

Plasmid name	Plasmid number	Description	Source
OSTIR-9myc-URA3	pKD243	ADH1p-OsTIR1-9Myc	Nishimura et al., 2009
AID-9myc-NAT	pKD244	AID-9myc-NAT	Nishimura et al., 2009
AID-9myc-HPH	pKD245	AID-9myc-HPH	Nishimura et al., 2009
mcd1-Q266-3FLAG-URA3	pKD511	pVG285 mcd1-Q266-3FLAG	Eng et al., 2014
MCD1-3FLAG-URA3	pKD517	MCD1-3FLAG	This study
rad50lo-URA3	pKD513	pJT23 pSIVura-SpeI-prom-Rad50(L116A, I119A, T127A, L128A)-term-KpnI	Kissling et al., 2022
RAD50-URA3	pKD514	pJT25, pSIVura-SpeI-prom-Rad50-term-KpnI	Kissling et al., 2022

Table S2.

Plasmids used in this study

Primer	Name	Sequence	Use
776	F OGG1	CAATGGTGTAGGCCCCAAAG	Reference gene
777	R OGG1	ACGATGCCATCCATGTGAAGT	Reference gene
1124	F MATa	AGTTTCAGCTTTCCGCAACAG	Quantify DSB efficiency at MATa
47	R MATa	CGTCACCACGTACTTCAGCATAA	Quantify DSB efficiency at MATa

Table S3.

qPCR primers used in this study

Movie S1.

yKD1177 E S9 Repair, green spot, division

Movie S2.

yKD1177 E S9 Repair, red spot, division

Movie S3.

yKD1177 E S8 No Repair, no division

Movie S4.

yKD1177 E S11 No repair, division

Results not included in Article 1:

- **Cohesin depletion does not alter resection**
- **Rad17 is not required for DSB end-tethering**
- **Rtt107 is not required for DSB end-tethering**

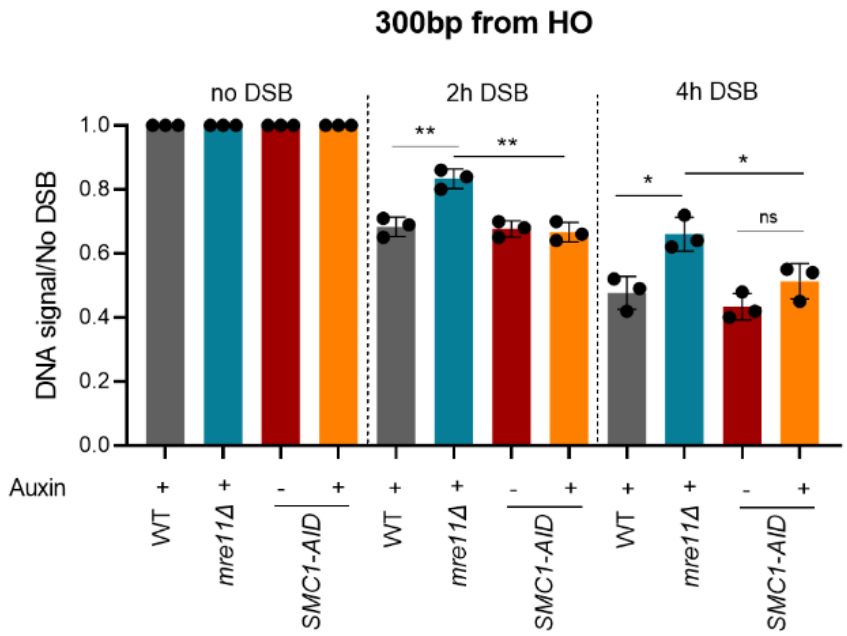

Figure 1. Cohesin depletion does not alter resection. qPCR analysis of DNA content in a region 300bp from the inducible HO DSB site. Time points were taken at 0 (no DSB), 2 and 4 hours after DSB induction. DNA content is presented as a ratio between the value at each time point, divided by the no DSB control. Strains were incubated with (+) or without (-) auxin as indicated on graph. Black stars indicate statistical differences (*= p<0,05; **= p<0,01; ***= p<0,005; ****= p<0,001). Shaded area indicates the 95% confidence interval of the fitting of 3 experiments per data set.

Result

Exo1 DSB end-tethering is dependent on its ability to form ssDNA. Therefore, we tested if cohesin might disrupt end tethering by altering resection. In our qPCR assay, a reduction in the ratio indicates less DNA was present at the given time point compared to the no DSB control. Thus we could determine the level of resection. In WT cells, the ratio reduced to 0.68 at 2h post DSB, and 0.48 at 4h post DSB. In mre11 null cells the ratio reduced to 0.83 and 0.66 at 2 and 4h post DSB respectively, indicating that resection had slowed compared to WT cells. In contrast, the ratio reduced to 0.66 and 0.51 at 2 and 4h post DSB in Smc1 depleted cells. This demonstrates that loss of cohesin does not affect rates of resection. As such, loss of end tethering in cohesin depleted cells is not explained by reduced availability of ssDNA.

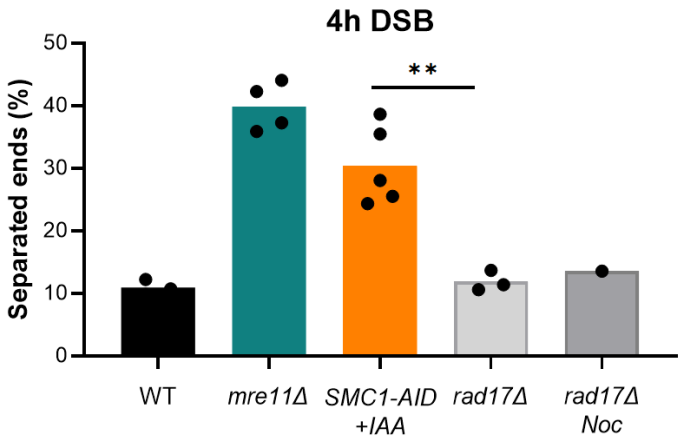

Figure 2. Rad17 is not required for DSB end-tethering. Percentage of cells with separated ends in the indicated strains after 4 hours DSB induction. Black stars indicate statistical differences (*= p<0,05; **= p<0,01; ***= p<0,005; ****= p<0,001). Shaded area indicates the 95% confidence interval of the fitting of 3 experiments per data set.

Result

A recent paper used Hi-C to measure chromosome contacts between both sides of an inducible DSB (Piazza et al., 2021). These contacts were lost in the absence of mre11, and as such were attributed to the tethering of DSB ends. The authors also implicated Rad17 of the 9-1-1 clamp in DSB end-tethering. Therefore, we tested DSB end-tethering in rad17 null cells using our live-cell microscopy assay. In contrast to Piazza et al., loss of Rad17 did not increase end separation in our system. This contradiction is important, as in contrast to our study, they did not observe loss of contacts upon depletion of cohesin subunits. These discrepancies will be addressed in detail in the discussion. This experiment was also performed in the presence of nocodazole, replicating the conditions used in the Piazza et al., study. End separation did not increase in the presence of nocodazole. However, this was only performed once and should be repeated.

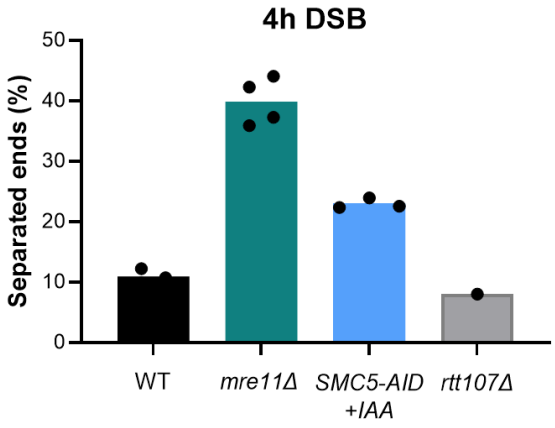

Figure 3. Rtt107 is not required for DSB end-tethering. Percentage of cells with separated ends in the indicated strains after 4 hours DSB induction. Black stars indicate statistical differences (*= p<0,05; **= p<0,01; ***= p<0,005; ****= p<0,001). Shaded area indicates the 95% confidence interval of the fitting of 3 experiments per data set.

Result

We demonstrate that Smc5/6 is important for DSB end-tethering in the cohesin pathway. In line with this, cohesin recruitment to DSBs is dependent on Smc5/6. We hypothesized that two Smc5/6 properties could recruit it to DNA DSBs and be important for cohesin end-tethering. One possibility is that Smc5/6 senses resected DSB ends through a domain in its hinge that preferentially binds ssDNA (Alt et al., 2017). The second is through an interacting partner, Rtt107, which was shown to be important for enrichment of Smc5/6 at DSBs (Leung et al., 2011). Rtt107 knockout did not increase end separation, indicating that it is not essential for DSB end tethering. Interestingly, Smc5/6 levels were still moderately elevated in the immediate vicinity of the DSB in absence of Rtt107 (Leung et al., 2011). This indicates that the Smc5/6 ssDNA binding affinity might be sufficient for recruitment to resected DNA at DSBs. These levels are sufficient for performing its role in promoting cohesin dependent end tethering. It would be interesting to determine if Rtt107 deletion reduces cohesin dependent genome compaction. It should also be checked if this residual recruitment is dependent on its ssDNA binding domain. This experiment was only performed once and as such should be repeated.

Article 2 – Telomere protein arrays stall DNA loop extrusion by condensin

Telomeres stall DNA loop extrusion by condensin

Brian T. Analikwu[1]*, Alice Deshayes[2]*, Jaco van der Torre[1], Thomas Guérin[3], Allard J. Katan[1], Claire Béneut[2], Roman Barth[1], Jamie Phipps[2], Vittore Scolari[4], Xavier Veaute[2], Christopher Barrington[5], Didier Busso[2], Frank Uhlmann[3], Karine Dubrana[2], Stefano Mattarocci[2$], Cees Dekker[1$], Stéphane Marcand[2$]

[1] Kavli Institute of Nanoscience Delft, Delft University of Technology, Delft, the Netherlands

[2] Université Paris-Saclay, Université Paris-Cité, CEA, Inserm, Institut de biologie François Jacob, UMR Stabilité Génétique Cellules Souches et Radiations, Fontenay-aux-Roses, France

[3] Chromosome Segregation Laboratory, The Francis Crick Institute, London, United Kingdom

[4] Institut Curie, PSL Research University, Sorbonne Université, Paris, France

[5] Bioinformatics and biostatistics, The Francis Crick Institute, London, United Kingdom

* Shared first author with equal contribution

[$] Corresponding authors: stefano.mattarocci@inserm.fr, c.dekker@tudelft.nl, stephane.marcand@cea.fr

ABSTRACT

DNA loop extrusion by SMC proteins is a key process underlying chromosomal organization. It is unknown how loop extruders interact with telomeres where DNA is covered with a dense array of proteins. Using complementary *in vivo* and *in vitro* single-molecule approaches, we study the interaction between loop-extruding condensin and Rap1, the DNA-binding telomeric protein of *Saccharomyces cerevisiae*. We show that dense linear Rap1 arrays can completely halt DNA loop extrusion, where the blocking efficiency depends on the array length and the DNA gap size between neighboring proteins. In cells, Rap1 arrays are found to act as contact insulators and to accumulate condensin at their borders, with direct implications for the resolution of dicentric chromosomes produced by telomere fusions. Our findings show that linear arrays of DNA-bound proteins can efficiently halt DNA loop extrusion by SMC proteins, which may impact cellular processes from telomere functions to transcription and DNA repair.

Keywords: telomere; condensin; SMC complexes; loop extrusion; dicentric chromosome; S. cerevisiae; single-molecule assay; chromatin

INTRODUCTION

Telomeres are essential protein-DNA complexes that ensure that chromosome ends escape the pathways acting on broken DNA ends. They consist of long stretches of DNA with repetitions of short motifs tightly covered by sequence-specific DNA-binding proteins such as Rap1 in budding yeast[1–4]. Because of the tight packing, access to telomere DNA is restricted for DNA-processing events such as transcription, DNA repair, and replication[5–12].

Here, we aim to shed light on the handling of such a tight DNA coverage at telomeres by a key organizer of chromosomal structure, the SMC complex (Structural Maintenance of Chromosomes) condensin. SMC complexes are motor proteins that extrude loops of DNA to organize chromatin into higher-order structures[13–20]. Condensin compacts chromosomes during mitosis via DNA loop extrusion[21–25] and is essential to chromosome segregation[26,27]. Condensin consists of two ATPase SMC coiled-coil subunits (Smc2 and Smc4), a kleisin (Brn1 in budding yeast), and two HEAT-repeat subunits (Ycs4 and Ycg1 in budding yeast). Yeast condensin acts as a monomeric protein complex that anchors DNA at the Brn1-Ycg1 interface and extrudes DNA into a loop from this anchoring point[15,18,28,29]. DNA loop extrusion is driven by ATP-dependent conformational changes and multiple dynamic DNA-protein contacts[18,30–32].

It is currently intensely studied whether loop extrusion by condensin and other SMC complexes can be blocked by DNA-binding proteins that may act as roadblocks for loop extrusion[33–37]. The DNA-binding protein CTCF, known to demarcate the boundaries of topologically associated domains (TADs)[35,38], was recently shown to block the SMC complex cohesin in a direction- and force-dependent manner through specific chemical interactions[34]. In the absence of a biochemical interaction, SMC complexes were, by contrast, found to be remarkably efficient at passing isolated physical roadblocks on the DNA *in vitro*[37]. However, in cells, chromosome-bound roadblocks are often not present as single obstacles at low density. For instance, RNA polymerases have been reported to stall SMC complexes at highly transcribed genes, perhaps as a consequence of DNA coverage by so-called polymerase trains[33,39–42].

Our previous work suggested that condensin may stall at telomeres[12]. Upon studying dicentric chromosome breakage in *Saccharomyces cerevisiae*, we found that dicentrics resulting from accidental telomere-telomere fusions preferentially broke at the fusion points[43] during abscission (septum closure in yeast)[12,44,45]. This restored the parental karyotype, therefore providing a backup pathway for telomere protection and genome stability. Breakage at telomere fusions requires two specific actors, namely condensin and the telomere DNA-binding protein Rap1. Condensin stalling by arrays of Rap1 might favour their capture at the abscission point, which would explain dicentric preferential breakage at telomere-telomere fusions[12].

Here we employ both *in vitro* single-molecule and *in vivo* approaches to directly address how arrays of Rap1 impact condensin-driven loop extrusion. Dense and tightly bound telomeric repeats provide a unique setting to systematically and mechanistically study this interaction. We show that telomere-Rap1 arrays inserted exogenously within a chromosome lead to an accumulation of condensin at their borders yielding a local boundary to chromatin compaction. By studying encounters between individual loop-extruding condensin complexes and Rap1 arrays in single-molecule visualizations, we show how ~100 nm arrays can stall condensin by physically blocking the loop extrusion with near-100% efficiency. Stalling is modulated by DNA tension and requires a high protein density on the DNA as small intra-array gaps sharply decrease the blocking. These results (i) impact our mechanistic biophysical understanding of DNA loop extrusion beyond single objects on the DNA, providing a unique example of linear protein arrays that block loop extrusion with an unprecedently high efficiency, (ii) provide evidence for the hypothesis that telomere-telomere fusions preferentially break at fusion points due to a force focusing organized by Rap1-mediated condensin stalling, (iii) uncovered a new feature of telomeres and (iv) more generally highlight the intricate interplay between SMC-driven chromosomal structure, local DNA stiffness, and protein occupancy.

RESULTS

Condensin is enriched at the border of Rap1 arrays

Stalling of condensin-driven DNA loop extrusion at dense telomere Rap1 arrays would result in a local accumulation of condensin at the edges of these arrays (**Fig. 1A**). To test this hypothesis, we engineered Rap1 binding-site arrays with a site density akin to native telomere sequences[12,46] into the genome. These arrays of 16 Rap1 sites consisted of pairs of two neighboring Rap1 sites (mutually separated by 1 bp) that were separated by a constant gap that was set at either 6 or 35-bp (**Fig. 1B** and Methods). Subsequently, we used chromatin immunoprecipitation (ChIP) to map condensin-DNA interactions in the vicinity of these arrays (**Fig. 1C, Fig. S1A**). To maximize the odds of condensin encountering the Rap1-bound array, we crosslinked cells that were synchronized in late anaphase (30 minutes after release from a *cdc15-2*^{ts} arrest)[12,22,45] because condensin-dependent chromosome-arm compaction in yeast peaks in anaphase[22].

We observed that an array of 16 closely spaced Rap1 sites (i.e., a dense array with 6-bp gaps) led to a 5-fold increase in the occurrence of condensin at the border of the array, relative to the level observed with an array made of mutated DNA sites that are incapable of binding Rap1[12] (**Fig. 1C**). This condensin accumulation decreased with the distance from the array, indicating that the accumulation was most strongly localized at the edge of the Rap1 array. We saw a similar local condensin enrichment at the border

of a native telomere (**Fig. S1B**). These data are in agreement with previous reports of condensin enrichment at the border of telomeres in budding yeast, fission yeast, and vertebrates during mitosis[47–49].

If this higher condensin abundancy resulted from the stalling of condensin-driven loop extrusion at the Rap1 array, a lower density of Rap1 sites could potentially alleviate this higher abundancy, for example by exposing bare DNA segments within the array that condensin could contact during the process of loop extrusion. To investigate this, we tested an array of 16 Rap1 sites that were spaced with a 35-bp bare DNA linker between every two successive sites (**Fig. 1B**). Since Rap1 binds uncooperatively to each site[50], such a spacer length should only impact the Rap1 density but not its high affinity[50]. As anticipated, lowering the Rap1 density strongly reduced the condensin accumulation at the border of the array (**Fig. 1C**). We conclude that condensin loop extrusion stalls at high-density Rap1 telomere arrays, but not at sparse arrays with a lower Rap1 density. Because the sparse arrays are longer than the dense arrays, this stalling is primarily due to the high local density of proteins rather than the length of the array.

To assess whether loop extrusion stalling is due to a purely physical blockade of the protein array, as opposed to possible chemical interactions, we engineered the 35-bp linker sequence to contain a *LacO* site that can be bound by lacI, thus filling the gaps between the Rap1 proteins. Notably, LacI and Rap1 bind their respective site with similar affinities[50–52]. The expression of LacI in cells harboring these 35-bp linker sequences resulted in a strongly increased abundancy of condensin at the border of the array, to the same level as the 6-bp spaced dense array (**Fig. 1C**). These findings indicate that DNA loop extrusion by condensin is stalled by the protein array due to mere physical interactions, rather than due to chemical interactions with Rap1 specifically – implying that any long dense protein array on DNA will stall condensin-driven loop extrusion.

High-density Rap1 arrays stall loop extrusion *in vitro*

Previous *in vitro* experiments showed that, surprisingly, most single DNA-binding proteins hardly pose any barrier to loop-extruding condensin[37]. Condensin can even pass 200 nm DNA-bound beads that are larger than its ring size and accommodate those into the extruded loop[37]. Here, we used the same single-molecule-visualization assay to test whether high-density Rap1 arrays alone block loop extrusion. To this end, we inserted a Rap1 array into a long (42-kb) DNA molecule. The DNA constructs were incubated with purified and fluorescently labeled Rap1 at a 5x to 7x excess of protein to the number of Rap1 binding sites. Then, Rap1-bound DNA was flushed into a flow channel with a pegylated and biotinylated surface to which the biotinylated ends of the DNA molecules attached via biotin-streptavidin binding (**Fig. 2A**). Rap1 bound efficiently and specifically to its binding site under these conditions showing a near-100% binding efficiency and negligible off-target binding (see methods and **Fig. S2A-C**), in line with its high affinity *in vitro* ($K_D \approx$

3 nM)[50,52,53]. The residence time of Rap1 was measured under our imaging conditions (see methods and **Fig. S2D-G**), showing that Rap1 stayed bound to its binding site for much longer than our acquisition time for loop extrusion experiments (median residence time: 166 min, compared to <30 min acquisition). From these data we concluded that our linear Rap1 arrays were saturated with bound Rap1 proteins during the single-molecule experiments.

After binding our Rap1 protein arrays in the flow cells, we next added condensin (see Methods) to observe encounters between the arrays and loop-extruding condensin. High-density linear Rap1 arrays (16 Rap1 binding sites with 6-bp gap – same as used *in vivo*) were found to clearly stall loop extrusion. This was first visualized qualitatively in a buffer flow that was applied perpendicular to the direction in which DNA was inserted. **Figure 2B** shows the typical blocking behavior where a DNA loop (cyan) developed and got stalled as soon as it encountered the Rap1 array (red); **Figure 2C** shows a passing event, where the condensin bypassed the Rap1 array and accommodated that into the extruded DNA loop. To quantify blocking in the absence of any flow (avoiding effects of the flow-associated force), imaging was performed after buffer flow was stopped. Analysis on resulting kymographs (which show the fluorescent intensity along the DNA versus time) was performed as previously described[20]. To discern stalling from passing events, we defined 'stalling' as an event that displayed a vanishingly small distance between the Rap1 array and the extruded loop, as well as a plateau in both the loop size and the moving mean squared displacement (MSD) (see Methods and ref. [37]). By contrast, in passing events, the loop continued to grow and the moving MSD increased upon an encounter (cf. **Fig. 2B** and **Fig. 2C** for kymograph analysis). Subsequently, we estimated the blocking efficiency as the number of stalling events relative to the total number of encounters.

The high-density linear Rap1 arrays with 16 consecutively bound Rap1 proteins were found to very efficiently stall loop extrusion, with a blocking efficiency of 83 ± 8% (N=84) (**Fig. 2F**). This is an extremely high blocking efficiency, higher than measured for any other DNA-binding protein[37], and higher than measured for encounters between cohesin and CTCF which involve chemical interactions[34]. For a block of only two Rap1 binding sites, the blocking efficiency was by contrast very low (9 ± 8%, N=44), allowing condensin-mediated loop extrusion to simply pass Rap1 into its loop in the vast majority of encounters (**Fig. 2F**). Furthermore, we found that binding of merely the Rap1 DNA-binding domain (DBD, fragment 310-608 omitting the N- and C-termini of Rap1) to the high-density 16 Rap1-site array also blocked loop-extruding condensin with a high efficiency (72 ± 11%, N=65), similar to the full-length protein (i.e., no significant difference). This shows that it is the coverage of the DNA by protein, be it Rap1 or solely its DBD, which underlies efficient blocking of loop extrusion.

By contrast, sparse Rap1 arrays with 35-bp gaps between Rap1 tandems (as in **Fig. 1**), showed a very low blocking efficiency (12 ± 9%, N=49) similar to that for only two adjacent binding sites. Inserting LacI protein

into the gaps of the low-density array did, however, restore a high blocking efficiency (67 ± 22%, N=18), showing that the linear protein filament provides efficient blockage of DNA loop extrusion. In agreement with the *in vivo* findings (**Fig. 1C**), this demonstrates that stalling is primarily due to the high local density of proteins in the ~100 nm long array. The experiments with truncated Rap1 (DBD) and with LacI insertions indicate that there is no specific protein-protein interaction between Rap1 and condensin, but instead that stalling is due to a physical rather than a biochemical interaction.

Stalling of loop extrusion depends on array density, array length, and DNA tension

To better understand the underlying biophysical mechanism of loop extrusion stalling by the Rap1 arrays, we tested the dependence of stalling on a variety of parameters. First, we systematically examined the effects of array density on stalling. We performed our single-molecule loop-extrusion assay with Rap1 arrays that had increasingly larger gaps in between pairs of Rap1 proteins on the DNA (**Fig. 1B**). Building on our prior observation that another SMC complex, cohesin, is blocked by CTCF in a tension-dependent manner[34], we furthermore characterized the blocking efficiency as a function of DNA tension (ranging from 0-0.2 pN) exerted on the DNA at the time of encounter. These forces are well below the stalling force of condensin, which we previously reported at ~1 pN [54].

We observed an approximately linear dependence of the blocking efficiency on the gap size in all force regimes (**Fig. 3A**). While at relatively high tensions (>0.13 pN), a near-100% blocking was observed for the densest (6-bp gap) array, the blocking efficiency monotonously reduced with increasing gap sizes, to ~10% for the 35-bp gap array. At lower DNA tension, the blocking efficiency was reduced for all arrays. The monotonous decrease of the blocking efficiency with gap size did not, within the finite signal-to noise ratio, show a clear threshold-like behavior that one would expect if there were an enabling gap size that allows condensin to make contacts within the array.

To dissect the relation between loop extrusion stalling and the length of Rap1 arrays, we next measured the blocking efficiency of dense arrays (i.e., only 6-bp gaps) with 2, 6, 8, or 16 binding sites, i.e., arrays whose length ranges from 10 to 93 nm (see **Table S2**). We observed a strong increase of the blocking efficiency with array length for all force regimes, see **Fig. 3B**, where blocking was negligible for a single Rap1 pair, but very pronounced for the 16x Rap1 array. Interestingly, the blocking efficiency exhibits a more pronounced effect of the DNA tension at higher array lengths. This suggests that local bending of DNA, which is hampered at higher DNA tension, may be important to ongoing DNA loop extrusion[18,31,32].

These data show that stalling depends on array density as well as array length. Notably, in the lowest force regime, even the longest of the dense Rap1 arrays (16x Rap1 with 6-bp gaps) can still pass into the loop for

a sizeable fraction (~50%) of the encounters, which prompts us to hypothesize that condensin can occasionally grab even beyond the longest 93 nm array, in accordance with our previous measurements of the step sizes that showed that condensin occasionally makes steps larger than its ~40 nm diameter[54,55]. The biophysical process of loop extrusion likely involves a large conformational change of the SMC complex[18,30,32] as well as the polymer dynamics of the DNA (with its local Rap1 array) which is set by thermal fluctuations and polymer stiffness. Hence, we next turned to investigate how Rap1 influences the polymer properties of DNA.

To investigate how the stiffness of the Rap1 arrays depends on their density, we analyzed the structure of the arrays using atomic force microscopy (AFM). **Figure 3C** shows typical images of DNA molecules with bound Rap1 proteins, for a variety of gap sizes. The 16 Rap1 protein arrays with small (6 bp) to medium (20 bp) gaps were found to act as fairly stiff rods (in accordance with a previous report[56]) whereas the arrays became more flexible as the gap increased further to 35-bp (**Fig. 3C-E**), approaching the flexibility of bare DNA. To quantify the data, we measured the end-to-end lengths of the Rap1 arrays and normalized that to the measured contour length (**Fig. 3D**). For the densest arrays, the normalized end-to-end length approached unity, i.e., the end-to-end length thus roughly equaled the contour length, indicating that these arrays behave like stiff rods that do not bend over their length. Since the end-to-end length is only very weakly dependent on the stiffness in this length regime, quantitative conclusions about the intrinsic stiffness of the arrays cannot be drawn from these data. By contrast, the normalized end-to-end length decreased to a value of ~0.6 for the 35-bp gap arrays with a wide distribution, indicating a greater freedom to take on different possible conformations which points to a greater flexibility. Interestingly, the mean absolute end-to-end length displayed in **Figure 3E** was found to be approximately constant with gap size. As illustrated in the insets to **Figure 3E**, this implies that the end-to-end length of the stiff 6-bp array (which equals the 93 nm contour length) happens to be about the same as the end-to-end length of the highly flexible 35-bp array which has a contour length of 162 nm. Taken together, we conclude that the denser arrays are also stiffer, which may contribute to their loop extrusion blocking efficiency.

Condensin stalling at dense Rap1 arrays induces local chromatin decompaction in anaphase

Condensin stalling at Rap1 arrays should change local chromatin compaction in cells where condensin is active. We tested this prediction using a microscopy-based approach. We tagged two positions that were 48-kb apart on a chromosome arm with distinct LacO and TetO arrays that were bound by mCherry and GFP respectively[57] (**Fig. 4A**). By measuring the projected 2D distance between these two spots, we inferred the local degree of chromosome folding. The median distance between the two spots decreased in cells in anaphase compared to G1 cells. This chromosome compaction did, however, not occur in condensin-depleted cells (**Fig. 4A**, *smc2-AID* +IAA), indicating that it resulted from condensin activity during anaphase[22,58–61].

The insertion of a dense array (16 Rap1 sites with 6-bp gap) half-way between the two fluorescently tagged positions was found to have no impact in G1 cells (**Fig. 4A**), which was expected given the low condensin activity. It also indicates that the local DNA stiffening of the array had no impact on the chromosome compaction at this scale. In cells in anaphase, however, inclusion of the dense array increased the median distance between the two spots to ~400 nm, equivalent to the low compaction seen in G1. This indicates that a Rap1-bound array caused a local chromatin decompaction during anaphase. Lowering the Rap1 density of the array restored the anaphase compaction (cf. 30-bp gap in **Fig. 4A**). The sensitivity to Rap1 density shows that it is the condensin stalling at the array that causes the observed chromatin decompaction by preventing the formation of larger loops that brings the two spots in closer proximity.

To further validate this result, we used a MicroC approach[62,63] to quantify the frequency of contacts between adjacent chromatin regions in cells synchronized in late anaphase. Strikingly, a dense Rap1 array (16 Rap1 sites with 6-bp gaps) reduced the contacts of the telomere-proximal chromosome region with the rest of the chromosome arm (**Fig. 4B**, **Fig. S3**), the expected outcome of condensin stalling at the dense array. A sparse array (35-bp gaps, **Fig. 4B**, **Fig. S3**) and an array of mutated DNA sites incapable of binding Rap1 (**Fig. S3**) failed to insulate the telomere-proximal region, in accordance with condensin being able to extrude these arrays in an unhindered way. This shows that the reduced contact frequency caused by the dense array stems from a reduced frequency of loops that would bring DNA together from the two sides separated by the array.

Preferential breakage of dicentric chromosomes near Rap1 arrays is another anticipated outcome of condensin stalling at the arrays (**Fig. 4C**)[12]. We used this readout to test arrays with various Rap1 densities. Rap1 arrays of 16 binding sites with gaps ranging from 6 to 35-bp were inserted in a conditional dicentric chromosome, whose one centromere can be reversibly inactivated (**Fig. 4C**). To monitor dicentric breakage by abscission, we reactivated the conditional centromere in cells synchronously released from a G1 arrest. Cells were harvested either prior to dicentric breakage (nocodazole arrest) or after dicentric breakage in the next G1 (alpha factor arrest). Chromosome fragments were separated by Pulse Field Gel Electrophoresis (PFGE) and detected by Southern blot. In the absence of Rap1 arrays between centromeres, dicentric breakage preferentially occurred near the centromeres (**Fig. S4**)[12,45].

We observed a strong dependence of dicentric breakage on the gap size. Only high-density arrays focused the breakage at the array, while low-density arrays with gaps of 30 and 35-bp failed to do so (**Fig. 4D**). Ectopic expression of bacterial LacI restored a strong breakage at the arrays with the 35-bp gap sequence containing a *LacO* site, as reported previously[12]. This effect was attenuated when utilizing a LacI* allele with

a reduced *LacO* affinity (**Fig. 4D**)[64]. These *in vivo* results further indicate that continuous high-affinity protein binding along the array on DNA is a key feature needed to stall condensin.

DISCUSSION

This work shows that DNA coverage by a telomere protein strongly modulates condensin loop extrusion activity *in vivo* and *in vitro*. DNA-loop-extruding condensin stalls at encounters with telomere-like arrays of Rap1 protein bound on DNA in a length- and density-dependent manner. While individual DNA-bound roadblocks can easily pass into the extruded loop[37], a dense coverage of DNA by proteins halts loop extrusion. Such a stalling of loop extrusion results in a local boundary to chromosomal compaction during anaphase. Notably, these telomeric protein arrays exhibit a remarkable stability as the Rap1 residence time on DNA is of the order of hours (**Fig. S2E**), which is much longer than the inverse stepping rate of the loop extrusion.

Our observations have implications for our biophysical understanding of loop extrusion by SMC complexes. Rap1 binding into a closely spaced array that covers the DNA makes this region inaccessible to a loop extruder. We found that small gaps in the array facilitate passage, and larger gaps of ~30-bp even allow unhindered loop extrusion through the array (**Fig. 1C**, **Fig. 2F**, **Fig. 3A**, **Fig. 4**). While the data thus clearly point to a steric hindrance effect where Rap1 precludes the availability of DNA as a substrate for loop extrusion, it is of interest to ask whether the increased local stiffness plays a role as well, since Rap1 binding stiffens the DNA. Such a stiffening can potentially hinder loop extrusion in two ways. First, it may be energetically costly to reel the new DNA within the SMC lumen due to its reduced flexibility, as current models for loop extrusion predict a significant bending of DNA during a loop extrusion step[18,32,54,55,65–68]. Second, a stiffer Rap1 array positions the next freely accessible DNA further away from condensin, making it less likely that the SMC can reach beyond the array. While we observed differences between Rap1 arrays of varying length and density, it is difficult to disentangle the effects of density and stiffness, and therefore we cannot unambiguously determine the relative importance of the stiffness. The data call for a detailed mechanistic model and simulations of loop extrusion of DNA with a local array of varying stiffness. Summing up, we conclude that the dense linear protein arrays stall condensin by reducing the amount of freely accessible DNA that can be grabbed and processed by condensin, as well as potentially by inhibiting the incorporation of the array into the loop and by distancing the freely accessible DNA to positions beyond the array.

Condensin stalling by Rap1 at telomere-telomere fusions favours dicentric breakage near the fusion points. This mechanism provides a back-up for telomere protection and contributes to genome stability[43]. As corroborated by microscopy and MicroC analyses (**Fig. 4A&B**), we find that dense Rap1 arrays establish

boundaries to loop extrusion during anaphase, resulting in local chromatin insulation. This reveals a mechanism underlying the positioning of dicentric breakage at telomere-telomere fusions. In anaphase, the connection of centromeres to the spindle poles stretches dicentric anaphase bridges. As telophase progresses, the disassembly of the mitotic spindle and the detachment of the spindle poles from the cell cortex allow condensin to recoil the dicentric bridges prior to septum closure[12,45]. Condensin stalling at telomere-telomere fusions will favour the creation of two distinct domains, one in each nuclear lobe, out of the two chromosome regions that are separated by the fusion point. This spatial insulation will direct the telomere-telomere fusion toward the midzone, where the septum grows, thus resulting in its entrapment and breakage by abscission.

Our findings show that the repeated nature of telomeres and the consequential dense DNA coverage yield a unique 1D property: the ability to inhibit protein machines acting along the DNA. The blocking of SMC-driven loop extrusion could apply more broadly to other activities whose control is important to telomere functions. Apart from its role in resolving dicentric chromosomes, it is conceivable that condensin stalling at native unfused telomeres contributes to their accurate segregation (**Fig. S5**). Without such stalling, loop extrusion would proceed unhindered until the end of chromosomes, where condensin would run off the DNA, leaving the chromosome ends uncompacted. Instead, a stalling of loop extrusion at the chromosome ends ensures their individualization and proper compaction, facilitating their correct segregation prior to cell division. In this way, condensin stalling at telomeres might further contribute to genome stability.

As we found that extended linear protein filaments can stall condensin-driven loop extrusion remarkably efficiently, it is of interest to ask whether this result can be generalized, i.e., whether linear protein filaments more generally block SMCs to extrude loops of DNA. Several observations indicate that this indeed may be the case. DNA repair of double-stranded breaks (DSBs) features a stage where DNA is coated with dense protein arrays, and it was reported that cohesin accumulates at these filaments[69,70]. While it is commonly assumed that cohesin is specifically loaded at DSB sites[70], loop extrusion could play a role in targeting cohesin to these sites[71,72]. Furthermore, it was shown that highly transcribed genes significantly slow down loop-extruding SMC complexes[33,40,41]. Possibly this can be attributed to a local dense coverage of DNA by RNA-polymerases that line up in long 'trains'. Finally, as the linker length needed for loop extrusion through Rap1 arrays approximates the average spacing between nucleosomes[73], it will be of interest to see if dense nucleosome fibres block SMCs. The tension that condensin can exert on chromatin (<1 pN[15]) is insufficient to unwrap nucleosomes[74] but may be sufficient to stretch them[75,76], which could help to expose the internucleosomal DNA for capture by the SMC complex during loop extrusion, a hypothesis that remains to be tested.

Loop extrusion stands as a universally conserved mechanism across the SMC family[15–17,19,20,32]. While we presented a detailed study of condensin and Rap1 in *S. cerevisiae,* we estimate that our findings have a general significance and likely also hold for other SMCs and other protein filaments – providing an important control element for chromosome organization.

MATERIALS & METHODS

Strains

All yeast strains used in this study are listed in **Table S1**.

Cell cycle synchronization

To synchronized cells in late anaphase (ChIP and MicroC experiments), exponentially growing cells carrying the *cdc15-2* thermosensitive allele were arrested at restrictive temperature (36°C) for about 90 minutes prior to be shifted back at permissive temperature (25°C) for 30 minutes. To assess dicentric breakage, cells growing exponentially in galactose-containing synthetic medium (*CEN6* OFF) were arrested in G1 with α-factor (10^{-7} M). Cells were released from the G1 arrest with two washes in glucose-containing rich medium (YPD). Half the culture was complemented with nocodazole (5 µg/mL) to arrest the cells in G2/M. The other half was complemented with α-factor (10^{-7} M) about one hour after the washes to arrest the cells in the next G1.

Pulse-Field Gel Electrophoretic (PFGE) and Southern blot

Yeast DNA embedded in agarose plugs was prepared as described [12] with minor modification (see supplementary information). Pulse-field gel electrophoresis was carried out in a 0.9% agarose gel in 0.5× TBE at 14°C with a CHEF DR III from Bio-Rad with a constant switch time of 20 s during 24 h. Gel-Red labeled DNA was detected by a Typhoon scanner. DNA transferred to a nitrocellulose member was hybridized with ^{32}P-labeled *TUB2* (chr. 6 probe) and *POL4* (chr. 3 probe) fragment as previously described [12].

Distance measurements by microscopy of cells

Exponential growing cells (0.8 OD) in rich medium (YPD) were washed in synthetic medium prior to live-cell imaging with a wide-field inverted microscope (Leica DMI-6000B) equipped with Adaptive Focus Control to eliminate Z drift, a 100×/1.4 NA immersion objective with a Prior NanoScanZ Nanopositioning Piezo Z Stage System, a CMOS camera (ORCA-Flash4.0; Hamamatsu), and a solid-state light source (SpectraX, Lumencore). The system is piloted by MetaMorph software (Molecular Device). 2mM Indole-3-acetic acid (IAA) was added to exponential growing *smc2-AID* cells in YPD for 1 hour prior to imaging.

GFP and mCherry two-color images were acquired over 19 focal steps of 0.2µm using solid state 475 and 575nm diodes and appropriate filters (GFP-mRFP filter; excitation: double BP, 450–490/550–590nm and dichroic double BP 500–550/600–665nm; Chroma Technology Corp.). Acquisition of both

wavelengths was completed on each focal plane with an exposure time of 50ms, before 0.2µm steps, to minimise the possibility of array movement between acquisitions of each wavelength. A single bright-field image on one focal plane was acquired at each time point with an exposure of 50ms. All images shown are maximum intensity z projections of z-stack images.

Image analysis was achieved following processing with ImageJ Fiji software, using scripts written in ImageJ macro language. Briefly, local maxima that define GFP and mCherry fluorescent array positions were determined from 2D maximal projections of three-dimensional data sets. Fluorescent signals within cells were confirmed manually from 3 color merged images. The distance between the two closest GFP and mCherry maxima was calculated using their extracted XY coordinates in R software (v4.1.1).

ChIP

ChIP experiments were carried out as previously described with minor modifications [77,78].

MicroC-XL

Micro-C was done following a mixed protocol described previously[63,79] with minor modification. Briefly, 55 OD anaphase blocked yeast cultures were crosslinked with 3% formaldehyde for 15 min at 30°C. The reactions were quenched with 250 mM glycine at 30°C temperature for 5 min with agitation. Cells were pelleted by centrifugation at 4000 rpm at 4°C for 5 min and washed twice with water. Cells were then resuspended in Buffer Z (1M sorbitol, 50 mM Tris-HCl pH 7.4, 10 mM β-mercaptoethanol) and spheroplasted by addition of 250 ug/mL Zymolyase (MP08320932) at 30°C in an incubator at 200 rpm for 40 to 60 minutes. Spheroplasts were washed once by 4°C PBS and then pelleted at 4000 rpm at 4°C for 10 min. Pellets were re-crosslinked by addition of PBS supplemented with 3 mM disuccinimidyl glutarate (ThermoFisher #20593) and incubated at 30°C for 40 min with gentle shaking before quenching by addition of 400 mM final glycine for 5 minutes at 30°C. Cells were pelleted by centrifugation at 4000 rpm at 4°C for 10 min, washed once with ice-cold PBS and stored at −80°C. Pellets were treated as previously described[63] up to the decrosslink part. Decrosslink solution was added with an equal volume of Phenol:Chloroform:Isoamyl Alcohol (25:24:1), vortexed intensively centrifuged for 15 minutes at room temperature. The aqueous phase loaded and purified on ZymoClean column according to the manufacturer protocol. Dinucleosomes were purified and excised from a 3% NuSieve GTG agarose gel (Lonza #50081) using Zymoclean Gel DNA Recovery Kit (Zymo #D4008). Micro-C libraries were prepared using the NEBNext Ultra II DNA Library Prep Kit for Illumina (NEB #E7645) following[79] manufacturer instructions and sequenced on the Illumina NovaSeq 6000 platform.

Micro-C datasets were analysed using the Distiller pipeline (https://github.com/open2c/distiller, commit 8aa86e) to implement read filtering, alignment, PCR duplicate removal, and binning and balancing of replicate and sample matrices. Reads were aligned to W303 using bwa 0.17.7 and the

resulting maps filtered to remove low-quality alignments (MAPQ<30) and cis alignment pairs within 150 bp. Replicates were analysed independently, and their quality assessed before aggregation into sample-level datasets. Maps were visualized and explored using Higlass[80].

DNA preparation for single-molecule-visualization assay

42-kb Linear cosmid-i95 plasmids with inserted sequences were prepared as previously reported[37,81]. First, the i95-cosmid was linearized with PsiI-v2 (New England Biolabs). Second, the remaining 5'-phosphate groups were dephosphorylated using calf-intestinal alkaline phosphatase for 10 minutes at 37°C and finally heat inactivated for 20 min at 80°C (Quick CIP, New England Biolabs). The Rap1 arrays initially cloned in a pUC19-derived vector (**Table S2**) were digested with PvuII (New England Biolabs) and subsequently gel isolated. The fragments were ligated together by using a T4 DNA ligase in T4 ligase buffer (New England Biolabs), with 1 mM ATP overnight at 16°C. The final constructs were transformed into *E. coli* NEB 10-beta cells (New England Biolabs) and all constructs were sequence verified using plasmidsaurus Oxford Nanopore long read sequencing. Inserted sequences are listed in **Table S2**. To linearize these cosmids and prepare them for flow cell insertion, the cosmids were isolated using a Midiprep and a QIAfilter plasmid midi kit (QIAGEN). The cosmids were then digested for 2 hours at 37°C and heat-inactivated for 20 minutes at 80°C using SpeI-HF (New England Biolabs). Next, 5'-biotin handles were constructed by a PCR reaction from a pBluescript SK+ (StrataGene) using 5'-biotin primers JT337 (Bio- AGAATAGACCGAGATAGGGTTGAGTG) and JT338 (Bio-GGCAGGGTCGGAACAGGAGAG). The PCR fragment was then digested by the same procedure as for the large cosmid, resulting in ~600-bp 5'-biotin handles, which were mixed with the digested cosmids in a 10x excess before ligation by T4 DNA ligase in T4 ligase buffer (New England Biolabs) at 16°C overnight. The reaction was subsequently heat-inactivated at 65°C for 25 min. The final linear construct was cleanup using an ÄKTA Start (Cytiva), with a homemade gel filtration column containing 46 mL of Sephacryl S-1000 SF gel filtration media, run with TE + 150 mM NaCl buffer at 0.5 mL/min.

Protein purification and fluorescent labelling

His6-TEV-4G-ScRap1-1-827 (Rap1 full length) was induced with 0.5 mM isopropyl-β-D-thiogalactoside (IPTG) four hours at 30 °C into *E. coli* strain BL21 (DE3) STAR (Invitrogen). All of the subsequent protein purification steps were carried out at 4 °C. Cells were harvested, suspended in lysis buffer (50 mM Tris HCl [pH8@4 °C], 1M NaCl, 1 mM DTT, 20 mM Imidazole 1 mg/mL lysozyme, 1 mM 4-(2-aminoethyl) benzenesulphonyl fluoride (AEBSF), 10 mM benzaminide, 2 µM pepstatin) and disrupted by sonication. Extract was cleared by centrifugation at 186,000*g* for 1 hour at 4 °C and then incubated at 4 °C with NiNTA resin (QIAGEN) for 4 h. Mixture was poured into an Econo-Column®Chromatography column (BIO-RAD). After extensive washing of the resin first with buffer A (20 mM Tris HCl [pH8@4 °C], 500 mM NaCl, 1 mM DTT, 20 mM Imidazole) and then with buffer B (20 mM Tris HCl [pH8@4 °C], 100 mM NaCl, 1 mM DTT, 40 mM Imidazole), protein was eluted with buffer B complemented with 400 mM imidazole. Fractions

containing purified His6-TEV-4G-ScRap1-1-827 were pooled and applied to a ResourceQ 1ml column (Cytiva) equilibrated with buffer C (20 mM Tris HCl [pH8@4 °C], 100 mM NaCl, 1 mM DTT, 1mM EDTA). Protein was eluted with a 20 mL linear gradient of 0.1–1 M NaCl. Fractions containing the purified protein were pooled and directly applied to a 1 ml HiTrap Heparin HP column (Cytiva) equilibrated with buffer C. A 30 mL linear gradient of 0.1-0.8 M NaCl was performed. TEV protease was added to the pooled fractions containing purified His6-TEV-4G-ScRap1-1-827 and the mixture was directly dialyzed against buffer D (20 mM Tris HCl [pH8@4 °C], 150 mM NaCl, 1 mM DTT, 1mM EDTA) at 4°C overnight. The mixture was then incubated with NiNTA resin (QIAGEN) for 2 hours and the purified 4G-ScRap1-1-827 without its His6-TEV tag was recovered into the flow trough. Concentration was determined using Bradford protein assay with BSA as standard. 4G-ScRap1-310-608 (Rap1 DBD) was purified with the same protocol except the HiTrap Heparin HP column which was omitted.

Rap1 protein was subsequently labelled with Janelia Fluor 646 (JF646) using a sortase reaction followed by ÄKTA purification in a MonoQ column against a 1M NaCl gradient. The labelling efficiency of Rap1-JF646 was estimated to be about 70% from the fluorophore and protein concentrations. *S. cerevisiae* condensin was purified as described in Ganji et al.[15].

Single-molecule-visualization assay

For the single-molecule loop extrusion assay, flow cells were prepared as previously reported[15]. Briefly, glass slides and coverslips were cleaned using successive rounds of sonication in acetone and 1M KOH followed by piranha etching. The glass surface was functionalised using aminosalinization and the surface was passivated using mPEG-SVA (Laysan Bio) and MS(PEG)$_4$-NHS-Ester (Laysan Bio) in the presence of biotin-PEG-SVA (Laysan Bio). Before experiments, the flowcell was briefly incubated with streptavidin (MP Biomedicals) in T20 buffer (40 mM tris-HCl pH 8.0, 20 mM NaCl, 0.2 mM EDTA) and with 5 mg/ml BSA (ThermoFisher Scientific) also in T20 buffer. Rap1 was bound to the long linear constructs by incubating at room temperature at a 5-fold excess of protein to binding site for at least 1h in 100 mM KGlu, 2.5 mM $MgCl_2$, 20 mM Tris pH 7.4, 1 mM DTT, 0.25 mg/ml BSA. After incubation, the Rap1-DNA complex was flushed into the flowcell. DNA was visualized by adding 100 nM SytoxOrange (SxO) DNA dye. Unbound complexes were flushed out and the buffer was changed to loop extrusion/imaging buffer (50 mM KGlu, 2.5 mM $MgCl_2$, 40 mM Tris pH 7.5, 2 mM Trolox, 1 mM DTT, 0.25 mg/ml BSA, 5% glucose, 10 nM catalase, 18.75 nM glucose oxidase, 2 mM ATP). Purified yeast condensin was added at 2 nM in imaging buffer at a flow rate of 0.5 µL/min until loops were observed and the flow was stopped. Imaging was done with a HILO microscope, as previously described[15], with a red (637 nm, 15 mW) and a green laser (561 nm, 0.2 mW) in alternating light excitation mode.

Rap1-DNA binding efficiency, specificity, and residence time

Binding efficiency was estimated to be near-100% from fluorophore bleaching in our single-molecule fluorescence visualization assay. To this end, Rap1-JF646 was incubated with linear constructs that contain 2 tandem Rap1 binding sites. After flushing the binding reaction into the flow cell, bleaching was done at 25mW power with the 637 nm laser. Individual fluorescent spots were tracked and their fluorescence plotted as in **Fig. S2A**. The number of observed bleaching steps were counted for 46 spots using a step-finding hidden Markov model (sfHMM)[82]. As shown in **Fig. S2B**, half of the traces showed 1 and the other half showed 2 bleaching steps (50 ±14%, N=46). This distribution of bleaching steps is in good accordance with the 70% labelling efficiency, from which we expect to observe 54% of traces with a Rap1-JF646 signal to show two steps if both binding sites are occupied ($E^2/(E^2 + 2E(1-E))$, where E is the labelling efficiency). There is no significant difference between the expected 54% and our observed 50% (p=0.16, one-sided binomial test), indicating a near-100% binding efficiency. Binding specificity was visualized using the binding positions along the DNA molecule from the same bleaching experiment (**Fig. S2C**). The Rap1 binding sites were positioned at roughly 40% along the DNA.

To measure the residence time (**Fig. S2D-G**) of Rap1 to its binding site, we used an assay similar to that described above for determining the binding specificity. Briefly, we used a DNA construct with 2 tandem Rap1 binding sites, incubated with Rap1 at a ratio of protein to binding site of 10, for >1h at room temperature. Imaging was performed in the imaging buffer described above without ATP with an oxygen scavenger system to minimize photobleaching (50 mM KGlu, 2.5 mM $MgCl_2$, 40 mM Tris pH 7.5, 2 mM Trolox, 1 mM DTT, 0.25 mg/ml BSA, 5% glucose, 10 nM catalase, 18.75 nM glucose oxidase). The constructs were imaged for 3h with infrequent imaging (1 image per 4s) to reduce photobleaching for this long measurement. Data was analyzed similar to described above, where unbinding events were counted as a downward step in kymographs, and steps were analyzed using sfHMM[82].

Atomic force microscopy

For AFM imaging, short DNA fragments containing Rap1 binding site arrays were produced. The same Rap1 arrays as for the single-molecule loop extrusion were cut with PvuII (New England Biolabs) and fragments containing Rap1 repeats were separated from the backbone using a similar ÄKTA procedure as mentioned above: ÄKTA Start (Cytiva) with a homemade gel filtration column containing 46 mL of Sephacryl S-1000 SF gel filtration media, run with TE + 150 mM NaCl buffer at 0.5 mL/min. To concentrate the sample, we used the vacufuge plus speedvac (Eppendorf) to reduce the volume. Next, the Rap1 array fragments were dialyzed to water to remove excess salt. Final concentration of DNA fragments was between 1 and 14 nM.

Samples were prepared by mixing DNA at a concentration of 0.5 nM with Rap1 to a protein:binding site ratio of 4.1. We used the same fluorescently labelled full-length Rap1 proteins as in the single-molecule visualization assay. Samples were incubated in a similar buffer as for the single-molecule visualization assay:

100 mM KGlu, 20 mM Tris pH 7.4, 1 mM DTT. Some of the samples had slightly higher ratios of protein to binding site due to a calculation error, but we found no significant effect on the binding in this concentration regime.

For surface deposition and measurement, we prepared mica substrates by punching 3.2 mm mica discs from mica sheets (V4 grade, SPI supplies) and gluing them to magnetic stainless steel discs with 2-component epoxy glue. The mica discs were cleaved with adhesive tape before each preparation to provide a clean surface. To ensure stable adhesion of the DNA to the mica surface, poly-L-lysine (PLL) was deposited onto the mica at a concentration of 0.01% (w/v), incubated for 3 minutes, washed with pure water and dried in a stream of nitrogen. We found that shorter incubation of the PLL, as well as the use of poly-L-orthinine instead of PLL, would lead to incomplete coverage of the mica, which promoted alignment of parts of the DNA molecules along straight lines separated by angles of 60 degrees, presumably parallel to the crystal axes of the mica. DNA-Rap1 samples were incubated for 45-90 minutes at room temperature (21°C) and then 3 µl drops were deposited onto the PLL-coated mica substrates. After 1 minute, the sample was gently washed using 200 µl of buffer applied and extracted with two separate pipettes. The sample was then placed onto the microscope and imaged in buffer. The microscope was a Bruker Multimode, with NanoScope V controller and version 9.1 Nanoscope software. The imaging mode was PeakForce QNM, with a tapping frequency of 4 kHz and a force setpoint and amplitude manually tuned for optimal image quality, typically 100 pN and 12 nm. Images were acquired with a pixel size of 2 nm, and processed for subtraction of background artifacts using the 'align rows' and 'remove polynomial background' filters in Gwyddion[83].

To analyze the contour lengths and array end-to-end lengths, we used a homebuilt Matlab analysis package named DNAcontour. This package in the version that was used to produce the data presented here, is available at https://gitlab.tudelft.nl/allards-matlab-repo/allards-matlab-repo/-/tree/RAP1_paper/DNAcontour. To automatically select DNA molecules from AFM images, we first applied smoothing using a multi-pass Gaussian blur, followed by thresholding and filtering based on a potential DNA molecule's height, size, and aspect ratio. To calculate the trajectories of the DNA molecules, they were skeletonized and resulting branches were connected. The initial guess for trajectories was obtained by connecting the branches with Dijkstra's algorithm and taking the longest shortest path between endpoints. These trajectories were manually corrected where needed and the start- and endpoints of the Rap1 arrays were manually annotated. The obtained trajectories were then iteratively refined by optimizing the trajectories for the local maxima in a smooth curve. The end-to-end lengths were then calculated as the distance between the endpoints of the Rap1 arrays and the contour length was determined from the length of the DNA trajectories as shown in Fig. 3D.

ACKNOWLEDGMENTS

We thank Milos Tisma, Theo Koenig, Eric Le Cam, Olivier Pietrement, Gerard Mazón, Armelle Lengronne, Jonathan Heuze, Olivier Alibert, Stéphane Coulon, Sylvie Tournier, Pascal Bernard, Frédéric Beckouet, Sabrina Pobieaga and Florian Roisné-Hamelin for discussions, Anders Barth for help with determining the Rap1 labelling efficiency, and Eli van der Sluis and Ashmiani van den Berg for purifying condensin and LacI proteins. Research in the laboratory of S.M. was supported by grants from *Agence Nationale de la Recherche* (ANR-14-CE10-021 DICENS, ANR-15CE12-0007 DNA-Life), *Fondation ARC pour la Recherche sur le Cancer*, *Ligue contre le Cancer*, CEA Radiation biology program and GGP CEA EDF program. A.D. was supported by a PhD fellowship from CEA and a *Ligue contre le Cancer* young researcher grant. Research in the laboratory of C.D. was supported by ERC Advanced Grant 883684 (DNA looping) NWO grant OCENW.GROOT.2019.012, and the BaSyC program.

REFERENCES

1. de Lange, T. Shelterin-Mediated Telomere Protection. *Annu. Rev. Genet.* **52**, 223–247 (2018).

2. Wellinger, R. J. & Zakian, V. A. Everything You Ever Wanted to Know About *Saccharomyces cerevisiae* Telomeres: Beginning to End. *Genetics* **191**, 1073–1105 (2012).

3. Galati, A., Micheli, E. & Cacchione, S. Chromatin Structure in Telomere Dynamics. *Front. Oncol.* **3**, (2013).

4. Soman, A., Korolev, N. & Nordenskiöld, L. Telomeric chromatin structure. *Current Opinion in Structural Biology* **77**, 102492 (2022).

5. Negrini, S., Ribaud, V., Bianchi, A. & Shore, D. DNA breaks are masked by multiple Rap1 binding in yeast: implications for telomere capping and telomerase regulation. *Genes Dev.* **21**, 292–302 (2007).

6. Makovets, S., Herskowitz, I. & Blackburn, E. H. Anatomy and Dynamics of DNA Replication Fork Movement in Yeast Telomeric Regions. *Mol Cell Biol* **24**, 4019–4031 (2004).

7. Miller, K. M., Rog, O. & Cooper, J. P. Semi-conservative DNA replication through telomeres requires Taz1. *Nature* **440**, 824–828 (2006).

8. Maestroni, L. *et al.* Nuclear envelope attachment of telomeres limits TERRA and telomeric rearrangements in quiescent fission yeast cells. *Nucleic Acids Research* **48**, 3029–3041 (2020).

9. Marcand, S., Pardo, B., Gratias, A., Cahun, S. & Callebaut, I. Multiple pathways inhibit NHEJ at telomeres. *Genes Dev.* **22**, 1153–1158 (2008).

10. Zimmermann, M., Kibe, T., Kabir, S. & de Lange, T. TRF1 negotiates TTAGGG repeat-associated replication problems by recruiting the BLM helicase and the TPP1/POT1 repressor of ATR signaling. *Genes Dev.* **28**, 2477–2491 (2014).

11. Goto, G. H. *et al.* Binding of Multiple Rap1 Proteins Stimulates Chromosome Breakage Induction during DNA Replication. *PLoS Genet* **11**, e1005283 (2015).

12. Guérin, T. M. *et al.* Condensin-Mediated Chromosome Folding and Internal Telomeres Drive Dicentric Severing by Cytokinesis. *Molecular Cell* **75**, 131-144.e3 (2019).

13. Yatskevich, S., Rhodes, J. & Nasmyth, K. Organization of Chromosomal DNA by SMC Complexes. *Annu. Rev. Genet.* **53**, 445–482 (2019).

14. Goloborodko, A., Marko, J. F. & Mirny, L. A. Chromosome Compaction by Active Loop Extrusion. *Biophysical Journal* **110**, 2162–2168 (2016).

15. Ganji, M. *et al.* Real-time imaging of DNA loop extrusion by condensin. *Science* **360**, 102–105 (2018).

16. Davidson, I. F. *et al.* DNA loop extrusion by human cohesin. *Science* **366**, 1338–1345 (2019).

17. Taschner, M. & Gruber, S. *DNA segment capture by Smc5/6 holo-complexes*. http://biorxiv.org/lookup/doi/10.1101/2022.10.09.511515 (2022) doi:10.1101/2022.10.09.511515.

18. Shaltiel, I. A. *et al.* A hold-and-feed mechanism drives directional DNA loop extrusion by condensin. *Science* **376**, 1087–1094 (2022).

19. Liu, H. W. *et al.* DNA-measuring Wadjet SMC ATPases restrict smaller circular plasmids by DNA cleavage. *Molecular Cell* **82**, 4727-4740.e6 (2022).

20. Pradhan, B. *et al. The Smc5/6 complex is a DNA loop extruding motor*. http://biorxiv.org/lookup/doi/10.1101/2022.05.13.491800 (2022) doi:10.1101/2022.05.13.491800.

21. Lioy, V. S. *et al.* Multiscale Structuring of the E. coli Chromosome by Nucleoid-Associated and Condensin Proteins. *Cell* **172**, 771-783.e18 (2018).

22. Lazar-Stefanita, L. *et al.* Cohesins and condensins orchestrate the 4D dynamics of yeast chromosomes during the cell cycle. *EMBO J* **36**, 2684–2697 (2017).

23. Shintomi, K. *et al.* Mitotic chromosome assembly despite nucleosome depletion in *Xenopus* egg extracts. *Science* **356**, 1284–1287 (2017).

24. Gibcus, J. H. *et al.* A pathway for mitotic chromosome formation. *Science* **359**, eaao6135 (2018).

25. Dey, A., Shi, G., Takaki, R. & Thirumalai, D. Structural changes in chromosomes driven by multiple condensin motors during mitosis. *Cell Reports* **42**, 112348 (2023).

26. Cuylen, S., Metz, J., Hruby, A. & Haering, C. H. Entrapment of Chromosomes by Condensin Rings Prevents Their Breakage during Cytokinesis. *Developmental Cell* **27**, 469–478 (2013).

27. Renshaw, M. J. *et al.* Condensins Promote Chromosome Recoiling during Early Anaphase to Complete Sister Chromatid Separation. *Developmental Cell* **19**, 232–244 (2010).

28. Lee, B.-G., Rhodes, J. & Löwe, J. Clamping of DNA shuts the condensin neck gate. *Proc. Natl. Acad. Sci. U.S.A.* **119**, e2120006119 (2022).

29. Kschonsak, M. *et al.* Structural Basis for a Safety-Belt Mechanism That Anchors Condensin to Chromosomes. *Cell* **171**, 588-600.e24 (2017).

30. Diebold-Durand, M.-L. *et al.* Structure of Full-Length SMC and Rearrangements Required for Chromosome Organization. *Molecular Cell* **67**, 334-347.e5 (2017).

31. Nomidis, S. K., Carlon, E., Gruber, S. & Marko, J. F. DNA tension-modulated translocation and loop extrusion by SMC complexes revealed by molecular dynamics simulations. *Nucleic Acids Research* **50**, 4974–4987 (2022).

32. Dekker, C., Haering, C. H., Peters, J.-M. & Rowland, B. D. How do molecular motors fold the genome? *Science* **382**, 646–648 (2023).

33. Brandão, H. B. *et al.* RNA polymerases as moving barriers to condensin loop extrusion. *Proc. Natl. Acad. Sci. U.S.A.* **116**, 20489–20499 (2019).

34. Davidson, I. F. *et al.* CTCF is a DNA-tension-dependent barrier to cohesin-mediated loop extrusion. *Nature* **616**, 822–827 (2023).

35. Wendt, K. S. *et al.* Cohesin mediates transcriptional insulation by CCCTC-binding factor. *Nature 2008 451:7180* **451**, 796–801 (2008).

36. Li, Y. *et al.* The structural basis for cohesin–CTCF-anchored loops. *Nature* **578**, 472–476 (2020).

37. Pradhan, B. *et al.* SMC complexes can traverse physical roadblocks bigger than their ring size. *Cell Reports* **41**, 111491 (2022).

38. Nanni, L., Ceri, S. & Logie, C. Spatial patterns of CTCF sites define the anatomy of TADs and their boundaries. *Genome Biology* **21**, 197 (2020).

39. Rivosecchi, J. *et al.* RNA polymerase backtracking results in the accumulation of fission yeast condensin at active genes. *Life Sci. Alliance* **4**, e202101046 (2021).

40. Banigan, E. J. *et al.* Transcription shapes 3D chromatin organization by interacting with loop extrusion. *Proceedings of the National Academy of Sciences* **120**, e2210480120 (2023).

41. Lebreton, J., Colin, L., Chatre, E. & Bernard, P. RNA Pol II antagonises mitotic chromatin folding and chromosome segregation by condensin. 2023.08.08.552486 Preprint at https://doi.org/10.1101/2023.08.08.552486 (2023).

42. Zhang, H. *et al.* CTCF and R-loops are boundaries of cohesin-mediated DNA looping. *Molecular Cell* **83**, 2856-2871.e8 (2023).

43. Pobiega, S. & Marcand, S. Dicentric breakage at telomere fusions. *Genes Dev.* **24**, 720–733 (2010).

44. Guérin, T. M. & Marcand, S. Breakage in breakage–fusion–bridge cycle: an 80-year-old mystery. *Trends in Genetics* **38**, 641–645 (2022).

45. Lopez, V. *et al.* Cytokinesis breaks dicentric chromosomes preferentially at pericentromeric regions and telomere fusions. *Genes Dev.* **29**, 322–336 (2015).

46. Grossi, S., Bianchi, A., Damay, P. & Shore, D. Telomere Formation by Rap1p Binding Site Arrays Reveals End-Specific Length Regulation Requirements and Active Telomeric Recombination. *Mol Cell Biol* **21**, 8117–8128 (2001).

47. Colin, L. *et al.* Condensin positioning at telomeres by shelterin proteins drives sister-telomere disjunction in anaphase. *eLife* **12**, (2023).

48. Leonard, J. *et al.* Condensin Relocalization from Centromeres to Chromosome Arms Promotes Top2 Recruitment during Anaphase. *Cell Reports* **13**, 2336–2344 (2015).

49. Kim, J. H. *et al.* Condensin I associates with structural and gene regulatory regions in vertebrate chromosomes. *Nat Commun* **4**, 2537 (2013).

50. Williams, T. L., Levy, D. L., Maki-Yonekura, S., Yonekura, K. & Blackburn, E. H. Characterization of the Yeast Telomere Nucleoprotein Core. *Journal of Biological Chemistry* **285**, 35814–35824 (2010).

51. Falcon, C. M. & Matthews, K. S. Glycine Insertion in the Hinge Region of Lactose Repressor Protein Alters DNA Binding. *Journal of Biological Chemistry* **274**, 30849–30857 (1999).

52. Matot, B. *et al.* The orientation of the C-terminal domain of the Saccharomyces cerevisiae Rap1 protein is determined by its binding to DNA. *Nucleic Acids Research* **40**, 3197–3207 (2012).

53. Lickwar, C. R., Mueller, F., Hanlon, S. E., McNally, J. G. & Lieb, J. D. Genome-wide protein–DNA binding dynamics suggest a molecular clutch for transcription factor function. *Nature* **484**, 251–255 (2012).

54. Ryu, J.-K. *et al.* Condensin extrudes DNA loops in steps up to hundreds of base pairs that are generated by ATP binding events. *Nucleic Acids Research* **50**, 820–832 (2022).

55. Takaki, R., Dey, A., Shi, G. & Thirumalai, D. Theory and simulations of condensin mediated loop extrusion in DNA. *Nature Communications 2021 12:1* **12**, 1–10 (2021).

56. Le Bihan, Y.-V. *et al.* Effect of Rap1 binding on DNA distortion and potassium permanganate hypersensitivity. *Acta Crystallogr D Biol Crystallogr* **69**, 409–419 (2013).

57. Phipps, J. *et al.* Cohesin complex oligomerization maintains end-tethering at DNA double-strand breaks. 2023.11.08.566226 Preprint at https://doi.org/10.1101/2023.11.08.566226 (2023).

58. Lamothe, R., Costantino, L. & Koshland, D. E. The spatial regulation of condensin activity in chromosome condensation. *Genes Dev.* **34**, 819–831 (2020).

59. Bystricky, K., Heun, P., Gehlen, L., Langowski, J. & Gasser, S. M. Long-range compaction and flexibility of interphase chromatin in budding yeast analyzed by high-resolution imaging techniques. *Proc. Natl. Acad. Sci. U.S.A.* **101**, 16495–16500 (2004).

60. Vas, A. C. J., Andrews, C. A., Kirkland Matesky, K. & Clarke, D. J. In Vivo Analysis of Chromosome Condensation in *Saccharomyces cerevisiae*. *MBoC* **18**, 557–568 (2007).

61. Robellet, X. *et al.* A high-sensitivity phospho-switch triggered by Cdk1 governs chromosome morphogenesis during cell division. *Genes Dev.* **29**, 426–439 (2015).

62. Hsieh, T.-H. S. *et al.* Mapping Nucleosome Resolution Chromosome Folding in Yeast by Micro-C. *Cell* **162**, 108–119 (2015).

63. Costantino, L., Hsieh, T.-H. S., Lamothe, R., Darzacq, X. & Koshland, D. Cohesin residency determines chromatin loop patterns. *eLife* **9**, e59889 (2020).

64. Dubarry, M., Loïodice, I., Chen, C. L., Thermes, C. & Taddei, A. Tight protein–DNA interactions favor gene silencing. *Genes Dev.* **25**, 1365–1370 (2011).

65. Oldenkamp, R. & Rowland, B. D. A walk through the SMC cycle: From catching DNAs to shaping the genome. *Molecular cell* (2022) doi:10.1016/J.MOLCEL.2022.04.006.

66. Kim, E., Barth, R. & Dekker, C. Looping the Genome with SMC Complexes. *Annual Review of Biochemistry* **92**, 15–41 (2023).

67. Higashi, T. L., Pobegalov, G., Tang, M., Molodtsov, M. I. & Uhlmann, F. A Brownian ratchet model for DNA loop extrusion by the cohesin complex. *eLife* **10**, (2021).

68. Bauer, B. W. *et al.* Cohesin mediates DNA loop extrusion by a “swing and clamp” mechanism. *Cell* **184**, 5448-5464.e22 (2021).

69. Ström, L., Lindroos, H. B., Shirahige, K. & Sjögren, C. Postreplicative Recruitment of Cohesin to Double-Strand Breaks Is Required for DNA Repair. *Molecular Cell* **16**, 1003–1015 (2004).

70. Phipps, J. & Dubrana, K. DNA Repair in Space and Time: Safeguarding the Genome with the Cohesin Complex. *Genes* **13**, 198 (2022).

71. Haarhuis, J. H. I. *et al.* The Cohesin Release Factor WAPL Restricts Chromatin Loop Extension. *Cell* **169**, 693-707.e14 (2017).

72. Haarhuis, J. H. & Rowland, B. D. Cohesin: building loops, but not compartments. *The EMBO Journal* **36**, 3549–3551 (2017).

73. Brogaard, K., Xi, L., Wang, J.-P. & Widom, J. A map of nucleosome positions in yeast at base-pair resolution. *Nature* **486**, 496–501 (2012).

74. Ngo, T. T. M., Zhang, Q., Zhou, R., Yodh, J. G. & Ha, T. Asymmetric Unwrapping of Nucleosomes under Tension Directed by DNA Local Flexibility. *Cell* **160**, 1135–1144 (2015).

75. Marko, J. F. & Siggia, E. D. Bending and twisting elasticity of DNA. *Macromolecules* **27**, 981–988 (1994).

76. Kaczmarczyk, A. *et al.* Single-molecule force spectroscopy on histone H4 tail-cross-linked chromatin reveals fiber folding. *Journal of Biological Chemistry* **292**, 17506–17513 (2017).

77. Roisné-Hamelin, F. *et al.* Mechanism of MRX inhibition by Rif2 at telomeres. *Nat Commun* **12**, 2763 (2021).

78. Lescasse, R., Pobiega, S., Callebaut, I. & Marcand, S. End-joining inhibition at telomeres requires the translocase and polySUMO-dependent ubiquitin ligase Uls1. *EMBO J* **32**, 805–815 (2013).

79. Slobodyanyuk, E., Cattoglio, C. & Hsieh, T.-H. S. Mapping Mammalian 3D Genomes by Micro-C. in *Spatial Genome Organization: Methods and Protocols* 51–71 (Springer US, 2022). doi:10.1007/978-1-0716-2497-5_4.

80. Kerpedjiev, P. *et al.* HiGlass: web-based visual exploration and analysis of genome interaction maps. *Genome Biology* **19**, 125 (2018).

81. Tišma, M. *et al.* ParB proteins can bypass DNA-bound roadblocks via dimer-dimer recruitment. *Science Advances* **8**, eabn3299 (2022).

82. Liu, H. & Shima, T. A fast and objective hidden Markov modeling for accurate analysis of biophysical data with numerous states. doi:10.1101/2021.05.30.446337.

83. Nečas, D. & Klapetek, P. Gwyddion: an open-source software for SPM data analysis. *Open Physics* **10**, 181–188 (2012).

84. Baudry, L., Millot, G. A., Thierry, A., Koszul, R. & Scolari, V. F. Serpentine: a flexible 2D binning method for differential Hi-C analysis. *Bioinformatics* **36**, 3645–3651 (2020).

FIGURES

Figure 1. Condensin enrichment at the border of Rap1-bound arrays.

(A) Working hypothesis for condensin stalling at a Rap1-bound array. **(B)** Scheme illustrating the Rap1 arrays used in this study. Tandem repeats are used, meaning two consecutive Rap1 binding sites separated by a gap of which we control the size. The arrays with 35-bp gaps contain a LacO sequence to which LacI protein can bind. **(C)** ChIP analysis of Smc2-Myc in cells synchronized in late anaphase. The bars represent mean IP/Input values normalized to the signal at an ectopic position; error bars indicate standard deviation over 3 or more biological replicates. Unnormalized IP/Input values are shown in Fig. S1.

Figure 2. Dense Rap1 arrays are roadblocks to loop-extruding condensin in *in vitro* single-molecule experiments.

(A) Schematic overview of a 42 kb linearized DNA molecule with a Rap1 array sequence that is tethered to a glass surface through biotin-streptavidin. **(B)** Example of a stalling event. Side-flow images of DNA in cyan and a Rap1 array red. The time points represent the initial position of Rap1 on the DNA, followed by the initiation of a loop, the encounter between the loop and Rap1, and finally the position of the Rap1 array and the loop when flow is maximal, showing that the array is at the loop base for blocking events and passes into the loop for passing events. **(C)** Same as in panel B, but for a passing event. **(D)** Kymograph analysis of a blocking event in an experiment without applied flow. Normalized positions of DNA and Rap1 are shown, as well as the distance between the loop and the Rap1 (black), and the 51-frame moving MSD of Rap1 (red). Bottom plot shows the size of the loop in kb, calculated from the fraction of fluorescence intensity of the loop relative to the whole DNA. **(E)** Same as in panel D, but for a passing event. **(F)** Blocking fraction for various Rap1 arrays. 'DBD' indicates the use of the DNA-binding domain truncation of Rap1 as opposed to the full-length protein. '+LacI' indicates the addition of LacI protein. Error bars represent the 95% binomial confidence interval. *** indicates $p<10^{-3}$, and *ns* indicates no significant difference as determined by the Fisher exact test.

Figure 3. Rap1 array density and length modulate the stalling efficiency for condensin.

(A) Blocking efficiency of Rap1 arrays with 16 binding sites versus gap size. Blocking efficiency is denoted for three force ranges. Shaded areas represent the standard error of proportion. **(B)** Blocking efficiency of Rap1 arrays versus array length, for constant 6-bp gap size. **(C)** Representative images from AFM experiments for the Rap1 arrays of panel A, and for bare DNA. **(D)** Measured end-to-end lengths normalized by the measured contour length of Rap1 arrays from AFM. **(E)** End-to-end lengths, with the contour length (CL) of each construct shown above in nm. Red bars show the median of the population. The red line shows the average end-to-end length for the different constructs (93.8 nm).

Figure 4. Impact of Rap1-bound array on chromatin compaction in anaphase.

(A) A telomere-like Rap1 array causes local chromatin decompaction in anaphase. Representative images of cells at distinct cell cycle stages. In anaphase, the two sister chromatids are separated and the actomyosin ring (Myo1-GFP labelled) is open. In G1 cells, the ring is disassembled. Scale bars: 1 µm (pixel size: 65 nm). Distance between the two fluorescent spots shown in G1 cells and in anaphase cells. Black lines indicate median value, red lines quartiles value. Statistical significance is given by the Mann-Whitney test. **(B)** MicroC contact maps of chromosome 7 in cells synchronized in late anaphase. The ratios were determined using the Serpentine tool[84]. Whole-genome contact maps are shown in Fig. S3. **(C)** Condensin stalling at dense Rap1 arrays in dicentrics focuses entrapment and breakage by abscission. **(D)** Dicentric breakage at Rap1-bound arrays with varying gap sizes. The error bars represent the standard deviation over 3 biological replicates. Gels for each single experiment are shown in Fig. S4.

Fig. 1

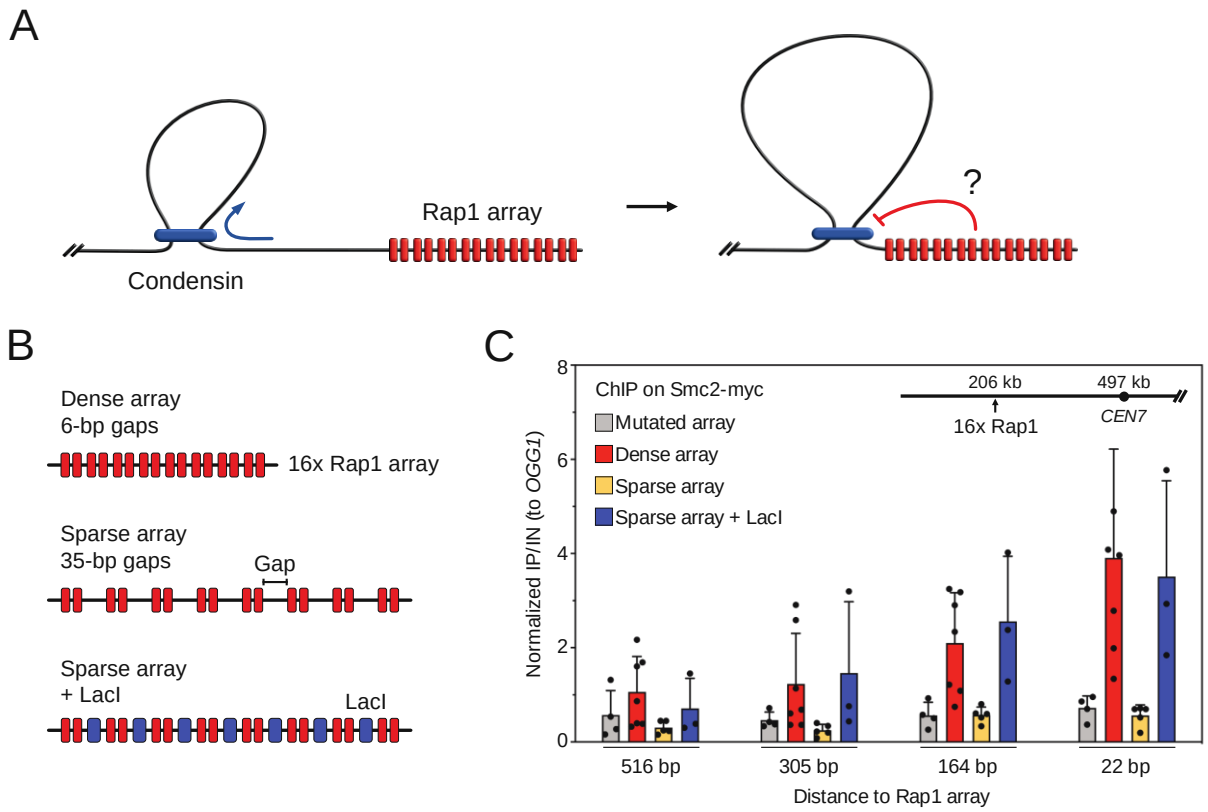
A
Rap1 array
Condensin
?
B
Dense array
6-bp gaps
16x Rap1 array
Sparse array
35-bp gaps
Gap
Sparse array
+ LacI
LacI
C
ChIP on Smc2-myc
Mutated array
Dense array
Sparse array
Sparse array + LacI
206 kb
497 kb
16x Rap1
CEN7
Normalized IP/IN (to OGG1)
0
2
4
6
8
516 bp
305 bp
164 bp
22 bp
Distance to Rap1 array

Fig. 2

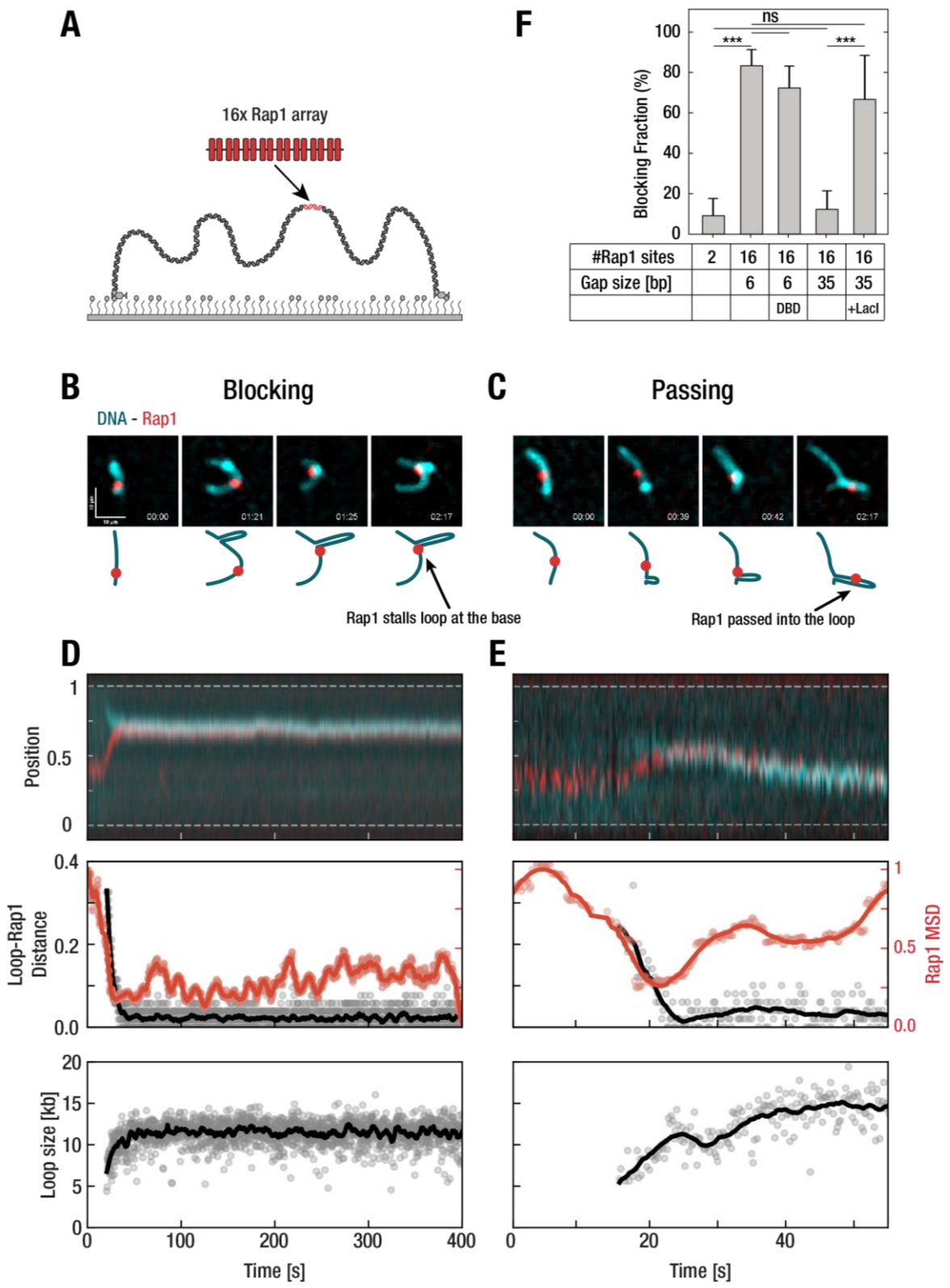
A
16x Rap1 array
F
ns
***
***
Blocking Fraction (%)
100
80
60
40
20
0
#Rap1 sites 2 16 16 16 16
Gap size [bp] 6 6 35 35
DBD +LacI
B
Blocking
C
Passing
DNA - Rap1
00:00
01:21
01:25
02:17
00:00
00:39
00:42
02:17
Rap1 stalls loop at the base
Rap1 passed into the loop
D
E
Position
1
0.5
0
Loop-Rap1 Distance
0.4
0.2
0.0
Rap1 MSD
1
0.5
0.0
Loop size [kb]
20
15
10
5
0
0
100
200
300
400
Time [s]
0
20
40
Time [s]

Fig. 3

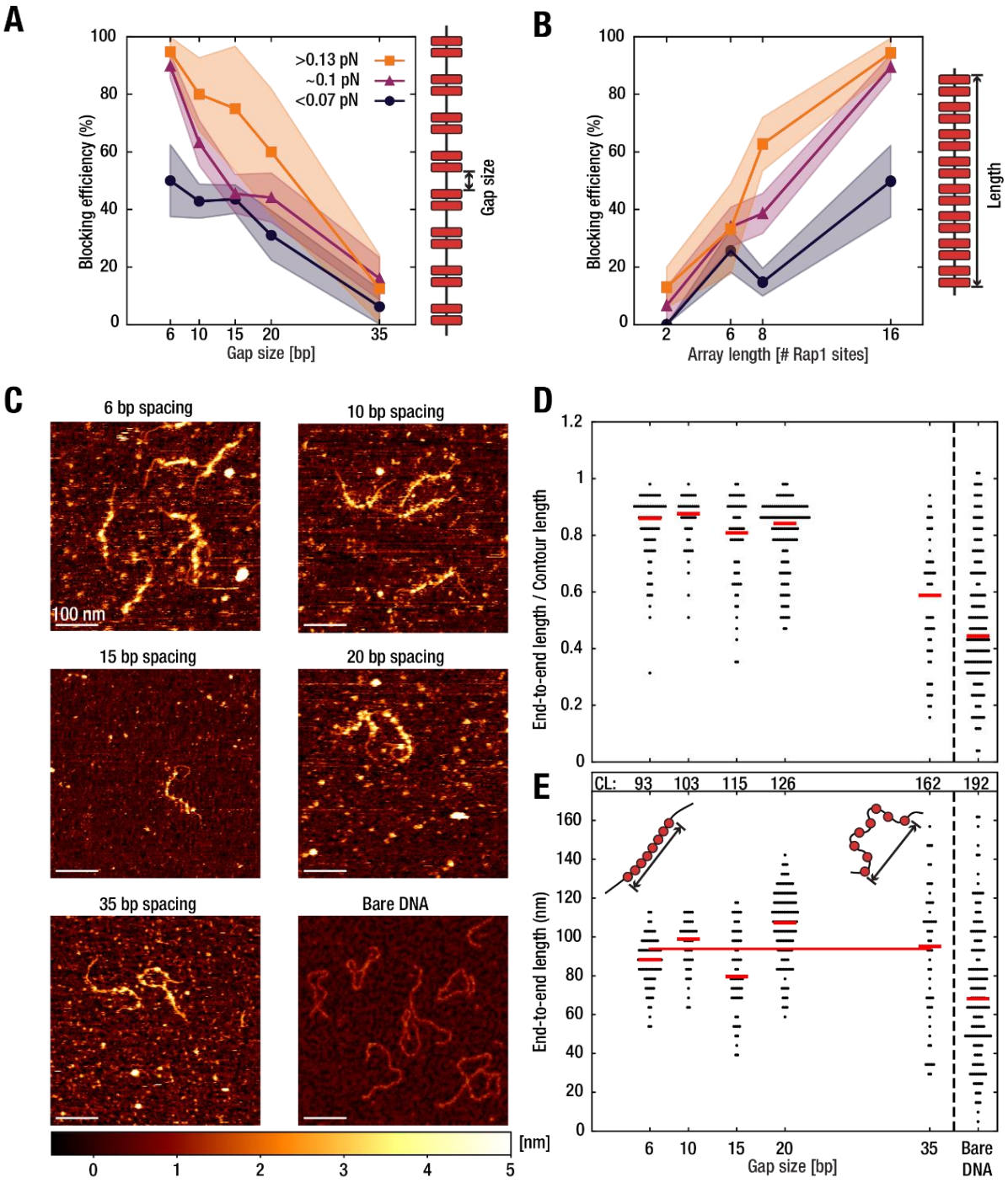
A
Blocking efficiency (%)
Gap size [bp]
>0.13 pN
~0.1 pN
<0.07 pN
Gap size
B
Blocking efficiency (%)
Array length [# Rap1 sites]
Length
C
6 bp spacing
10 bp spacing
100 nm
15 bp spacing
20 bp spacing
35 bp spacing
Bare DNA
[nm]
D
End-to-end length / Contour length
E
CL: 93 103 115 126 162 192
End-to-end length (nm)
Gap size [bp]
Bare DNA

Fig. 4

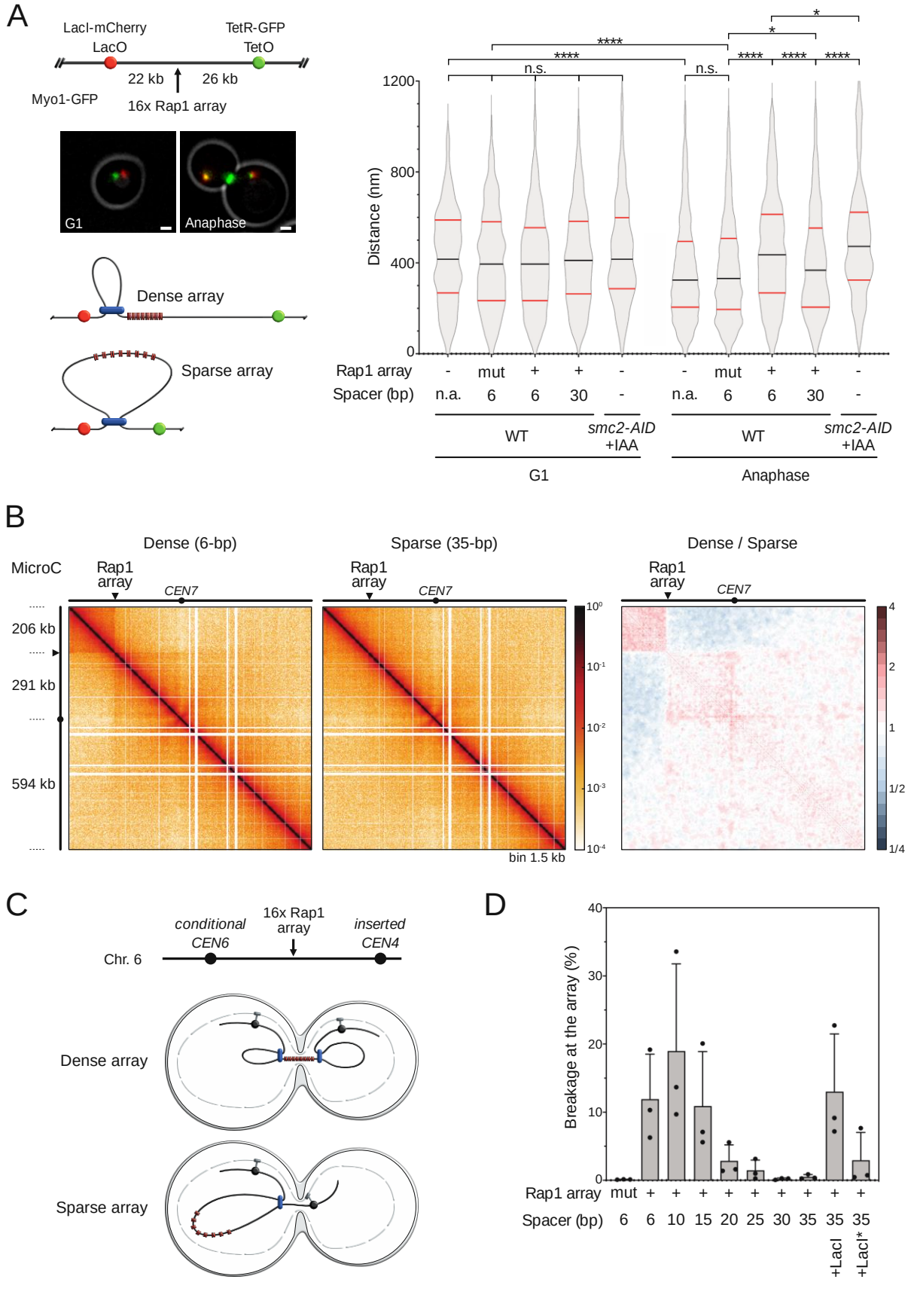
A
LacI-mCherry
LacO
TetR-GFP
TetO
22 kb
26 kb
Myo1-GFP
16x Rap1 array
G1
Anaphase
Dense array
Sparse array
Distance (nm)
1200
800
400
0
n.s.
n.s.
****
****
****
****
****
*
*
Rap1 array - mut + + - - mut + + -
Spacer (bp) n.a. 6 6 30 - n.a. 6 6 30 -
WT
smc2-AID +IAA
WT
smc2-AID +IAA
G1
Anaphase
B
Dense (6-bp)
Sparse (35-bp)
Dense / Sparse
MicroC
Rap1 array
CEN7
206 kb
291 kb
594 kb
bin 1.5 kb
C
conditional CEN6
16x Rap1 array
inserted CEN4
Chr. 6
Dense array
Sparse array
D
Breakage at the array (%)
40
30
20
10
0
Rap1 array mut + + + + + + + + +
Spacer (bp) 6 6 10 15 20 25 30 35 35 35
+LacI
+LacI*

Table S1: Yeast strains used in this study.

Name	Genotype	Figures
YCB212	*MATα cdc15-2ts smc2-AID-9myc::HPHBr NATr::16 Rap1 sites 6bp gaps in 7L at position 206707*	*1C, S1*
YCB214	*MATα cdc15-2ts NATr::16 Rap1 sites 6bp gaps in 7L at position 206707*	*1C, S1, 4B*
YCB215	*MATα cdc15-2ts*	*4B*
YCB257	*MATα cdc15-2ts smc2-AID-9myc::HPHBr NATr::16 mutated Rap1 sites 6bp gaps in 7L at position 206707*	*1C, S1*
YCB261	*MATα cdc15-2ts NATr::16 mutated Rap1 sites 6bp gaps in 7L at position 206707*	*1C, S1, 4B*
YCB542	*MATα cdc15-2ts smc2-AID-9myc::HPHBr NATr::16 Rap1 sites 35b gaps in 7L at position 206707*	*1C, S1*
YCB544	*MATα cdc15-2ts NATr::16 Rap1 sites 35bp gaps in 7L at position 206707*	*4B*
YCB550	*MATα cdc15-2ts NATr::14 Rap1 sites 35bp gaps in 7L at position 206707*	*1C, S1*
YCB551	*MATα cdc15-2ts smc2-AID-9myc::HPHBr NATr::16 Rap1 sites 35bp gaps in 7L at position 206707 ura3-1::lacI-mCherry::URA3*	*1C, S1*
YCB552	*MATα cdc15-2ts smc2-AID-9myc::HPHBr NATr::16 Rap1 sites 35bp gaps in 7L at position 206707 ura3-1::URA3*	*1C, S1*
YCB554	*MATα cdc15-2ts NATr::16 Rap1 sites 35bp gaps in 7L at position 206707 ura3-1::URA3*	*1C, S1*
YCB557	*MATα cdc15-2ts NATr::16 Rap1 sites 35bp gaps in 7L at position 206707 ura3-1::lacI-mCherry::URA3*	*1C, S1*
YAD82	*MATa bar1-Δ KANr-pGAL1-CEN6-pGAL1-skHIS3 ADE2 NATr::16 mutated Rap1 sites 25bp gaps in chromosome 6 at position 192140 CEN4::klLEU2 in chromosome 6 at position 245710*	S4
YAD83	*MATa bar1-Δ KANr-pGAL1-CEN6-pGAL1-skHIS3 ADE2 NATr::16 mutated Rap1 sites 6bp gaps in chromosome 6 at position 192140 CEN4::klLEU2 in chromosome 6 at position 245710*	S4
YAD86	*MATa bar1-Δ KANr-pGAL1-CEN6-pGAL1-skHIS3 ADE2 NATr::16 Rap1 sites 35bp gaps 6bp gaps in chromosome 6 at position 192140 CEN4::klLEU2 in chromosome 6 at position 245710*	S4
YAD97	*MATa bar1-Δ KANr-pGAL1-CEN6-pGAL1-skHIS3 ADE2 NATr::16 Rap1 sites 6bp gaps in chromosome 6 at position 192140 CEN4::klLEU2 in chromosome 6 at position 245710*	S4

YAD128	*MATa bar1-Δ KANr-pGAL1-CEN6-pGAL1-skHIS3 ADE2 NATr::16 mutated Rap1 sites 10bp gaps in chromosome 6 at position 192140 CEN4::klLEU2 in chromosome 6 at position 245710*	S4
YAD130	*MATa bar1-Δ KANr-pGAL1-CEN6-pGAL1-skHIS3 ADE2 NATr::16 mutated Rap1 sites 15bp gaps in chromosome 6 at position 192140 CEN4::klLEU2 in chromosome 6 at position 245710*	S4
YAD138	*MATa bar1-Δ KANr-pGAL1-CEN6-pGAL1-skHIS3 ADE2 NATr::16 mutated Rap1 sites 35bpgaps in chromosome 6 at position 192140 ura3-1::lacI-mCherry*::URA3 CEN4::klLEU2 in chromosome 6 at position 245710*	S4
YAD139	*MATa bar1-Δ KANr-pGAL1-CEN6-pGAL1-skHIS3 ADE2 NATr::16 mutated Rap1 sites 35bpgaps in chromosome 6 at position 192140 ura3-1::lacI-mCherry::URA3 CEN4::klLEU2 in chromosome 6 at position 245710*	S4
YAD148	*MATa bar1-Δ KANr-pGAL1-CEN6-pGAL1-skHIS3 ADE2 NATr::16 mutated Rap1 sites 20bp gaps in chromosome 6 at position 192140 CEN4::klLEU2 in chromosome 6 at position 245710*	S4
YAD184	*MATa bar1-Δ KANr-pGAL1-CEN6-pGAL1-skHIS3 ADE2 NATr::16 mutated Rap1 sites 30bp gaps in chromosome 6 at position 192140 CEN4::klLEU2 in chromosome 6 at position 245710*	S4
YAD267	*MATa hml::ADE1 hmr::ADE1 ade3::GALHO MATa::TetO-LEU2 0.5kb-CWH43::lacOpFX-TRP1 ura3::OsTIR1-URA3-LacI-mCherry-KanMx leu2::TetR-GFP-LEU2 Myo1-GFP::HPHBr*	4A
YAD 302	*MATa MATa hml::ADE1 hmr::ADE1 ade3::GALHO MATa::TetO-LEU2 0.5kb-CWH43::lacOpFX-TRP1 ura3::OsTIR1-URA3-LacI-mCherry-KanMx leu2::TetR-GFP-LEU2 Myo1-GFP::HPHB 16Rap1-6bp-gaps -at-chr.3-at-1670517::NATr*	4A
YAD317	*MATa MATa hml::ADE1 hmr::ADE1 ade3::GALHO MATa::TetO-LEU2 0.5kb-CWH43::lacOpFX-TRP1 ura3::OsTIR1-URA3-LacI-mCherry-KanMx leu2::TetR-GFP-LEU2 Myo1-GFP::HPHB no_Rap1-at-chr.3-at-1670517::NATr*	4A
YAD319	*MATa MATa hml::ADE1 hmr::ADE1 ade3::GALHO MATa::TetO-LEU2 0.5kb-CWH43::lacOpFX-TRP1 ura3::OsTIR1-URA3-LacI-mCherry-KanMx leu2::TetR-GFP-LEU2 Myo1-GFP::HPHB 16mutated-6bp-gaps-at-chr.3-at-1670517::NATr*	4A
YAD319	*MATa MATa hml::ADE1 hmr::ADE1 ade3::GALHO MATa::TetO-LEU2 0.5kb-CWH43::lacOpFX-TRP1 ura3::OsTIR1-URA3-LacI-mCherry-KanMx leu2::TetR-GFP-LEU2 Myo1-GFP::HPHB 16Rap1-30bp-gaps-at-chr.3-at-1670517::NATr*	4A
Lev915	*MATa MATa hml::ADE1 hmr::ADE1 ade3::GALHO MATa::TetO-LEU2 0.5kb-CWH43::lacOpFX-TRP1 ura3::OsTIR1-URA3-LacI-mCherry-KanMx leu2::TetR-GFP-LEU2 Myo1-GFP::HPHB smc2-AID-9myc::NATr*	4A

Table S2: Rap1 array sequences with their contour lengths in bp and nm. Rap1 binding sites are indicated in red. All arrays were initially created in a pUC19-BBB cloning vector where BamHI and BglII cloning sites (underlined) replace the pUC19 original polylinker: ---AGTGAATTGGGAC GGATCCTGATCAAGATCTAGCTTGGCGTAATCATGGT---.

Construct	Length [bp]	Length [nm]	Sequence
16Rap1-6bpGap	274	93	GGATCCGGTGTCTGGGTGTAAGGTGTATGGGTGTAGGATCTGGTGTCTGGGTG TAAGGTGTATGGGTGTAGGATCTGGTGTCTGGGTGTAAGGTGTATGGGTGTAG GATCTGGTGTCTGGGTGTAAGGTGTATGGGTGTAGGATCTGGTGTCTGGGTGT AAGGTGTATGGGTGTAGGATCTGGTGTCTGGGTGTAAGGTGTATGGGTGTAGG ATCTGGTGTCTGGGTGTAAGGTGTATGGGTGTAGGATCTGGTGTCTGGGTGTA AGGTGTATGGGTGTAAGATCT
16Rap1-10bpGap	302	103	GGATCCGGTGTCTGGGTGTAAGGTGTATGGGTGTAGGATCTGAATGGTGTCTG GGTGTAAGGTGTATGGGTGTAGGATCTGAATGGTGTCTGGGTGTAAGGTGTAT GGGTGTAGGATCTGAATGGTGTCTGGGTGTAAGGTGTATGGGTGTAGGATCTG AATGGTGTCTGGGTGTAAGGTGTATGGGTGTAGGATCTGAATGGTGTCTGGGT GTAAGGTGTATGGGTGTAGGATCTGAATGGTGTCTGGGTGTAAGGTGTATGGG TGTAGGATCTGAATGGTGTCTGGGTGTAAGGTGTATGGGTGTAAGATCT
16Rap1-15bpGap	337	115	GGATCCGGTGTCTGGGTGTAAGGTGTATGGGTGTAGGATCTGATCCATATGGTG TCTGGGTGTAAGGTGTATGGGTGTAGGATCTGATCCATATGGTGTCTGGGTGTA AGGTGTATGGGTGTAGGATCTGATCCATATGGTGTCTGGGTGTAAGGTGTATGG GTGTAGGATCTGATCCATATGGTGTCTGGGTGTAAGGTGTATGGGTGTAGGATC TGATCCATATGGTGTCTGGGTGTAAGGTGTATGGGTGTAGGATCTGATCCATATG GTGTCTGGGTGTAAGGTGTATGGGTGTAGGATCTGATCCATATGGTGTCTGGGT GTAAGGTGTATGGGTGTAAGATCT
16Rap1-20bpGap	372	126	GGATCCGGTGTCTGGGTGTAAGGTGTATGGGTGTAGGATCTGAACAATTCCAT ATGGTGTCTGGGTGTAAGGTGTATGGGTGTAGGATCTGAACAATTCCATATGGT GTCTGGGTGTAAGGTGTATGGGTGTAGGATCTGAACAATTCCATATGGTGTCTG GGTGTAAGGTGTATGGGTGTAGGATCTGAACAATTCCATATGGTGTCTGGGTGT AAGGTGTATGGGTGTAGGATCTGAACAATTCCATATGGTGTCTGGGTGTAAGG TGTATGGGTGTAGGATCTGAACAATTCCATATGGTGTCTGGGTGTAAGGTGTAT GGGTGTAGGATCTGAACAATTCCATATGGTGTCTGGGTGTAAGGTGTATGGGT GTAAGATCT
16Rap1-25bpGap	407	138	GGATCCGGTGTCTGGGTGTAAGGTGTATGGGTGTAGGATCTGACGCTCACAAT TCCATATGGTGTCTGGGTGTAAGGTGTATGGGTGTAGGATCTGACGCTCACAAT TCCATATGGTGTCTGGGTGTAAGGTGTATGGGTGTAGGATCTGACGCTCACAAT TCCATATGGTGTCTGGGTGTAAGGTGTATGGGTGTAGGATCTGACGCTCACAAT TCCATATGGTGTCTGGGTGTAAGGTGTATGGGTGTAGGATCTGACGCTCACAAT TCCATATGGTGTCTGGGTGTAAGGTGTATGGGTGTAGGATCTGACGCTCACAAT TCCATATGGTGTCTGGGTGTAAGGTGTATGGGTGTAGGATCTGACGCTCACAAT TCCATATGGTGTCTGGGTGTAAGGTGTATGGGTGTAAGATCT
16Rap1-30bpGap	442	150	GGATCCGGTGTCTGGGTGTAAGGTGTATGGGTGTAGGATCTGATTATCCGCTCA CAATTCCATATGGTGTCTGGGTGTAAGGTGTATGGGTGTAGGATCTGATTATCC GCTCACAATTCCATATGGTGTCTGGGTGTAAGGTGTATGGGTGTAGGATCTGAT TATCCGCTCACAATTCCATATGGTGTCTGGGTGTAAGGTGTATGGGTGTAGGAT CTGATTATCCGCTCACAATTCCATATGGTGTCTGGGTGTAAGGTGTATGGGTGTA GGATCTGATTATCCGCTCACAATTCCATATGGTGTCTGGGTGTAAGGTGTATGG

			GTGTAGGATCTGATTATCCGCTCACAATTCCATATGGTGTCTGGGTGTAAGGTG TATGGGTGTAAGATCT
16Rap1-35bpGap	477	162	GGATCCGGTGTCTGGGTGTAAGGTGTATGGGTGTAGGATCTGAAATTGTTATCC GCTCACAATTCCATATGGTGTCTGGGTGTAAGGTGTATGGGTGTAGGATCTGAA ATTGTTATCCGCTCACAATTCCATATGGTGTCTGGGTGTAAGGTGTATGGGTGTA GGATCTGAAATTGTTATCCGCTCACAATTCCATATGGTGTCTGGGTGTAAGGTG TATGGGTGTAGGATCTGAAATTGTTATCCGCTCACAATTCCATATGGTGTCTGGG TGTAAGGTGTATGGGTGTAGGATCTGAAATTGTTATCCGCTCACAATTCCATATG GTGTCTGGGTGTAAGGTGTATGGGTGTAGGATCTGAAATTGTTATCCGCTCACA ATTCCATATGGTGTCTGGGTGTAAGGTGTATGGGTGTAGGATCTGAAATTGTTA TCCGCTCACAATTCCATATGGTGTCTGGGTGTAAGGTGTATGGGTGTAAGATCT
2Rap1	29	10	GGATCCGGTGTCTGGGTGTAAGGTGTATGGGTGTAAGATCT
6Rap1-6bpGap	99	34	GGATCTGGTGTCTGGGTGTAAGGTGTATGGGTGTAGGATCTGGTGTCTGGGTG TAAGGTGTATGGGTGTAGGATCTGGTGTCTGGGTGTAAGGTGTATGGGTGTAA GATCT
8Rap1-6bpGap	134	46	GGATCCGGTGTCTGGGTGTAAGGTGTATGGGTGTAGGATCTGGTGTCTGGGTG TAAGGTGTATGGGTGTAGGATCTGGTGTCTGGGTGTAAGGTGTATGGGTGTAG GATCTGGTGTCTGGGTGTAAGGTGTATGGGTGTAAGATCT
12Rap1-6bpGap	204	69	GGATCCGGTGTCTGGGTGTAAGGTGTATGGGTGTAGGATCTGGTGTCTGGGTG TAAGGTGTATGGGTGTAGGATCTGGTGTCTGGGTGTAAGGTGTATGGGTGTAG GATCTGGTGTCTGGGTGTAAGGTGTATGGGTGTAGGATCTGGTGTCTGGGTGT AAGGTGTATGGGTGTAGGATCTGGTGTCTGGGTGTAAGGTGTATGGGTGTAAG ATCT

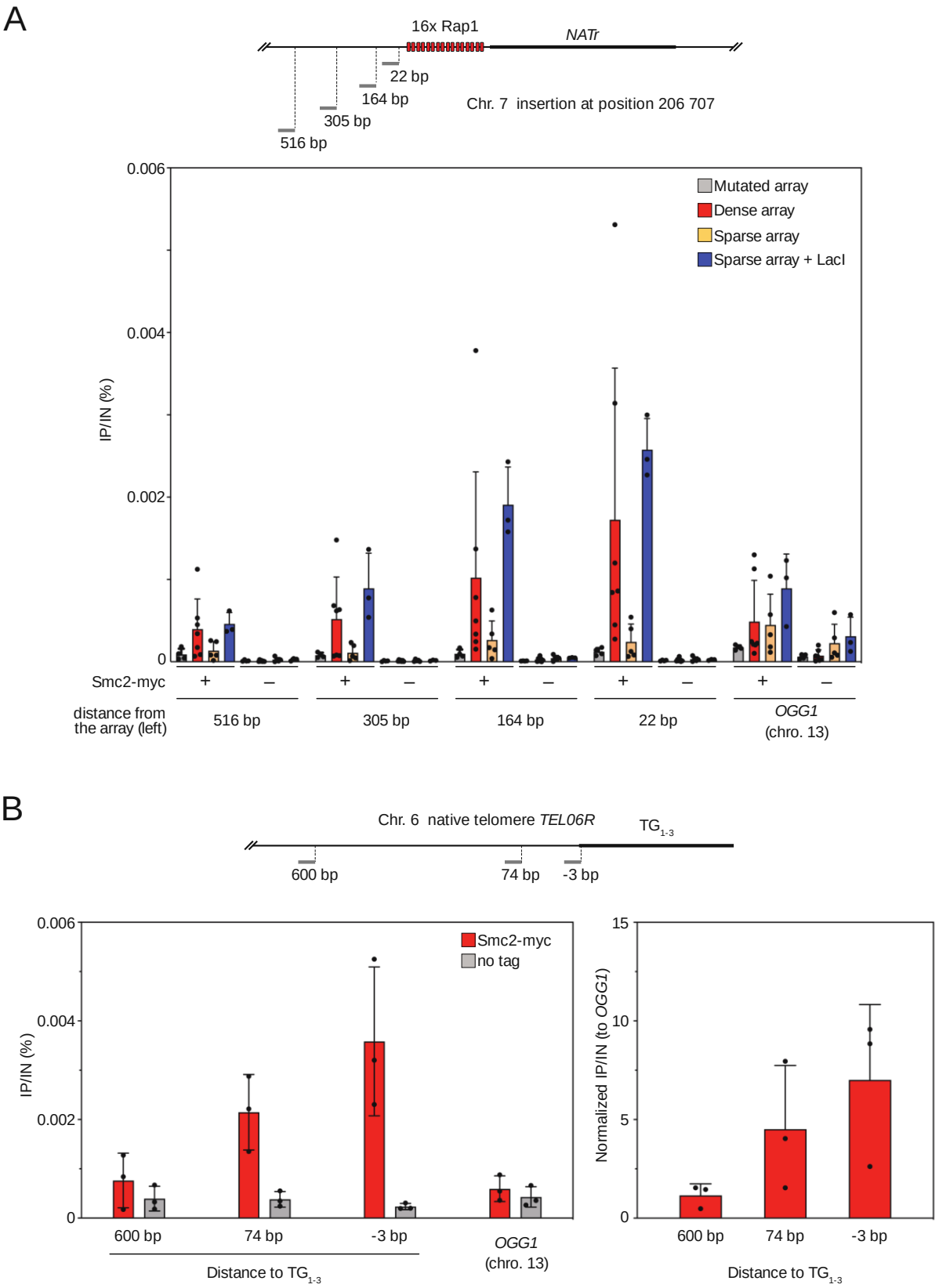

Fig. S1. ChIP analysis of Smc2-Myc in cells synchronized in late anaphase. (A) Individual IP/Input values from which the relative enrichment at Rap1 arrays shown in Fig.1C is derived**.** Error bars indicate standard deviation **(B)** Condensin enrichment at native telomere *TEL06R*. Left panel: Individual IP/Input values. Right panel: enrichment relative to an ectopic internal position. The bars represent mean IP/Input values; error bars indicate standard deviation over 3 biological replicates.

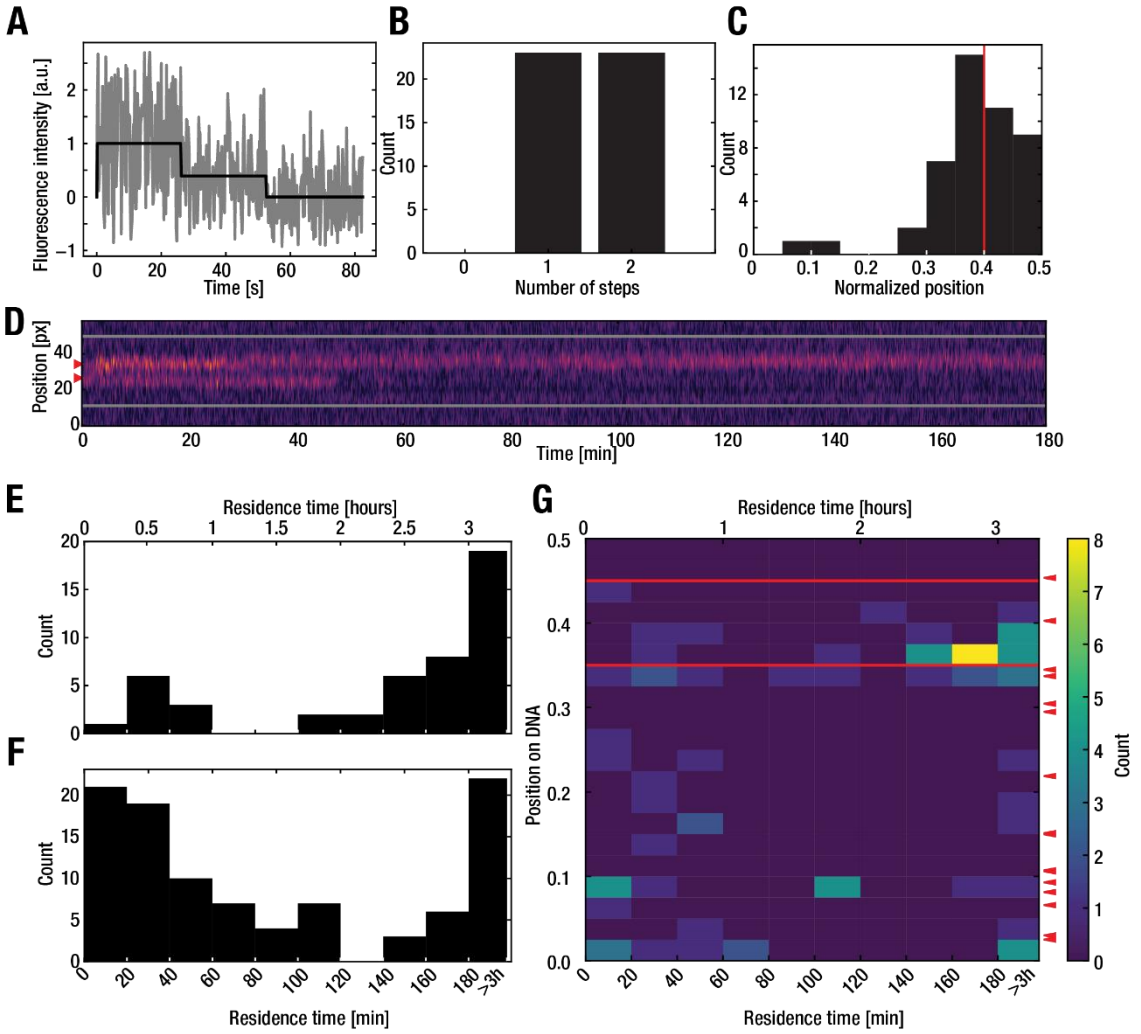

Fig. S2. Validation of binding efficiency, specificity, and residence time. (A-C) Bleaching assay under Rap1 DNA-binding conditions (see methods). **(A)** Representative bleaching curve of two Rap1-JF646 proteins bound to DNA (see methods). The raw fluorescence intensity is shown in grey and the steps are shown in black. **(B)** Histogram of identified bleaching steps (N=46). **(C)** Histogram of the positions of bleached Rap1-JF646 in (B). Positions are normalized by the end-to-end length. Distances are shown from 0-0.5 because we cannot distinguish directionality of the DNA molecules. **(D-G)** Residence time assay under imaging conditions (see methods). **(D)** Representative example of a kymograph that shows a Rap1 protein with a long and short residence time. The red arrows indicate the position of the Rap1 binding site located at 0.4 distance along the DNA (because we cannot distinguish top from bottom and our binding site is located asymmetrically along the DNA, we indicate both 0.4 and the mirrored 0.6 position, which is coincidentally located near several potential Rap1 sites within the i95-cosmid sequence). **(E)** Histogram of residence time measured for Rap1 proteins near the binding site position. Last bin (>3h) represents all proteins that were still present at the end of acquisition time. **(F)** Histogram of residence time measured for all off-target bound Rap1 proteins. **(G)** 2D histogram of the residence time (x-axis) and binding position (y-axis). Red lines indicate the positional bins from which on-target binding was aggregated to generate the histogram in (D). Red arrows indicate sites partially matching Rap1 consensus site (5'-RRKGNKYGGRTKY-3') within the i95-cosmid sequence.

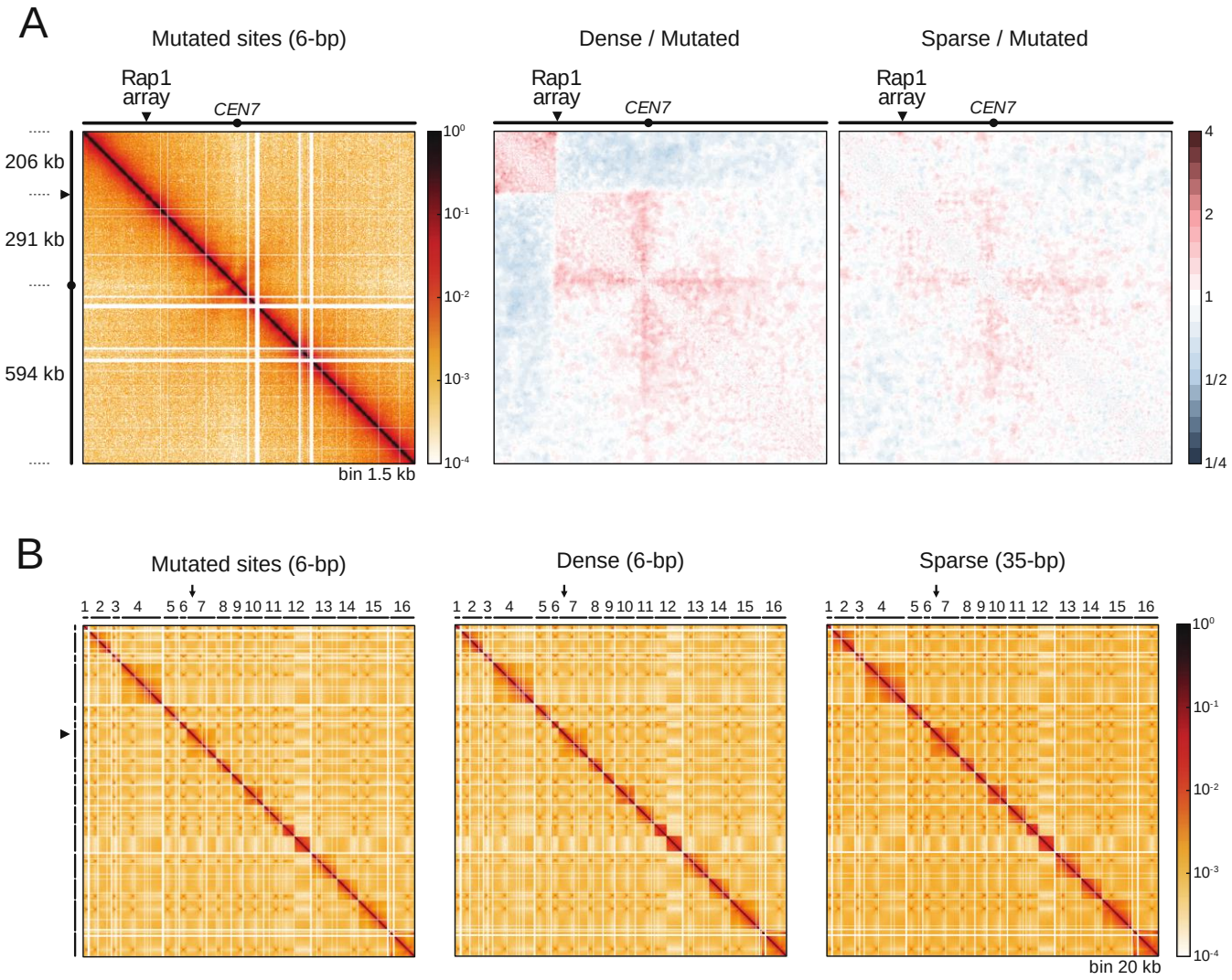

Fig. S3. MicroC at Rap1 arrays. (A) MicroC contact map of chromosome 7 where a control array of 16 mutated sites is inserted at position 206 707. Cells are synchronized in late anaphase. The ratios were determined using the Serpentine tool. We note that dense and sparse Rap1 arrays make frequent contact with the proximal native chromosome end. Unlikely to be related to condensin activity, these *cis*-contacts may stem instead from Rap1-dependent direct protein-protein interactions known to cluster telomeres[1]. (B) Whole-genome contact maps.

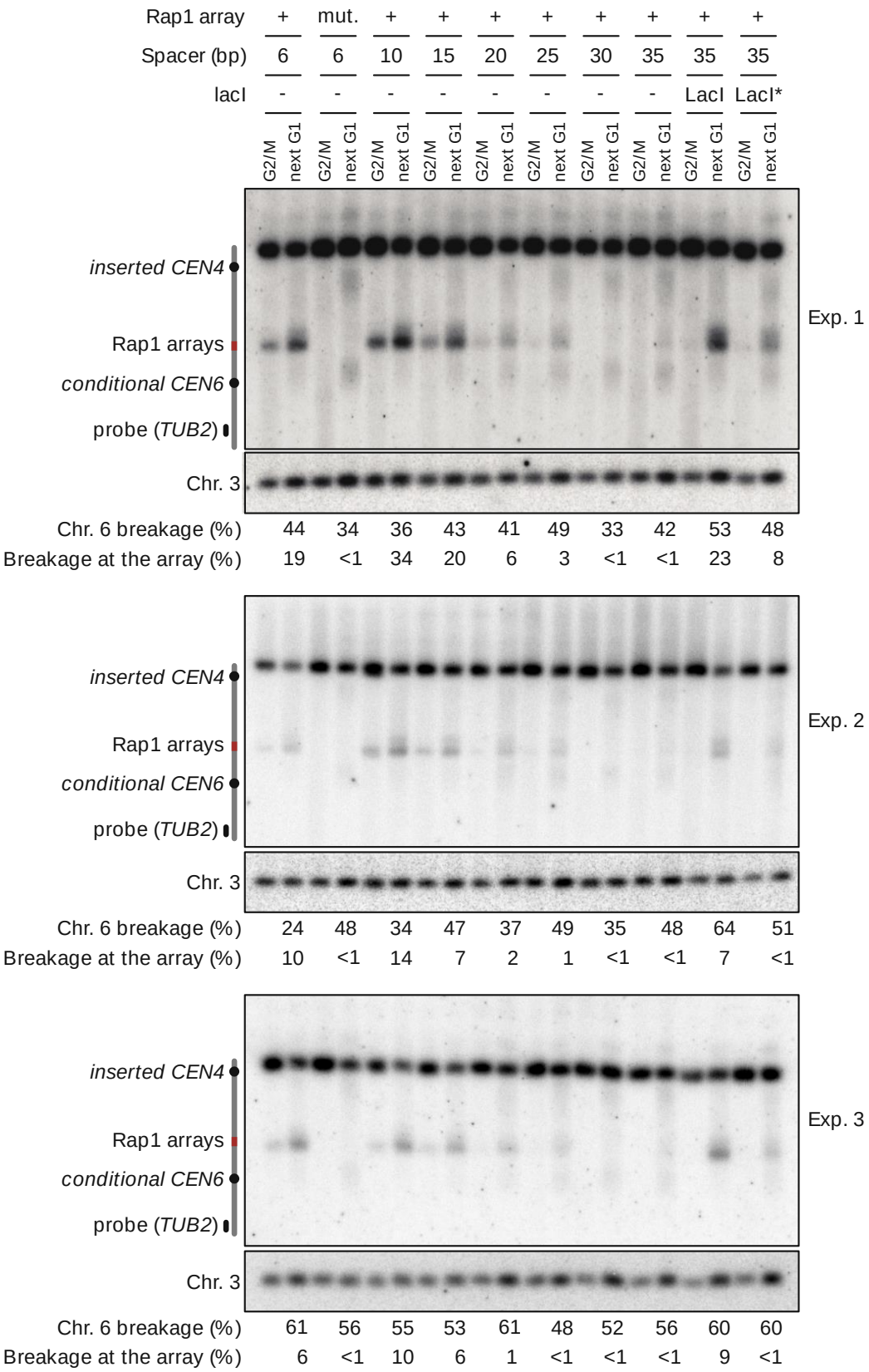

Fig.S4. Dicentric chromosome breakage. Individual gels from which the preferential dicentric breakage at Rap1 arrays shown in Fig.4C is derived.

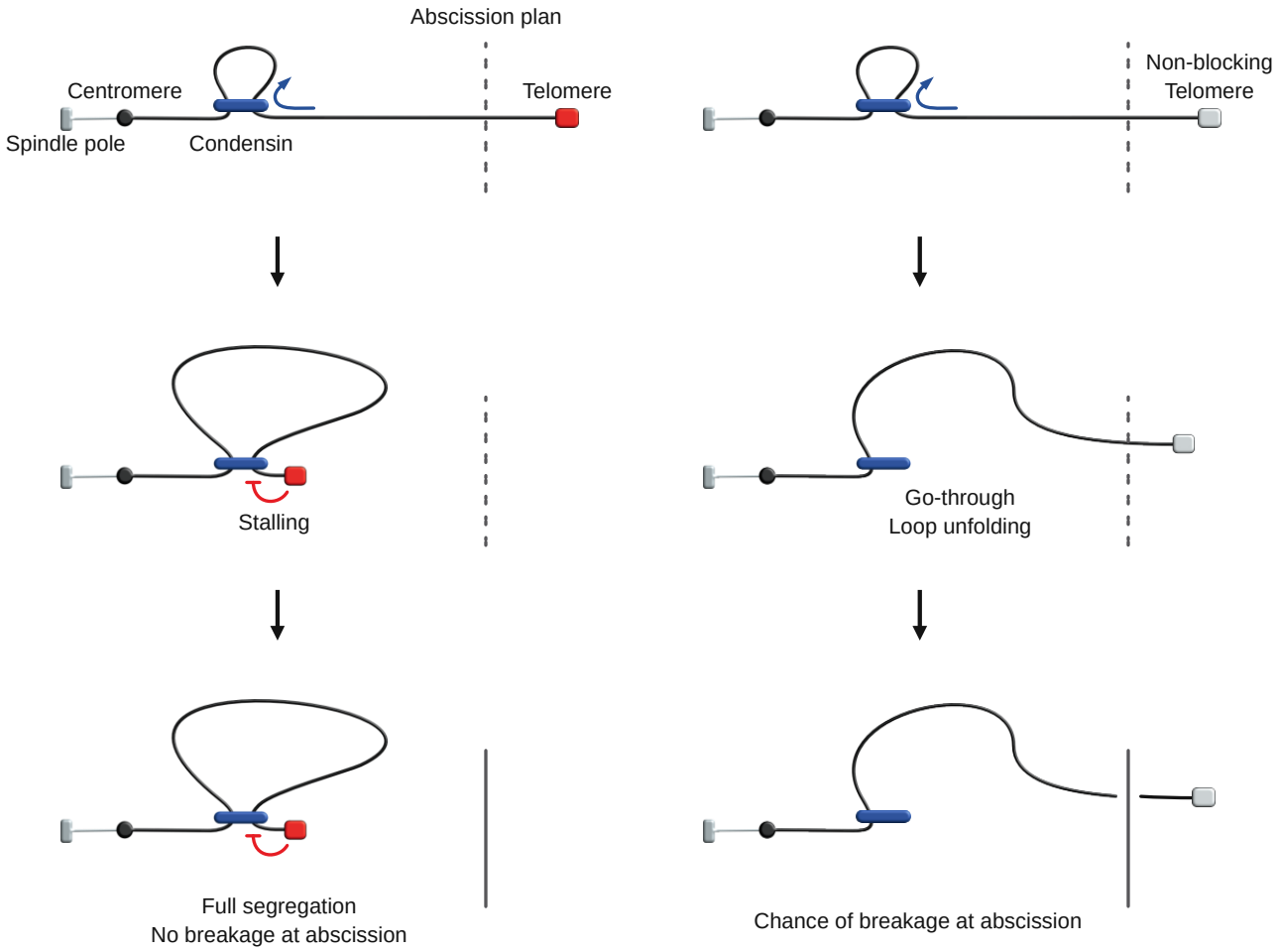

Fig.S5. Working model for a role of condensin stalling at native telomeres.

REFERENCES

1. Ruault, M. *et al.* Sir3 mediates long-range chromosome interactions in budding yeast. *Genome Res.* **31**, 411–425 (2021).

Chapter 3: Discussion

Discussion – overview

Throughout my thesis, I have primarily investigated how two DNA ends are held together following DNA DSBs. It has long been known that MRX performs DSB end-tethering in *S. cerevisiae* (Lobachev et al., 2004). We have added to this by demonstrating that MRX head oligomerization is required for end-tethering, in accordance with DNA tethering structures observed *in vitro* (Kissling et al., 2022; Rotheneder et al., 2023). We have also exposed the protein complex responsible for DSB end-tethering following resection, a pathway that was previously only known to rely on the exonuclease Exo1's ability to form ssDNA. Our work implicates oligomerization between cohesin complexes either side of the DSB in this pathway. We demonstrate this through our genetic analysis of *exo1* and SMC1-AID *exo1* mutants, which present similar levels of end-separation, unlike *mre11* SMC1-AID mutants. Following resection, DSB end-tethering is still important to prevent promiscuous repair events, albeit whilst providing freedom to search for a homologous donor. Ultimately, we show that cohesin end-tethering is indeed important for repair efficiency beyond maintaining sister chromatids in proximity, using a real-time microfluidic assay. Thus, MRX is immediately recruited to DSB ends for tethering, and cohesin plays a major role following resection (Figure 16).

Despite revealing cohesin's role in end-tethering and homology directed repair, our work raises many unanswered questions. Perhaps most importantly, we identified two genetically separable cohesin populations that act at DSBs, in a distinct manner from those responsible for strengthening sister chromatid cohesion. These two cohesin populations are individually responsible for compacting the DSB adjacent DNA, and tethering DSB ends for efficient repair. Strikingly, whereas Pds5 is not required for DSB dependent genome compaction, it is essential for DSB end tethering. This suggests that Pds5 differentially regulates tethering and loop forming cohesin at DSB ends. Questions remain about how Pds5 presence or absence defines and regulates these different populations at DSBs.

We also demonstrate that the Smc5/6 complex is important for DSB end-tethering. Despite this observation, we did not explore roles for Smc5/6 in end-tethering beyond its known role in recruiting cohesin to DSBs (De Piccoli et al., 2006). With Smc5/6 containing subunits with both ubiquitin and SUMO-ligase activity, Smc5/6 might play crucial roles in regulating the different cohesin populations at DSBs.

Throughout this chapter, I will identify questions that remain with regards to Smc5/6, cohesin and Pds5 dependent end-tethering. I will also discuss questions that remain in the DSB end-tethering field more globally, as well as for cohesin biology. In tandem, I will try to provide insights into how we could start to answer these questions.

Finally, I will discuss the observations made during my collaborative work with Stéphane Marcand's lab. The finding that telomeric protein arrays of a specific density and length stall loop extrusion provides an important tool for further understanding SMC complexes. Importantly, it explains how condensin is able to condense mitotic chromosomes, without extruding through the end of the linear structure.

Part 1 – Tethering questions raised by our study
Cohesin oligomerization and DNA DSB end-tethering

Our finding that cohesin oligomerization tethers DSBs demonstrates that this property is biologically relevant for bridging two DNA loci *in vivo*. What regulates cohesin oligomerization, and distinguishes oligomerizing and non-oligomerizing cohesin, remains unclear. Of note, Pds5 is necessary, independently of Smc3 acetylation, for *in vivo* oligomerization (Xiang and Koshland, 2021). However, an Mcd1/Scc1 mutant (*mcd1Q266*) that maintains its association to Pds5 does not form cohesin oligomers (Xiang and Koshland, 2021). This indicates that presence of Pds5 alone is not sufficient for this property. Importantly, both cohesin containing *mcd1Q266* and lacking Pds5 appear to maintain their loop forming capabilities at DSBs, but do not maintain DSB end-tethering (Phipps et al., 2023).

Cohesin dependent DSB end-tethering also provides an important tool for identifying cohesin properties that are important for oligomerization. Of note, Smc5/6 contains SUMO and ubiquitin ligase subunits, and is important for DSB end-tethering. Furthermore, SUMOylation by Mms21 is necessary for damage induced sister chromatid cohesion (McAleenan, et al., 2012). Pds5 also plays an important role in protecting cohesin from extensive SUMOylation (Psakhye et al., 2023). SUMOylation could thus regulate cohesin localization and oligomerization properties at DSBs. The importance of the Smc5/6 SUMO and ubiquitin ligase subunits for DSB end-tethering should also be determined by their depletion upon DSB induction. SUMO and ubiquitin profiles of Mcd1 in Pds5 depleted cells and *mcd1Q266* containing strains should be checked following DSB induction. Together, these result could provide important insights into how end-tethering cohesin's are defined.

We demonstrate that Pds5 and *mcd1Q266* mutants are still capable of forming DSB dependent genome compaction, showing that cohesin is still recruited to DSBs in these mutants (Figure 16). However, ChIP for cohesin subunits at DSBs in these mutants would provide confirmation. If cohesin is still enriched, we reinforce our finding that loss of end-tethering is truly dependent on loss of cohesin oligomerization.

Two cohesin populations at DSBs

Our observation of DSB adjacent genome compaction is in line with gH2Ax spreading away from DSBs by loop extrusion (Arnould et al., 2021). Unlike DSB end-tethering, this property is maintained in yeast cells lacking Pds5 (Phipps et al., 2023). This exposes two different populations of cohesin at DSBs. One that tethers DSB ends and requires Pds5, and another that compacts the genome and does not tether DSB ends nor requires Pds5 (Figure 16).

This finding correlates with another key observation at DSBs. It was previously described that *mre11Δ* cells have severely reduced levels of cohesin recruitment to DSBs (Unal et al., 2004). Surprisingly, we demonstrate that DSB end-separation increases upon cohesin depletion in *mre11Δ* cells (Figure 16). This indicates that some cohesin's are still recruited to DSBs in absence of *mre11Δ*, and that these are competent for end-tethering. Therefore, this cohesin population is independent of cohesin recruited in an MRX dependent manner.

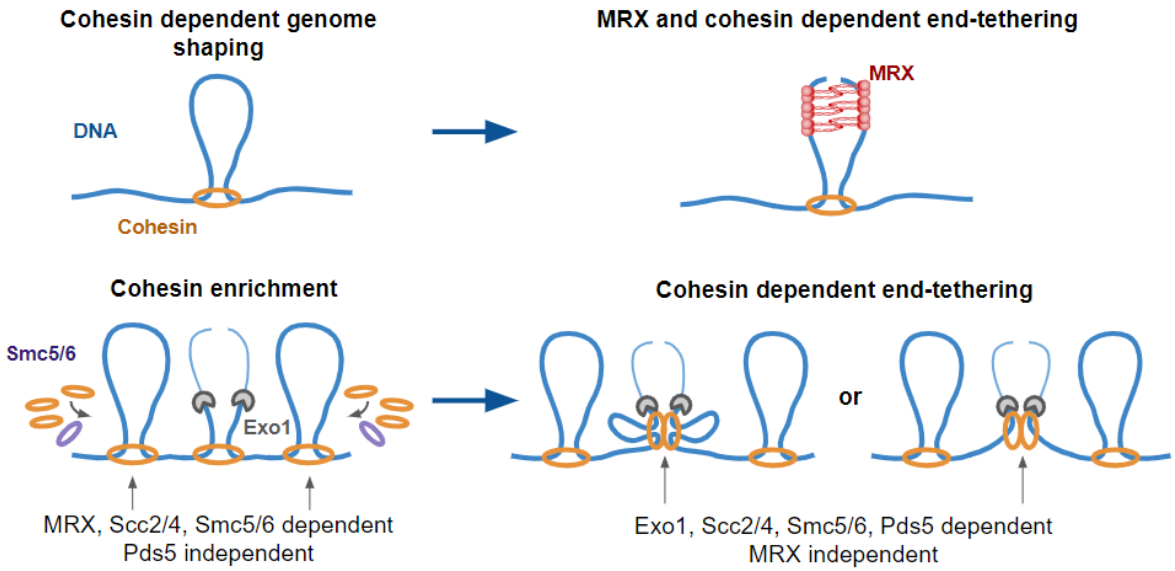

Figure 16. Models for DSB end-tethering in *Saccharomyces cerevisiae*. Upon DSB, MRX rapidly binds DNA ends. MRX complexes hold DNA ends together through physical bridging. Cohesin also assists in DSB end-tethering shortly after DSB formation, independently of MRX and Exo1, and likely relies on cohesin-dependent genome looping. Later, cohesin-dependent DSB end-tethering requires *de novo* cohesin enrichment by Scc2/4, acts in cooperation with Exo1 and Smc5/6, is independent of sister chromatid cohesion and loop formation, and likely relies on cohesin oligomerization. Unlike massive cohesin enrichment around DSBs, cohesin end-tethering does not require MRX. In contrast, Pds5, which is not required for DSB dependent loop formation around DSBs, is required for DSB end-tethering. As such, at least two cohesin populations act at DNA DSBs alongside those which strengthen sister chromatid cohesion. These populations ensure compaction of DSB adjacent chromatin and tethering of DSB ends.

Cohesin end-tethering and dependence on long-range resection

MRX plays an important role in initiating resection. However, in its absence, redundant exonucleases are able to compensate for its loss, performing long-range resection. This might explain why cohesin dependent end tethering is not disrupted by MRX. In line with this, we tested DSB end-tethering in cells lacking Rtt107. This mutant is interesting as it severely reduces Smc5/6 enrichment around DSBs, but not in the immediate vicinity of the break where it is still recruited (Leung et al., 2011). This is likely due to the Smc5/6 ssDNA binding domain, which gives it affinity for ssDNA-dsDNA junctions (Tanasie et al., 2022), and a redundant pathway for DSB recruitment. Interestingly, *rtt107* null cells were still able to perform DSB end-tethering (Section 4, Figure 3), indicating that the local enrichment of Smc5/6 at DSBs is sufficient to insure its role in cohesin dependent end-tethering.

In contrast to loss of MRX, loss of Exo1 leads to defects in long-range resection, and disrupt cohesin dependent end-tethering. Therefore, although we might expect to see enrichment of cohesin at DSBs in *exo1Δ* cells (due to MRXs presence), a reduction in Smc5/6 might be observed. This could explain why cohesin is not competent for DSB end-tethering in EXO1 null cells. Of note, Smc5/6 is typically required for cohesin enrichment at DSBs, so this result would be surprising. Perhaps instead, level of resection somehow dictates Smc5/6 activity. Without extensive resection, some factors that prevent cohesin from becoming competent for end-tethering might remain. ChIP for cohesin and Smc5/6 should be performed in *exo1Δ* and *mre11Δ* mutants. Our DSB compaction in cells lacking Exo1 and Mre11 would also provide an important readout for cohesin's activity in these mutants. If factors important for transforming cohesin into end-tethering cohesin are identified, and are absent at DBSs in cells lacking Exo1, we should artificially target them to the break. Thus potentially rescuing cohesin tethering in *exo1Δ* mutants.

This raises an important point about the role of long-range resection in the cohesin dependent end-tethering pathway. We observe higher end-separation in cohesin depleted cells compared to *exo1Δ* cells, despite them acting in the same pathway. This suggests that some cohesin tethering still takes place in absence of Exo1. To determine if this is due to ssDNA formation by redundant nucleases, we should also investigate end-separation upon Dna2-Sgs1 depletion. Long-range resection is defective in absence of both Dna2-Sgs1 and Exo1, with only short, MRX dependent ssDNA tracts formed (Zhu et al., 2008). In this double mutant, end-

separation levels should reach those seen in cohesin depleted cells. We did not previously check this due to an issue with genomic stability and loss of spots in *sgs1* mutants. However, use of the auxin induced degradation (AID) system for rapid conditional depletion of target proteins provides an opportunity to do so.

Smc3 acetylation and ATPase activity in end tethering

Finally, we should determine the dependence of cohesin DSB end-tethering on Smc3 acetylation/ATPase activity. Smc3 is acetylated for stable maintenance on chromosomes following cohesin establishment. Non-acetylable Smc3 K112R K113R (Smc3RR) containing complexes are active as ATPase's, but are sensitive to Wpl1 releasing (Rolef Ben-Shahar et al. 2008; Ünal et al. 2008). As such, Smc3RR coshesin can still be loaded on to chromosomes, but present sister chromatid cohesion defects. Interestingly, cohesin's oligomerization property is independent of Smc3 acetylation *in vivo* (Xiang and Koshland, 2021). As DSB end-tethering by cohesin is oligomerization dependent, enrichment of these mutant cohesin complexes at DSBs might be sufficient for DSB end-tethering, whilst presenting sister chromatid cohesion defects. This would be the first time that we separate loss of sister chromatid cohesion and maintenance of tethering when the sister is present (in absence of Cdc45 depletion). However, it is important to consider that loss of Smc3 acetylation may also lead to rapid turnover of the end-tethering cohesin population. Alternatively, we could check the dependence of end-tethering on the Smc3 targeting acetyltransferase, Eco1.

On the other hand, we could also test acetyl-mimicking cohesin's, which are ATPase deficient. Of note, the Smc3 K112Q K113Q mutant (Smc3QQ; Heidinger-Pauli et al., 2010) is severely compromised in cohesin loading (Hu et al., 2015). As cohesin DSB end-tethering is dependent on *de novo* enrichment at DSBs, we might observe loss of end-tethering due to lack of cohesin loading or loss of loop extrusion activity. However, Scc2/4 over expression was recently shown to rescue survival in Smc3QQ cells (Boardman et al., 2023). If the mechanisms that stimulate massive cohesin enrichment at DSBs are sufficient to load Smc3QQ containing cohesins should be tested. If this mutant is sufficient for end-tethering, we could also check compaction in the adjacent DNA. As loop extrusion requires cycles of ATP hydrolysis, this should be abolished.

Rad50 mutants and tethering, a rescue experiment for rad50lo

We demonstrated that a rad50 mutant deficient for head oligomerization (rad50lo) was not competent for DSB end-tethering (Kissling et al., 2022; Phipps et al., 2023). However, it is important to consider the effects of such mutations on functions beyond the targeted disruption. Structural changes may not only affect the dimerization ability of the complexes, but also the ability to bind DNA or initiate endonuclease or exonuclease activity. For example, the zinc hook has recently been shown to be important for DNA binding affinity in *E. coli* Mre11-Rad50. As such, the previous observation that the zinc hook is important for DSB end-tethering might be due to a disruption in DNA binding, and not loss of bridging through the hook (Lobachev et al., 2004).

DNA binding was checked *in vitro* for the *rad50lo* mutant. Although slightly reduced, it maintains DNA binding affinity. However its enrichment at DSBs should be tested by ChIP in our system. However, due to reduced Rad50 oligomerization, some decrease might be expected regardless. Reintroducing oligomerization properties to the rad50lo mutant would provide convincing evidence that oligomerization deficiency, and not disrupted DNA binding, explains the observed phenotype. We could achieve this through fusing inducible dimerization FKB domains to Rad50lo head domains, and seeing if inducing dimerization rescues DSB end-tethering. Furthermore, we should check this strain for its ability to perform NHEJ. MRX is essential for NHEJ. As such, ability to repair by NHEJ would demonstrate this is a separation of function mutant.

Remaining general questions around the nature of DSB end-tethering

Other general questions around the nature of DSB end-tethering remain. It is unknown if DNA ends transiently separate following DSB, before coming back into contact, or if they continuously stay in proximity. If they do separate, the time for the ends to come back together, and the mechanism that drives the attraction, are unknown. We could begin to investigate these questions through microfluidics experiments, continuously following individual cells following DSB. Two types of experiment can be imagined. In the first case, we could track DSB end-tethering in individual cells over long periods, taking images every 10

minutes as we did during our repair assay. As our repair movies were performed using the DSB end-tethering strains, I could already begin investigating this question. It would provide important insights into the stability and dynamics of DSB end-tethering mechanisms. For the second case, we could acquire images rapidly in the immediate time after DSB induction, as is often performed when tracking DNA movement *in vivo* (Dion et al., 2012; Dion and Gasser, 2013). Due to the difficulty of knowing exactly when a DSB is induced in our system, an alternative approach could be imagined. One option would be to fuse split fluorescent proteins to components of the NHEJ complex. Formation of the NHEJ complex at a DSB should result in an immediate fluorescent signal, detectable by microscopy. If this signal disappears, either synapsis has failed, or repair has taken place. If the signal reappears, this would indicate that the previous loss of signal was due to loss of synapsis. Performing these experiments in cells lacking Dnl4, in which cells cannot ligate the DNA, might provide proof of principle. It would also be important to repress the expression of HO after DSB induction, to ensure that signal reappearance is not due to a new break being formed.

Part 2 – Understanding discrepancies with conflicting studies

Discrepancies with Hi-C view of DSB end-tethering data

A recent budding yeast study, which induced DSBs and measured Hi-C detectable contacts either side of the break, concluded that cohesin was not required for this process. Instead, the authors proposed a mechanism that is dependent on the 9-1-1 clamp, which binds at the ssDNA-dsDNA junction (Piazza et al., 2021). The reason for this discrepancy is hard to explain, particularly as we did not detect increased end-separation in absence of Rad17, a 9-1-1 component (Chapter 4, Figure 2).

These differences might be due to the techniques used to detect end-separation in each study. One notable difference between our assay and that used in Piazza et al.'s study is that we observe end-tethering in live cells by microscopy. In contrast, Hi-C requires a fixation step, ligation of proximal/crosslinked DNAs, and sequencing of purified DNA fragments, giving a pairwise contact readout. Of note, fragments containing ssDNA will not be ligated during this process, and as such these contacts will be lost. Thus, these observations might be sensitive to levels of resection. Of note, the contact structure is lost in mutants with resection defects. However, how this would lead to loss of the DSB contact structure (LIP) in mutants with delayed resection that maintain end-tethering is unclear. Perhaps the structure observed during this assay represents something other than DSB end-tethering. Higher resolution 3C techniques such as Micro-C might be an important control for understanding what these DSB dependent contacts represent.

The Hi-C assay measures contacts at a population level. In contrast, at 4h post DSB in our assay we are only able to quantify end tethering in roughly 30% of cells, which still contain spots. However, quantifiable cells nearly double in cells lacking Mre11, in which we also see an important affect of cohesin depletion. Furthermore, in our repair assay in absence of the sister chromatid (-Cdc45), we note reduction of repair events from 44% to 16% upon depletion of cohesin. This correlates to a ~75% reduction in repair events, far higher than the 30% end-separation that we are able to detect. This argues against the fact that what we see is only relevant to a small population of cells. To take this further, we should quantify end-tethering throughout time course movies. This would allow us to track end-tethering in all cells before spots are resected, and provide proof of the general requirement for cohesin in end-tethering. Interestingly, Piazza et al. and others have observed increased attempted ectopic repair

events or translocations in cells lacking cohesin (Gelot et al., 2016). Piazza et al. attribute this to loss of cohesin and DSB dependent chromosome individualisation. However, it could also indicate a loss of DSB end-tethering.

Beyond this, our system might create a particular situation where loop extrusion is stalled by the ectopic arrays introduced into the DSB adjacent DNA. Of note, the DSB site used in the Piazza et al. study appears to be a cohesin-associated region. As such, some degree of insulation is observed even in absence of DSB. Why or if this would create a dependence on cohesin for DSB end-tethering in one case but not the other is unclear.

An important step in understanding our observation could be to observe what happens to the ssDNA in the absence of cohesin and end-tethering. To do this, we could induce a DSB and follow tagged Rad51 (Liu et al., 2023) in our strain with LacO and TetO arrays, and a strain without arrays inserted. Loss of end-tethering is likely to also separate the NPF filament. Although resection and filament formation would be altered in *exo1* and *mre11* mutants, these would provide controls to confirm separation of the NPF. If the Rad51 NPF does separate, we could observe the effect of cohesin loss on DSB end-tethering in different chromosome contexts, which could also describe the discrepancy between studies. We could also introduce arrays at the locus in which Piazza et al. induce the DSB, and see if loss of cohesin increases end-separation by microscopy in this context. Ultimately, it is unclear why the differences between these two studies exist. Following the Rad51 NPF in the absence of these factors might provide an important validation of our observation.

Rad52 in DSB end-tethering

Rad52 was previously proposed to be important for DSB end-tethering (Kaye et al., 2004). However, preliminary results from our laboratory (not included in this thesis) indicate that Rad52 is not required in our system. This raises questions about how the system we use might be important for detecting different tethering events. Kaye et al. used a strain in which the fluorescent binding arrays were 50kbp from the DSB site. In contrast, our strain only has 5-7kbp before resection starts to proceed through the arrays. This means that in our assay, we cannot measure separation between ends with extensive resection. For a ssDNA binding protein such as Rad52, the amount of ssDNA available might be important for its tethering

function. It is possible that after a certain level of resection, end- tethering is passed over to ssDNA binding proteins. As Rad52 is important for nucleating the Rad51 NPF, it should be checked if this tethering is performed by Rad52 or Rad51. To investigate this further I could use strains available in our laboratory in which the arrays are also 50kb from the DSB.

Discrepancies with *in vivo* microscopy assays in yeast and humans

In yeast, *in vivo* studies identify MRX as important for early end tethering, and shows there is much less dependence on the NHEJ factors interrogated in NHEJ synapsis studies. Similarly, in human cell lines, loss of Ku only led to a maximum of 10% end-separation (Soutoglou et al., 2007). Perhaps surprisingly, MRN and Smc1 knockdown (KD) resulted in even less DSB end separation in this assay. These results are striking, as they do not correlate with the importance of Ku in forming the human synaptic complex, or MRX and cohesin's role in yeast. One possible explanation for these results is that an unidentified factor carries this function in humans. Alternatively, redundant and compensating pathways might exist. Furthermore, the conditions of this assay might not be robust, or the assay itself might not be sensitive enough to detect end-separation. Of note, end separation was determined significantly after DSB induction (24 hours), as such separation may only have been detectable in cells where NHEJ was prevented (Ku KD). Protein depletion was also achieved using siRNA, it would be interesting to see if rapid depletion using the AID system changed the outcome. Tracking the ends in this system in long microfluidics time course experiments could expose the role of other actors.

Part 3 – Remaining question in cohesin biology

Understanding cohesin oligomerization

Other ways to demonstrate oligomerization dependent cohesin functions should be pursued. First, it would be interesting to check if this mutant still performs loop extrusion *in vitro*, which we might expect considering the ability of mcd1Q266 containing cohein to compact DSB adjacent DNA. We could then check if *the mcd1Q266* mutant forms Hi-C detectable loops. Looking for cohesin dependent contacts that are lost in *mcd1Q266* mutant cells would allow for differentiation between loop extrusion and oligomerization dependent interactions. Furthermore, oligomerization might bring many genomic loci together into a cohesin oligomerization dependent hub. Therefore, molecular methods capable of capturing multiple simultaneous interactions should be used (Zhang and Ma, 2020). This is important as the current gold standard proximity ligation assays (Hi-C; Micro-C) quantify pairwise interactions. Once identified, candidate loci/interactions could be validated by microscopy techniques such as FISH.

Clearly, many other SMC/cohesin oligomerization questions remain. Xiang and Koshland described both off chromosome and on chromosome clusters, the biological significance of these two populations remains unclear. Perhaps an answer lies in the observed enrichment of cohesin at DSBs (Caron et al., 2012; Unal et al., 2004; Strom et al., 2004; Potts et al., 2006); in which case, off chromosome clustered cohesin could represent a pool of readily available cohesin's for rapid response. Xiang and Koshland also described cohesin oligomerization peaking in S phase, before reducing in G2/M, why this happens is not clear, but may indicate an association with replication.

Alternative mechanisms for loop formation

Alternative mechanisms for loop formation have long been proposed. Strong evidence for an extrusion independent mechanism of loop formation came recently (Guerin et al., 2023). Here, cohesin mutants unable to extrude loops *in vitro* were still able to form cohesin dependent chromosome contacts. How these contacts were formed is unclear. One possibility is cohesin oligomerization. As such, it would be interesting to see if Hi-C contacts are

maintained when using these loop extrusion mutants in concert with the *mcd1Q266* allele. Another possibility is that these mutants form loops through a cohesin-DNA capture mechanism. Here, cohesin's which come into contact with far loci would form a loop by topologically loading DNA into the SMC compartment. How such a DNA capture mechanism would work remains unclear, possibilities include capture in a similar fashion to replication coupled sister chromatid cohesion, but if this would require ssDNA, or could topologically entrap a second DNA through another mechanism, is unknown. An interesting way to test this possibility would be to fuse FKB domains to the proposed domains through which cohesin opens (Gruber et al., 2006), and see if *in vivo* loop formation is still possible when this interface cannot open. However, important controls for cohesin's ability to form loops *in vitro*, and associate to DNA *in vivo* would be necessary if loops were abolished. Interestingly, cohesin-DNA capture also presents a mechanism by which loop extrusion barriers could be bypassed.

Interpreting Alphafold predictions for Wpl1 mediated cohesin releasing

The interplay between the core cohesin complex and its HAWKs, and the affect this has on loading, translocation and cohesin releasing are complex, with the full story yet to be fully described. However, use of Alphafold provides satisfactory and testable hypotheses for how these interactions regulate cohesin's function, particularly when considering their correlation with historical experimental observations. Of note, Alphafold predicts that a conserved patch in Wpl1's C-terminal domain sequesters alpha-helices in Scc1's N-terminal domain, holding the Scc1-Smc3 interface open and promoting cohesin releasing (Nasmyth et al., 2023). Although this provides an appealing hypothesis for how Wpl1 mediates cohesin releasing, it will be necessary to validate this model experimentally before wide acceptance in the community. Observing the effect genetic disruption in the Wpl1 C-terminal domain has on releasing activity, as well as solving structures of the Wpl1 and Scc1 domains in question to confirm the predicted interaction, present ideal starting points. Furthermore, Alphafold predicts that Smc3 acetylation in yeast prevents an essential interaction with Scc3 and Smc3 for Wpl1 dependent releasing of cohesin. Genetic data already confirms that the Scc3 domain in question is essential for Wpl1 mediated cohesin releasing (Rowland et al., 2023). Solving the structure of this interaction would be important for validating this model. Insights into why Smc3 acetylation alone is sufficient to abrogate Wpl1 activity would also come from

investigating if Wpl1 is still recruited to Pds5 in yeast when Smc3 is acetylated, as Sororin is not present and thereby does not occupy the Pds5-Wpl1 interface as in humans.

Scc2 for loop extrusion vs sister cohesion

Another curiosity comes in the regulation of cohesin activity by Scc2/4. Scc2/4 is essential for cohesin loading at the end of G1 and during replication coupled cohesion establishment (capturing a second DNA), as well as for translocation during loop extrusion (Davidson et al., 2019; Minamino et al., 2023; Srinivasan et al., 2020). However, it remains to be demonstrated what prevents cohesin from being topologically loaded onto the chromosome during the loop extrusion process. A possible explanation is the lack of active replication, as cohesion establishment relies on the presence of the replication machinery and ssDNA capture (Xu et al., 2007; Minamino et al., 2023). In their absence, cohesin might be free to continue through cycles of ATP hydrolysis and perform loop extrusion. However, cohesin associates with chromosomes in G1, and is sensitive to unloading by Wpl1, suggesting that DNA may be topologically entrapped within the cohesin ring (Kueng et al., 2006; Chan et al., 2012). Despite this, unlike cohesin's loaded during G2/M phase, Scc2 is required for maintaining cohesin association to chromatin during G1 phase (Srinivasan et al., 2019; Srinivasan et al., 2020). This might suggest it is instead pseudotopologcally loaded on to the DNA in an Scc2/4-Kleisin dependent mechanism as described for loop extrusion (Shaltiel et al., 2022). Alternatively, these cohesin's could be topologically loaded inside the cohesin ring without Smc3 acetylation, Scc2 would be required to prevent Pds5-Wpl1 binding and unloading, or for dynamic cycles of cohesin re-loading if it is unloaded. Ultimately, this suggests that other factors are likely important for regulating the shift between cohesive and loop extruding cohesin's, and as such, these mechanisms remain to be fully understood. As cohesin is not believed to be topologically loaded onto chromsomes during loop extrusion (Shatiel et al., 2022), it also remains unclear how Wpl1 mediates cohesin releasing to negatively regulate loop extrusion.

It would also be interesting to know how cohesin composition is regulated. In particular, what infers some complexes to contain Pds5, and others Scc2. Is this based on chance encounters between these two HAWKs and available cohesin complexes, or is this actively regulated. At

sister chromatid cohesion, it is likely that Scc2 dissociates following its loading function, at this point, is there an active mechanism that promotes exchange for Pds5, which is important for Smc3 acetylation.

Part 4 – Stalling condensin loop extrusion

We show that dense linear Rap1 arrays stall DNA loop extrusion *in vitro*, with the blocking efficiency depending on the length of the array and the size of the DNA gap between neighboring proteins (Analikwa, Deshayes et al. 2023). The length threshold for blocking loop extrusion sat at 100nm, which is larger than the SMC arm length. It is likely that loop extrusion was halted due to condensin being unable to grab upstream DNA to which Rap1 was bound.

In vivo, Rap1 arrays in the chromosome generate insulated domains that accumulate condensin at their borders, with direct implications for the resolution of dicentric chromosomes produced by telomere fusions (Guerin et al., 2019). This is important due to condensin's canonical function in condensing mitotic chromosomes. Condensation is an important step for ensuring chromosome compaction, which prevents trailing chromosome segments from remaining in the mother nucleus upon division. The absence of a barrier to loop extrusion at telomeres could hinder condensation. If condensin were to fall off chromosomes, condensation may be defective, and as such, chromosomes may not migrate effectively during segregation.

Interestingly, the density required to stall condensin also correlated with increased DNA stiffness. Lack of flexibility could theoretically prevent passage of the DNA into the lumen during loop extrusion, providing another mechanism to halt this process. Due to the dynamic and non-linear nature of nuclear DNA, it is possible that condensin could bypass a barrier if it comes into contact with DNA beyond the Rap1 array. However, if DNA must perform a double passage through the SMC ring during the proposed power stroke step of loop extrusion, the presence of a stiff filament that cannot bend might present a further barrier.

Of note, passing events did occur in ~20% of cases. Therefore, condensin might be able to reach around the array and continue loop extrusion, suggesting that this stiff fibre/DNA might not need to pass into the SMC ring. However, it cannot be ruled out that this is due to transient Rap1 turnover providing DNA substrate for condensin to grab through the array. One way to challenge this hypothesis could be to increase the length of DNA molecules used in these assays. This could increase the probability of condensin contacting DNA beyond the array, and might increase the number of passing events. In contrast, the number of passing events due to Rap1 turnover should remain the same.

In any case, our *in vivo* Micro-C experiments demonstrated that the Rap1 array generated a strong insulated domain that prevented loop expansion on a chromosome arm. This suggests that in the nuclear context, condensin cannot pass the array by going around it. Whether this is due to preventing condensin from contacting the next DNA section in its loop extrusion cycle, or also due to the presence of a stiff fibre that cannot enter the SMC lumen, remains to be defined. Modelling of the likelihood of DNA beyond the Rap1 array meeting the stalled condensin *in vivo* would provide insight into the probability of these events occurring.

Theoretically, the Rap1 array should be able to stall loop extrusion by cohesin through the same mechanism that it prevents condensin. However, unlike condensin, cohesin has been demonstrated to loop extrude bi-directionally *in vitro* (Davidson et al., 2019; Ganji et al., 2018), and switches direction upon coming into contact with CTCF (Davidson et al., 2023). Furthermore, a cohesin dependent striped contact pattern appears away from DSBs *in vivo*, indicating directional switching upon encountering a DNA end (Arnould et al., 2021). Cohesin switching or stalling in the presence of the Rap1 array would provide insights into whether switching is an intrinsic property of cohesin upon encountering a barrier, or if specific properties at DSB or CTCF boundaries regulate this. CTCF not only switched cohesin loop extrusion direction, but also led to events in which loops started to shrink. It would be interesting to know if hypothetical cohesin-Rap1 array stalling also shares this property, which was not observed for condensin so far. Of note, cohesin interacts directly with CTCF (Li et al., 2020), and its boundary effect depends on the direction of the encounter (Rao et al., 2014). This is particularly interesting as the nature of the interaction with CTCF and the Rap1 array would therefore be different (chemical vs physical), providing regulatory insights.

References

Adane, B., Alexe, G., Seong, B. K. A., Lu, D., Hwang, E. E., Hnisz, D., Lareau, C. A., Ross, L., Lin, S., Dela Cruz, F. S., Richardson, M., Weintraub, A. S., Wang, S., Iniguez, A. B., Dharia, N. V., Conway, A. S., Robichaud, A. L., Tanenbaum, B., Krill-Burger, J. M., Vazquez, F., … Stegmaier, K. (2021). STAG2 loss rewires oncogenic and developmental programs to promote metastasis in Ewing sarcoma. *Cancer cell*, *39*(6), 827–844.e10.

Agashe, S., Joseph, C. R., Reyes, T. A. C., Menolfi, D., Giannattasio, M., Waizenegger, A., Szakal, B., & Branzei, D. (2021). Smc5/6 functions with Sgs1-Top3-Rmi1 to complete chromosome replication at natural pause sites. *Nature communications*, *12*(1), 2111.

Almedawar, S., Colomina, N., Bermúdez-López, M., Pociño-Merino, I., & Torres-Rosell, J. (2012). A SUMO-dependent step during establishment of sister chromatid cohesion. *Current biology : CB*, *22*(17), 1576–1581.

Alt, A., Dang, H. Q., Wells, O. S., Polo, L. M., Smith, M. A., McGregor, G. A., Welte, T., Lehmann, A. R., Pearl, L. H., Murray, J. M., & Oliver, A. W. (2017). Specialized interfaces of Smc5/6 control hinge stability and DNA association. *Nature communications*, *8*, 14011.

Analikwu, B. T., Deshayes, A., Béneut, C., Barth, R., Phipps, J., Scolar, V., Barrington, C., Busso, D., Uhlmann, F., Dubrana, K., Mattarocci, S., Dekker, C., & Marcand, S. (2023). Telomere protein arrays stall DNA loop extrusion by condensin. *bioRxiv 2023.10.29.564563;*

Anand, R., Ranjha, L., Cannavo, E., & Cejka, P. (2016). Phosphorylated CtIP Functions as a Co-factor of the MRE11-RAD50-NBS1 Endonuclease in DNA End Resection. *Molecular cell*, *64*(5), 940–950.

Andrews, E. A., Palecek, J., Sergeant, J., Taylor, E., Lehmann, A. R., & Watts, F. Z. (2005). Nse2, a component of the Smc5-6 complex, is a SUMO ligase required for the response to DNA damage. *Molecular and cellular biology*, *25*(1), 185–196.

Andriuskevicius, T., Kotenko, O., & Makovets, S. (2018). Putting together and taking apart: assembly and disassembly of the Rad51 nucleoprotein filament in DNA repair and genome stability. *Cell stress*, *2*(5), 96–112.

Arnould, C., Rocher, V., Finoux, A. L., Clouaire, T., Li, K., Zhou, F., Caron, P., Mangeot, P. E., Ricci, E. P., Mourad, R., Haber, J. E., Noordermeer, D., & Legube, G. (2021). Loop extrusion as a mechanism for formation of DNA damage repair foci. *Nature*, *590*(7847), 660–665.

Arnould, C., Rocher, V., Saur, F., Bader, A. S., Muzzopappa, F., Collins, S., Lesage, E., Le Bozec, B., Puget, N., Clouaire, T., Mangeat, T., Mourad, R., Ahituv, N., Noordermeer, D., Erdel, F., Bushell, M., Marnef, A., & Legube, G. (2023). Chromatin compartmentalization regulates the response to DNA damage. *Nature*, *623*(7985), 183–192.

Arumugam, P., Gruber, S., Tanaka, K., Haering, C. H., Mechtler, K., & Nasmyth, K. (2003). ATP hydrolysis is required for cohesin's association with chromosomes. *Current biology : CB*, *13*(22), 1941–1953.

Aymard, F., Bugler, B., Schmidt, C. K., Guillou, E., Caron, P., Briois, S., Iacovoni, J. S., Daburon, V., Miller, K. M., Jackson, S. P., & Legube, G. (2014). Transcriptionally active chromatin recruits homologous recombination at DNA double-strand breaks. *Nature structural & molecular biology*, *21*(4), 366–374.

Ba, Z., Lou, J., Ye, A. Y., Dai, H. Q., Dring, E. W., Lin, S. G., Jain, S., Kyritsis, N., Kieffer-Kwon, K. R., Casellas, R., & Alt, F. W. (2020). CTCF orchestrates long-range cohesin-driven V(D)J recombinational scanning. *Nature*, *586*(7828), 305–310.

Bastié, N., Chapard, C., Dauban, L., Gadal, O., Beckouët, F., & Koszul, R. (2022). Smc3 acetylation, Pds5 and Scc2 control the translocase activity that establishes cohesin-dependent chromatin loops. *Nature structural & molecular biology*, *29*(6), 575–585.

Bastié, Chapard, Nejmi, Mboumba, Thierry, Beckouët, Koszul. (2023) Sister chromatid cohesion halts DNA loop expansion. *bioRxiv, 2023.07.31.551217*.

Batté, A., Brocas, C., Bordelet, H., Hocher, A., Ruault, M., Adjiri, A., Taddei, A., & Dubrana, K. (2017). Recombination at subtelomeres is regulated by physical distance, double-strand break resection and chromatin status. *The EMBO journal*, *36*(17), 2609–2625.

Bauer, B. W., Davidson, I. F., Canena, D., Wutz, G., Tang, W., Litos, G., Horn, S., Hinterdorfer, P., & Peters, J. M. (2021). Cohesin mediates DNA loop extrusion by a "swing and clamp" mechanism. *Cell*, *184*(21), 5448–5464.e22.

Bazzano, D., Lomonaco, S., & Wilson, T. E. (2021). Mapping yeast mitotic 5' resection at base resolution reveals the sequence and positional dependence of nucleases in vivo. *Nucleic acids research*, *49*(22), 12607–12621.

Becker, E., Meyer, V., Madaoui, H., & Guerois, R. (2006). Detection of a tandem BRCT in Nbs1 and Xrs2 with functional implications in the DNA damage response. *Bioinformatics (Oxford, England)*, *22*(11), 1289–1292.

Beckouët, F., Hu, B., Roig, M. B., Sutani, T., Komata, M., Uluocak, P., Katis, V. L., Shirahige, K., & Nasmyth, K. (2010). An Smc3 acetylation cycle is essential for establishment of sister chromatid cohesion. *Molecular cell*, *39*(5), 689–699.

Beckouët, F., Srinivasan, M., Roig, M. B., Chan, K. L., Scheinost, J. C., Batty, P., Hu, B., Petela, N., Gligoris, T., Smith, A. C., Strmecki, L., Rowland, B. D., & Nasmyth, K. (2016). Releasing Activity Disengages Cohesin's Smc3/Scc1 Interface in a Process Blocked by Acetylation. *Molecular cell*, *61*(4), 563–574.

Bekker-Jensen, S., Lukas, C., Kitagawa, R., Melander, F., Kastan, M. B., Bartek, J., & Lukas, J. (2006). Spatial organization of the mammalian genome surveillance machinery in response to DNA strand breaks. *The Journal of cell biology*, *173*(2), 195–206.

Rolef Ben-Shahar, T., Heeger, S., Lehane, C., East, P., Flynn, H., Skehel, M., & Uhlmann, F. (2008). Eco1-dependent cohesin acetylation during establishment of sister chromatid cohesion. *Science (New York, N.Y.)*, *321*(5888), 563–566.

Berkovich, E., Monnat, R. J., Jr, & Kastan, M. B. (2007). Roles of ATM and NBS1 in chromatin structure modulation and DNA double-strand break repair. *Nature cell biology*, *9*(6), 683–690.

Birkenbihl, R. P., & Subramani, S. (1992). Cloning and characterization of rad21 an essential gene of Schizosaccharomyces pombe involved in DNA double-strand-break repair. *Nucleic acids research*, *20*(24), 6605–6611.

Bloom, M. S., Koshland, D., & Guacci, V. (2018). Cohesin Function in Cohesion, Condensation, and DNA Repair Is Regulated by Wpl1p via a Common Mechanism in *Saccharomyces cerevisiae*. *Genetics*, *208*(1), 111–124.

Boardman, K., Xiang, S., Chatterjee, F., Mbonu, U., Guacci, V., & Koshland, D. (2023). A model for Scc2p stimulation of cohesin's ATPase and its inhibition by acetylation of Smc3p. *Genes & development*, *37*(7-8), 277–290.

Bonetti, D., Villa, M., Gobbini, E., Cassani, C., Tedeschi, G., & Longhese, M. P. (2015). Escape of Sgs1 from Rad9 inhibition reduces the requirement for Sae2 and functional MRX in DNA end resection. *EMBO reports*, *16*(3), 351–361.

Bordelet, H., Costa, R., Brocas, C., Dépagne, J., Veaute, X., Busso, D., Batté, A., Guérois, R., Marcand, S., & Dubrana, K. (2022). Sir3 heterochromatin protein promotes non-homologous end joining by direct inhibition of Sae2. *The EMBO journal*, *41*(1), e108813.

Borges, V., Lehane, C., Lopez-Serra, L., Flynn, H., Skehel, M., Rolef Ben-Shahar, T., & Uhlmann, F. (2010). Hos1 deacetylates Smc3 to close the cohesin acetylation cycle. *Molecular cell*, *39*(5), 677–688.

Börner, G. V., Hochwagen, A., & MacQueen, A. J. (2023). Meiosis in budding yeast. *Genetics*, *225*(2), iyad125.

Brouwer, I., Sitters, G., Candelli, A., Heerema, S. J., Heller, I., de Melo, A. J., Zhang, H., Normanno, D., Modesti, M., Peterman, E. J., & Wuite, G. J. (2016). Sliding sleeves of XRCC4-XLF bridge DNA and connect fragments of broken DNA. *Nature*, *535*(7613), 566–569.

Buehl, C. J., Goff, N. J., Hardwick, S. W., Gellert, M., Blundell, T. L., Yang, W., Chaplin, A. K., & Meek, K. (2023). Two distinct long-range synaptic complexes promote different aspects of end processing prior to repair of DNA breaks by non-homologous end joining. *Molecular cell*, *83*(5), 698–714.e4.

Bürmann, F., Lee, B. G., Than, T., Sinn, L., O'Reilly, F. J., Yatskevich, S., Rappsilber, J., Hu, B., Nasmyth, K., & Löwe, J. (2019). A folded conformation of MukBEF and cohesin. *Nature structural & molecular biology*, *26*(3), 227–236.

Busslinger, G. A., Stocsits, R. R., van der Lelij, P., Axelsson, E., Tedeschi, A., Galjart, N., & Peters, J. M. (2017). Cohesin is positioned in mammalian genomes by transcription, CTCF and Wapl. *Nature*, *544*(7651), 503–507.

Callebaut, I., & Mornon, J. P. (1997). From BRCA1 to RAP1: a widespread BRCT module closely associated with DNA repair. *FEBS letters*, *400*(1), 25–30.

Cannavo, E., & Cejka, P. (2014). Sae2 promotes dsDNA endonuclease activity within Mre11-Rad50-Xrs2 to resect DNA breaks. *Nature*, *514*(7520), 122–125.

Cannavo, E., Johnson, D., Andres, S. N., Kissling, V. M., Reinert, J. K., Garcia, V., Erie, D. A., Hess, D., Thomä, N. H., Enchev, R. I., Peter, M., Williams, R. S., Neale, M. J., & Cejka, P. (2018). Regulatory control of DNA end resection by Sae2 phosphorylation. *Nature communications*, *9*(1), 4016.

Caron, P., Aymard, F., Iacovoni, J. S., Briois, S., Canitrot, Y., Bugler, B., Massip, L., Losada, A., & Legube, G. (2012). Cohesin protects genes against γH2AX Induced by DNA double-strand breaks. *PLoS genetics*, *8*(1), e1002460.

Casari, E., Rinaldi, C., Marsella, A., Gnugnoli, M., Colombo, C. V., Bonetti, D., & Longhese, M. P. (2019). Processing of DNA Double-Strand Breaks by the MRX Complex in a Chromatin Context. *Frontiers in molecular biosciences*, *6*, 43.

Cassani, C., Gobbini, E., Wang, W., Niu, H., Clerici, M., Sung, P., & Longhese, M. P. (2016). Tel1 and Rif2 Regulate MRX Functions in End-Tethering and Repair of DNA Double-Strand Breaks. *PLoS biology*, *14*(2), e1002387.

Cejka, P., & Symington, L. S. (2021). DNA End Resection: Mechanism and Control. *Annual review of genetics*, *55*, 285–307.

Chan, K. L., Gligoris, T., Upcher, W., Kato, Y., Shirahige, K., Nasmyth, K., & Beckouët, F. (2013). Pds5 promotes and protects cohesin acetylation. *Proceedings of the National Academy of Sciences of the United States of America*, *110*(32), 13020–13025.

Chapard, C., Jones, R., van Oepen, T., Scheinost, J. C., & Nasmyth, K. (2019). Sister DNA Entrapment between Juxtaposed Smc Heads and Kleisin of the Cohesin Complex. *Molecular cell*, *75*(2), 224–237.e5.

Chaplin, A. K., Hardwick, S. W., Stavridi, A. K., Buehl, C. J., Goff, N. J., Ropars, V., Liang, S., De Oliveira, T. M., Chirgadze, D. Y., Meek, K., Charbonnier, J. B., & Blundell, T. L. (2021). Cryo-EM of NHEJ supercomplexes provides insights into DNA repair. *Molecular cell*, *81*(16), 3400–3409.e3.

Chappidi, N., De Gregorio, G., & Ferrari, S. (2019). Replication stress-induced Exo1 phosphorylation is mediated by Rad53/Pph3 and Exo1 nuclear localization is controlled by 14-3-3 proteins. *Cell division*, *14*, 1.

Ray Chaudhuri, A., & Nussenzweig, A. (2017). The multifaceted roles of PARP1 in DNA repair and chromatin remodelling. *Nature reviews. Molecular cell biology*, *18*(10), 610–621.

Cheblal, A., Challa, K., Seeber, A., Shimada, K., Yoshida, H., Ferreira, H. C., Amitai, A., & Gasser, S. M. (2020). DNA Damage-Induced Nucleosome Depletion Enhances Homology Search Independently of Local Break Movement. *Molecular cell*, *80*(2), 311–326.e4.

Chen, L., Trujillo, K., Ramos, W., Sung, P., & Tomkinson, A. E. (2001). Promotion of Dnl4-catalyzed DNA end-joining by the Rad50/Mre11/Xrs2 and Hdf1/Hdf2 complexes. *Molecular cell*, *8*(5), 1105–1115.

Chen, S., Lee, L., Naila, T., Fishbain, S., Wang, A., Tomkinson, A. E., Lees-Miller, S. P., & He, Y. (2021). Structural basis of long-range to short-range synaptic transition in NHEJ. *Nature*, *593*(7858), 294–298.

Chen, S., Vogt, A., Lee, L., Naila, T., McKeown, R., Tomkinson, A. E., Lees-Miller, S. P., & He, Y. (2023). Cryo-EM visualization of DNA-PKcs structural intermediates in NHEJ. *Science advances*, *9*(22), eadg2838.

Chen, X., & Tomkinson, A. E. (2011). Yeast Nej1 is a key participant in the initial end binding and final ligation steps of nonhomologous end joining. *The Journal of biological chemistry*, *286*(6), 4931–4940.

Chimthanawala, A., Parmar, J. J., Kumar, S., Iyer, K. S., Rao, M., & Badrinarayanan, A. (2022). SMC protein RecN drives RecA filament translocation for in vivo homology search. *Proceedings of the National Academy of Sciences of the United States of America*, *119*(46), e2209304119.

Chiolo, I., Minoda, A., Colmenares, S. U., Polyzos, A., Costes, S. V., & Karpen, G. H. (2011). Double-strand breaks in heterochromatin move outside of a dynamic HP1a domain to complete recombinational repair. *Cell*, *144*(5), 732–744.

Choudhary, K., Itzkovich, Z., Alonso-Perez, E., Bishara, H., Dunn, B., Sherlock, G., & Kupiec, M. (2022). S. cerevisiae Cells Can Grow without the Pds5 Cohesin Subunit. *mBio*, *13*(4), e0142022.

Ciosk, R., Shirayama, M., Shevchenko, A., Tanaka, T., Toth, A., Shevchenko, A., & Nasmyth, K. (2000). Cohesin's binding to chromosomes depends on a separate complex consisting of Scc2 and Scc4 proteins. *Molecular cell*, *5*(2), 243–254.

Clouaire, T., Rocher, V., Lashgari, A., Arnould, C., Aguirrebengoa, M., Biernacka, A., Skrzypczak, M., Aymard, F., Fongang, B., Dojer, N., Iacovoni, J. S., Rowicka, M., Ginalski, K., Côté, J., & Legube, G. (2018). Comprehensive Mapping of Histone Modifications at DNA Double-Strand Breaks Deciphers Repair Pathway Chromatin Signatures. *Molecular cell*, *72*(2), 250–262.e6.

Collier, J. E., Lee, B. G., Roig, M. B., Yatskevich, S., Petela, N. J., Metson, J., Voulgaris, M., Gonzalez Llamazares, A., Löwe, J., & Nasmyth, K. A. (2020). Transport of DNA within cohesin involves clamping on top of engaged heads by Scc2 and entrapment within the ring by Scc3. *eLife*, *9*, e59560.

Collier, J. E., & Nasmyth, K. A. (2022). DNA passes through cohesin's hinge as well as its Smc3-kleisin interface. *eLife*, *11*, e80310.

Collins, P. L., Purman, C., Porter, S. I., Nganga, V., Saini, A., Hayer, K. E., Gurewitz, G. L., Sleckman, B. P., Bednarski, J. J., Bassing, C. H., & Oltz, E. M. (2020). DNA double-strand breaks induce H2Ax phosphorylation domains in a contact-dependent manner. *Nature communications*, *11*(1), 3158.

Copsey, A., Tang, S., Jordan, P. W., Blitzblau, H. G., Newcombe, S., Chan, A. C., Newnham, L., Li, Z., Gray, S., Herbert, A. D., Arumugam, P., Hochwagen, A., Hunter, N., & Hoffmann, E. (2013). Smc5/6 coordinates formation and resolution of joint molecules with chromosome morphology to ensure meiotic divisions. *PLoS genetics*, *9*(12), e1004071.

Costantino, L., Hsieh, T. S., Lamothe, R., Darzacq, X., & Koshland, D. (2020). Cohesin residency determines chromatin loop patterns. *eLife*, *9*, e59889.

Dai, H. Q., Hu, H., Lou, J., Ye, A. Y., Ba, Z., Zhang, X., Zhang, Y., Zhao, L., Yoon, H. S., Chapdelaine-Williams, A. M., Kyritsis, N., Chen, H., Johnson, K., Lin, S., Conte, A., Casellas, R., Lee, C. S., & Alt, F. W. (2021). Loop extrusion mediates physiological Igh locus contraction for RAG scanning. *Nature*, *590*(7845), 338–343.

D'Ambrosio, L. M., & Lavoie, B. D. (2014). Pds5 prevents the PolySUMO-dependent separation of sister chromatids. *Current biology : CB*, *24*(4), 361–371.

D'Amours, D., & Jackson, S. P. (2001). The yeast Xrs2 complex functions in S phase checkpoint regulation. *Genes & development*, *15*(17), 2238–2249.

Dauban, L., Montagne, R., Thierry, A., Lazar-Stefanita, L., Bastié, N., Gadal, O., Cournac, A., Koszul, R., & Beckouët, F. (2020). Regulation of Cohesin-Mediated Chromosome Folding by Eco1 and Other Partners. *Molecular cell*, *77*(6), 1279–1293.e4.

Davidson, I. F., Barth, R., Zaczek, M., van der Torre, J., Tang, W., Nagasaka, K., Janissen, R., Kerssemakers, J., Wutz, G., Dekker, C., & Peters, J. M. (2023). CTCF is a DNA-tension-dependent barrier to cohesin-mediated loop extrusion. *Nature*, *616*(7958), 822–827.

Davidson, I. F., & Peters, J. M. (2021). Genome folding through loop extrusion by SMC complexes. *Nature reviews. Molecular cell biology*, *22*(7), 445–464.

Davidson, I. F., Bauer, B., Goetz, D., Tang, W., Wutz, G., & Peters, J. M. (2019). DNA loop extrusion by human cohesin. *Science (New York, N.Y.)*, *366*(6471), 1338–1345.

De Koninck, M., & Losada, A. (2016). Cohesin Mutations in Cancer. *Cold Spring Harbor perspectives in medicine*, *6*(12), a026476.

Deardorff, M. A., Bando, M., Nakato, R., Watrin, E., Itoh, T., Minamino, M., Saitoh, K., Komata, M., Katou, Y., Clark, D., Cole, K. E., De Baere, E., Decroos, C., Di Donato, N., Ernst, S., Francey, L. J., Gyftodimou, Y., Hirashima, K., Hullings, M., Ishikawa, Y., … Shirahige, K. (2012). HDAC8 mutations in Cornelia de Lange syndrome affect the cohesin acetylation cycle. *Nature*, *489*(7415), 313–317.

DeFazio, L. G., Stansel, R. M., Griffith, J. D., & Chu, G. (2002). Synapsis of DNA ends by DNA-dependent protein kinase. *The EMBO journal*, *21*(12), 3192–3200.

Dekker, C., Haering, C. H., Peters, J. M., & Rowland, B. D. (2023). How do molecular motors fold the genome?. *Science (New York, N.Y.)*, *382*(6671), 646–648.

Desai-Mehta, A., Cerosaletti, K. M., & Concannon, P. (2001). Distinct functional domains of nibrin mediate Mre11 binding, focus formation, and nuclear localization. *Molecular and cellular biology*, *21*(6), 2184–2191.

Deshpande, I., Seeber, A., Shimada, K., Keusch, J. J., Gut, H., & Gasser, S. M. (2017). Structural Basis of Mec1-Ddc2-RPA Assembly and Activation on Single-Stranded DNA at Sites of Damage. *Molecular cell*, *68*(2), 431–445.e5.

Deshpande, R. A., & Wilson, T. E. (2007). Modes of interaction among yeast Nej1, Lif1 and Dnl4 proteins and comparison to human XLF, XRCC4 and Lig4. *DNA repair*, *6*(10), 1507–1516.

Diebold-Durand, M. L., Lee, H., Ruiz Avila, L. B., Noh, H., Shin, H. C., Im, H., Bock, F. P., Bürmann, F., Durand, A., Basfeld, A., Ham, S., Basquin, J., Oh, B. H., & Gruber, S. (2017). Structure of Full-Length SMC and Rearrangements Required for Chromosome Organization. *Molecular cell*, *67*(2), 334–347.e5.

Dimitrova, N., Chen, Y. C., Spector, D. L., & de Lange, T. (2008). 53BP1 promotes non-homologous end joining of telomeres by increasing chromatin mobility. *Nature*, *456*(7221), 524–528.

Dinkelmann, M., Spehalski, E., Stoneham, T., Buis, J., Wu, Y., Sekiguchi, J. M., & Ferguson, D. O. (2009). Multiple functions of MRN in end-joining pathways during isotype class switching. *Nature structural & molecular biology*, *16*(8), 808–813.

Dion, V., Kalck, V., Horigome, C., Towbin, B. D., & Gasser, S. M. (2012). Increased mobility of double-strand breaks requires Mec1, Rad9 and the homologous recombination machinery. *Nature cell biology*, *14*(5), 502–509.

Yasunori Horikoshi, Hiroki Shima, Jiying Sun, Wataru Kobayashi, Volker J. Schmid, Hiroshi Ochiai, Lin Shi, Atsuhiko Fukuto, Yasuha Kinugasa, Hitoshi Kurumizaka, Tsuyoshi Ikura, Yolanda Markaki, Shin-ichi Tate, Kazuhiko Igarashi, Thomas Cremer, & Satoshi Tashiro. (2021). Distinctive nuclear zone for RAD51-mediated homologous recombinational DNA repair. *BioRxiv, 2021.11.29.470307.*

Dumont, A., Mendiboure, N., Savocco, J., Anani, L., Moreau, P., Modolo, L., Jost, D., & Piazza, A. (2023). Mechanism of homology search expansion during recombinational DNA break repair. *bioRxiv 2023.12.01.569403*

Ellenberger, T., & Tomkinson, A. E. (2008). Eukaryotic DNA ligases: structural and functional insights. *Annual review of biochemistry*, *77*, 313–338.

Emerson, C. H., & Bertuch, A. A. (2016). Consider the workhorse: Nonhomologous end-joining in budding yeast. *Biochemistry and cell biology, 94*(5), 396–406.

Forte, G., Boteva, L., Conforto, F., Gilbert, N., Cook, P. R., & Marenduzzo, D. (2024). Bridging condensins mediate compaction of mitotic chromosomes. *The Journal of cell biology*, *223*(1), e202209113.

Fousteri, M. I., & Lehmann, A. R. (2000). A novel SMC protein complex in Schizosaccharomyces pombe contains the Rad18 DNA repair protein. *The EMBO journal*, *19*(7), 1691–1702.

Friedel, A. M., Pike, B. L., & Gasser, S. M. (2009). ATR/Mec1: coordinating fork stability and repair. *Current opinion in cell biology*, *21*(2), 237–244.

Fu, J., Zhou, S., Xu, H., Liao, L., Shen, H., Du, P., & Zheng, X. (2023). ATM-ESCO2-SMC3 axis promotes 53BP1 recruitment in response to DNA damage and safeguards genome integrity by stabilizing cohesin complex. *Nucleic acids research*, *51*(14), 7376–7391.

Fudenberg, G., Imakaev, M., Lu, C., Goloborodko, A., Abdennur, N., & Mirny, L. A. (2016). Formation of Chromosomal Domains by Loop Extrusion. *Cell reports*, *15*(9), 2038–2049.

Gandhi, R., Gillespie, P. J., & Hirano, T. (2006). Human Wapl is a cohesin-binding protein that promotes sister-chromatid resolution in mitotic prophase. *Current biology : CB*, *16*(24), 2406–2417.

Ganji, M., Shaltiel, I. A., Bisht, S., Kim, E., Kalichava, A., Haering, C. H., & Dekker, C. (2018). Real-time imaging of DNA loop extrusion by condensin. *Science (New York, N.Y.)*, *360*(6384), 102–105.

Gao, Y., Chaudhuri, J., Zhu, C., Davidson, L., Weaver, D. T., & Alt, F. W. (1998). A targeted DNA-PKcs-null mutation reveals DNA-PK-independent functions for KU in V(D)J recombination. *Immunity*, *9*(3), 367–376.

García-Nieto, A., Patel, A., Li, Y., Oldenkamp, R., Feletto, L., Graham, J. J., Willems, L., Muir, K. W., Panne, D., & Rowland, B. D. (2023). Structural basis of centromeric cohesion protection. *Nature structural & molecular biology*, *30*(6), 853–859.

Gassler, J., Brandão, H. B., Imakaev, M., Flyamer, I. M., Ladstätter, S., Bickmore, W. A., Peters, J. M., Mirny, L. A., & Tachibana, K. (2017). A mechanism of cohesin-dependent loop extrusion organizes zygotic genome architecture. *The EMBO journal*, *36*(24), 3600–3618.

Gelot, C., Guirouilh-Barbat, J., Le Guen, T., Dardillac, E., Chailleux, C., Canitrot, Y., & Lopez, B. S. (2016). The Cohesin Complex Prevents the End Joining of Distant DNA Double-Strand Ends. *Molecular cell*, *61*(1), 15–26.

Gelot, C., Guirouilh-Barbat, J., & Lopez, B. S. (2018). The Cohesion complex maintains genome stability by preventing end joining of distant DNA ends in S phase. *Molecular & cellular oncology*, *5*(3), e1154123.

Gerguri, T., Fu, X., Kakui, Y., Khatri, B. S., Barrington, C., Bates, P. A., & Uhlmann, F. (2021). Comparison of loop extrusion and diffusion capture as mitotic chromosome formation pathways in fission yeast. *Nucleic acids research*, *49*(3), 1294–1312.

Gibcus, J. H., Samejima, K., Goloborodko, A., Samejima, I., Naumova, N., Nuebler, J., Kanemaki, M. T., Xie, L., Paulson, J. R., Earnshaw, W. C., Mirny, L. A., & Dekker, J. (2018). A pathway for mitotic chromosome formation. *Science (New York, N.Y.)*, *359*(6376), eaao6135.

Gligoris, T., & Löwe, J. (2016). Structural Insights into Ring Formation of Cohesin and Related Smc Complexes. *Trends in cell biology*, *26*(9), 680–693.

Glynn, E. F., Megee, P. C., Yu, H. G., Mistrot, C., Unal, E., Koshland, D. E., DeRisi, J. L., & Gerton, J. L. (2004). Genome-wide mapping of the cohesin complex in the yeast Saccharomyces cerevisiae. *PLoS biology*, *2*(9), E259.

Golfier, S., Quail, T., Kimura, H., & Brugués, J. (2020). Cohesin and condensin extrude DNA loops in a cell cycle-dependent manner. *eLife*, *9*, e53885.

Goodarzi, A. A., Noon, A. T., Deckbar, D., Ziv, Y., Shiloh, Y., Löbrich, M., & Jeggo, P. A. (2008). ATM signaling facilitates repair of DNA double-strand breaks associated with heterochromatin. *Molecular cell*, *31*(2), 167–177.

Graham, T. G., Walter, J. C., & Loparo, J. J. (2016). Two-Stage Synapsis of DNA Ends during Non-homologous End Joining. *Molecular cell*, *61*(6), 850–858.

Gruber, S., Arumugam, P., Katou, Y., Kuglitsch, D., Helmhart, W., Shirahige, K., & Nasmyth, K. (2006). Evidence that loading of cohesin onto chromosomes involves opening of its SMC hinge. *Cell*, *127*(3), 523–537.

Gruber, S., Haering, C. H., & Nasmyth, K. (2003). Chromosomal cohesin forms a ring. *Cell*, *112*(6), 765–777.

Guacci, V., & Koshland, D. (2012). Cohesin-independent segregation of sister chromatids in budding yeast. *Molecular biology of the cell*, *23*(4), 729–739.

Guérin, T. M., Béneut, C., Barinova, N., López, V., Lazar-Stefanita, L., Deshayes, A., Thierry, A., Koszul, R., Dubrana, K., & Marcand, S. (2019). Condensin-Mediated Chromosome Folding and Internal Telomeres Drive Dicentric Severing by Cytokinesis. *Molecular cell*, *75*(1), 131–144.e3.

Guérin, T. M., Barrington, C., Pobegalov, G., Molodtsov, M. I., & Uhlmann, F. (2023). Cohesin chromatin loop formation by an extrinsic motor. *bioRxiv 2023.11.30.569410*

Gutierrez-Escribano, P., Newton, M. D., Llauró, A., Huber, J., Tanasie, L., Davy, J., Aly, I., Aramayo, R., Montoya, A., Kramer, H., Stigler, J., Rueda, D. S., & Aragon, L. (2019). A conserved ATP- and Scc2/4-dependent activity for cohesin in tethering DNA molecules. *Science advances*, *5*(11), eaay6804.

Haering, C. H., Farcas, A. M., Arumugam, P., Metson, J., & Nasmyth, K. (2008). The cohesin ring concatenates sister DNA molecules. *Nature*, *454*(7202), 297–301.

Haering, C. H., Löwe, J., Hochwagen, A., & Nasmyth, K. (2002). Molecular architecture of SMC proteins and the yeast cohesin complex. *Molecular cell*, *9*(4), 773–788.

Hammel, M., Yu, Y., Fang, S., Lees-Miller, S. P., & Tainer, J. A. (2010). XLF regulates filament architecture of the XRCC4·ligase IV complex. *Structure (London, England : 1993)*, *18*(11), 1431–1442.

Hammet, A., Magill, C., Heierhorst, J., & Jackson, S. P. (2007). Rad9 BRCT domain interaction with phosphorylated H2AX regulates the G1 checkpoint in budding yeast. *EMBO reports*, *8*(9), 851–857.

Hansen A. S. (2020). CTCF as a boundary factor for cohesin-mediated loop extrusion: evidence for a multi-step mechanism. *Nucleus (Austin, Tex.)*, *11*(1), 132–148.

Hara, K., Zheng, G., Qu, Q., Liu, H., Ouyang, Z., Chen, Z., Tomchick, D. R., & Yu, H. (2014). Structure of cohesin subcomplex pinpoints direct shugoshin-Wapl antagonism in centromeric cohesion. *Nature structural & molecular biology*, *21*(10), 864–870.

Hauer, M. H., & Gasser, S. M. (2017). Chromatin and nucleosome dynamics in DNA damage and repair. *Genes & development*, *31*(22), 2204–2221.

He, J., Shi, L. Z., Truong, L. N., Lu, C. S., Razavian, N., Li, Y., Negrete, A., Shiloach, J., Berns, M. W., & Wu, X. (2012). Rad50 zinc hook is important for the Mre11 complex to bind chromosomal DNA double-stranded breaks and initiate various DNA damage responses. *The Journal of biological chemistry*, *287*(38), 31747–31756.

He, P., & Yang, W. (2018). Template and primer requirements for DNA Pol θ-mediated end joining. *Proceedings of the National Academy of Sciences of the United States of America*, *115*(30), 7747–7752.

Heidinger-Pauli, J. M., Onn, I., & Koshland, D. (2010). Genetic evidence that the acetylation of the Smc3p subunit of cohesin modulates its ATP-bound state to promote cohesion establishment in Saccharomyces cerevisiae. *Genetics*, *185*(4), 1249–1256.

Heidinger-Pauli, J. M., Unal, E., & Koshland, D. (2009). Distinct targets of the Eco1 acetyltransferase modulate cohesion in S phase and in response to DNA damage. *Molecular cell*, *34*(3), 311–321.

Herrmann, G., Lindahl, T., & Schär, P. (1998). Saccharomyces cerevisiae LIF1: a function involved in DNA double-strand break repair related to mammalian XRCC4. *The EMBO journal*, *17*(14), 4188–4198.

Higashi, T. L., Eickhoff, P., Sousa, J. S., Locke, J., Nans, A., Flynn, H. R., Snijders, A. P., Papageorgiou, G., O'Reilly, N., Chen, Z. A., O'Reilly, F. J., Rappsilber, J., Costa, A., & Uhlmann, F. (2020). A Structure-Based Mechanism for DNA Entry into the Cohesin Ring. *Molecular cell*, *79*(6), 917–933.e9.

Higashi, T. L., Pobegalov, G., Tang, M., Molodtsov, M. I., & Uhlmann, F. (2021). A Brownian ratchet model for DNA loop extrusion by the cohesin complex. *eLife*, *10*, e67530.

Hill, L., Ebert, A., Jaritz, M., Wutz, G., Nagasaka, K., Tagoh, H., Kostanova-Poliakova, D., Schindler, K., Sun, Q., Bönelt, P., Fischer, M., Peters, J. M., & Busslinger, M. (2020). Wapl repression by Pax5 promotes V gene recombination by Igh loop extrusion. *Nature*, *584*(7819), 142–147.

Hirano T. (2012). Condensins: universal organizers of chromosomes with diverse functions. *Genes & development*, *26*(15), 1659–1678.

Hopfner, K. P., Craig, L., Moncalian, G., Zinkel, R. A., Usui, T., Owen, B. A., Karcher, A., Henderson, B., Bodmer, J. L., McMurray, C. T., Carney, J. P., Petrini, J. H., & Tainer, J. A. (2002). The Rad50 zinc-hook is a structure joining Mre11 complexes in DNA recombination and repair. *Nature*, *418*(6897), 562–566.

Hopfner, K. P., Karcher, A., Shin, D. S., Craig, L., Arthur, L. M., Carney, J. P., & Tainer, J. A. (2000). Structural biology of Rad50 ATPase: ATP-driven conformational control in DNA double-strand break repair and the ABC-ATPase superfamily. *Cell*, *101*(7), 789–800.

Horigome, C., Bustard, D. E., Marcomini, I., Delgoshaie, N., Tsai-Pflugfelder, M., Cobb, J. A., & Gasser, S. M. (2016). PolySUMOylation by Siz2 and Mms21 triggers relocation of DNA breaks to nuclear pores through the Slx5/Slx8 STUbL. *Genes & development*, *30*(8), 931–945.

Hozé, N., Ruault, M., Amoruso, C., Taddei, A., & Holcman, D. (2013). Spatial telomere organization and clustering in yeast Saccharomyces cerevisiae nucleus is generated by a random dynamics of aggregation-dissociation. *Molecular biology of the cell*, *24*(11), 1791–S10.

Iacovoni, J. S., Caron, P., Lassadi, I., Nicolas, E., Massip, L., Trouche, D., & Legube, G. (2010). High-resolution profiling of gammaH2AX around DNA double strand breaks in the mammalian genome. *The EMBO journal*, *29*(8), 1446–1457.

Ivanov, E. L., Sugawara, N., Fishman-Lobell, J., & Haber, J. E. (1996). Genetic requirements for the single-strand annealing pathway of double-strand break repair in Saccharomyces cerevisiae. *Genetics*, *142*(3), 693–704.

Ivanov, M. P., Ladurner, R., Poser, I., Beveridge, R., Rampler, E., Hudecz, O., Novatchkova, M., Hériché, J. K., Wutz, G., van der Lelij, P., Kreidl, E., Hutchins, J. R., Axelsson-Ekker, H., Ellenberg, J., Hyman, A. A., Mechtler, K., & Peters, J. M. (2018). The replicative helicase MCM recruits cohesin acetyltransferase ESCO2 to mediate centromeric sister chromatid cohesion. *The EMBO journal*, *37*(15), e97150.

Iwasaki, D., Hayashihara, K., Shima, H., Higashide, M., Terasawa, M., Gasser, S. M., & Shinohara, M. (2016). The MRX Complex Ensures NHEJ Fidelity through Multiple Pathways Including Xrs2-FHA-Dependent Tel1 Activation. *PLoS genetics*, *12*(3), e1005942.

Jackson, S. P., & Bartek, J. (2009). The DNA-damage response in human biology and disease. *Nature*, *461*(7267), 1071–1078.

Janssen, A., Breuer, G. A., Brinkman, E. K., van der Meulen, A. I., Borden, S. V., van Steensel, B., Bindra, R. S., LaRocque, J. R., & Karpen, G. H. (2016). A single double-strand break system reveals repair dynamics and mechanisms in heterochromatin and euchromatin. *Genes & development*, *30*(14), 1645–1657.

Jeppsson, Pradhan, Sutani, Sakata, Igarashi, Berta, Kanno, Nakato, Shirahige, Kim, & Björkegren. (2023). Loop-extruding Smc5/6 organizes transcription-induced positive DNA supercoils. *BioRxiv*, 2023.06.20.545053.

Jeppsson, K., Sakata, T., Nakato, R., Milanova, S., Shirahige, K., & Björkegren, C. (2022). Cohesin-dependent chromosome loop extrusion is limited by transcription and stalled replication forks. *Science advances*, *8*(23), eabn7063.

Karl, L. A., Peritore, M., Galanti, L., & Pfander, B. (2022). DNA Double Strand Break Repair and Its Control by Nucleosome Remodeling. *Frontiers in genetics*, *12*, 821543.

Käshammer, L., Saathoff, J. H., Lammens, K., Gut, F., Bartho, J., Alt, A., Kessler, B., & Hopfner, K. P. (2019). Mechanism of DNA End Sensing and Processing by the Mre11-Rad50 Complex. *Molecular cell*, *76*(3), 382–394.e6.

Kaur, M., Blair, J., Devkota, B., Fortunato, S., Clark, D., Lawrence, A., Kim, J., Do, W., Semeo, B., Katz, O., Mehta, D., Yamamoto, N., Schindler, E., Al Rawi, Z., Wallace, N., Wilde, J. J., McCallum, J., Liu, J., Xu, D., Jackson, M., … Krantz, I. D. (2023). Genomic analyses in Cornelia de Lange Syndrome and related diagnoses: Novel candidate genes, genotype-phenotype correlations and common mechanisms. *American journal of medical genetics. Part A*, *191*(8), 2113–2131.

Kaushik, A., Than, T., Petela, N. J., Voulgaris, M., Percival, C., Daniels, P., Rafferty, J. B., Nasmyth, K. A., & Hu, B. (2023). Conformational dynamics of cohesin/Scc2 loading complex are regulated by Smc3 acetylation and ATP binding. *Nature communications*, *14*(1), 5929.

Kaye, J. A., Melo, J. A., Cheung, S. K., Vaze, M. B., Haber, J. E., & Toczyski, D. P. (2004). DNA breaks promote genomic instability by impeding proper chromosome segregation. *Current biology : CB*, *14*(23), 2096–2106.

Kikuchi, S., Borek, D. M., Otwinowski, Z., Tomchick, D. R., & Yu, H. (2016). Crystal structure of the cohesin loader Scc2 and insight into cohesinopathy. *Proceedings of the National Academy of Sciences of the United States of America*, *113*(44), 12444–12449.

Kilic, S., Lezaja, A., Gatti, M., Bianco, E., Michelena, J., Imhof, R., & Altmeyer, M. (2019). Phase separation of 53BP1 determines liquid-like behavior of DNA repair compartments. *The EMBO journal*, *38*(16), e101379.

Kim, S. T., Xu, B., & Kastan, M. B. (2002). Involvement of the cohesin protein, Smc1, in Atm-dependent and independent responses to DNA damage. *Genes & development*, *16*(5), 560–570.

Kim, Y., Shi, Z., Zhang, H., Finkelstein, I. J., & Yu, H. (2019). Human cohesin compacts DNA by loop extrusion. *Science (New York, N.Y.)*, *366*(6471), 1345–1349.

Kinoshita, K., Tsubota, Y., Tane, S., Aizawa, Y., Sakata, R., Takeuchi, K., Shintomi, K., Nishiyama, T., & Hirano, T. (2022). A loop extrusion-independent mechanism contributes to condensin I-mediated chromosome shaping. *The Journal of cell biology*, *221*(3), e202109016.

Kissling, V. M., Reginato, G., Bianco, E., Kasaciunaite, K., Tilma, J., Cereghetti, G., Schindler, N., Lee, S. S., Guérois, R., Luke, B., Seidel, R., Cejka, P., & Peter, M. (2022). Mre11-Rad50 oligomerization promotes DNA double-strand break repair. *Nature communications*, *13*(1), 2374.

Klein, F., Mahr, P., Galova, M., Buonomo, S. B., Michaelis, C., Nairz, K., & Nasmyth, K. (1999). A central role for cohesins in sister chromatid cohesion, formation of axial elements, and recombination during yeast meiosis. *Cell*, *98*(1), 91–103.

Koole, W., van Schendel, R., Karambelas, A. E., van Heteren, J. T., Okihara, K. L., & Tijsterman, M. (2014). A Polymerase Theta-dependent repair pathway suppresses extensive genomic instability at endogenous G4 DNA sites. *Nature communications*, *5*, 3216.

Krawczyk, P. M., Borovski, T., Stap, J., Cijsouw, T., ten Cate, R., Medema, J. P., Kanaar, R., Franken, N. A., & Aten, J. A. (2012). Chromatin mobility is increased at sites of DNA double-strand breaks. *Journal of cell science*, *125*(Pt 9), 2127–2133.

Kueng, S., Hegemann, B., Peters, B. H., Lipp, J. J., Schleiffer, A., Mechtler, K., & Peters, J. M. (2006). Wapl controls the dynamic association of cohesin with chromatin. *Cell*, *127*(5), 955–967.

Ladurner, R., Kreidl, E., Ivanov, M. P., Ekker, H., Idarraga-Amado, M. H., Busslinger, G. A., Wutz, G., Cisneros, D. A., & Peters, J. M. (2016). Sororin actively maintains sister chromatid cohesion. *The EMBO journal*, *35*(6), 635–653.

Lee, B. G., Roig, M. B., Jansma, M., Petela, N., Metson, J., Nasmyth, K., & Löwe, J. (2016). Crystal Structure of the Cohesin Gatekeeper Pds5 and in Complex with Kleisin Scc1. *Cell reports*, *14*(9), 2108–2115.

Lee, B. G., Merkel, F., Allegretti, M., Hassler, M., Cawood, C., Lecomte, L., O'Reilly, F. J., Sinn, L. R., Gutierrez-Escribano, P., Kschonsak, M., Bravo, S., Nakane, T., Rappsilber, J., Aragon, L., Beck, M., Löwe, J., & Haering, C. H. (2020). Cryo-EM structures of holo condensin reveal a subunit flip-flop mechanism. *Nature structural & molecular biology*, *27*(8), 743–751.

Lee, C. S., Lee, K., Legube, G., & Haber, J. E. (2014). Dynamics of yeast histone H2A and H2B phosphorylation in response to a double-strand break. *Nature structural & molecular biology*, *21*(1), 103–109.

Lee, K., & Lee, S. E. (2007). Saccharomyces cerevisiae Sae2- and Tel1-dependent single-strand DNA formation at DNA break promotes microhomology-mediated end joining. *Genetics*, *176*(4), 2003–2014.

Lee, K., Zhang, Y., & Lee, S. E. (2008). Saccharomyces cerevisiae ATM orthologue suppresses break-induced chromosome translocations. *Nature*, *454*(7203), 543–546.

Lemaître, C., Grabarz, A., Tsouroula, K., Andronov, L., Furst, A., Pankotai, T., Heyer, V., Rogier, M., Attwood, K. M., Kessler, P., Dellaire, G., Klaholz, B., Reina-San-Martin, B., & Soutoglou, E. (2014). Nuclear position dictates DNA repair pathway choice. *Genes & development*, *28*(22), 2450–2463.

Lengronne, A., Katou, Y., Mori, S., Yokobayashi, S., Kelly, G. P., Itoh, T., Watanabe, Y., Shirahige, K., & Uhlmann, F. (2004). Cohesin relocation from sites of chromosomal loading to places of convergent transcription. *Nature*, *430*(6999), 573–578.

Lengronne, A., McIntyre, J., Katou, Y., Kanoh, Y., Hopfner, K. P., Shirahige, K., & Uhlmann, F. (2006). Establishment of sister chromatid cohesion at the S. cerevisiae replication fork. *Molecular cell*, *23*(6), 787–799.

Leung, G. P., Brown, J. A., Glover, J. N., & Kobor, M. S. (2016). Rtt107 BRCT domains act as a targeting module in the DNA damage response. *DNA repair*, *37*, 22–32.

Leung, G. P., Lee, L., Schmidt, T. I., Shirahige, K., & Kobor, M. S. (2011). Rtt107 is required for recruitment of the SMC5/6 complex to DNA double strand breaks. *The Journal of biological chemistry*, *286*(29), 26250–26257.

Li, K., Bronk, G., Kondev, J., & Haber, J. E. (2020). Yeast ATM and ATR kinases use different mechanisms to spread histone H2A phosphorylation around a DNA double-strand break. *Proceedings of the National Academy of Sciences of the United States of America*, *117*(35), 21354–21363.

Li, Y., Muir, K. W., Bowler, M. W., Metz, J., Haering, C. H., & Panne, D. (2018). Structural basis for Scc3-dependent cohesin recruitment to chromatin. *eLife*, *7*, e38356.

Lieber, M. R., Ma, Y., Pannicke, U., & Schwarz, K. (2003). Mechanism and regulation of human non-homologous DNA end-joining. *Nature reviews. Molecular cell biology*, *4*(9), 712–720.

Lilienthal, I., & Kanno, T. (2013). Inhibition of the Smc5/6 Complex during Meiosis Perturbs Joint Molecule Formation and Resolution without Significantly Changing Crossover or Non-crossover Levels. *PLOS Genetics*, *9*(11).

Betts Lindroos, H., Ström, L., Itoh, T., Katou, Y., Shirahige, K., & Sjögren, C. (2006). Chromosomal association of the Smc5/6 complex reveals that it functions in differently regulated pathways. *Molecular cell*, *22*(6), 755–767.

Lioy, V. S., Cournac, A., Marbouty, M., Duigou, S., Mozziconacci, J., Espéli, O., Boccard, F., & Koszul, R. (2018). Multiscale Structuring of the E. coli Chromosome by Nucleoid-Associated and Condensin Proteins. *Cell*, *172*(4), 771–783.e18.

Lioy, V. S., Lorenzi, J. N., Najah, S., Poinsignon, T., Leh, H., Saulnier, C., Aigle, B., Lautru, S., Thibessard, A., Lespinet, O., Leblond, P., Jaszczyszyn, Y., Gorrichon, K., Varoquaux, N., Junier, I., Boccard, F., Pernodet, J. L., & Bury-Moné, S. (2021). Dynamics of the compartmentalized Streptomyces chromosome during metabolic differentiation. *Nature communications*, *12*(1), 5221.

Lioy, V. S., Cournac, A., Marbouty, M., Duigou, S., Mozziconacci, J., Espéli, O., Boccard, F., & Koszul, R. (2018). Multiscale Structuring of the E. coli Chromosome by Nucleoid-Associated and Condensin Proteins. *Cell*, *172*(4), 771–783.e18.

Lisby, M., Barlow, J. H., Burgess, R. C., & Rothstein, R. (2004). Choreography of the DNA damage response: spatiotemporal relationships among checkpoint and repair proteins. *Cell*, *118*(6), 699–713.

Liu, H. W., Roisné-Hamelin, F., Beckert, B., Li, Y., Myasnikov, A., & Gruber, S. (2022). DNA-measuring Wadjet SMC ATPases restrict smaller circular plasmids by DNA cleavage. *Molecular cell*, *82*(24), 4727–4740.e6.

Liu, S., Miné-Hattab, J., Villemeur, M., Guerois, R., Pinholt, H. D., Mirny, L. A., & Taddei, A. (2023). Publisher Correction: In vivo tracking of functionally tagged Rad51 unveils a robust strategy of homology search. *Nature structural & molecular biology*, *30*(10), 1607.

Lobachev, K., Vitriol, E., Stemple, J., Resnick, M. A., & Bloom, K. (2004). Chromosome fragmentation after induction of a double-strand break is an active process prevented by the RMX repair complex. *Current biology : CB*, *14*(23), 2107–2112.

Ma, J. L., Kim, E. M., Haber, J. E., & Lee, S. E. (2003). Yeast Mre11 and Rad1 proteins define a Ku-independent mechanism to repair double-strand breaks lacking overlapping end sequences. *Molecular and cellular biology*, *23*(23), 8820–8828.

Ma, Y., Lu, H., Tippin, B., Goodman, M. F., Shimazaki, N., Koiwai, O., Hsieh, C. L., Schwarz, K., & Lieber, M. R. (2004). A biochemically defined system for mammalian nonhomologous DNA end joining. *Molecular cell*, *16*(5), 701–713.

Marston A. L. (2014). Chromosome segregation in budding yeast: sister chromatid cohesion and related mechanisms. *Genetics*, *196*(1), 31–63.

Matsuzaki, K., Shinohara, A., & Shinohara, M. (2008). Forkhead-associated domain of yeast Xrs2, a homolog of human Nbs1, promotes nonhomologous end joining through interaction with a ligase IV partner protein, Lif1. *Genetics*, *179*(1), 213–225.

McAleenan, A., Cordon-Preciado, V., Clemente-Blanco, A., Liu, I. C., Sen, N., Leonard, J., Jarmuz, A., & Aragón, L. (2012). SUMOylation of the α-kleisin subunit of cohesin is required for DNA damage-induced cohesion. *Current biology : CB*, *22*(17), 1564–1575.

Menchon, G., Bombarde, O., Trivedi, M., Négrel, A., Inard, C., Giudetti, B., Baltas, M., Milon, A., Modesti, M., Czaplicki, G., & Calsou, P. (2016). Structure-Based Virtual Ligand Screening on the XRCC4/DNA Ligase IV Interface. *Scientific reports*, *6*, 22878.

Mimitou, E. P., & Symington, L. S. (2010). Ku prevents Exo1 and Sgs1-dependent resection of DNA ends in the absence of a functional MRX complex or Sae2. *The EMBO journal*, *29*(19), 3358–3369.

Mimori, T., & Hardin, J. A. (1986). Mechanism of interaction between Ku protein and DNA. *The Journal of biological chemistry*, *261*(22), 10375–10379.

Minamino, M., Bouchoux, C., Canal, B., Diffley, J. F. X., & Uhlmann, F. (2023). A replication fork determinant for the establishment of sister chromatid cohesion. *Cell*, *186*(4), 837–849.e11.

Minamino, M., Ishibashi, M., Nakato, R., Akiyama, K., Tanaka, H., Kato, Y., Negishi, L., Hirota, T., Sutani, T., Bando, M., & Shirahige, K. (2015). Esco1 Acetylates Cohesin via a Mechanism Different from That of Esco2. *Current biology : CB*, *25*(13), 1694–1706.

Minamino, M., Higashi, T. L., Bouchoux, C., & Uhlmann, F. (2018). Topological *in vitro* loading of the budding yeast cohesin ring onto DNA. *Life science alliance*, *1*(5), e201800143.

Miné-Hattab, J., & Rothstein, R. (2012). Increased chromosome mobility facilitates homology search during recombination. *Nature cell biology*, *14*(5), 510–517.

Miné-Hattab, J., Heltberg, M., Villemeur, M., Guedj, C., Mora, T., Walczak, A. M., Dahan, M., & Taddei, A. (2021). Single molecule microscopy reveals key physical features of repair foci in living cells. *eLife*, *10*, e60577.

Mojumdar, A., Sorenson, K., Hohl, M., Toulouze, M., Lees-Miller, S. P., Dubrana, K., Petrini, J. H. J., & Cobb, J. A. (2019). Nej1 Interacts with Mre11 to Regulate Tethering and Dna2 Binding at DNA Double-Strand Breaks. *Cell reports*, *28*(6), 1564–1573.e3.

Mojumdar, A., Adam, N., & Cobb, J. A. (2022). Nej1 interacts with Sae2 at DNA double-stranded breaks to inhibit DNA resection. *The Journal of biological chemistry*, *298*(6), 101937.

Moreno-Herrero, F., de Jager, M., Dekker, N. H., Kanaar, R., Wyman, C., & Dekker, C. (2005). Mesoscale conformational changes in the DNA-repair complex Rad50/Mre11/Nbs1 upon binding DNA. *Nature*, *437*(7057), 440–443.

Mortensen, U. H., Bendixen, C., Sunjevaric, I., & Rothstein, R. (1996). DNA strand annealing is promoted by the yeast Rad52 protein. *Proceedings of the National Academy of Sciences of the United States of America*, *93*(20), 10729–10734.

Muir, K. W., Li, Y., Weis, F., & Panne, D. (2020). The structure of the cohesin ATPase elucidates the mechanism of SMC-kleisin ring opening. *Nature structural & molecular biology*, *27*(3), 233–239.

Murayama, Y., & Uhlmann, F. (2015). DNA Entry into and Exit out of the Cohesin Ring by an Interlocking Gate Mechanism. *Cell*, *163*(7), 1628–1640.

Murayama, Y., Samora, C. P., Kurokawa, Y., Iwasaki, H., & Uhlmann, F. (2018). Establishment of DNA-DNA Interactions by the Cohesin Ring. *Cell*, *172*(3), 465–477.e15.

Murayama, Y., & Uhlmann, F. (2014). Biochemical reconstitution of topological DNA binding by the cohesin ring. *Nature*, *505*(7483), 367–371.

Murphy, C. M., Xu, Y., Li, F., Nio, K., Reszka-Blanco, N., Li, X., Wu, Y., Yu, Y., Xiong, Y., & Su, L. (2016). Hepatitis B Virus X Protein Promotes Degradation of SMC5/6 to Enhance HBV Replication. *Cell reports*, *16*(11), 2846–2854.

Myler, L. R., Gallardo, I. F., Soniat, M. M., Deshpande, R. A., Gonzalez, X. B., Kim, Y., Paull, T. T., & Finkelstein, I. J. (2017). Single-Molecule Imaging Reveals How Mre11-Rad50-Nbs1 Initiates DNA Break Repair. *Molecular cell*, *67*(5), 891–898.e4.

Nagai, S., Dubrana, K., Tsai-Pflugfelder, M., Davidson, M. B., Roberts, T. M., Brown, G. W., Varela, E., Hediger, F., Gasser, S. M., & Krogan, N. J. (2008). Functional targeting of DNA damage to a nuclear pore-associated SUMO-dependent ubiquitin ligase. *Science (New York, N.Y.)*, *322*(5901), 597–602.

Nakada, D., Matsumoto, K., & Sugimoto, K. (2003). ATM-related Tel1 associates with double-strand breaks through an Xrs2-dependent mechanism. *Genes & development*, *17*(16), 1957–1962.

Nakai, W., Westmoreland, J., Yeh, E., Bloom, K., & Resnick, M. A. (2011). Chromosome integrity at a double-strand break requires exonuclease 1 and MRX. *DNA repair*, *10*(1), 102–110.

Nasmyth, K. A., Lee, B. G., Roig, M. B., & Löwe, J. (2023). What AlphaFold tells us about cohesin's retention on and release from chromosomes. *eLife*, *12*, RP88656.

Nishiyama, T., Ladurner, R., Schmitz, J., Kreidl, E., Schleiffer, A., Bhaskara, V., Bando, M., Shirahige, K., Hyman, A. A., Mechtler, K., & Peters, J. M. (2010). Sororin mediates sister chromatid cohesion by antagonizing Wapl. *Cell*, *143*(5), 737–749.

Noble, D., Kenna, M. A., Dix, M., Skibbens, R. V., Unal, E., & Guacci, V. (2006). Intersection between the regulators of sister chromatid cohesion establishment and maintenance in budding yeast indicates a multi-step mechanism. *Cell cycle (Georgetown, Tex.)*, *5*(21), 2528–2536.

Noon, A. T., Shibata, A., Rief, N., Löbrich, M., Stewart, G. S., Jeggo, P. A., & Goodarzi, A. A. (2010). 53BP1-dependent robust localized KAP-1 phosphorylation is essential for heterochromatic DNA double-strand break repair. *Nature cell biology*, *12*(2), 177–184.

Ocampo-Hafalla, M., Muñoz, S., Samora, C. P., & Uhlmann, F. (2016). Evidence for cohesin sliding along budding yeast chromosomes. *Open biology*, *6*(6), 150178.

Oh, J., Al-Zain, A., Cannavo, E., Cejka, P., & Symington, L. S. (2016). Xrs2 Dependent and Independent Functions of the Mre11-Rad50 Complex. *Molecular cell*, *64*(2), 405–415.

Oldenkamp, R., & Rowland, B. D. (2022). A walk through the SMC cycle: From catching DNAs to shaping the genome. *Molecular cell*, *82*(9), 1616–1630.

Ouyang, Z., Zheng, G., Tomchick, D. R., Luo, X., & Yu, H. (2016). Structural Basis and IP6 Requirement for Pds5-Dependent Cohesin Dynamics. *Molecular cell*, *62*(2), 248–259.

Paciotti, V., Clerici, M., Lucchini, G., & Longhese, M. P. (2000). The checkpoint protein Ddc2, functionally related to S. pombe Rad26, interacts with Mec1 and is regulated by Mec1-dependent phosphorylation in budding yeast. *Genes & development*, *14*(16), 2046–2059.

Palecek, J. J., & Gruber, S. (2015). Kite Proteins: a Superfamily of SMC/Kleisin Partners Conserved Across Bacteria, Archaea, and Eukaryotes. *Structure (London, England : 1993)*, *23*(12), 2183–2190.

Palmbos, P. L., Wu, D., Daley, J. M., & Wilson, T. E. (2008). Recruitment of Saccharomyces cerevisiae Dnl4-Lif1 complex to a double-strand break requires interactions with Yku80 and the Xrs2 FHA domain. *Genetics*, *180*(4), 1809–1819.

Paull, T. T., & Gellert, M. (1998). The 3' to 5' exonuclease activity of Mre 11 facilitates repair of DNA double-strand breaks. *Molecular cell*, *1*(7), 969–979.

Paulsen, J., Liyakat Ali, T. M., Nekrasov, M., Delbarre, E., Baudement, M. O., Kurscheid, S., Tremethick, D., & Collas, P. (2019). Long-range interactions between topologically associating domains shape the four-dimensional genome during differentiation. *Nature genetics*, *51*(5), 835–843.

Pebernard, S., Perry, J. J., Tainer, J. A., & Boddy, M. N. (2008). Nse1 RING-like domain supports functions of the Smc5-Smc6 holocomplex in genome stability. *Molecular biology of the cell*, *19*(10), 4099–4109.

Peng, J. C., & Karpen, G. H. (2009). Heterochromatic genome stability requires regulators of histone H3 K9 methylation. *PLoS genetics*, *5*(3), e1000435.

Petela, N. J., Gligoris, T. G., Metson, J., Lee, B. G., Voulgaris, M., Hu, B., Kikuchi, S., Chapard, C., Chen, W., Rajendra, E., Srinivisan, M., Yu, H., Löwe, J., & Nasmyth, K. A. (2018). Scc2 Is a Potent Activator of Cohesin's ATPase that Promotes Loading by Binding Scc1 without Pds5. *Molecular cell*, *70*(6), 1134–1148.e7.

Petela, N. J., Gonzalez Llamazares, A., Dixon, S., Hu, B., Lee, B. G., Metson, J., Seo, H., Ferrer-Harding, A., Voulgaris, M., Gligoris, T., Collier, J., Oh, B. H., Löwe, J., & Nasmyth, K. A. (2021). Folding of cohesin's coiled coil is important for Scc2/4-induced association with chromosomes. *eLife*, *10*, e67268.

Peters J. M. (2021). How DNA loop extrusion mediated by cohesin enables V(D)J recombination. *Current opinion in cell biology*, *70*, 75–83.

Peters, J. M., & Nishiyama, T. (2012). Sister chromatid cohesion. *Cold Spring Harbor perspectives in biology*, *4*(11), a011130.

Pfister, S. X., Ahrabi, S., Zalmas, L. P., Sarkar, S., Aymard, F., Bachrati, C. Z., Helleday, T., Legube, G., La Thangue, N. B., Porter, A. C., & Humphrey, T. C. (2014). SETD2-dependent histone H3K36 trimethylation is required for homologous recombination repair and genome stability. *Cell reports*, *7*(6), 2006–2018.

Phipps, J., & Dubrana, K. (2022). DNA Repair in Space and Time: Safeguarding the Genome with the Cohesin Complex. *Genes*, *13*(2), 198.

Phipps, J., Dubrana, K. (2023). Cohesin complex oligomerization maintains end-tethering at DNA double-strand breaks. *bioRxiv 2023.11.08.566226*

Piazza, A., Bordelet, H., Dumont, A., Thierry, A., Savocco, J., Girard, F., & Koszul, R. (2021). Cohesin regulates homology search during recombinational DNA repair. *Nature cell biology*, *23*(11), 1176–1186.

De Piccoli, G., Cortes-Ledesma, F., Ira, G., Torres-Rosell, J., Uhle, S., Farmer, S., Hwang, J. Y., Machin, F., Ceschia, A., McAleenan, A., Cordon-Preciado, V., Clemente-Blanco, A., Vilella-Mitjana, F., Ullal, P., Jarmuz, A., Leitao, B., Bressan, D., Dotiwala, F., Papusha, A., Zhao, X., … Aragón, L. (2006). Smc5-Smc6 mediate DNA double-strand-break repair by promoting sister-chromatid recombination. *Nature cell biology*, *8*(9), 1032–1034.

Potts, P. R., Porteus, M. H., & Yu, H. (2006). Human SMC5/6 complex promotes sister chromatid homologous recombination by recruiting the SMC1/3 cohesin complex to double-strand breaks. *The EMBO journal*, *25*(14), 3377–3388.

Potts, P. R., & Yu, H. (2005). Human MMS21/NSE2 is a SUMO ligase required for DNA repair. *Molecular and cellular biology*, *25*(16), 7021–7032.

Pradhan, B., Barth, R., Kim, E., Davidson, I. F., Bauer, B., van Laar, T., Yang, W., Ryu, J. K., van der Torre, J., Peters, J. M., & Dekker, C. (2022). SMC complexes can traverse physical roadblocks bigger than their ring size. *Cell reports*, *41*(3), 111491.

Pradhan, B., Kanno, T., Umeda Igarashi, M., Loke, M. S., Baaske, M. D., Wong, J. S. K., Jeppsson, K., Björkegren, C., & Kim, E. (2023). The Smc5/6 complex is a DNA loop-extruding motor. *Nature*, *616*(7958), 843–848.

Psakhye, I., & Branzei, D. (2021). SMC complexes are guarded by the SUMO protease Ulp2 against SUMO-chain-mediated turnover. *Cell reports*, *36*(5), 109485.

Psakhye, I., Kawasumi, R., Abe, T., Hirota, K., & Branzei, D. (2023). PCNA recruits cohesin loader Scc2 to ensure sister chromatid cohesion. *Nature structural & molecular biology*, *30*(9), 1286–1294.

Rankin, S., Ayad, N. G., & Kirschner, M. W. (2005). Sororin, a substrate of the anaphase-promoting complex, is required for sister chromatid cohesion in vertebrates. *Molecular cell*, *18*(2), 185–200.

Rao, H., Uhlmann, F., Nasmyth, K., & Varshavsky, A. (2001). Degradation of a cohesin subunit by the N-end rule pathway is essential for chromosome stability. *Nature*, *410*(6831), 955–959.

Rao, S. S. P., Huang, S. C., Glenn St Hilaire, B., Engreitz, J. M., Perez, E. M., Kieffer-Kwon, K. R., Sanborn, A. L., Johnstone, S. E., Bascom, G. D., Bochkov, I. D., Huang, X., Shamim, M. S., Shin, J., Turner, D., Ye, Z., Omer, A. D., Robinson, J. T., Schlick, T., Bernstein, B. E., Casellas, R., … Aiden, E. L. (2017). Cohesin Loss Eliminates All Loop Domains. *Cell*, *171*(2), 305–320.e24.

Rass, E., Grabarz, A., Plo, I., Gautier, J., Bertrand, P., & Lopez, B. S. (2009). Role of Mre11 in chromosomal nonhomologous end joining in mammalian cells. *Nature structural & molecular biology*, *16*(8), 819–824.

Reddy, G., Golub, E. I., & Radding, C. M. (1997). Human Rad52 protein promotes single-strand DNA annealing followed by branch migration. *Mutation research*, *377*(1), 53–59.

Revenkova, E., Focarelli, M. L., Susani, L., Paulis, M., Bassi, M. T., Mannini, L., Frattini, A., Delia, D., Krantz, I., Vezzoni, P., Jessberger, R., & Musio, A. (2009). Cornelia de Lange syndrome mutations in SMC1A or SMC3 affect binding to DNA. *Human molecular genetics*, *18*(3), 418–427.

Riballo, E., Kühne, M., Rief, N., Doherty, A., Smith, G. C., Recio, M. J., Reis, C., Dahm, K., Fricke, A., Krempler, A., Parker, A. R., Jackson, S. P., Gennery, A., Jeggo, P. A., & Löbrich, M. (2004). A pathway of double-

strand break rejoining dependent upon ATM, Artemis, and proteins locating to gamma-H2AX foci. *Molecular cell*, *16*(5), 715–724.

Rinaldi, C., Pizzul, P., Casari, E., Mangiagalli, M., Tisi, R., & Longhese, M. P. (2023). The Ku complex promotes DNA end-bridging and this function is antagonized by Tel1/ATM kinase. *Nucleic acids research*, *51*(4), 1783–1802.

Rogakou, E. P., Boon, C., Redon, C., & Bonner, W. M. (1999). Megabase Chromatin Domains Involved in DNA Double-Strand Breaks In Vivo. *The Journal of Cell Biology*, *146*.

Roig, M. B., Löwe, J., Chan, K. L., Beckouët, F., Metson, J., & Nasmyth, K. (2014). Structure and function of cohesin's Scc3/SA regulatory subunit. *FEBS letters*, *588*(20), 3692–3702.

Rooney, S., Sekiguchi, J., Zhu, C., Cheng, H. L., Manis, J., Whitlow, S., DeVido, J., Foy, D., Chaudhuri, J., Lombard, D., & Alt, F. W. (2002). Leaky Scid phenotype associated with defective V(D)J coding end processing in Artemis-deficient mice. *Molecular cell*, *10*(6), 1379–1390.

Ropars, V., Drevet, P., Legrand, P., Baconnais, S., Amram, J., Faure, G., Márquez, J. A., Piétrement, O., Guerois, R., Callebaut, I., Le Cam, E., Revy, P., de Villartay, J. P., & Charbonnier, J. B. (2011). Structural characterization of filaments formed by human Xrcc4-Cernunnos/XLF complex involved in nonhomologous DNA end-joining. *Proceedings of the National Academy of Sciences of the United States of America*, *108*(31), 12663–12668.

Rotheneder, M., Stakyte, K., van de Logt, E., Bartho, J. D., Lammens, K., Fan, Y., Alt, A., Kessler, B., Jung, C., Roos, W. P., Steigenberger, B., & Hopfner, K. P. (2023). Cryo-EM structure of the Mre11-Rad50-Nbs1 complex reveals the molecular mechanism of scaffolding functions. *Molecular cell*, *83*(2), 167–185.e9.

Rowland, B. D., Roig, M. B., Nishino, T., Kurze, A., Uluocak, P., Mishra, A., Beckouët, F., Underwood, P., Metson, J., Imre, R., Mechtler, K., Katis, V. L., & Nasmyth, K. (2009). Building sister chromatid cohesion: smc3 acetylation counteracts an antiestablishment activity. *Molecular cell*, *33*(6), 763–774.

Roy, U., Kwon, Y., Marie, L., Symington, L., Sung, P., Lisby, M., & Greene, E. C. (2021). The Rad51 paralog complex Rad55-Rad57 acts as a molecular chaperone during homologous recombination. *Molecular cell*, *81*(5), 1043–1057.e8.

van Ruiten, M. S., van Gent, D., Sedeño Cacciatore, Á., Fauster, A., Willems, L., Hekkelman, M. L., Hoekman, L., Altelaar, M., Haarhuis, J. H. I., Brummelkamp, T. R., de Wit, E., & Rowland, B. D. (2022). The cohesin acetylation cycle controls chromatin loop length through a PDS5A brake mechanism. *Nature structural & molecular biology*, *29*(6), 586–591.

Ryu, J. K., Bouchoux, C., Liu, H. W., Kim, E., Minamino, M., de Groot, R., Katan, A. J., Bonato, A., Marenduzzo, D., Michieletto, D., Uhlmann, F., & Dekker, C. (2021). Bridging-induced phase separation induced by cohesin SMC protein complexes. *Science advances*, *7*(7), eabe5905.

Ryu, J. K., Rah, S. H., Janissen, R., Kerssemakers, J. W. J., Bonato, A., Michieletto, D., & Dekker, C. (2022). Condensin extrudes DNA loops in steps up to hundreds of base pairs that are generated by ATP binding events. *Nucleic acids research*, *50*(2), 820–832.

Ryu, T., Spatola, B., Delabaere, L., Bowlin, K., Hopp, H., Kunitake, R., Karpen, G. H., & Chiolo, I. (2015). Heterochromatic breaks move to the nuclear periphery to continue recombinational repair. *Nature cell biology*, *17*(11), 1401–1411.

Sakai, Y., Mochizuki, A., Kinoshita, K., Hirano, T., & Tachikawa, M. (2018). Modeling the functions of condensin in chromosome shaping and segregation. *PLoS computational biology*, *14*(6), e1006152.

Sallmyr, A., & Tomkinson, A. E. (2018). Repair of DNA double-strand breaks by mammalian alternative end-joining pathways. *The Journal of biological chemistry*, *293*(27), 10536–10546.

Sanborn, A. L., Rao, S. S., Huang, S. C., Durand, N. C., Huntley, M. H., Jewett, A. I., Bochkov, I. D., Chinnappan, D., Cutkosky, A., Li, J., Geeting, K. P., Gnirke, A., Melnikov, A., McKenna, D., Stamenova, E. K., Lander, E. S., & Aiden, E. L. (2015). Chromatin extrusion explains key features of loop and domain formation in wild-type and engineered genomes. *Proceedings of the National Academy of Sciences of the United States of America*, *112*(47), E6456–E6465.

Sanchez, Y., Bachant, J., Wang, H., Hu, F., Liu, D., Tetzlaff, M., & Elledge, S. J. (1999). Control of the DNA damage checkpoint by chk1 and rad53 protein kinases through distinct mechanisms. *Science (New York, N.Y.)*, *286*(5442), 1166–1171.

Schalbetter, S. A., Fudenberg, G., Baxter, J., Pollard, K. S., & Neale, M. J. (2019). Principles of meiotic chromosome assembly revealed in S. cerevisiae. *Nature communications*, *10*(1), 4795.

Schär, P., Fäsi, M., & Jessberger, R. (2004). SMC1 coordinates DNA double-strand break repair pathways. *Nucleic acids research*, *32*(13), 3921–3929..

Schiller, C. B., Seifert, F. U., Linke-Winnebeck, C., & Hopfner, K. P. (2014). Structural studies of DNA end detection and resection in homologous recombination. *Cold Spring Harbor perspectives in biology*, *6*(10), a017962.

Schwartz, M. F., Duong, J. K., Sun, Z., Morrow, J. S., Pradhan, D., & Stern, D. F. (2002). Rad9 phosphorylation sites couple Rad53 to the Saccharomyces cerevisiae DNA damage checkpoint. *Molecular cell*, *9*(5), 1055–1065.

Schwarzer, W., Abdennur, N., Goloborodko, A., Pekowska, A., Fudenberg, G., Loe-Mie, Y., Fonseca, N. A., Huber, W., Haering, C. H., Mirny, L., & Spitz, F. (2017). Two independent modes of chromatin organization revealed by cohesin removal. *Nature*, *551*(7678), 51–56.

Seif-El-Dahan, M., Kefala-Stavridi, A., Frit, P., Hardwick, S. W., Chirgadze, D. Y., Maia De Oliviera, T., Andreani, J., Britton, S., Barboule, N., Bossaert, M., Pandurangan, A. P., Meek, K., Blundell, T. L., Ropars, V., Calsou, P., Charbonnier, J. B., & Chaplin, A. K. (2023). PAXX binding to the NHEJ machinery explains functional redundancy with XLF. *Science advances*, *9*(22), eadg2834.

Serrano, D., Cordero, G., Kawamura, R., Sverzhinsky, A., Sarker, M., Roy, S., Malo, C., Pascal, J. M., Marko, J. F., & D'Amours, D. (2020). The Smc5/6 Core Complex Is a Structure-Specific DNA Binding and Compacting Machine. *Molecular cell*, *80*(6), 1025–1038.e5.

Sexton, T., Yaffe, E., Kenigsberg, E., Bantignies, F., Leblanc, B., Hoichman, M., Parrinello, H., Tanay, A., & Cavalli, G. (2012). Three-dimensional folding and functional organization principles of the Drosophila genome. *Cell*, *148*(3), 458–472.

Sfeir, A., & Symington, L. S. (2015). Microhomology-Mediated End Joining: A Back-up Survival Mechanism or Dedicated Pathway?. *Trends in biochemical sciences*, *40*(11), 701–714.

Shaltiel, I. A., Datta, S., Lecomte, L., Hassler, M., Kschonsak, M., Bravo, S., Stober, C., Ormanns, J., Eustermann, S., & Haering, C. H. (2022). A hold-and-feed mechanism drives directional DNA loop extrusion by condensin. *Science (New York, N.Y.)*, *376*(6597), 1087–1094.

Shao, Z., Davis, A. J., Fattah, K. R., So, S., Sun, J., Lee, K. J., Harrison, L., Yang, J., & Chen, D. J. (2012). Persistently bound Ku at DNA ends attenuates DNA end resection and homologous recombination. *DNA repair*, *11*(3), 310–316.

Shi, Z., Gao, H., Bai, X. C., & Yu, H. (2020). Cryo-EM structure of the human cohesin-NIPBL-DNA complex. *Science (New York, N.Y.)*, *368*(6498), 1454–1459.

Shroff, R., Arbel-Eden, A., Pilch, D., Ira, G., Bonner, W. M., Petrini, J. H., Haber, J. E., & Lichten, M. (2004). Distribution and dynamics of chromatin modification induced by a defined DNA double-strand break. *Current biology : CB*, *14*(19), 1703–1711.

Simsek, D., Brunet, E., Wong, S. Y.-W., Katyal, S., Gao, Y., Lou, J., Zhang, L., Li, J., Rebar, E. J., Gregory, P. D., & Jasin, M. (2011). DNA Ligase III Promotes Alternative Nonhomologous End-Joining during Chromosomal Translocation Formation. *PLoS Genetics*, *7*(6).

Sjögren, C., & Nasmyth, K. (2001). Sister chromatid cohesion is required for postreplicative double-strand break repair in Saccharomyces cerevisiae. *Current biology : CB*, *11*(12), 991–995.

Skibbens, R. V., Corson, L. B., Koshland, D., & Hieter, P. (1999). Ctf7p is essential for sister chromatid cohesion and links mitotic chromosome structure to the DNA replication machinery. *Genes & development*, *13*(3), 307–319.

Soutoglou, E., Dorn, J. F., Sengupta, K., Jasin, M., Nussenzweig, A., Ried, T., Danuser, G., & Misteli, T. (2007). Positional stability of single double-strand breaks in mammalian cells. *Nature cell biology*, *9*(6), 675–682.

Srinivasan, M., Scheinost, J. C., Petela, N. J., Gligoris, T. G., Wissler, M., Ogushi, S., Collier, J. E., Voulgaris, M., Kurze, A., Chan, K. L., Hu, B., Costanzo, V., & Nasmyth, K. A. (2018). The Cohesin Ring Uses Its Hinge to Organize DNA Using Non-topological as well as Topological Mechanisms. *Cell*, *173*(6), 1508–1519.e18.

Srinivasan, M., Fumasoni, M., Petela, N. J., Murray, A., & Nasmyth, K. A. (2020). Cohesion is established during DNA replication utilising chromosome associated cohesin rings as well as those loaded de novo onto nascent DNAs. *eLife*, *9*, e56611.

Ström, L., Lindroos, H. B., Shirahige, K., & Sjögren, C. (2004). Postreplicative recruitment of cohesin to double-strand breaks is required for DNA repair. *Molecular cell*, *16*(6), 1003–1015.

Ström, L., Karlsson, C., Lindroos, H. B., Wedahl, S., Katou, Y., Shirahige, K., & Sjögren, C. (2007). Postreplicative formation of cohesion is required for repair and induced by a single DNA break. *Science (New York, N.Y.)*, *317*(5835), 242–245.

Sun, Z., Hsiao, J., Fay, D. S., & Stern, D. F. (1998). Rad53 FHA domain associated with phosphorylated Rad9 in the DNA damage checkpoint. *Science (New York, N.Y.)*, *281*(5374), 272–274.

Surcel, A., Koshland, D., Ma, H., & Simpson, R. T. (2008). Cohesin Interaction with Centromeric Minichromosomes Shows a Multi-Complex Rod-Shaped Structure. *PLoS ONE*, *3*(6).

Sutani, T., Kawaguchi, T., Kanno, R., Itoh, T., & Shirahige, K. (2009). Budding yeast Wpl1(Rad61)-Pds5 complex counteracts sister chromatid cohesion-establishing reaction. *Current biology : CB*, *19*(6), 492–497.

Sweeney, F. D., Yang, F., Chi, A., Shabanowitz, J., Hunt, D. F., & Durocher, D. (2005). Saccharomyces cerevisiae Rad9 acts as a Mec1 adaptor to allow Rad53 activation. *Current biology : CB*, *15*(15), 1364–1375.

Tadi, S. K., Tellier-Lebègue, C., Nemoz, C., Drevet, P., Audebert, S., Roy, S., Meek, K., Charbonnier, J. B., & Modesti, M. (2016). PAXX Is an Accessory c-NHEJ Factor that Associates with Ku70 and Has Overlapping Functions with XLF. *Cell reports*, *17*(2), 541–555.

Tanasie, N. L., Gutiérrez-Escribano, P., Jaklin, S., Aragon, L., & Stigler, J. (2022). Stabilization of DNA fork junctions by Smc5/6 complexes revealed by single-molecule imaging. *Cell reports*, *41*(10), 111778.

Tang, J., Li, Z., Wu, Q., Irfan, M., Li, W., & Liu, X. (2022). Role of Paralogue of XRCC4 and XLF in DNA Damage Repair and Cancer Development. *Frontiers in immunology*, *13*, 852453.

Tang, J., Cho, N. W., Cui, G., Manion, E. M., Shanbhag, N. M., Botuyan, M. V., Mer, G., & Greenberg, R. A. (2013). Acetylation limits 53BP1 association with damaged chromatin to promote homologous recombination. *Nature structural & molecular biology*, *20*(3), 317–325.

Tang, M., Pobegalov, G., Tanizawa, H., Chen, Z. A., Rappsilber, J., Molodtsov, M., Noma, K. I., & Uhlmann, F. (2023). Establishment of dsDNA-dsDNA interactions by the condensin complex. *Molecular cell*, *83*(21), 3787–3800.e9.

Taschner, M., Basquin, J., Steigenberger, B., Schäfer, I. B., Soh, Y. M., Basquin, C., Lorentzen, E., Räschle, M., Scheltema, R. A., & Gruber, S. (2021). Nse5/6 inhibits the Smc5/6 ATPase and modulates DNA substrate binding. *The EMBO journal*, *40*(15), e107807.

Tedeschi, A., Wutz, G., Huet, S., Jaritz, M., Wuensche, A., Schirghuber, E., Davidson, I. F., Tang, W., Cisneros, D. A., Bhaskara, V., Nishiyama, T., Vaziri, A., Wutz, A., Ellenberg, J., & Peters, J. M. (2013). Wapl is an essential regulator of chromatin structure and chromosome segregation. *Nature*, *501*(7468), 564–568.

Tisi, R., Vertemara, J., Zampella, G., & Longhese, M. P. (2020). Functional and structural insights into the MRX/MRN complex, a key player in recognition and repair of DNA double-strand breaks. *Computational and structural biotechnology journal*, *18*, 1137–1152.

Tong, K., & Skibbens, R. V. (2015). Pds5 regulators segregate cohesion and condensation pathways in Saccharomyces cerevisiae. *Proceedings of the National Academy of Sciences of the United States of America*, *112*(22), 7021–7026.

Tothova, Z., Valton, A. L., Gorelov, R. A., Vallurupalli, M., Krill-Burger, J. M., Holmes, A., Landers, C. C., Haydu, J. E., Malolepsza, E., Hartigan, C., Donahue, M., Popova, K. D., Koochaki, S., Venev, S. V., Rivera, J., Chen, E., Lage, K., Schenone, M., D'Andrea, A. D., Carr, S. A., … Ebert, B. L. (2021). Cohesin mutations alter DNA damage repair and chromatin structure and create therapeutic vulnerabilities in MDS/AML. *JCI insight*, *6*(3), e142149.

Tseng, S. F., Gabriel, A., & Teng, S. C. (2008). Proofreading activity of DNA polymerase Pol2 mediates 3'-end processing during nonhomologous end joining in yeast. *PLoS genetics*, *4*(4), e1000060.

Tsouroula, K., Furst, A., Rogier, M., Heyer, V., Maglott-Roth, A., Ferrand, A., Reina-San-Martin, B., & Soutoglou, E. (2016). Temporal and Spatial Uncoupling of DNA Double Strand Break Repair Pathways within Mammalian Heterochromatin. *Molecular cell*, *63*(2), 293–305.

Tsukamoto, Y., Mitsuoka, C., Terasawa, M., Ogawa, H., & Ogawa, T. (2005). Xrs2p regulates Mre11p translocation to the nucleus and plays a role in telomere elongation and meiotic recombination. *Molecular biology of the cell*, *16*(2), 597–608.

Tubbs, A., & Nussenzweig, A. (2017). Endogenous DNA Damage as a Source of Genomic Instability in Cancer. *Cell*, *168*(4), 644–656.

Uhlmann, F., Wernic, D., Poupart, M. A., Koonin, E. V., & Nasmyth, K. (2000). Cleavage of cohesin by the CD clan protease separin triggers anaphase in yeast. *Cell*, *103*(3), 375–386.

Unal, E., Arbel-Eden, A., Sattler, U., Shroff, R., Lichten, M., Haber, J. E., & Koshland, D. (2004). DNA damage response pathway uses histone modification to assemble a double-strand break-specific cohesin domain. *Molecular cell*, *16*(6), 991–1002.

Unal, E., Heidinger-Pauli, J. M., Kim, W., Guacci, V., Onn, I., Gygi, S. P., & Koshland, D. E. (2008). A molecular determinant for the establishment of sister chromatid cohesion. *Science (New York, N.Y.)*, *321*(5888), 566–569.

Unal, E., Heidinger-Pauli, J. M., & Koshland, D. (2007). DNA double-strand breaks trigger genome-wide sister-chromatid cohesion through Eco1 (Ctf7). *Science (New York, N.Y.)*, *317*(5835), 245–248.

Uziel, T., Lerenthal, Y., Moyal, L., Andegeko, Y., Mittelman, L., & Shiloh, Y. (2003). Requirement of the MRN complex for ATM activation by DNA damage. *The EMBO journal*, *22*(20), 5612–5621.

Vazquez Nunez, R., Polyhach, Y., Soh, Y. M., Jeschke, G., & Gruber, S. (2021). Gradual opening of Smc arms in prokaryotic condensin. *Cell reports*, *35*(4), 109051.

Vialard, J. E., Gilbert, C. S., Green, C. M., & Lowndes, N. F. (1998). The budding yeast Rad9 checkpoint protein is subjected to Mec1/Tel1-dependent hyperphosphorylation and interacts with Rad53 after DNA damage. *The EMBO journal*, *17*(19), 5679–5688.

Vignard, J., Mirey, G., & Salles, B. (2013). Ionizing-radiation induced DNA double-strand breaks: a direct and indirect lighting up. *Radiotherapy and oncology : journal of the European Society for Therapeutic Radiology and Oncology*, *108*(3), 362–369.

Vilenchik, M. M., & Knudson, A. G. (2003). Endogenous DNA double-strand breaks: production, fidelity of repair, and induction of cancer. *Proceedings of the National Academy of Sciences of the United States of America*, *100*(22), 12871–12876.

Villarreal, D. D., Lee, K., Deem, A., Shim, E. Y., Malkova, A., & Lee, S. E. (2012). Microhomology directs diverse DNA break repair pathways and chromosomal translocations. *PLoS genetics*, *8*(11), e1003026.

Vogt, A., & He, Y. (2023). Structure and mechanism in non-homologous end joining. *DNA repair*, *130*, 103547.

Vogt, A., He, Y., & Lees-Miller, S. P. (2023). How to fix DNA breaks: new insights into the mechanism of non-homologous end joining. *Biochemical Society transactions*, *51*(5), 1789–1800.

Vrouwe, M. G., Elghalbzouri-Maghrani, E., Meijers, M., Schouten, P., Godthelp, B. C., Bhuiyan, Z. A., Redeker, E. J., Mannens, M. M., Mullenders, L. H., Pastink, A., & Darroudi, F. (2007). Increased DNA damage sensitivity of Cornelia de Lange syndrome cells: evidence for impaired recombinational repair. *Human molecular genetics*, *16*(12), 1478–1487.

Walker, J. R., Corpina, R. A., & Goldberg, J. (2001). Structure of the Ku heterodimer bound to DNA and its implications for double-strand break repair. *Nature*, *412*(6847), 607–614.

Watanabe, Y., & Nurse, P. (1999). Cohesin Rec8 is required for reductional chromosome segregation at meiosis. *Nature*, *400*(6743), 461–464.

Watrin, E., & Peters, J. M. (2009). The cohesin complex is required for the DNA damage-induced G2/M checkpoint in mammalian cells. *The EMBO journal*, *28*(17), 2625–2635.

Weitzer, S., Lehane, C., & Uhlmann, F. (2003). A model for ATP hydrolysis-dependent binding of cohesin to DNA. *Current biology : CB*, *13*(22), 1930–1940.

Wells, J. N., Gligoris, T. G., Nasmyth, K. A., & Marsh, J. A. (2017). Evolution of condensin and cohesin complexes driven by replacement of Kite by Hawk proteins. *Current biology : CB*, *27*(1), R17–R18.

Wheeler, E. C., Martin, B. J. E., Doyle, W. C., Gorelov, R. A., Donahue, M., Jann, J. C., Abdel-Wahab, O., Taylor, J., Seiler, M., Belizaire, R., Adelman, K., & Tothova, Z. (2022). Splicing modulators impair DNA damage response and induce killing of cohesin-mutant MDS/AML. *Blood* 2022; 140 (Supplement 1): 6888–6889.

Wiktor, J., Gynnå, A. H., Leroy, P., Larsson, J., Coceano, G., Testa, I., & Elf, J. (2021). Author Correction: RecA finds homologous DNA by reduced dimensionality search. *Nature*, *600*(7887), E11.

Wilson, T. E., Grawunder, U., & Lieber, M. R. (1997). Yeast DNA ligase IV mediates non-homologous DNA end joining. *Nature*, *388*(6641), 495–498.

Wright, W. D., Shah, S. S., & Heyer, W. D. (2018). Homologous recombination and the repair of DNA double-strand breaks. *The Journal of biological chemistry*, *293*(27), 10524–10535.

Wu, D., Topper, L. M., & Wilson, T. E. (2008). Recruitment and dissociation of nonhomologous end joining proteins at a DNA double-strand break in Saccharomyces cerevisiae. *Genetics*, *178*(3), 1237–1249.

Wu, P. Y., Frit, P., Meesala, S., Dauvillier, S., Modesti, M., Andres, S. N., Huang, Y., Sekiguchi, J., Calsou, P., Salles, B., & Junop, M. S. (2009). Structural and functional interaction between the human DNA repair proteins DNA ligase IV and XRCC4. *Molecular and cellular biology*, *29*(11), 3163–3172.

Wu, W., Wang, M., Wu, W., Singh, S. K., Mussfeldt, T., & Iliakis, G. (2008). Repair of radiation induced DNA double strand breaks by backup NHEJ is enhanced in G2. *DNA repair*, *7*(2), 329–338.

Wutz, G., Ladurner, R., St Hilaire, B. G., Stocsits, R. R., Nagasaka, K., Pignard, B., Sanborn, A., Tang, W., Várnai, C., Ivanov, M. P., Schoenfelder, S., van der Lelij, P., Huang, X., Dürnberger, G., Roitinger, E., Mechtler, K., Davidson, I. F., Fraser, P., Lieberman-Aiden, E., & Peters, J. M. (2020). ESCO1 and CTCF enable formation of long chromatin loops by protecting cohesin^{STAG1} from WAPL. *eLife*, *9*, e52091.

Wutz, G., Várnai, C., Nagasaka, K., Cisneros, D. A., Stocsits, R. R., Tang, W., Schoenfelder, S., Jessberger, G., Muhar, M., Hossain, M. J., Walther, N., Koch, B., Kueblbeck, M., Ellenberg, J., Zuber, J., Fraser, P., &

Peters, J. M. (2017). Topologically associating domains and chromatin loops depend on cohesin and are regulated by CTCF, WAPL, and PDS5 proteins. *The EMBO journal*, *36*(24), 3573–3599.

Xaver, M., Huang, L., Chen, D., & Klein, F. (2013). Smc5/6-Mms21 Prevents and Eliminates Inappropriate Recombination Intermediates in Meiosis. *PLOS Genetics*, *9*(12).

Xiang, S., & Koshland, D. (2021). Cohesin architecture and clustering in vivo. *eLife*, *10*, e62243.

Xie, A., Kwok, A., & Scully, R. (2009). Role of mammalian Mre11 in classical and alternative nonhomologous end joining. *Nature structural & molecular biology*, *16*(8), 814–818.

Xie, B., Sanford, E. J., Hung, S. H., Wagner, M. M., Heyer, W. D., & Smolka, M. B. (2023). Multi-Step Control of Homologous Recombination by Mec1/ATR Ensures Robust Suppression of Gross Chromosomal Rearrangements. *bioRxiv : the preprint server for biology*, 2023.11.21.568146.

Xiong, B., Lu, S., & Gerton, J. L. (2010). Hos1 is a lysine deacetylase for the Smc3 subunit of cohesin. *Current biology : CB*, *20*(18), 1660–1665.

Xu, H., Boone, C., & Brown, G. W. (2007). Genetic dissection of parallel sister-chromatid cohesion pathways. *Genetics*, *176*(3), 1417–1429.

Yang, J. H., Brandão, H. B., & Hansen, A. S. (2023). DNA double-strand break end synapsis by DNA loop extrusion. *Nature communications*, *14*(1), 1913.

Yano, K., Morotomi-Yano, K., Lee, K. J., & Chen, D. J. (2011). Functional significance of the interaction with Ku in DNA double-strand break recognition of XLF. *FEBS letters*, *585*(6), 841–846.

Yatskevich, S., Rhodes, J., & Nasmyth, K. (2019). Organization of Chromosomal DNA by SMC Complexes. *Annual review of genetics*, *53*, 445–482.

Yoshimura, A., Sutani, T., & Shirahige, K. (2021). Functional control of Eco1 through the MCM complex in sister chromatid cohesion. *Gene*, *784*, 145584.

Yu, T. Y., Garcia, V. E., & Symington, L. S. (2019). CDK and Mec1/Tel1-catalyzed phosphorylation of Sae2 regulate different responses to DNA damage. *Nucleic acids research*, *47*(21), 11238–11249.

Yu, X., Chini, C. C., He, M., Mer, G., & Chen, J. (2003). The BRCT domain is a phospho-protein binding domain. *Science (New York, N.Y.)*, *302*(5645), 639–642.

Yu, X., & Gabriel, A. (2004). Reciprocal translocations in Saccharomyces cerevisiae formed by nonhomologous end joining. *Genetics*, *166*(2), 741–751.

Yu, Y., Li, S., Ser, Z., Sanyal, T., Choi, K., Wan, B., Kuang, H., Sali, A., Kentsis, A., Patel, D. J., & Zhao, X. (2021). Integrative analysis reveals unique structural and functional features of the Smc5/6 complex. *Proceedings of the National Academy of Sciences of the United States of America*, *118*(19), e2026844118.

Zhang, N., Jiang, Y., Mao, Q., Demeler, B., Tao, Y. J., & Pati, D. (2013). Characterization of the Interaction between the Cohesin Subunits Rad21 and SA1/2. *PLOS ONE*, *8*(7).

Zhang, N., Kuznetsov, S. G., Sharan, S. K., Li, K., Rao, P. H., & Pati, D. (2008). A handcuff model for the cohesin complex. *The Journal of cell biology*, *183*(6), 1019–1031.

Zhang, N., & Pati, D. (2009). Handcuff for sisters: a new model for sister chromatid cohesion. *Cell cycle (Georgetown, Tex.)*, *8*(3), 399–402.

Zhang, R., & Ma, J. (2020). MATCHA: Probing multi-way chromatin interaction with hypergraph representation learning. *Cell systems*, *10*(5), 397–407.e5.

Zhang, S., Yajima, H., Huynh, H., Zheng, J., Callen, E., Chen, H. T., Wong, N., Bunting, S., Lin, Y. F., Li, M., Lee, K. J., Story, M., Gapud, E., Sleckman, B. P., Nussenzweig, A., Zhang, C. C., Chen, D. J., & Chen, B. P. (2011). Congenital bone marrow failure in DNA-PKcs mutant mice associated with deficiencies in DNA repair. *The Journal of cell biology*, *193*(2), 295–305.

Zhang, Y., Hefferin, M. L., Chen, L., Shim, E. Y., Tseng, H. M., Kwon, Y., Sung, P., Lee, S. E., & Tomkinson, A. E. (2007). Role of Dnl4-Lif1 in nonhomologous end-joining repair complex assembly and suppression of homologous recombination. *Nature structural & molecular biology*, *14*(7), 639–646.

Zhao, B., Watanabe, G., Morten, M. J., Reid, D. A., Rothenberg, E., & Lieber, M. R. (2019). The essential elements for the noncovalent association of two DNA ends during NHEJ synapsis. *Nature communications*, *10*(1), 3588.

Zhu, Z., Chung, W. H., Shim, E. Y., Lee, S. E., & Ira, G. (2008). Sgs1 helicase and two nucleases Dna2 and Exo1 resect DNA double-strand break ends. *Cell*, *134*(6), 981–994.

Zuin, J., & Franke, V. (2014). A Cohesin-Independent Role for NIPBL at Promoters Provides Insights in CdLS. *PLOS Genetics*, *10*(2).

Sommaire en français

Chapitre 1 Introduction

1) Réparation des cassures double brin de l'ADN

Les cassures double brin d'ADN (DSB) sont étonnamment fréquentes et se produisent à chaque cycle cellulaire (Vilenchik et Knudson, 2003). Les sources endogènes de DSB comprennent les stress reçus lors des processus liés au métabolisme de l'ADN tels que la réplication. Cependant, des sources extrinsèques, notamment les rayonnements ionisants et les agents génotoxiques, génèrent également des DSB (Vignard et al., 2013). S'ils ne sont pas réparés, les DSB peuvent entraîner une perte de chromosomes et, s'ils sont mal réparés, des mutations ponctuelles, une perte d'hétérozygotie et des réarrangements chromosomiques (Jackson et Bartek, 2009). Tout cela conduisant à l'oncogenèse ou à la mort cellulaire (Tubbs et Nussenzweig, 2017).

Chez les eucaryotes, y compris la levure et les humains, les DSB sont principalement réparés par deux mécanismes : la ligation d'extrémités non homologues (NHEJ) et la recombinaison homologue (HR ; Figure 1). Le NHEJ ligature deux extrémités DSB de manière indépendante de l'homologie (Emerson et Bertuch, 2016). Bien que précis lorsque la religature a lieu sans modification des extrémités d'ADN cassées, le NHEJ peut entraîner une altération du génome par la perte ou l'ajout de nucléotides (Tseng et al., 2008) ou la formation de translocations chromosomiques (Yu et Gabriel, 2004). En revanche, la HR utilise une séquence donneuse homologue intacte pour reconstituer l'ADN brisé. En règle générale, l'utilisation de la chromatide sœur homologue pendant la HR entraîne une réparation fidèle des cassures de l'ADN (Wright et al., 2018). En revanche, un transfert de mutation ou une perte d'hétérozygotie peut survenir si la HR est réalisée entre allèles ou séquences hétérologues. Bien que NHEJ et HR soient les voies prédominantes utilisées pour la réparation des DSB, d'autres mécanismes moins fidèles sont observés. Si le NHEJ est compromis, une réparation par des voies de jonction d'extrémité alternative (a-EJ) peut avoir lieu. Par exemple, la réparation par Microhomology-Mediated End Joining (MMEJ) utilise des micro-homologie d'environ 4 à 20 pb situées de part et d'autre des DSB, qui sont exposées après une résection limitée des extrémités, et génère de petites délétions (Figure 1 ; Sallmyr et Tomkinson, 2018). Alternativement, la réparation par appariement de simple brin (SSA) peut être utilisée pour la

réparation si la résection révèle des répétitions homologues directes plus longues, dans un processus qui supprime également la séquence génomique qui les séparait (Figure 1 ; Sallmyr et Tomkinson, 2018).

2) Pontage des extrémités des cassures double brin

Rassembler deux extrémités d'ADN pour la réparation des DSB est l'une des premières et des plus cruciales étapes du processus de réparation. Si les extrémités ne parviennent pas à se trouver, la réparation ne peut pas avoir lieu et des événements néfastes tels que des translocations chromosomiques peuvent survenir.

Ceci est particulièrement important si l'on considère la nature dynamique de la chromatine. Bien que le génome soit activement replié et ordonné au sein du noyau, cette organisation n'est pas statique, avec des loci chromosomiques uniques explorant des volumes d'un rayon de 0,5 à 1 µm dans tous les organismes (Lanctot et al., 2007). En outre, un certain nombre d'études ont décrit des modifications du mouvement de la chromatine en réponse aux dommages de l'ADN. Chez *S. cerevisiae*, la mobilité du site d'ADN endommagé et de l'ensemble du génome augmentent en réponse aux dommages (Figure 3A ; (Dion et al., 2012 ; Miné-Hattab et al., 2012). Une augmentation du mouvement des DSB est également décrite chez la drosophile et les cellules de mammifères (Chiolo et al. ., 2011 ; Krawczyk et al., 2012). L'augmentation du mouvement de la chromatine pourrait augmenter la probabilité de rencontre des extrémités cassées séparées pour permettre le NHEJ (Dimitrova et Chen, 2008). Cependant, en l'absence de pontage efficace des extrémités, l'augmentation du mouvement pourrait promouvoir la séparation des extrémités cassées et conduire à des événements de réparation ectopique entre plusieurs DSB.

De nombreuses études *in vitro* et *in vivo* ont tenté de déchiffrer comment se produit le pontage des extrémités du DSB. Des travaux théoriques récents suggèrent qu'il est peu probable que l'association des extrémités séparées résulte de la diffusion passive (Yang et al., 2023). Au lieu de cela, des mécanismes pontant activement les extrémités des DSB ont été identifiés. Des études menées chez le *Xénope* et dans les cellules humaines impliquent des membres du complexe NHEJ (Graham et al., 2016 ; Zhao et al., 2019). Chez la levure, le complexe MRX et la formation d'ADNsb par l'exonucléase Exo1 ont été impliqués (Lobachev et al., 2004 ; Nakai et al., 2011). Généralement, les techniques utilisées définissent deux

niveaux de pontage des extrémité des DSB. Le premier se concentre sur la synapse qui a lieu avant la religature pendant le NHEJ, qui relie les extrémités de l'ADN à l'échelle de l'Angström (Vogt et He, 2023). La seconde suit les extrémités des DSB *in vivo*, démontrant l'existence d'un pontage des extrémités des DSB dans le contexte nucléaire à une plus grande échelle (Lobachev et al., 2004 ; Lee et al., 2008 ; Nakai et al., 2011).

Le mécanisme assurant le pontage des extrémités après la formation d'ADN simple brin (ADNsb) par résection est mal compris. *In vivo*, des analyses basées sur la microscopie chez la levure démontrent que les extrémités restent attachées même pendant la résection. Ceci est en accord avec le fait que les protéines liant l'ADNsb telles que RPA et Rad52 forment un foyer unique en réponse à une cassure double brin (Lisby et al., 2004) et qu'un seul filament Rad51 est observé lors de la recherche d'homologie coordonnée par les deux côtés du DSB (Liu et al., 2023 ; Dumont et al. , 2023). La manière dont l'alignement des filaments d'ADNsb est réalisé et la manière dont l'ADN adjacent est maintenu ensemble dans ce contexte reste à déchiffrer.

D'autres questions demeurent également. Par exemple, on ne sait pas si les extrémités de l'ADN cassé se séparent transitoirement, ou si elles restent constamment à proximité. Si elles se séparent, le moment où les extrémités se rejoignent et le mécanisme qui les ponte restent à définir . Il est également important de considérer le DSB dans le contexte de la fibre chromatine : si un DSB se produit sur l'ADN enroulé autour d'un nucléosome, le nucléosome peut-il contrecarer la séparation des extrémités cassées ? Les nucléosomes à proximité des DSB sont activement remodelés (Leonhard et al., 2022), mais on ne sait pas si ce processus facilite le recrutement de facteurs pontant les extrémités. Les facteurs de pontage pourraient également jouer un rôle dans l'expulsion des nucléosomes des sites cassés. Il sera techniquement difficile de répondre à ces questions, mais elles sont essentielles pour comprendre le pontage des extrémités des DSB *in vivo*.

3) Cohésine

La cohésine est un complexe SMC multiprotéique en forme d'anneau, initialement identifié chez la levure bourgeonnante et conservé chez presque tous les eucaryotes. Le complexe a été décrit pour la première fois pour son rôle dans la cohésion des chromatides sœurs, maintenue de la phase S à l'anaphase et essentielle pour la ségrégation équitable des chromosomes (Figure 6B ; Marston et al., 2014). Cependant, la cohésine est de plus en plus impliquée dans de nouvelles fonctions, notamment dans l'organisation 3D de la chromatine par la formation de boucles intra-chromatides à longue distance (Figure 6C ; Zuin et al., 2014 ; Dauban et al., 2020).

3E) Cohésion des chromatides sœurs

La cohésine est chargée sur les chromosomes juste avant la phase S par Scc2/4 (Ciosk et al., 2000), ce qui provoque un changement de conformation dans le complexe de cohésine et stimule son activité ATPase (Petela et al., 2018). Lorsque la machinerie de réplication rencontre la cohésine, elle est utilisée pour piéger topologiquement la chromatide sœur nouvellement répliquée, dans un processus appelé établissement de la cohésion (Figure 8). Ce piégeage maintient les chromatides sœurs ensemble jusqu'à la division cellulaire (maintien de la cohésion). La cohésine est ensuite complètement éliminée des chromosomes avant l'anaphase pour une division équitable des produits de réplication entre les cellules filles (dissociation ; Uhlmann et al., 2000 ; Haering et coll., 2008 ; Ivanov et Nasmyth, 2005). Deux voies redondantes permettent le piégeage de l'ADN par la cohésine (Xu et al., 2007). La première établit la cohésion par conversion des cohésines préchargées lorsque la réplication passe à travers l'anneau de cohésine. (Lengronne et al., 2006 ; Srinivasin et al., 2020). La deuxième correspond à la capture de novo de l'ADN double bin synthétisé par la réplication du brin principal et l'ADN simple brin généré par réplication discontinue du deuxième brin (Skibbens et al., 1999 ; Minamino et al., 2023). Ces deux voies ne s'excluent pas mutuellement. Ensemble, ils sont essentiels à l'établissement d'une bonne cohésion (Rolef Ben-Shahar et al., 2008 ; Unal et al., 2008 ; Xu et al., 2007 ; Zhang et al., 2008). Un processus couplé à la réplication ouvre l'anneau de cohésine et lui permet d'embrasser les deux produits de réplication (Gruber et al., 2006 ; Collier et Nasmyth 2022 ; Minamino et al., 2023). Une fois

chargée, la cohésine liée à Pds5 stimule l'acétylation de Smc3 par l'acétyltransférase Eco1$^{ESCO1/ESCO2}$(Noble et al., 2006 ; Chan et al., 2013). L'acétylation de Smc3 favorise le maintien de la cohésion en antagonisant la libération de la cohésine par Wpl1^{WAPL} (Heidinger-Pauli et al., 2009 ; Ladurner et al., 2016).

Chez l'homme, la libération de cohésine est régulée par deux vagues de dissociation de la cohésine des chromosomes. Dans la première vague, la cohésine devient sensible à l'activité de libération de WAPL en raison de l'inactivation et de la dissociation de Sororin de Pds5 (Marston, 2014 ; Peters et Nishiyama 2012). La cohésine centromèrique est protégée au cours de cette vague initiale et n'est éliminée qu'avant la ségrégation chromosomique et la division cellulaire. La cohésine centromérique est éliminée lors de la deuxième vague suite au clivage de Scc1 par une cystéine protéase, la Separase (Marston, 2014 ; Peters et Nishiyama 2012). Chez la levure, l'acétylation de Smc3 seule suffit à protéger la cohésine de l'activité Wpl1. En tant que telles, les cohésines cohésives ne sont supprimées qu'au début de l'anaphase, via le clivage de Scc1 par Esp1 (Separase ; Marston, 2014 ; Peters et Nishiyama 2012).

3F) Cohesin et formation de boucles

Les génomes eucaryotes sont organisés à plusieurs niveaux et existent finalement dans un état hautement replié. Le premier niveau de repliement de la chromatine consiste en l'enroulement périodique de la double hélice d'ADN autour d'un noyau d'octamères d'histone pour former des fibres nucléosomales de chromatine. Ces fibres sont ensuite organisées en domaines topologiquement associés (TAD), qui ont des limites définies et présentent des interactions locales accrues en leur sein et une diminution des interactions entre eux (Davidson et Peters, 2021 ; Sexton et al., 2012). Le génome des mammifères est divisé en une succession de TAD, dont la taille varie de plusieurs dizaines de kilobases à 1 à 2 Mb d'ADN, tandis que chez la levure, des structures plus petites de type TAD ont été décrites (50 à 100 kb chez S. pombe et 5 Ko dans*S. cerevisiae*).

Les modèles actuels proposent que la cohésine forme des TAD par extrusion de boucles entre des protéines barrières telles que CTCF chez les mammifères ou les CAR (régions associées à la cohésine) chez la levure (Dauban et al., 2020 ; Constatino et al., 2020 ; Rao et al., 2017 ;

Schwarzer et al., 2017 ; Wutz et al., 2017). La cohésine contribue également à l'organisation d'ordre supérieur des TAD, en TAD cliques, dans lesquelles des interactions accrues sont observées entre TAD distants, de manière constitutive ou dynamique (Paulsen et al., 2019). La contribution de la cohésine à l'individualisation des domaines chromosomiques impose une contrainte sur la distance entre les séquences dans le noyau. Cela explique l'importance de la cohésine pour un large éventail de processus liés à l'ADN, qui vont au-delà de son rôle dans la cohésion des chromatides sœurs. Ceux-ci incluent la régulation de la transcription des gènes et, de manière significative, la réponse aux dommages à l'ADN chez la levure et les mammifères (Phipps et Dubrana, 2022). Surtout, cette contrainte pourrait favoriser ou défavoriser les contacts entre les séquences d'ADN lors de la réparation de l'ADN et moduler à la fois la réponse aux dommages de l'ADN et l'issue de leur réparation.

Divers domaines de liaison à l'ADN dans le complexe de cohésine, ainsi que le partenaire de chargement $Scc2^{NIPBL}$, se sont révélés essentiels pour l'activité d'extrusion de boucles par la cohésine humaine *in vitro* (Davidson et al., 2019 ; Bauer et al., 2021). Les changements de conformation dépendant de la liaison de l'ATP et de l'ADN au sein du complexe cohésine facilitent le passage de la molécule d'ADN entre les sites de liaison de l'ADN. Cependant, même si un consensus se construit, la séquence et l'ordre de ces événements restent flous, et plusieurs modèles sont proposés (Bauer et al., 2021 ; Davidson et Peters, 2021 ; Dekker et al., 2023 ; Shaltiel et al., 2022). ; Yatskevic et al., 2019).

L'extrusion de boucles par la levure et le complexe de cohésine humain a été démontrée *in vitro* (Figure 11A ; Davidson et al., 2019 ; Guerin et al., 2023). Dans ces tests, l'ADN est attaché à une lame de verre, incubée avec la cohésine, de l'ATP et $Scc2^{NIPBL}$, et l'expansion d'une boucle d'ADN est visualisée par des techniques de microscopie. Avant cela, les conclusions sur la capacité de la cohésine à former des boucles avaient été tirées pour la première fois à partir d'observations selon lesquelles les cellules humaines déficiente pour WAPL généraient des chromosomes en interphase super condensés (Tedeschi et al., 2013). Les cartes de contact Hi-C ont ensuite démontré des contacts intra-chromosomiques à longue distance, dont les bornes corrélaient avec les pics de cohésine détectés par ChIP, et qui étaient abolies par la déplétion des cohésines (Figure 11B ; Rao et al., 2017 ; Schwarzer et al., 2017 ; Wutz et al., 2017 ; Dauban et al., 2020 ; Costatino et al., 2020). *In vivo,* la preuve de l'extrusion de boucles elle-même est ensuite venue de l'observation selon laquelle les la taille des boucles

dépendantes de la cohésine, observées par Hi-C, augmente lorsque le temps de résidence de la cohésine est augmenté en absence de Wpl1^{WAPL} ou de Pds5 (Dauban et al., 2020 ; Costatino et al., 2020). Malgré cela, il existe des données suggérant que l'extrusion de boucle n'est pas le seul mécanisme permettant à la cohésine de former des contacts d'ADN intra-chromosomiques. En effet, des complexes mutants incapables d'extruder des boucles *in vitro* sont encore capable de former des boucles dépendantes de la cohésine *in vivo* (Guérin et al., 2023). Les différentes manières par lesquelles la cohésine forme des boucles chromosomiques coexistent probablement in vivo.

3G) Oligomérisation des cohésines

Au-delà de l'extrusion de boucles *in vitro,* des études ont démontré la capacité de la cohésine de levure bourgeonnante à relier et à compacter les molécules d'ADN grâce à des interactions cohésine-cohésine (Gutierrez et al., 2019 ; Xiang et Koshland, 2021 ; Ryu et al., 2021). Bien que cela n'ait pas encore été observé pour la cohésine humaine, la cohésine de levure en interaction avec l'ADN forme des condensats moléculaires *in vitro*, conduisant à un pontage des molécules d'ADN (Figure 14 ; Ryu et al., 2021). De plus, des travaux récents chez la levure ont également démontré la formation d'oligomères de cohésine in vivo, grâce à un test de ligature de proximité (Xiand et Koshland, 2021). La signification biologique de ces observations reste à définir. Cependant, de récentes observations en Cryo-EM du complexe MRX de levure ont révélé qu'il partage la capacité à former des condensats, qui joueraient un role important dans le pontages des extrémités des DSB et la signalisation des dommages à l'ADN. Des motifs essentiels ont été identifiés dans la protéine Rad50 (Kissling et al., 2021). Il reste à déterminer si des motifs équivalent sont conservés dans la cohésine et sont pertinents pour la formation d'oligomères.

Il est intéressant de noter qu'un corpus de littérature s'accumule également sur la formation de condensat par la condensine. Une étude théorique a proposé que l'extrusion de boucles de condensine à elle seule n'est pas suffisante pour reproduire les niveaux observés de condensation des chromosomes mitotiques (Sakai et al., 2018 PLOS ; Gerguri et al., 2021 ; Forte et al., 2024). De plus, les auteurs démontrent qu'une oligomérisation des condensines telles que celle observée pour la cohésine par Ryu et al., ainsi que par Xiang et Koshland,

permettrait d'atteindre ces niveaux de condensation. De manière frappante, des amas de condensine ont également été visualisés in vivo chez la levure et sur les chromosomes mitotiques de *Xénope* (Gerguri et al., 2021 ; Kinoshita et al., 2022).

4) Cohésine et réparation

En parallèle de l'importance croissante de la cohésine dans la formation du génome par la formation de boucles, de nouveaux aspects de la contribution de la cohésine à la signalisation et à la réparation des dommages à l'ADN apparaissent. Le rôle des cohésines dans la réparation de l'ADN a en réalité été découvert avant son rôle dans la cohésion des chromatides sœurs. En effet, il y a plus de 30 que le gène Rad21^{Scc1} de la levure S. pombe est connu pour son rôle dans la résistance aux rayonnements ionisants (Birkenbihl et Subramani, 1992). Depuis, la cohésine est de plus en plus impliquée dans la réparation des dommages à l'ADN. Sa fonction dans la réparation de l'ADN a d'abord été liée à sa capacité à maintenir la cohésion des chromatides sœurs au niveau des DSB pour faciliter la RH. La cohésine a également été proposée dans la régulation du NHEJ chez la levure et dans les cellules humaines (Schar et al., 2004 ; Gelot et al., 2016). Des travaux plus récents montrent que la formation de boucles par la cohésine régule également la réponse aux dommages de l'ADN et limite la recherche d'homologie pendant la HR (Arnould et al., 2021 ; Piazza et al., 2021).

4A) Recrutement des cohésines aux DSB

Des études chez la levure et les mammifères ont démontré que la cohésine est recrutée aux DSB (Caron et al., 2012 ; Unal et al., 2004 ; Strom et al., 2004 ; Potts et al., 2006). Cependant, comment la cohésine est enrichie et régulée aux DSB reste à décrire en détail. Chez la levure et chez l'homme, le complexe de chargement de cohésine Scc2/4$^{NIPBL\text{-}Mau2}$ est essentiel pour l'enrichissement de la cohésine au niveau des DSB. Cependant, Scc2/4$^{NIPBL\text{-}Mau2}$ étant aussi nécessaire pour l'extrusion de boucles et l'établissement de la cohésion (Davidson et al., 2019 ; Guerin et al., 2023 ; Minamino et al., 2015), il reste à déterminer l'enrichissement des cohésines aux DSB resulte d'un chargement *de novo* ou de la mobilisation des cohésines préchargées via l'extrusion de boucles (Arnould et al., 2021 ; Strom et al., 2004 ; Unal et al., 2004). Il est frappant de constater que les composants clés des points de contrôle des

dommages à l'ADN sont importants pour le recrutement de la cohésine aux DSB. Le complexe MRX^{MRN} et la kinase $Tel1^{ATM}$ sont nécessaires à la fois chez la levure et chez l'homme (Unal et al., 2004, Arnould et al., 2021). De plus, chez la levure γH2AX et les kinases $Mec1^{ATR}$ et Chk1 sont également importantes (Unal et al., 2004). La SUMOylation de la sous-unité de cohésine Scc1 par la SUMO ligase Mms21 (Mms21/Nse2 chez l'homme) facilite également le recrutement de la cohésine au niveau des DSB de levure (McAleenan et al., 2012). La liaison de la cohésine aux DSB est négativement contrôlée par l'ubiquitine ligase Uls1 dépendante de SUMO, dont l'absence augmente les niveaux de MRX et de cohésine au DSB (Cheblal et al., 2020).

4B) Extrusion de boucles par les cohésines et réparation

De multiples observations démontrent que la cohésion des chromatides sœurs n'est pas le rôle exclusif de la cohésine dans la réparation du DSB. Par exemple, un enrichissement en cohésine dépendant de Scc2 est nécessaire pour une réparation efficace des DSB formés dans les cellules bloquées G2/M dans lesquelles la cohésion des chromatides sœurs est maintenue par la cohésine chargée phase S (ainsi qu'un mécanisme dépendant de MRX ; Strom 2004 ; Potts 2006 ; Seeber et al. ., 2016).

Plus récemment, l'extrusion de boucles dépendante de la cohésine a été impliquée dans la signalisation et la réparation des DSB. L'un des premiers événements de signalisation suite à l'induction des DSB est la phosphorylation de H2A (γH2AX chez les mammifères) par les PI3-kinases $Tel1^{ATM}$, $Mec1^{ATR}$ et DNA-PK (chez les mammifères) (Jackson et Bartek, 2009 ; Shroff et al., 2004). γH2AX peut se propager sur 50 à 100 Kb chez la levure (Lee et al., 2014 ; Shroff et al., 2004) et sur 1 à 2 Mb de la chromatine adjacente chez les mammifères (Berkovich et al., 2007 ; Iacovoni et al., 2010), alors que les kinases semblent être liées près des extrémités DSB. Des études récentes sur des cellules humaines ont démontré que les TAD dépendants de la cohésine sont des unités fonctionnelles de la réponse aux dommages de l'ADN, via la propagation de γH2AX (Arnould et al., 2021 ; Collins et al., 2020). Des données de Hi-C et de ChIP-seq ont démontré que les contacts entre le site cassé et les loci chromosomiques distants en *cis* sont importants pour l'établissement des domaines γH2AX, l'interactome du site de cassure étant fortement corrélé à la densité et à la propagation de γH2AX (Collins et al., 2020). Ces domaines sont largement définis par les TAD, la perturbation des TAD étendant la

propagation de γH2AX (Collins et al., 2020). De plus, les DSB agissent comme un obstacle à la translocation de la cohésine chez la levure et les humains (Arnould et al., 2021 ; Piazza et al., 2021), la cohésine extrudant des boucles en s'éloignant des DSB. Par conséquent, l'activité d'extrusion de boucles de cohésine semble jouer un rôle dans la propagation de γH2AX, au-delà de son rôle dans la définition de TAD (Arnould et al., 2021). Ces observations soutiennent un modèle dans lequel les cohésines, ancrées aux extrémités DSB où se trouve la kinase, facilitent la phosphorylation de H2Ax lorsque la chromatine passe à travers l'anneau de cohésine pendant l'extrusion de la boucle (Figure 15B). Il est intéressant de noter que la propagation de γH2Ax n'est pas exclusivement corrélée aux TAD individuels, la propagation trans chez la levure et chez l'homme se produisant de manière dépendante de la cohésine ; dans ce contexte, un mécanisme de capture de l'ADN en *trans* par les cohésines pourrait entrer en jeu (Lee et al., 2014).

Les boucles de cohésine favorisent également la réparation des séquences d'ADN proximales en limitant les interactions chromosomiques et éventuellement le mouvement du DSB. En effet, l'interactome autour d'une DSB est modifié en l'absence de cohésine, ce qui entraîne une augmentation des contacts à l'échelle du génome (Figure 15C ; Piazza et al., 2021). De plus, la déplétion de la cohésine augmente la mobilité des DSB au-delà du mouvement accru induit par la cassure elle-même dans les cellules de levure sauvage (Figure 15A ; Cheblal et al., 2020). Ensemble, ces données mettent en évidence la contribution de la cohésine liée au DSB. La cohésine entraîne les contacts entre les DSB et les séquences proximales via l'extrusion de boucles, participant à la signalisation des dommages à l'ADN par la propagation de γH2AX et favorisant la réparation intra-chromosomique. La cohésine restreint également le mouvement du DSB, limitant les interactions trans, favorisant ainsi la réparation avec des séquences proximales. Il convient de noter que la perte des boucles et de la cohésion des chromatides sœurs pourrait contribuer à une augmentation du mouvement et des interactions interchromosomiques.

Résultats

Les résultats de mes travaux doctoraux seront divisés en deux sections. La première contient mon travail principal, dans lequel nous avons identifié le role des cohésines dans le pontage des extrémités des cassures double brin de l'ADN. Ces travaux sont présentés sous la forme d'un article récemment publié sur BioRxiv et actuellement en cours d'évaluation à Nature Cell Biology (https://doi.org/10.1101/2023.11.08.566226).

Des résultats supplémentaires, qui n'ont pas été inclus dans la version finale de l'article, mais qui fournissent néanmoins des informations complémentaires sont présentées à la suite du manuscrit soumis.

Le second est un projet auquel j'ai contribué en collaboration avec le groupe de Stéphane Marcand, qui décrit comment les protéines télomériques bloquent l'extrusion des boucles par les condensines. Cet article est également publié sur BioRxiv et est actuellement en cours d'évaluation à Cell (https://doi.org/10.1101/2023.10.29.564563). Ma contribution à ce projet a été la construction de la souche de base utilisée pour les expériences de microscopie de la figure 4, l'établissement du pipeline utilisé pour l'analyse de ces expériences, ainsi que la réalisation et l'analyse des expériences de microscopie. J'ai également eu le plaisir de partager des réunions de laboratoire avec le groupe de Stéphane, qui ont donné lieu à de nombreuses conversations fructueuses sur ce sujet et d'autres, pour lesquelles je suis extrêmement reconnaissant.

J'ai également contribué à la planification et à l'analyse d'expériences de microscopie dans un article du groupe d'Eric Coïc, en collaboration avec Laurent Maloisel, qui ont été critiques pour le processus de révision. Cet article, publié dans PLOS Genetics (https://doi.org/10.1371/journal.pgen.1010639), décrit les rôles clés des paralogues Rad51, Rad55 et Rad57, dans la stabilisation du filament Rad51. Rad55 et Rad57 sont importants pour contrecarrer la synthèse de polymérase de translésion sujette aux erreurs au niveau des brèches d'ADN simple brin et favoriser la réparation par recombinaison homologue. Cet article est consultable en annexe.

Chapitre 5 : Discussion

On sait depuis longtemps que MRX participe au pontage des extrémités des DSB chez *S. cerevisiae*. Notre travail met en évidence l'importance de l'oligomérisation de la cohésine pontage des extrémités des DSB après résection de ceux-ci par Exo1. Contrairement à MRX, qui agit précocement, le pontage des extrémités cassées par la cohésine nécessite la formation d'ADN simple brin, comme le montre notre analyse génétique des mutants déficient pour Exo1 et doublement déficient pour les cohésine et Exo1 (SMC1-AID exo1Δ**)**. En effet, à ces moments tardifs, la machinerie cNHEJ n'est pas présente au niveau des DSB et la formation de l'ADN simple brin a commencé avant la réparation par HR. Dans ce contexte, le maintien des extrémités DSB à proximité est important pour éviter les événements de réparation aléatoires, tout en laissant la liberté de rechercher un donneur homologue comme matrice de réparation. Nous montrons que le pontage des extrémités de la cohésine est en effet important pour l'efficacité de la réparation à l'aide d'un test spécifique en temps réel. Malgré la révélation du rôle de la cohésine dans la réparation au travers du pontage des extrémités cassées, des questions demeurent quant à la régulation de ce processus.

Annex

genes

MDPI

Review

DNA Repair in Space and Time: Safeguarding the Genome with the Cohesin Complex

Jamie Phipps and Karine Dubrana *

UMR Stabilité Génétique Cellules Souches et Radiations, INSERM, iRCM/IBFJ CEA, Université de Paris and Université Paris-Saclay, F-92265 Fontenay-aux-Roses, France; jamie.phipps@cea.fr
* Correspondence: karine.dubrana@cea.fr; Tel.: +33-146-5493-43

Abstract: DNA double-strand breaks (DSBs) are a deleterious form of DNA damage, which must be robustly addressed to ensure genome stability. Defective repair can result in chromosome loss, point mutations, loss of heterozygosity or chromosomal rearrangements, which could lead to oncogenesis or cell death. We explore the requirements for the successful repair of DNA DSBs by non-homologous end joining and homology-directed repair (HDR) mechanisms in relation to genome folding and dynamics. On the occurrence of a DSB, local and global chromatin composition and dynamics, as well as 3D genome organization and break localization within the nuclear space, influence how repair proceeds. The cohesin complex is increasingly implicated as a key regulator of the genome, influencing chromatin composition and dynamics, and crucially genome organization through folding chromosomes by an active loop extrusion mechanism, and maintaining sister chromatid cohesion. Here, we consider how this complex is now emerging as a key player in the DNA damage response, influencing repair pathway choice and efficiency.

Keywords: DNA repair; NHEJ; homologous recombination; chromatin; nuclear organization; chromatin dynamics; cohesin

Citation: Phipps, J.; Dubrana, K. DNA Repair in Space and Time: Safeguarding the Genome with the Cohesin Complex. *Genes* **2022**, *13*, 198. https://doi.org/10.3390/genes13020198

Academic Editor: Josee Guirouilh-Barbat

Received: 24 December 2021
Accepted: 20 January 2022
Published: 22 January 2022

Publisher's Note: MDPI stays neutral with regard to jurisdictional claims in published maps and institutional affiliations.

1. Introduction: DNA Double-Strand Breaks Repair and Genome Stability

To ensure genome stability, DNA damage by both endogenous and extrinsic sources must be dealt with robustly. Without effective mechanisms to detect and repair assaults on the genome, diseases such as cancer can arise [1]. DNA double-strand breaks (DSBs) are particularly deleterious. If unrepaired, DSBs can result in chromosome loss and, if repaired incorrectly, can lead to point mutations, loss of heterozygosity and chromosomal rearrangements [2], all of which could lead to oncogenesis or cell death.

In eukaryotes, including yeast and humans, DSBs are predominantly repaired by two mechanisms: non-homologous end joining (NHEJ), and homologous recombination (HR; Figure 1). NHEJ ligates two DSB ends in a homology-independent manner [3]. Although accurate when re-ligation takes place without DNA processing, NHEJ can lead to genome alteration by the loss or addition of nucleotides [4] or chromosomal translocations [5]. In contrast, HR uses an intact homologous donor sequence to reconstitute broken DNA. Typically, use of the homologous sister chromatid during HR results in faithful DNA DSB repair, although, if performed between alleles or heterologous sequences, transfer of mutation or loss of heterozygosity can occur. Although NHEJ and HR are the predominant pathways used for DNA DSB repair, other mechanisms are also observed; however, these are often less faithful. If NHEJ is compromised, repair by alternative end joining (a-EJ) pathways can take place. Repair by microhomology-mediated end joining (MMEJ) is dependent on the annealing of roughly 4–20 bp of microhomology close to both ends of the DSB, which are exposed after limited end resection, and generates small deletions [6]. Alternatively, longer direct homologous repeats that are unmasked by resection can be repaired by single-strand annealing (SSA), in a process that also sees the loss of the genomic sequence that once separated them [6].

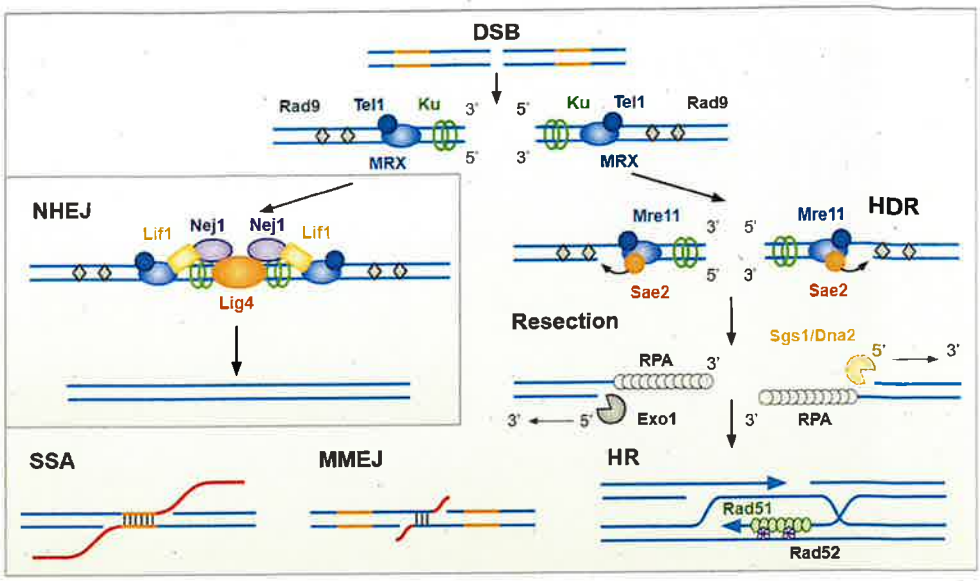

Figure 1. DNA double-strand break repair pathways. DNA double-strand breaks (DSBs) can be repaired by direct re-ligation of broken ends (non-homologous end joining, NHEJ), or through using a homologous template (homology-directed repair, HDR). On the occurrence of a DSB, DNA damage response factors Ku, MRX, Tel1 and Rad9 are recruited to the damaged site. If repair by NHEJ is favored, Lif1, Nej1 and Lig4 are recruited, and broken DNA is re-ligated (see Table 1 for human orthologs). HDR requires the formation of 3′ single-stranded-DNA (ssDNA) overhangs at the DSB site in a process known as resection. Resection is initiated by the endonuclease activity of Mre11 upon stimulation by Sae2 and proceeds due to the activity of the redundant exonucleases Exo1 and Sgs1/Dna2. The 3′ ssDNA overhangs are stabilized by replication protein A (RPA). Rad52 mediates the replacement of RPA for Rad51. Typically, resected Rad51-bound DSB ends undergo repair by homologous recombination (HR), invading the DNA duplex of the replicated sister chromatid for use as a template for faithful DNA DSB repair. Although NHEJ and HR are the canonical DSB repair pathways, other mechanisms are also observed. Repair by microhomology-mediated end joining (MMEJ) is dependent on short ~4–20 bp homologous sequences situated close to the DSB on either side of the break. These short homologous sequences can anneal with one another, sealing the DSB, but generating small deletions (in red). Alternatively, unmasking of longer direct homologous repeats (in orange) can lead to repair by single-strand annealing (SSA), a process that also sees the loss of the genomic sequence that once separated them (in red).

Upon DSB, the first repair pathway engaged is NHEJ, which relies on the rapid recruitment of the KU heterodimer (along with DNA-PK in mammalian cells; Table 1) and the XRCC4–XLF–Ligase IV ligation complex [7]. If ligation fails, DNA resection is initiated at the break site by the Mre11/Sae2^{CtIP} complex, unmasking short 3′-single-stranded DNA (ssDNA) overhangs of 60–70 bp [8–10]. This limited resection may unmask short direct repeats, the annealing of which, followed by DNA synthesis by DNA polymerases (Pol θ in mammals, Polδ and Pol4 in yeast) mediate repair by MMEJ [6]. If resection proceeds further, mediated by the partially redundant nuclease activity of Dna2/Sgs1^{BLM} and Exo1 [10], longer 3′-ssDNA overhangs are generated that can engage in homology-directed repair (HDR). The 3′-ssDNA overhangs are rapidly stabilized by replication protein A (RPA), which in turn is replaced by the Rad51 recombinase via the Rad52 recombinase mediator. The resulting right-handed helical filament can invade the homologous donor DNA duplex, ultimately leading to DNA synthesis and the sealing of the DSB, followed by resolution of intermediate recombination structures. Long-range resection may also unmask longer direct repeats that can anneal in a Rad52-dependent manner to mediate repair by SSA. Resolution of SSA intermediates is achieved by the Rad1–Rad10 complex, which removes the 3′ non-homologous tail generated. This pathway does not require the

invasion of a donor DNA duplex and is, therefore, Rad51 independent (for more details on the mechanisms see [11,12]).

Table 1. Repair factors in *Saccharomyces. cerevisiae*, functions and orthologs in *Schizosaccharomyces. pombe* and humans.

S. cerevisiae	*S. pombe*	Human	Complex	Function
Yku70	Pku70	KU70	KU (DNA-PK)	NHEJ repair factor
Yku80	Pku80	KU80		
-	-	DNA-PKcs		
Lif1	Xrc4	XRCC4	XRCC4–XLF–Ligase IV	
Nej1	Xlf1	NHEJ1 (XLF)		
Dnl4	Lig4	LIG4 (Ligase IV)		
Mre11	Mre11	MRE11	MRX (MRN)	NHEJ/HDR factor
Rad50	Rad50	RAD50		
Xrs2	Nbs1	NBS1		
Sae2	Ctp1	CTIP	-	HDR factor
Dna2	Dna2	DNA2	Dna2/Sgs1 (BLM)	
Sgs1	Rqh1	BLM		
Exo1	Exo1	EXO1	-	
Rad51	Rad51	RAD51	-	
Rad52	Rad52	RAD52	-	
Rad1	Rad16	ERCC4	Rad1–Rad10 (ERCC1–XPF)	
Rad10	Swi10	ERCC1		
Rad9	Crb2	TP53BP1 (53BP1)	-	DNA damage signaling
Tel1	Tel1	ATM	-	
Mec1	Rad3	ATR	-	
Chk1	Chk1	CHEK1	-	

Repair pathway choice, thus, relies primarily on resection initiation, which is highly regulated at several levels. Notably, the stage of the cell cycle plays a key role, with HR favored in the S phase due to the stimulation of resection by cyclin-dependent kinases (CDKs). The local sequence context, chromatin composition and fiber dynamics, as well as the global nuclear architecture, also regulate repair pathway choice and repair completion. In this review, we explore the requirements for successful NHEJ and homology-directed repair (HDR), particularly, the local chromatin context of the broken DNA molecule, the movement dynamics of DSB ends, the global chromatin context that makes the donor sequence permissive to homology search and the influence of nuclear structures and localization within the nuclear space on DSB repair. We consider how this affects repair choice and efficiency, and throughout, we discuss how the cohesin complex modulates these aspects and is emerging as a key player in DNA repair.

2. Cohesin Structure and Loop Extrusion Activity in *Saccharomyces cerevisiae* and Humans

Cohesin is a multiprotein, ring-shaped complex, which was initially identified in budding yeast, and is conserved in almost all eukaryotes (Figure 2A). The complex was first described to hold sister chromatids together from S phase to anaphase, entrapping them to ensure equal division of chromosomes (Figure 2B; [13]). However, cohesin has increasingly been implicated in novel functions, including the 3D organization of chromatin by the formation of long-range intrachromatid loops (Figure 2C; [14,15]), likely by the extrusion of chromatin in a symmetrical manner [16,17].

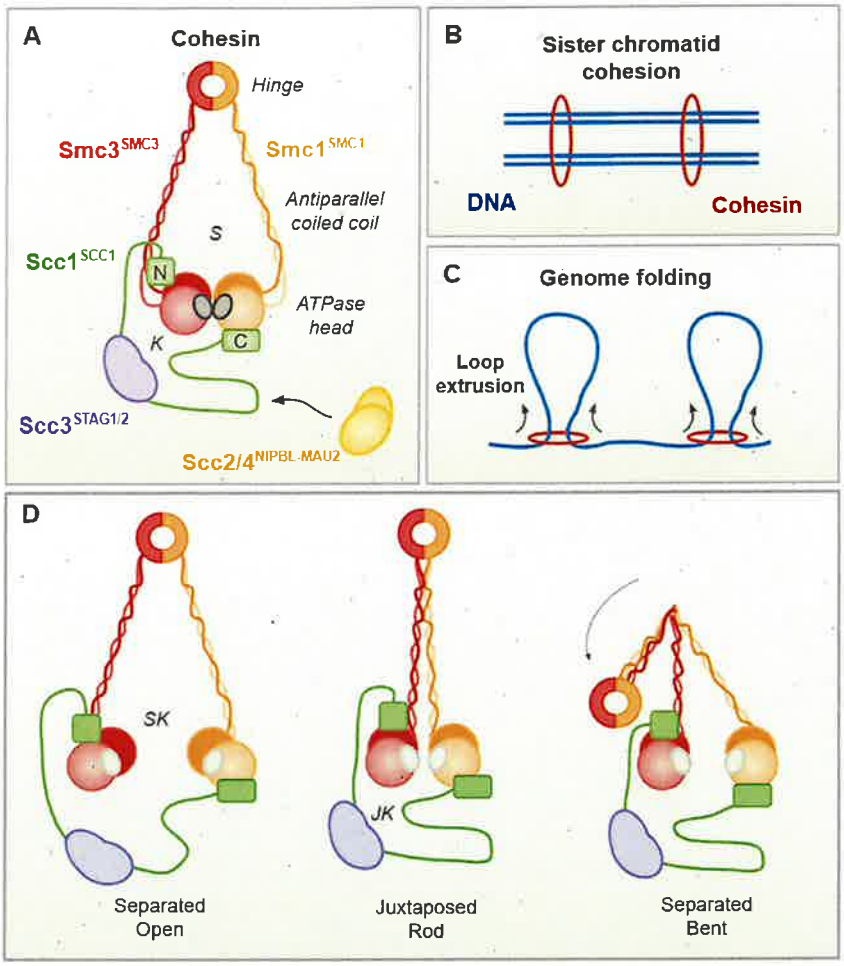

Figure 2. Cohesin structure and molecular functions. (**A**) The cohesin complex, shown in the ATP-bound state, has four core subunits: the structural maintenance of chromosomes proteins, Smc1 and Smc3, the kleisin Scc1 and the kleisin-associating $Scc3^{STAG1/2}$. The loading complex $Scc2/4^{NIPBLA/NIPBLB-Mau2}$ interacts with cohesin through Scc1. SMC proteins consist of ATPase head and hinge domains, and a long antiparallel coiled-coil arm. In the ATP-bound state, closed SMC (S) and kleisin (K) compartments are observed. (**B**) Cohesin holds sister chromatids together from S phase to anaphase. (**C**) Cohesin forms long-range intrachromatid loops, likely by a symmetrical extrusion process. (**D**) Cohesin can exist in multiple conformations determined by ATP binding (SMC heads engaged) and hydrolysis (SMC heads juxtaposed/separated). When separated, the coiled-coil arms generate one open SMC–kleisin (SK) compartment. In the juxtaposed state, the SMC coiled coils align, generating a rod-shaped complex, with a juxtaposed kleisin (JK) compartment. Alignment of the coiled coil is permissive to bending at an elbow region within the arms, bringing the hinge domain into close contact with the SMC3 head domain.

In *S. cerevisiae*, cohesin consists of four core and essential subunits: the structural maintenance of chromosomes (SMC) proteins, Smc1 and Smc3, the kleisin Scc1 and the kleisin-associating Scc3 (Figure 2A; [18,19]). The following are the human orthologs: SMC1, SMC3, SCC1 and STAG1/STAG2, respectively (Figure 2A; Table 2). SMC proteins consist of "head" and "hinge" domains, separated by a long antiparallel coiled-coil arm. The head comprises the N and C terminal domains that, respectively, provide the A and B motifs of a Walker ATPase [20]. The hinge is generated where the coiled coil, which separates the two halves of the head domain, reverses direction. Smc1 and Smc3 heterodimerize through their hinge domains, as well as making contacts through their head domains, which are essential

for ATPase activity [18,21]. The Scc1 subunit binds Smc3 at its N terminal and Smc1 at its C terminal, generating separate Smc and kleisin compartments when the ATPase heads are engaged, upon the binding of two ATP molecules. The Scc3 subunit binds to the central domain of Scc1, completing the cohesin complex [18,22].

Table 2. Cohesin subunits in *S. cerevisiae*, functions and orthologs in *S. pombe* and humans.

S. cerevisiae	*S. pombe*	Human	Complex	Function
Smc1	Psm1	SMC1A/B	Cohesin	Genome organization Sister chromatid cohesion
Smc3	Psm3	SMC3		
Scc1	Rad21	SCC1		
Scc3	Psc3	STAG1/2		
Scc2	Mis4	NIPBLA/B	Scc2/4 (NIPBL–Mau2)	Cohesin loading partner
Scc4	Ssl3	Mau2		
Pds5	Pds5	PDS5	-	Cohesin regulator
Wpl1	Wpl1	WAPL		
Eco1	Eso1	ESCO1/2	-	Cohesin separase
Esp1	Cut1	ESPL1		
Smc5	Smc5	SMC5	SMC5/6	DNA/chromatin processing
Smc6	Smc6	SMC6		
Mms21	Nse2	NSE2		Ubiquitin ligase

Other proteins, such as Scc2/Scc4 (NIPBLA/NIPBLB–Mau2 in humans), Pds5 (PDS5A/PDS5B in humans) and Wpl1 (WAPL in humans) also bind to the complex, through the Scc1 recruitment platform (Figure 2A; Table 2; [23–25]). These dynamic interactions facilitate cohesin loading (Scc2/4) and dissociation (Wpl1) or, in the case of Pds5, have a dual role in the establishment and maintenance of sister chromatid cohesion, as well as dissociation through recruiting Wpl1 [26,27]. Cohesin is loaded onto chromosomes prior to the S phase by Scc2/4, which causes a conformational change in the cohesin complex. This opens the cohesin ring and allows it to embrace DNA, potentially through the hinge domains or the Smc3–Scc1 interface [27–29]. Once loaded, Smc3 acetylation by the acetyltransferase Eco1 (ESCO1 and ESCO2 in humans) stabilizes cohesin chromosome embracement by antagonizing Wpl1 [30,31]. At this point, a DNA-replication-coupled process leads to cohesin-dependent cohesion of sister chromatids [32,33]. Timely sister chromatid separation is regulated by Scc1 cleavage by a cysteine protease, separase (Esp1 in *S. cerevisiae*), during the anaphase [13,34].

Various conformations of the human cohesin complex have been identified by advanced microscopy techniques, which provide insight into how it facilitates both its sister chromatid cohesion and loop extrusion functions. These in vitro studies indicate that the ATPase SMC heads can be engaged, separated or juxtaposed, in a dynamic manner that is regulated by ATP binding (engaged) and hydrolysis (separated/juxtaposed) (Figure 2; reviewed in [19,29,35]). Engagement of the ATPase heads upon ATP binding confers a conformation in which the coiled-coil arms are separated, generating distinct SMC and kleisin compartments (Figure 2A). In the ATP-unbound state, ATPase heads can be separated or juxtaposed. When separated, the coiled-coil arms do not align, generating one open SMC–kleisin compartment (Figure 2D). In the juxtaposed state, the SMC coiled-coils align, generating a rod-shaped complex, in which only a juxtaposed kleisin compartment is present (Figure 2D). Alignment of the coiled coil is permissive to bending at an elbow region within the arms, which can bring the hinge domain into close contact with the SMC3 head domain (Figure 2D; [29]).

Crucially, various DNA binding domains throughout the cohesin complex, as well as the loading partner NIPBL, have been shown to be essential for in vitro loop extrusion activity by human cohesin [29]. It appears that ATP- and DNA-binding-dependent conformation changes within the cohesin complex facilitate the passing over of the DNA molecule between DNA binding sites, although the full sequence and order of these events remains unclear, with multiple models being proposed [16,19,29]. The importance of DNA

entrapment within the different compartments of the complex also remains unclear for the loop extrusion process.

Loop extrusion by the budding yeast cohesin complex has not been formally demonstrated. However, the observation of cohesin-dependent loops, which expand when cohesin residency time is increased by Wpl1 depletion, argues in favor of loop extrusion [15,36]. Furthermore, in vitro studies have demonstrated the ability of budding yeast cohesin to bridge DNA molecules and compact DNA [37,38]. Unlike human cohesin, yeast cohesin forms molecular condensates upon interactions with DNA, leading to pronounced clustering [38,39]. Although the biological significance of this in vitro observation remains to be fully demonstrated, recent cryo-EM observations of budding yeast MRX, also an SMC family complex, revealed that it shares an ability to form large condensates, and crucially responsible protein motifs were identified [40]. Whether these motifs in Mre11 are conserved in cohesin and are relevant for their clustering activity remains to be determined.

The loop extrusion activity of the cohesin complex has revealed its importance for a broad range of DNA-related processes that go beyond its role in sister chromatid cohesion. These include regulation of gene transcription and, significantly, the DNA damage response in both yeast and mammals [41], due to its ability to shape the genome, and influence chromatin composition and nuclear architecture on multiple levels.

3. Chromosome Organization within the Nuclear Space and Cohesin Contribution

Eukaryotic genomes are organized at multiple levels, and ultimately exist in a highly folded state. The first level of chromatin folding consists of the periodic wrapping of the DNA double helix around a core of histone octamers to form nucleosomal chromatin fibers. These fibers are further organized into topologically associated domains (TADs), which have defined boundaries and exhibit increased local interactions within them and decreased interactions between them [35,42]. The mammalian genome is partitioned into a succession of TADs, which range in size from tens of kilobases to 1–2 Mb of DNA, whereas in yeast, smaller TAD-like structures have been described (50–100 kb in *S. pombe* and 5 kb in *S. cerevisiae*). Current models propose that cohesin forms TADs by loop extrusion between boundary proteins such as CTCF in mammals, or CARs (cohesin-associated regions) in yeast [15,36,43–45]. Cohesin also contributes to the higher-order organization of TADs, into TAD cliques, in which increased interactions are observed between distant TADs, in a constitutive or dynamic manner [46]. The contribution of cohesin to the individualization of chromosome domains imposes a constraint on the distance between sequences in the nucleus. This constraint could favor or disfavor contacts between DNA sequences during DNA repair and modulate both the DNA damage response and outcome, as supported by recent studies described below.

On a larger scale, chromatin is separated into different states with distinct characteristics, defined by specific histone variants, post-translational modifications (PTMs) and chromatin-binding proteins. Traditionally, two broad categories of chromatin states are distinguished, the transcriptionally active euchromatin and the densely packed and repressive heterochromatin, that overlap respectively with two compartments, A or B, defined by increased long-range interchromosomal interactions [47–49]. Cohesin is not required to form these compartments and rather appears to counteract their folding, as cohesin depletion results in an enhancement of A/B compartmentalization, as observed by increased contrast in Hi-C contact patterns [43–45,50,51]. Conversely, increasing loop formation by the depletion of WAPL or PDS5 strongly inhibits chromatin compartmentalization [45]. How cohesin opposes compartment formation remains to be defined experimentally. However, polymer simulations suggest that this could be achieved by cohesin-mediated loop extrusion [52].

Heterochromatin itself is subdivided into the ubiquitous constitutive heterochromatin, associated with highly repetitive sequences [53], and the more dynamic and often developmentally regulated facultative heterochromatin [54]. Heterochromatin can be associated with nuclear structures, including the nuclear lamina, forming lamina-associated domains,

further organizing chromosomes within the nucleus [55]. An intriguing link exists between pericentromeric heterochromatin and cohesin in several organisms. In vertebrates, despite previous conflicting reports, a recent study demonstrated that haspin, the inhibitor of the cohesin-releasing factor WAPL, interacts with the heterochromatin protein HP1 in pericentromeric heterochromatin [56]. This interaction prevents premature dissociation of centromeric cohesin and ensures that cohesion is protected in pericentromeric heterochromatin at early stages of mitosis [56]. Haspin also cooperates with cohesin in interphase to ensure robust polycomb-dependent homeotic gene silencing in *Drosophila* [57]. In *S. pombe*, the Psc3 (Scc3 in budding yeast) cohesin subunit directly interacts with the heterochromatin protein Swi6, which ensures cohesin recruitment and cohesion establishment at centromeres but is also important to ensure the genomic integrity of the heterochromatic mating type locus [58]. Finally, cohesin is enriched in subtelomeric regions and is required for their transcriptional repression in both fission and budding yeast through mechanisms that remain to be deciphered [59,60]. How cohesin shapes these compacted regions and whether this influences gene expression or DNA repair remains an open question.

Beyond these substructures and compartments, chromosomes fold on themselves, defining chromosome territories with few interchromosomal interactions in mammals [48,61]. Additionally, homologous chromosomes are separated in the somatic cells of most diploid organisms [62–65] and are even more distant than expected in human cells, an organization that appears to be actively defined [66]. These characteristics are likely to be significant in disfavoring recombination events between distinct chromosomes, but this remains to be experimentally tested. In yeast, chromosome territories are less clear, but the spatial arrangement of chromosomes imposed by the tethering of the centromeres at one pole and the clustering of telomeres at the nuclear periphery [67,68] favors interactions between clustered sequences. Several studies have revealed a clear correlation between physical distance and recombination efficiency, with closest loci recombining with higher efficiency [69–72]. Beyond physical distance, other factors influence recombination efficiency. For example, in vivo studies have shown that limiting the rate of resection can increase recombination efficiency at some subtelomeric and intrachromosomal DSBs [71,72], demonstrating a relationship between the rate of resection and successful homology search (reviewed in [73]).

Although the genome is actively folded and ordered within the nucleus, this organization is not static, and movement of the chromatin fiber is observed to a similar extent in all organisms, with single loci exploring volumes with a radius of 0.5 to 1 µm [74]. In normal conditions, chromatin exhibits a subdiffusive motion, reflecting constrained movement. The first constraint on chromatin motion is linked to its polymeric nature and its higher-order folding. In addition, external factors such as crowding and viscoelastic properties of the environment, as well as interaction with nuclear substructures, in particular with the nuclear membrane, also impinge on motion (reviewed in [75,76]). Chromatin motion is an energy-dependent process that is reduced upon glucose starvation or the depletion of intracellular ATP [77–79]. Part of this dependency on ATP could be linked to ATP-dependent chromatin remodelers that have been shown to drive enhanced chromatin mobility (reviewed in [75,76]). In *S. cerevisiae*, the cell cycle stage also has a dramatic effect on motion, which is restrained during the S phase and is much more dynamic during G1. Reduced motion in the S phase is replication and cohesin dependent, as S phase inactivation of cohesin restores mobility to G1 levels [80,81]. This S-phase-specific effect has led to the proposal that the cohesion between sister chromatids restrains chromatin motion. However, chromatin mobility is constant throughout the interphase in mammals, with depletion of cohesin also increasing chromatin mobility [82,83]. This suggests a sister chromatid cohesion independent role for cohesin in influencing chromatin motion, which could rely on its ATP-dependent loop extrusion activity. While chromatin motion is regulated in a conserved manner, its significance for cellular processes is far from clear. Indeed, a number of studies have described changes in chromatin motion in response to DNA damage, while the relevance of these changes for DNA repair have not been fully defined.

4. Genome Folding and Chromatin Dynamics Modulate DNA Repair

The final 3D architecture of the genome, defined through the combined influence of its structure at multiple levels, as well as the nuclear structures to which it is associated, provides both structural and regulatory functions that modulate DNA repair.

Breaks induced in different chromatin contexts lead to varied responses to DSBs, supporting a role of pre-established chromatin marks in DSB repair choice. Indeed, DSB repair pathway usage and efficiency in various chromatin environments has been addressed by employing genome-wide analysis of repair in euchromatic DSB sites [84] or the repair of specific heterochromatic sites [72,85–93]. The various forms of chromatin interfere with the recruitment of DSB repair proteins, thus contributing to DSB processing and DNA repair pathway choice. HR was shown to be the prevalent repair mechanism for endonuclease-induced DSB sites in transcriptionally active genes in human cell lines, while noncoding or silent euchromatic sequences exhibit a preference for NHEJ [84,94]. The H3K36me3 histone mark, typical of actively transcribed euchromatin, is thought to promote HR through the recruitment of the protein LEDGF, which mediates the recruitment of CtIP and, therefore, triggers ssDNA formation, Rad51 loading and HR initiation [84,95,96]. In parallel, the active chromatin mark H4K16-Ac, catalyzed by the TIP60 acetyltransferase, inhibits the binding of the anti-resection and pro-NHEJ factor 53BP1, thus favoring resection and HR commitment [97]. In contrast, H3K27me3-associated heterochromatin, or chromatin targeted to the repressive nuclear lamina, was shown to favor repair by NHEJ or alt-NHEJ through an undefined mechanism [89].

Paradoxically, the repair of DSBs in constitutive heterochromatic regions also appears to rely heavily on HR in different organisms [85,90,98,99], as observed in repeat-rich regions in G2 mouse cells [92,100] and in *Drosophila* pericentromeric heterochromatin [88]. This is partially due to the heterochromatin protein HP1, which recruits BRCA1 [101] to promote resection, as well as the recruitment of TIP60 by H3K9me3, which may promote decompaction of the DSB-flanking chromatin [102]. This decompaction is accompanied by the exclusion of the DSB to the periphery of the heterochromatin clusters, as observed in both *Drosophila* and mice [88,92,103]. In *Drosophila*, but not in mammals, exclusion from heterochromatin domains is followed by migration to the nuclear periphery, where HR takes place [88]. These studies support a model in which HR is actively repressed in heterochromatin domains. These relocation events, which isolate resected DSB from the bulk of heterochromatin, are proposed to help prevent recombination between the highly repetitive heterochromatic sequences, limiting sequence loss. Recent reports analyzing repair outcomes at unique genomic sites cleaved by meganucleases or CRISPR-Cas9 found no major change in the balance between NHEJ and HR when comparing heterochromatin and euchromatin [91,104]. However, observations in *Drosophila* suggest that heterochromatic repair might require specific DSB-induced chromatin modifications, involving a histone demethylase, to achieve the same NHEJ/HR balance seen in euchromatin [105]. The exact mechanism at work is still under investigation.

Lastly, a high-throughput study using CRISPR-Cas9 cleavage of a unique cassette inserted throughout the genome by a PiggyBac transposase optimized system has addressed the repair of DSB sites by NHEJ and MMEJ, depending on the chromatin context [106]. Although NHEJ is generally the most frequent repair pathway, how it is outcompeted by MMEJ varies depending on the chromatin context. Notably, the H3K27me3 heterochromatin mark favors MMEJ at the expense of NHEJ, suggesting it could promote resection initiation [106].

In *S. cerevisiae*, heterochromatin clearly modulates repair pathway choice through the control of resection at several levels [72,93]. The compacted chromatin structure modulates long-range resection through a still unknown mechanism [72]. In addition, Sir3, the mammalian HP1 functional ortholog, suppresses resection initiation through direct interaction and inhibition of the MRX^{MRN} activator $Sae2^{CtIP}$. This in turn promotes NHEJ and protects heterochromatin from unscheduled HR [93]. Notably, although delayed by resection inhibition, HR repair is proficient in yeast heterochromatin. Limiting resection

is of particular importance at subtelomeric DSBs as it avoids loss of chromosome end sequences and favors repair by conservative HR [72].

Beyond the chromatin context, an increasing number of studies have highlighted the contribution of higher-order chromatin structures, chromosome organization and interaction with nuclear substructures, such as the nuclear membrane, to DNA damage signaling and repair. As previously stated, the successive layers of genome folding—from TADs, TAD cliques, compartments and whole chromosome territories to chromosome positioning within the nucleus—each constrain contact between genomic sequences. These structures likely regulate HR, which is highly dependent on contact between the damaged DNA and the homologous template [73]. Furthermore, they could elicit the illegitimate rejoining of DNA ends by NHEJ, resulting in deleterious translocations.

Genome folding also defines the 3D context in which the DSB response propagates. For example, γH2AX spreading is largely influenced by the folding of chromosomes into TADs, with TAD boundaries correlating with the extent of γ2AX spreading [107]. Furthermore, CTCF-binding sites, which define TAD borders, are enriched around γH2AX foci [108,109]. A functional relationship is further supported by the failure of CTCF-deficient cells to properly assemble γH2AX foci, as well as recent data depicting a role for cohesin in foci formation [108,110]. Importantly, TAD-defined spreading may not be the exclusive mechanism for the propagation of DNA damage response factors, as other proteins, such as 53BP1, can spread over several TADs or sub-TADs in a manner that only partially relies on cohesin [109]. Whether chromosome folding has other functions in repair remains to be investigated. If the pre-existing chromatin architecture is important for the DNA damage response, it is also widely affected in response to DNA damage. Notably, chromatin marks and histone variants are deposited de novo on DSB-flanking sequences, including typical heterochromatin marks. This, along with variations in the chromatin compaction around DSB, plays a central role in DSB repair pathway choice (for a review see [111]). Higher-order chromatin folding is also modified, with the strengthening of TAD boundaries [112,113], an enrichment of TAD cliques and the formation of a new interaction-based subcompartment (D compartment) that groups damaged sequences with nondamaged loci enriched in chromatin marks typical of active transcription (H2AZac, H3K4me3 and H3K79me2; [113]).

These modifications are likely sustained by the increased chromatin dynamics observed in response to DNA damage. Indeed, in *S. cerevisiae*, both the damaged DNA site and the whole undamaged genome increase mobility (Figure 3A; [114,115]). Increased DSB motion has also been observed in *Drosophila* and mammalian cells [88,116]. DNA repair factors, chromatin remodeling complexes and the activity of actin filaments and microtubules have been identified as key elements that facilitate increased DSB chromatin motion (see [117,118] for more details). In budding yeast, decompaction of the chromatin fiber, associated with histone loss, is a key factor in increased chromatin dynamics [119]. This decompaction extends globally, with potential HR donor sequences also becoming more accessible and exploring larger nuclear volumes [80]. Enhanced chromatin movement was first proposed to increase the probability that separated DSB ends find each other prior to NHEJ [120] or to increase the rate of homology search during HDR [114,115]. However, recent work in budding yeast has demonstrated that the mobility of DSB ends was not rate limiting for timely HDR [80]. In this study, the absence of SUMO-dependent ubiquitin ligase Uls1 was shown to compromise local DSB movement, whilst maintaining increased global genome dynamics, DSB resection, checkpoint activation, histone degradation and chromatin decompaction [80]. Despite reduced DSB mobility, homology-directed strand invasion was not delayed, indicating that movement of the break is not limiting for the homology search [80]. Whether global genome mobility is critical for HR efficiency remains to be demonstrated.

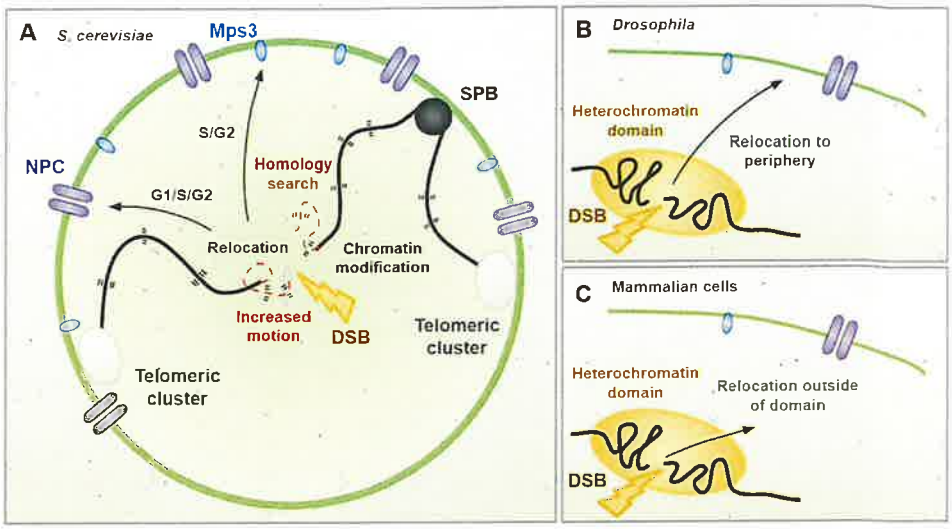

Figure 3. Chromatin dynamics in response to DNA double-strand breaks (DSBs). (**A**) In *S. cerevisiae*, chromosome centromeres are tethered to the spindle pole body (SPB), and telomeres cluster at the nuclear periphery. Upon DSB both local and global processing of the chromatin fiber alter its properties. These chromatin modifications lead to increased chromatin motion of DSB ends and the global genome, which likely assists in the homology search process. Persistent DSBs relocate to the nuclear periphery, through either interaction with the nuclear pore complex (NPC) or Mps3, in a cell-cycle-dependent manner, to assist repair by alternative mechanisms. (**B**) In *Drosophila*, heterochromatic DSBs move out of heterochromatin domains and to the nuclear periphery to facilitate faithful repair. (**C**) In mammalian cells, heterochromatic DSBs move out of heterochromatin domains, but not to the nuclear periphery, to facilitate DSB repair.

Despite this, increased chromatin mobility could facilitate efficient DSB repair in numerous other ways. These include by moving DNA DSBs outside of repair-repressive domains or into domains that favor repair. In line with this, several types of DNA lesions, including DSBs, have been shown to migrate to the nuclear periphery in budding and fission yeast (Figure 3A) and *Drosophila* (Figure 3B; [88,121–124]). In budding yeast, they associate with two distinct sites, either the nuclear pore complex (NPC) throughout the cell cycle, or the inner nuclear membrane SUN protein, Mps3, in the S/G2 phase. Relocation of DNA lesions to Mps3 or the NPC requires distinct signaling mechanisms, promoting distinct DNA repair pathways (extensively reviewed in [125]). Although relocation of DSBs to the nuclear periphery has not been observed in mammalian cells, displacement of DSBs is nonetheless observed, as demonstrated by DSB relocation outside of heterochromatic domains (Figure 3C; [126]). This is consistent with the need to relocate difficult to repair breaks outside of compartments that are repressive for some repair pathways and to move them towards more favorable environments in which repair could take place. Although a number of studies have described some of the actors required for DSB perinuclear localization, the precise molecular mechanism, from DNA damage to contact with perinuclear anchors, remains to be solved. Similarly, how Mps3 and the NPC define subnuclear compartments favoring repair is still unknown.

5. Cohesin in Repair

With the emerging importance of cohesin in shaping the genome by loop extrusion, new aspects of cohesin contribution to DNA damage signaling and repair are appearing.

A role for cohesin in DNA repair was in fact discovered before its well-described role in sister chromatid cohesion, with the *S. pombe* Rad21 gene being identified for providing resistance to ionizing radiation [127]. Since then, cohesin has increasingly been implicated in DNA damage repair, although its function in this was first linked to its capacity to

maintain sister chromatid cohesion at the DSB site, to facilitate HDR. Studies in yeast and mammals have demonstrated that cohesin is recruited to DNA DSB sites [107,128–130]. How cohesin is enriched and regulated at DSBs remains to be fully described. In yeast and humans, the cohesin loading complexes Scc2/4 and NIPBL–Mau2, respectively, are essential for the enrichment of cohesin at DSBs, suggesting de novo loading is responsible, not rearrangement of preloaded cohesin [128,129,131]. However, the recent finding that NIPBL is required for loop extrusion [16] highlights a possibility for a loop-extrusion-dependent accumulation of preloaded cohesin at DSBs. Strikingly, key components of the DNA damage checkpoint (DDC), the response mechanism that enables the detection and repair of DSBs, are important for cohesin DSB recruitment. MRX^{MRN} and the $Tel1^{ATM}$ kinase are required both in yeast and humans [41,128,131], and γH2AX, the $Mec1^{ATR}$ and Chk1 kinases are also important for cohesin enrichment at DSBs in yeast [128]. Sumoylation of the cohesin subunit Scc1 by the SUMO ligase Mms21 (Mms21/Nse2 in humans) also assists recruitment of cohesin at yeast DSBs [132]. Cohesin binding at DSBs is kept in check by the SUMO-dependent ubiquitin ligase Uls1, whose absence increases MRX and cohesin levels at DSB [80].

The Mms21 SUMO ligase is itself recruited to DSBs by another DSB-binding SMC, the essential Smc5/Smc6 (SMC5/6) complex [133], originally identified in *S. pombe* in genetic screens probing for increased radiation sensitivity [134,135]. Interestingly, SMC5/6 monomers and the holistic complex, including Mms21/Nse2, have been shown to have ssDNA binding affinity, through novel and unique hub and latch domains not found in the other SMC family proteins [136]. Like cohesin, SMC5/6 is enriched in the 25 kb region flanking the DSB [137,138]. Furthermore, knockdown (KD) of the SMC5/6 complex was shown to reduce cohesin loading at DSBs [130]. Crucially, KD of cohesin alone, or together with SMC5/6, resulted in the same reduction in HR events by sister chromatid exchange, indicating that these two complexes act in the same DNA repair pathway [130]. These observations may suggest that the SMC5/6 complex acts as a sensor for DSB ends, leading to the recruitment of the cohesin complex to the DSB. How SMC5/6 senses DSB ends is unknown. One possible hypothesis could be that the ssDNA formed by DSB end resection is detected through the SMC5/6 ssDNA-binding motifs [136]. Another possible mechanism could be linked to the deposition of γH2AX in the DSB-adjacent chromatin. Indeed, Rtt107, a γH2AX-binding protein with which SMC5/6 can interact, is necessary for the enrichment of SMC5/6 at DSBs [139].The full functional role SMC5/6 plays in DNA repair remains unclear, including the mechanism by which it leads to cohesin recruitment. Furthermore, it is possible that SMC5/6 plays roles beyond cohesin recruitment, as demonstrated by the importance of the SUMOylation activity of its Nse2 subunit for the relocation of heterochromatic DSBs in *Drosophila* [90] and DSB interaction with the nuclear periphery in yeast [140]. Whether cohesin is also relevant to these responses remains to be tested.

At DSB sites, local cohesin loading, which is dispensable for sister chromatid cohesion, is key for efficient repair. Indeed, impairing cohesin de novo loading at DSB, in experimental settings that do not affect sister chromatid cohesion, impinges on DNA repair [129,130]. Cohesin has also been proposed to regulate NHEJ in both yeast [141] and human cells [142] through an unknown mechanism.

More recently, the ability of cohesin to shape individual chromosomes through loop extrusion has been implicated in DNA DSB signaling and repair. One of the first signaling events following DSB induction is the phosphorylation of H2A (H2AX in mammals) by the $Tel1^{ATM}$, $Mec1^{ATR}$ and DNA-PK (only in mammals) PI3-kinases [2,143]. γH2AX can spread over 50–100 kb in yeast [143,144] and over 1–2 Mb of the adjacent chromatin in mammals [145,146] while the kinases appear to be bound close to the DSB ends. Recent studies in human cells have now demonstrated how cohesin-dependent TADs are functional units of the DNA damage response, through γH2AX spreading [131,147]. Hi-C and ChIP-seq data have demonstrated that contacts between the DSB site and distant *cis* chromosome loci are important for establishing γH2AX domains, with the interactome of the break site correlating strongly with the density and spread of γH2AX [147]. These domains are

largely defined to TADs, with TAD disruption extending γH2AX spreading into adjacent TADs [147]. Furthermore, DSB sites act as a cohesin translocation roadblock in both yeast and humans [131,148], with cohesin extruding loops away from DSB sites. Therefore, a role for cohesin loop extrusion activity in γH2AX spreading could be imagined, beyond its role in defining TADs with increased interaction [131]. These observations support a model in which cohesin complexes, anchored at DSB ends where the kinase is located, facilitate phosphorylation of H2A as chromatin passes through the cohesin ring during loop extrusion (Figure 4B). In budding yeast, γH2A propagates in both *cis*, and *trans* between nearby genomic regions of different chromosomes [144]; however, the contribution of the cohesin complex and chromosome folding has not been tested.

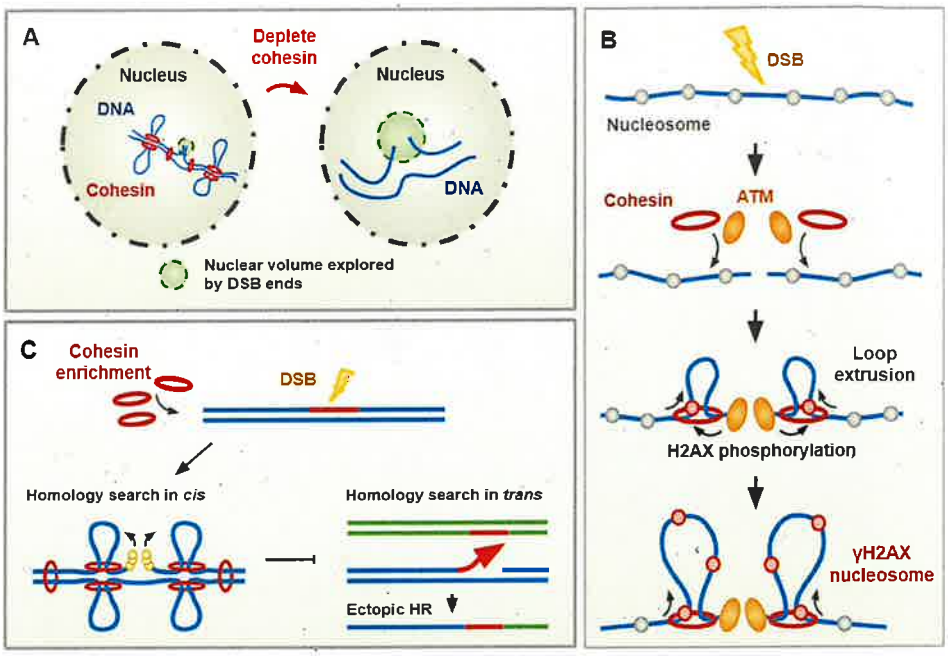

Figure 4. Cohesin contributes to DNA damage signaling and repair. (**A**) Cohesion of sister chromatids restricts chromatin mobility. Cohesin also restricts chromatin mobility in response to DNA damage, with the nuclear volume explored by DSB ends increasing upon cohesin disruption. (**B**) Cohesin-dependent TADs are functional units of the DNA damage response, through γH2Ax spreading. Loop-extrusion activity away from a DSB site drives γH2Ax spreading by the PI3 kinase ATM, allowing the establishment of γH2Ax domains. (**C**) Genome-wide loading of cohesin upon DSB leads to the individualization of chromosomes. Loss of cohesin leads to an increase in interchromosomal interactions and decrease in *cis* dsDNA sampling. Individualization of chromosomes may disfavor ectopic repair events by restraining the homology search process. Preventing interchromosome recombination demonstrates a key role for cohesin in safeguarding the genome against genome instability.

Loop extrusion by the cohesin complex has also been implicated in the random rearrangement of antibody gene segments of the mouse immune system through a repair process named V(D)J (for a detailed review see [149]). V(D)J recombination is triggered by the programmed formation of DSBs by the RAG endonuclease and results in repair between distant sequences arranged in tandem. Segments destined for rearrangement are interspersed by CTCF sites, which Hi-C data has revealed act as loop anchors and boundaries, limiting contacts and repair between more distant segments [150,151]. Further supporting a functional role for loop extrusion, depletion of cohesin reduces long-range interactions and recombination between distal segments [150], whereas downregulation of WAPL, and

thus increasing the size of cohesin-mediated loops, favors repair between more distant segments [152]. Therefore, loop extrusion by cohesin appears to favor intrachromosomal DNA repair between proximal sequences.

Beyond its loop extrusion activity, cohesin may also favor repair with proximal DNA sequences by restricting DSB motion. Indeed, cohesin depletion increases DSB movement beyond the heightened movement observed at DSB sites in WT yeast cells [80]. Accordingly, the interactome around the DSB is altered in absence of cohesin, resulting in increased genome-wide contacts, at the expense of *cis* intrachromosomal interactions (Figure 4C) [148].

Together, these data highlight the contribution of DSB-bound cohesin. Cohesin drives contact between DSB ends and proximal sequences through loop extrusion, participating in DNA damage signaling through γH2AX spreading and promoting intrachromosomal repair. Cohesin also restrains DSB motion, restricting *trans* interactions, further favoring repair with proximal sequences.

Cohesin enrichment is also enhanced genome wide in response to DSB induction [153,154]. In yeast, this enrichment at undamaged sites globally tightens sister chromatid cohesion [30,154]. Similar to the establishment of the S phase cohesion, DSB-induced global cohesin loading relies on Scc2/4, Eco1-mediated Smc3 acetylation and cohesin sumoylation [132,155]. Additionally, DSB-induced phosphorylation of Scc1 by the Chk1 checkpoint kinase is required to allow subsequent Scc1 acetylation by Eco1. Scc1 acetylation counteracts Wpl1 activity, stabilizing cohesin on chromosomes [30,156]. DSB-induced cohesin stabilization may act redundantly with the Chk1-mediated phosphorylation and stabilization of Pds1, antagonizing the activity of the Esp1 separase to delay the metaphase–anaphase transition. In line with this, cohesin accumulates on chromatin upon formation of DNA DSBs [113,130,157] and is involved in the DNA-damage-induced intra-S and G2/M checkpoint activation in human cells [158].

In addition to this, enhanced genome-wide loading of cohesin could mediate the individualization of chromosomes, therefore disfavoring ectopic repair events [148]. Indeed, Hi-C experiments upon HO-induced DSBs in *S. cerevisiae* demonstrated that HR repair occurs in a chromatin context spatially shaped at the global level by cohesin [148]. Whether this relies on pre-existing or de novo loaded cohesin remains to be determined. Cohesin appears to mediate chromosome individualization, reducing overall interchromosomal interactions, which may also restrain the homology search process and promote *cis* dsDNA sampling (Figure 4C) [148]. Accordingly, cohesin depletion increases DSB contacts and favors recombination with the rest of the genome [148]. Importantly, biasing the homology search in *cis* may safeguard the genome against genome instability.

6. Conclusions

While the importance of chromatin composition and organization for DNA repair has become increasingly clear, more work is now required to precisely define the actors and molecular mechanisms at work in these processes. In particular, deciphering how chromatin compaction and the protein or DNA modifications associated with heterochromatin regulate DNA repair pathway choice is crucial, particularly in regard to the development of genome editing tools for therapeutic approaches.

The cohesin complex and its activity as a molecular motor, capable of forming chromatin loops, has emerged as a key player in detecting and responding to DNA damage and, therefore, promoting DNA repair and genome stability. Recent advancements in our knowledge of how this complex works and the technology available for observing its functions at a molecular level, make it likely that we will continue to see novel roles attributed to cohesin for correct DNA repair in the near future. How cohesin interacts with heterochromatin and whether its role there is relevant for DNA repair has not yet been addressed and should be investigated.

A better understanding of cohesin function in DNA repair could be particularly relevant for understanding how cohesin dysfunction affects tumorigenesis. Indeed, cohesin is frequently deregulated in cancer cells, notably in bladder cancer and myeloid

neoplasms [159]. The fact that tumors mutated for cohesin have increased sensitivity to DNA damaging agents and PARP inhibitors further suggests a link to their role in DNA repair. Understanding the role of cohesin in DNA repair is, thus, particularly relevant to human health.

Author Contributions: This review was written and edited by J.P. and K.D. All authors have read and agreed to the published version of the manuscript.

Funding: This work was funded by grants from Fondation pour la Recherche Médicale (DEP20131128535), the European Research Council under the European Community's Seventh Framework Program (FP7/2007 2013/European Research Council Grant Agreement 281287), the Fondation ARC pour la Recherche sur le Cancer (PJA-20191209432), the CEA Radiation biology program and the EDF. J.P. was supported by a fellowship from the CEA—IRTELIS Ph.D. program.

Institutional Review Board Statement: Not applicable.

Informed Consent Statement: Not applicable.

Data Availability Statement: Not applicable.

Acknowledgments: We thank members of the Dubrana and Marcand laboratory for helpful discussions. We apologize to our colleagues whose studies are not cited here due to space limitations.

Conflicts of Interest: The authors declare no conflict of interest.

References

1. Tubbs, A.; Nussenzweig, A. Endogenous DNA Damage as a Source of Genomic Instability in Cancer. *Cell* **2017**, *168*, 644–656. [CrossRef]
2. Jackson, S.P.; Bartek, J. The DNA-damage response in human biology and disease. *Nature* **2009**, *461*, 1071–1078. [CrossRef]
3. Emerson, C.H.; Bertuch, A.A. Consider the workhorse: Nonhomologous end-joining in budding yeast 1. *Biochem. Cell Biol.* **2016**, *94*, 396–406. [CrossRef] [PubMed]
4. Tseng, S.-F.; Gabriel, A.; Teng, S.-C. Proofreading activity of DNA polymerase Pol2 mediates 3′-end processing during nonhomologous end joining in yeast. *PLoS Genet.* **2008**, *4*, e1000060. [CrossRef]
5. Yu, X.; Gabriel, A. Reciprocal translocations in Saccharomyces cerevisiae formed by nonhomologous end joining. *Genetics* **2004**, *166*, 741–751. [CrossRef] [PubMed]
6. Sallmyr, A.; Tomkinson, A.E. Repair of DNA double-strand breaks by mammalian alternative end-joining pathways. *J. Biol. Chem.* **2018**, *293*, 10536–10546. [CrossRef]
7. Chang, H.H.Y.; Pannunzio, N.R.; Adachi, N.; Lieber, M.R. Non-homologous DNA end joining and alternative pathways to double-strand break repair. *Nat. Rev. Mol. Cell Biol.* **2017**, *21*, 296–506. [CrossRef] [PubMed]
8. Bazzano, D.; Lomonaco, S.; Wilson, T.E. Mapping yeast mitotic 5′ resection at base resolution reveals the sequence and positional dependence of nucleases in vivo. *Nucleic Acids Res.* **2021**, *49*, 12607–12621. [CrossRef]
9. Tisi, R.; Vertemara, J.; Zampella, G.; Longhese, M.P. Functional and structural insights into the MRX/MRN complex, a key player in recognition and repair of DNA double-strand breaks. *Comput. Struct. Biotechnol. J.* **2020**, *18*, 1137–1152. [CrossRef]
10. Cejka, P.; Symington, L.S. DNA End Resection: Mechanism and Control. *Annu. Rev. Genet.* **2021**, *55*, 285–307. [CrossRef]
11. Heyer, W.-D.; Ehmsen, K.T.; Liu, J. Regulation of homologous recombination in eukaryotes. *Annu. Rev. Genet.* **2010**, *44*, 113–139. [CrossRef] [PubMed]
12. Symington, L.S. DNA repair: Making the cut. *Nature* **2014**, *514*, 39–40. [CrossRef] [PubMed]
13. Marston, A.L. Chromosome Segregation in Budding Yeast: Sister Chromatid Cohesion and Related Mechanisms. *Genetics* **2014**, *196*, 31–63. [CrossRef] [PubMed]
14. Zuin, J.; Dixon, J.R.; van der Reijden, M.I.J.A.; Ye, Z.; Kolovos, P.; Brouwer, R.W.W.; van de Corput, M.P.C.; van de Werken, H.J.G.; Knoch, T.A.; van IJcken, W.F.J.; et al. Cohesin and CTCF differentially affect chromatin architecture and gene expression in human cells. *Proc. Natl. Acad. Sci. USA* **2014**, *111*, 996–1001. [CrossRef]
15. Dauban, L.; Montagne, R.; Thierry, A.; Lazar-Stefanita, L.; Bastié, N.; Gadal, O.; Cournac, A.; Koszul, R.; Beckouët, F. Regulation of Cohesin-Mediated Chromosome Folding by Eco1 and Other Partners. *Mol. Cell* **2020**, *77*, 1279–1293.e4. [CrossRef] [PubMed]
16. Davidson, I.F.; Bauer, B.; Goetz, D.; Tang, W.; Wutz, G.; Peters, J.M. DNA loop extrusion by human cohesin. *Science* **2019**, *366*, 1338–1345. [CrossRef] [PubMed]
17. Golfier, S.; Quail, T.; Kimura, H.; Brugués, J. Cohesin and condensin extrude DNA loops in a cell cycle-dependent manner. *eLife* **2020**, *9*, e53885. [CrossRef]
18. Gligoris, T.; Löwe, J. Structural Insights into Ring Formation of Cohesin and Related Smc Complexes. *Trends Cell Biol.* **2016**, *26*, 680–693. [CrossRef]

19. Yatskevich, S.; Rhodes, J.; Nasmyth, K. Organization of Chromosomal DNA by SMC Complexes. *Annu. Rev. Genet.* **2019**, *53*, 445–482. [CrossRef]
20. Hopfner, K.P.; Karcher, A.; Shin, D.S.; Craig, L.; Arthur, L.M.; Carney, J.P.; Tainer, J.A. Structural biology of Rad50 ATPase: ATP-driven conformational control in DNA double-strand break repair and the ABC-ATPase superfamily. *Cell* **2000**, *101*, 789–800. [CrossRef]
21. Weitzer, S.; Lehane, C.; Uhlmann, F. A Model for ATP Hydrolysis-Dependent Binding of Cohesin to DNA. *Curr. Biol.* **2003**, *13*, 1930–1940. [CrossRef]
22. Roig, M.B.; Löwe, J.; Chan, K.-L.; Beckouët, F.; Metson, J.; Nasmyth, K. Structure and function of cohesin's Scc3/SA regulatory subunit. *FEBS Lett.* **2014**, *588*, 3692–3702. [CrossRef]
23. Kikuchi, S.; Borek, D.M.; Otwinowski, Z.; Tomchick, D.R.; Yu, H. Crystal structure of the cohesin loader Scc2 and insight into cohesinopathy. *Proc. Natl. Acad. Sci. USA* **2016**, *113*, 12444–12449. [CrossRef] [PubMed]
24. Lee, B.-G.; Roig, M.B.; Jansma, M.; Petela, N.; Metson, J.; Nasmyth, K.; Löwe, J. Crystal Structure of the Cohesin Gatekeeper Pds5 and in Complex with Kleisin Scc1. *Cell Rep.* **2016**, *14*, 2108–2115. [CrossRef]
25. Hara, K.; Zheng, G.; Qui, Q.; Liu, H.; Ouyang, Z.; Chen, Z.; Tomchick, D.R.; Yu, H. Structure of cohesin subcomplex pinpoints direct shugoshin-Wapl antagonism in centromeric cohesion. *Nat. Struct. Mol. Biol.* **2014**, *21*, 864–870. [CrossRef] [PubMed]
26. Ciosk, R.; Shirayama, M.; Shevchenko, A.; Tanaka, T.; Toth, A.; Shevchenko, A.; Nasmyth, K. Cohesin's binding to chromosomes depends on a separate complex consisting of Scc2 and Scc4 proteins. *Mol. Cell* **2000**, *5*, 243–254. [CrossRef]
27. Murayama, Y.; Uhlmann, F. DNA Entry into and Exit out of the Cohesin Ring by an Interlocking Gate Mechanism. *Cell* **2015**, *163*, 1628–1640. [CrossRef]
28. Gruber, S.; Arumugam, P.; Katou, Y.; Kuglitsch, D.; Helmhart, W.; Shirahige, K.; Nasmyth, K. Evidence that loading of cohesin onto chromosomes involves opening of its SMC hinge. *Cell* **2006**, *127*, 523–537. [CrossRef]
29. Bauer, B.W.; Davidson, I.F.; Canena, D.; Wutz, G.; Tang, W.; Litos, G.; Horn, S.; Hinterdorfer, P.; Peters, J.M. Cohesin mediates DNA loop extrusion by a "swing and clamp" mechanism. *Cell* **2021**, *184*, 5448–5464.e22. [CrossRef] [PubMed]
30. Heidinger-Pauli, J.M.; Ünal, E.; Koshland, D. Distinct targets of the Eco1 acetyltransferase modulate cohesion in S phase and in response to DNA damage. *Mol. Cell* **2009**, *34*, 311–321. [CrossRef] [PubMed]
31. Ladurner, R.; Kreidl, E.; Ivanov, M.P.; Ekker, H.; Idarraga Amado, M.H.; Busslinger, G.A.; Wutz, G.; Cisneros, D.A.; Peters, J.M. Sororin actively maintains sister chromatid cohesion. *EMBO J.* **2016**, *35*, 635–653. [CrossRef]
32. Sherwood, R.; Takahashi, T.S.; Jallepalli, P.V. Sister acts: Coordinating DNA replication and cohesion establishment. *Genes Dev.* **2010**, *24*, 2723–2731. [CrossRef]
33. Zheng, G.; Kanchwala, M.; Xing, C.; Yu, H. MCM2-7-dependent cohesin loading during S phase promotes sister-chromatid cohesion. *eLife* **2018**, *7*, e33920. [CrossRef]
34. Peters, J.M.; Nishiyama, T. Sister chromatid cohesion. *Cold Spring Harb. Perspect. Biol.* **2012**, *4*, a011130. [CrossRef] [PubMed]
35. Davidson, I.F.; Peters, J.M. Genome folding through loop extrusion by SMC complexes. *Nat. Rev. Mol. Cell Biol.* **2021**, *22*, 445–464. [CrossRef] [PubMed]
36. Costantino, L.; Hsieh, T.-H.S.; Lamothe, R.; Darzacq, X.; Koshland, D. Cohesin residency determines chromatin loop patterns. *eLife* **2020**, *9*, e59889. [CrossRef] [PubMed]
37. Gutierrez-Escribano, P.; Newton, M.D.; Llauró, A.; Huber, J.; Tanasie, L.; Davy, J.; Aly, I.; Aramayo, R.; Montoya, A.; Kramer, H.; et al. A conserved ATP- And Scc2/4-dependent activity for cohesin in tethering DNA molecules. *Sci. Adv.* **2019**, *5*, eaay6804. [CrossRef] [PubMed]
38. Xiang, S.; Koshland, D. Cohesin architecture and clustering in vivo. *eLife* **2021**, *10*, 1–49. [CrossRef]
39. Ryu, J.-K.; Bouchoux, C.; Liu, H.W.; Kim, E.; Minamino, M.; de Groot, R.; Katan, A.J.; Bonato, A.; Marenduzzo, D.; Michieletto, D.; et al. Bridging-induced phase separation induced by cohesin SMC protein complexes. *Sci. Adv.* **2021**, *7*, eabe5905. [CrossRef]
40. Kissling, V.; Reginato, G.; Bianco, E.; Kasaciunaite, K. Mre11-Rad50 oligomerization promotes DNA double-strand break repair. *Res. Sq.* **2021**. [CrossRef]
41. Litwin, I.; Pilarczyk, E.; Wysocki, R. The Emerging Role of Cohesin in the DNA Damage Response. *Genes* **2018**, *9*, 581. [CrossRef]
42. Sexton, T.; Yaffe, E.; Kenigsberg, E.; Bantignies, F.; Leblanc, B.; Hoichman, M.; Parrinello, H.; Tanay, A.; Cavalli, G. Three-Dimensional Folding and Functional Organization Principles of the Drosophila Genome. *Cell* **2012**, *148*, 458–472. [CrossRef] [PubMed]
43. Rao, S.S.P.; Huang, S.-C.; Glenn St Hilaire, B.; Engreitz, J.M.; Perez, E.M.; Kieffer-Kwon, K.-R.; Sanborn, A.L.; Johnstone, S.E.; Bascom, G.D.; Bochkov, I.D.; et al. Cohesin Loss Eliminates All Loop Domains. *Cell* **2017**, *171*, 305–320.e24. [CrossRef]
44. Schwarzer, W.; Abdennur, N.; Goloborodko, A.; Pekowska, A.; Fudenberg, G.; Loe-Mie, Y.; Fonseca, N.A.; Huber, W.; Haering, C.; Mirny, L.; et al. Two independent modes of chromatin organization revealed by cohesin removal. *Nature* **2017**, *551*, 51–56. [CrossRef]
45. Wutz, G.; Várnai, C.; Nagasaka, K.; Cisneros, D.A.; Stocsits, R.R.; Tang, W.; Schoenfelder, S.; Jessberger, G.; Muhar, M.; Hossain, M.J.; et al. Topologically associating domains and chromatin loops depend on cohesin and are regulated by CTCF, WAPL, and PDS5 proteins. *EMBO J.* **2017**, *36*, 3573–3599. [CrossRef]

46. Paulsen, J.; Liyakat Ali, T.M.; Nekrasov, M.; Delbarre, E.; Baudement, M.-O.; Kurscheid, S.; Tremethick, D.; Collas, P. Long-range interactions between topologically associating domains shape the four-dimensional genome during differentiation. *Nat. Genet.* **2019**, *51*, 835–843. [CrossRef] [PubMed]
47. Lieberman Aiden, E.; van Berkum, N.L.; Williams, L.; Imakaev, M.; Ragoczy, T.; Telling, A.; Amit, I.; Lajoie, B.R.; Sabo, P.J.; Dorschner, M.O.; et al. Comprehensive Mapping of Long-Range Interactions Reveals Folding Principles of the Human Genome. *Science* **2009**, *326*, 289–293. [CrossRef]
48. Rao, S.S.P.; Huntley, M.H.; Durand, N.C.; Stamenova, E.K.; Bochkov, I.D.; Robinson, J.T.; Sanborn, A.L.; Machol, I.; Omer, A.D.; Lander, E.S.; et al. A 3D Map of the Human Genome at Kilobase Resolution Reveals Principles of Chromatin Looping. *Cell* **2014**, *159*, 1665–1680. [CrossRef] [PubMed]
49. Sexton, T.; Yaffe, E. Chromosome Folding: Driver or Passenger of Epigenetic State? *Cold Spring Harb. Perspect. Biol.* **2015**, *7*, a018721. [CrossRef]
50. Gassler, J.; Brandão, H.B.; Imakaev, M.; Flyamer, I.M.; Ladstatter, S.; Bickmore, W.A.; Peters, J.M.; Mirny, L.A.; Tachibana, K. A mechanism of cohesin-dependent loop extrusion organizes zygotic genome architecture. *EMBO J.* **2017**, *36*, 3600–3618. [CrossRef] [PubMed]
51. Haarhuis, J.H.I.; van der Weide, R.H.; Blomen, V.A.; Yáñez-Cuna, J.O.; Amendola, M.; van Ruiten, M.S.; Krijger, P.H.L.; Teunissen, H.; Medema, R.H.; van Steensel, B.; et al. The Cohesin Release Factor WAPL Restricts Chromatin Loop Extension. *Cell* **2017**, *169*, 693–707.e14. [CrossRef] [PubMed]
52. Nuebler, J.; Fudenberg, G.; Imakaev, M.; Abdennur, N.; Mirny, L.A. Chromatin organization by an interplay of loop extrusion and compartmental segregation. *Proc. Natl. Acad. Sci. USA* **2018**, *115*, E6697–E6706. [CrossRef]
53. Padeken, J.; Zeller, P.; Gasser, S.M. ScienceDirect Repeat DNA in genome organization and stability. *Curr. Opin. Genet. Dev.* **2015**, *31*, 12–19. [CrossRef] [PubMed]
54. Trojer, P.; Reinberg, D. Facultative heterochromatin: Is there a distinctive molecular signature? *Mol. Cell* **2007**, *28*, 1–13. [CrossRef]
55. Penagos-Puig, A.; Furlan-Magaril, M. Heterochromatin as an Important Driver of Genome Organization. *Front. Cell Dev. Biol.* **2020**, *8*, 579137. [CrossRef] [PubMed]
56. Yi, Q.; Chen, Q.; Liang, C.; Yan, H.; Zhang, Z.; Xiang, X.; Zhang, M.; Qi, F.; Zhou, L.; Wang, F. HP1 links centromeric heterochromatin to centromere cohesion in mammals. *EMBO Rep.* **2018**, *19*, e45484. [CrossRef]
57. Fresán, U.; Rodríguez-Sánchez, M.A.; Reina, O.; Corces, V.G.; Lluisa Espinàs, M. Haspin kinase modulates nuclear architecture and Polycomb-dependent gene silencing. *PLoS Genet.* **2020**, *16*, e1008962. [CrossRef]
58. Nonaka, N.; Kitajima, T.; Yokobayashi, S.; Xiao, G.; Yamamoto, M.; Grewal, S.I.S.; Watanabe, Y. Recruitment of cohesin to heterochromatic regions by Swi6/HP1 in fission yeast. *Nat. Cell Biol.* **2002**, *4*, 89–93. [CrossRef]
59. Kothiwal, D.; Laloraya, S. A SIR-independent role for cohesin in subtelomeric silencing and organization. *Proc. Natl. Acad. Sci. USA* **2019**, *116*, 5659–5664. [CrossRef]
60. Dheur, S.; Saupe, S.J.; Genier, S.; Vazquez, S.; Javerzat, J.-P. Role for cohesin in the formation of a heterochromatic domain at fission yeast subtelomeres. *Mol. Cell. Biol.* **2011**, *31*, 1088–1097. [CrossRef]
61. Cremer, T.; Cremer, M. Chromosome Territories. *Cold Spring Harb. Perspect. Biol.* **2010**, *2*, a003889. [CrossRef]
62. Cremer, M.; von Hase, J.; Volm, T.; Brero, A.; Kreth, G.; Walter, J.; Fischer, C.; Solovei, I.; Cremer, C.; Cremer, T. Non-random radial higher-order chromatin arrangements in nuclei of diploid human cells. *Chromosome Res.* **2001**, *9*, 541–567. [CrossRef] [PubMed]
63. Lorenz, A.; Fuchs, J.; Burger, R.; Loidl, J. Chromosome pairing does not contribute to nuclear architecture in vegetative yeast cells. *Eukaryot. Cell* **2003**, *2*, 856–866. [CrossRef] [PubMed]
64. Rong, Y.S.; Golic, K.G. The homologous chromosome is an effective template for the repair of mitotic DNA double-strand breaks in drosophila. *Genetics* **2003**, *165*, 1831–1842. [CrossRef] [PubMed]
65. Joyce, E.F.; Erceg, J.; Wu, C.-T. ScienceDirect Pairing and anti-pairing: A balancing act in the diploid genome. *Curr. Opin. Genet. Dev.* **2016**, *37*, 119–128. [CrossRef]
66. Heride, C.; Ricoul, M.; Kiêu, K.; von Hase, J.; Guillemot, V.; Cremer, C.; Dubrana, K.; Sabatier, L. Distance between homologous chromosomes results from chromosome positioning constraints. *J. Cell. Sci.* **2010**, *123*, 4063–4075. [CrossRef]
67. Taddei, A.; Schober, H.; Gasser, S.M. The Budding Yeast Nucleus. *Cold Spring Harb. Perspect. Biol.* **2010**, *2*, a000612. [CrossRef]
68. Albert, B.; Léger-Silvestre, I.; Normand, C.; Gadal, O. Nuclear organization and chromatin dynamics in yeast: Biophysical models or biologically driven interactions? *BBA Gene. Regul. Mech.* **2012**, *1819*, 468–481. [CrossRef]
69. Burgess, S.M.; Kleckner, N. Collisions between yeast chromosomal loci in vivo are governed by three layers of organization. *Genes Dev.* **1999**, *13*, 1871–1883. [CrossRef]
70. Agmon, N.; Liefshitz, B.; Zimmer, C.; Fabre, E.; Kupiec, M. Effect of nuclear architecture on the efficiency of double-strand break repair. *Nat. Cell Biol.* **2013**, *15*, 694–699. [CrossRef]
71. Lee, C.-S.; Wang, R.W.; Chang, H.-H.; Capurso, D.; Segal, M.R.; Haber, J.E. Chromosome position determines the success of double-strand break repair. *Proc. Natl. Acad. Sci. USA* **2016**, *113*, E146–E154. [CrossRef]
72. Batté, A.; Brocas, C.; Bordelet, H.; Hocher, A.; Ruault, M.; Adjiri, A.; Taddei, A.; Dubrana, K. Recombination at subtelomeres is regulated by physical distance, double-strand break resection and chromatin status. *EMBO J.* **2017**, *36*, 2609–2625. [CrossRef] [PubMed]
73. Bordelet, H.; Dubrana, K. Keep moving and stay in a good shape to find your homologous recombination partner. *Curr. Genet.* **2019**, *65*, 29–39. [CrossRef] [PubMed]

74. Lanctot, C.; Cheutin, T.; Cremer, M.; Cavalli, G.; Cremer, T. Dynamic genome architecture in the nuclear space: Regulation of gene expression in three dimensions. *Nat. Rev. Genet.* **2007**, *8*, 104–115. [CrossRef] [PubMed]
75. Zimmer, C.; Fabre, E. Chromatin mobility upon DNA damage: State of the art and remaining questions. *Curr. Genet.* **2019**, *65*, 1–9. [CrossRef]
76. Shukron, O.; Seeber, A.; Amitai, A.; Holcman, D. Advances Using Single-Particle Trajectories to Reconstruct Chromatin Organization and Dynamics. *Trends Genet.* **2019**, *35*, 685–705. [CrossRef] [PubMed]
77. Heun, P.; Laroche, T.; Shimada, K.; Furrer, P.; Gasser, S.M. Chromosome dynamics in the yeast interphase nucleus. *Science* **2001**, *294*, 2181–2186. [CrossRef]
78. Joyner, R.P.; Tang, J.H.; Helenius, J.; Dultz, E.; Brune, C.; Holt, L.J.; Huet, S.; Mueller, D.J.; Weis, K. A glucose-starvation response regulates the diffusion of macromolecules. *eLife* **2016**, *5*, e09376. [CrossRef]
79. Weber, S.C.; Spakowitz, A.J.; Theriot, J.A. Nonthermal ATP-dependent fluctuations contribute to the in vivo motion of chromosomal loci. *Proc. Natl. Acad. Sci. USA* **2012**, *109*, 7338–7343. [CrossRef] [PubMed]
80. Cheblal, A.; Challa, K.; Seeber, A.; Shimada, K.; Yoshida, H.; Ferreira, H.C.; Amitai, A.; Gasser, S.M. DNA Damage-Induced Nucleosome Depletion Enhances Homology Search Independently of Local Break Movement. *Mol. Cell* **2020**, *80*, 311–326.e4. [CrossRef]
81. Dion, V.; Kalck, V.; Seeber, A.; Schleker, T.; Gasser, S.M. Cohesin and the nucleolus constrain the mobility of spontaneous repair foci. *EMBO Rep.* **2013**, *14*, 984–991. [CrossRef] [PubMed]
82. Ashwin, S.S.; Nozaki, T.; Maeshima, K.; Sasai, M. Organization of fast and slow chromatin revealed by single-nucleosome dynamics. *Proc. Natl. Acad. Sci. USA* **2019**, *116*, 19939–19944. [CrossRef]
83. Nozaki, T.; Imai, R.; Tanbo, M.; Nagashima, R.; Tamura, S.; Tani, T.; Joti, Y.; Tomita, M.; Hibino, K.; Kanemaki, M.T.; et al. Dynamic Organization of Chromatin Domains Revealed by Super-Resolution Live-Cell Imaging. *Mol. Cell* **2017**, *67*, 282–293.e7. [CrossRef] [PubMed]
84. Aymard, F.; Bugler, B.; Schmidt, C.K.; Guillou, E.; Caron, P.; Briois, S.; Iacovoni, J.S.; Daburon, V.; Miller, K.M.; Jackson, S.P.; et al. Transcriptionally active chromatin recruits homologous recombination at DNA double-strand breaks. *Nat. Struct. Mol. Biol.* **2014**, *21*, 366–374. [CrossRef] [PubMed]
85. Goodarzi, A.A.; Noon, A.T.; Deckbar, D.; Ziv, Y.; Shiloh, Y.; Löbrich, M.; Jeggo, P.A. ATM signaling facilitates repair of DNA double-strand breaks associated with heterochromatin. *Mol. Cell* **2008**, *31*, 167–177. [CrossRef]
86. Peng, J.C.; Karpen, G.H. Heterochromatic Genome Stability Requires Regulators of Histone H3 K9 Methylation. *PLoS Genet.* **2009**, *5*, e1000435. [CrossRef] [PubMed]
87. Noon, A.T.; Shibata, A.; Rief, N.; Löbrich, M.; Stewart, G.S.; Jeggo, P.A.; Goodarzi, A.A. 53BP1-dependent robust localized KAP-1 phosphorylation is essential for heterochromatic DNA double-strand break repair. *Nat. Cell Biol.* **2010**, *12*, 177–184. [CrossRef] [PubMed]
88. Chiolo, I.; Minoda, A.; Colmenares, S.U.; Polyzos, A.; Costes, S.V.; Karpen, G.H. Double-strand breaks in heterochromatin move outside of a dynamic HP1a domain to complete recombinational repair. *Cell* **2011**, *144*, 732–744. [CrossRef]
89. Lemaître, C.; Grabarz, A.; Tsouroula, K.; Andronov, L.; Furst, A.; Pankotai, T.; Heyer, V.; Rogier, M.; Attwood, K.M.; Kessler, P.; et al. Nuclear position dictates DNA repair pathway choice. *Genes Dev.* **2014**, *28*, 2450–2463. [CrossRef]
90. Ryu, T.; Spatola, B.; Delabaere, L.; Bowlin, K.; Hopp, H.; Kunitake, R.; Karpen, G.H.; Chiolo, I. Heterochromatic breaks move to the nuclear periphery to continue recombinational repair. *Nat. Cell Biol.* **2015**, *17*, 1401–1411. [CrossRef]
91. Janssen, A.; Breuer, G.A.; Brinkman, E.K.; van der Meulen, A.I.; Borden, S.V.; van Steensel, B.; Bindra, R.S.; LaRocque, J.R.; Karpen, G.H. A single double-strand break system reveals repair dynamics and mechanisms in heterochromatin and euchromatin. *Genes Dev.* **2016**, *30*, 1645–1657. [CrossRef] [PubMed]
92. Tsouroula, K.; Furst, A.; Rogier, M.; Heyer, V.; Maglott-Roth, A.; Ferrand, A.; Reina-San-Martin, B.; Soutoglou, E. Temporal and Spatial Uncoupling of DNA Double Strand Break Repair Pathways within Mammalian Heterochromatin. *Mol. Cell* **2016**, *63*, 293–305. [CrossRef] [PubMed]
93. Bordelet, H.; Costa, R.; Brocas, C.; Dépagne, J.; Veaute, X.; Busso, D.; Batté, A.; Guerois, R.; Marcand, S.; Dubrana, K. Sir3 heterochromatin protein promotes non-homologous end joining by direct inhibition of Sae2. *EMBO J.* **2022**, *41*, e108813. [CrossRef]
94. Clouaire, T.; Rocher, V.; Lashgari, A.; Arnould, C.; Aguirrebengoa, M.; Biernacka, A.; Skrzypczak, M.; Aymard, F.; Fongang, B.; Dojer, N.; et al. Comprehensive Mapping of Histone Modifications at DNA Double-Strand Breaks Deciphers Repair Pathway Chromatin Signatures. *Mol. Cell* **2018**, *72*, 250–262.e6. [CrossRef]
95. Clouaire, T.; Legube, G. DNA double strand break repair pathway choice: A chromatin based decision? *Nucleus* **2015**, *6*, 107–113. [CrossRef]
96. Pfister, S.X.; Ahrabi, S.; Zalmas, L.-P.; Sarkar, S.; Aymard, F.; Bachrati, C.Z.; Helleday, T.; Legube, G.; La Thangue, N.B.; Porter, A.C.G.; et al. SETD2-dependent histone H3K36 trimethylation is required for homologous recombination repair and genome stability. *Cell Rep.* **2014**, *7*, 2006–2018. [CrossRef]
97. Tang, J.; Cho, N.W.; Cui, G.; Manion, E.M.; Shanbhag, N.M.; Botuyan, M.V.; Mer, G.; Greenberg, R.A. Acetylation limits 53BP1 association with damaged chromatin to promote homologous recombination. *Nat. Struct. Mol. Biol.* **2013**, *20*, 317–325. [CrossRef]
98. Geuting, V.; Reul, C.; Loebrich, M. ATM Release at Resected Double-Strand Breaks Provides Heterochromatin Reconstitution to Facilitate Homologous Recombination. *PLoS Genet.* **2013**, *9*, e1003667. [CrossRef]

99. Kakarougkas, A.; Ismail, A.; Klement, K.; Goodarzi, A.A.; Conrad, S.; Freire, R.; Shibata, A.; Löbrich, M.; Jeggo, P.A. Opposing roles for 53BP1 during homologous recombination. *Nucleic Acids Res.* **2013**, *41*, 9719–9731. [CrossRef] [PubMed]
100. Beucher, A.; Birraux, J.; Tchouandong, L.; Barton, O.; Shibata, A.; Conrad, S.; Goodarzi, A.A.; Krempler, A.; Jeggo, P.A.; brich, M.L.O. ATM and Artemis promote homologous recombination of radiation-induced DNA double-strand breaks in G2. *EMBO J.* **2009**, *28*, 3413–3427. [CrossRef]
101. Lee, Y.-H.; Kuo, C.-Y.; Stark, J.M.; Shih, H.-M.; Ann, D.K. HP1 promotes tumor suppressor BRCA1 functions during the DNA damage response. *Nucleic Acids Res.* **2013**, *41*, 5784–5798. [CrossRef] [PubMed]
102. Ayrapetov, M.K.; Gursoy-Yuzugullu, O.; Xu, C.; Xu, Y.; Price, B.D. DNA double-strand breaks promote methylation of histone H3 on lysine 9 and transient formation of repressive chromatin. *Proc. Natl. Acad. Sci. USA* **2014**, *111*, 9169–9174. [CrossRef] [PubMed]
103. Amaral, N.; Ryu, T.; Li, X.; Chiolo, I. Nuclear Dynamics of Heterochromatin Repair. *Trends Genet.* **2017**, *33*, 86–100. [CrossRef] [PubMed]
104. Kallimasioti-Pazi, E.M.; Thelakkad Chathoth, K.; Taylor, G.C.; Meynert, A.; Ballinger, T.; Kelder, M.J.E.; Lalevee, S.; Sanli, I.; Feil, R.; Wood, A.J. Heterochromatin delays CRISPR-Cas9 mutagenesis but does not influence the outcome of mutagenic DNA repair. *PLoS Biol.* **2018**, *16*, e2005595. [CrossRef]
105. Janssen, A.; Colmenares, S.U.; Lee, T.; Karpen, G.H. Timely double-strand break repair and pathway choice in pericentromeric heterochromatin depend on the histone demethylase dKDM4A. *Genes Dev.* **2019**, *33*, 103–115. [CrossRef]
106. Schep, R.; Brinkman, E.K.; Leemans, C.; Vergara, X.; van der Weide, R.H.; Morris, B.; van Schaik, T.; Manzo, S.G.; Peric-Hupkes, D.; van den Berg, J.; et al. Impact of chromatin context on Cas9-induced DNA double-strand break repair pathway balance. *Mol. Cell* **2021**, *81*, 2216–2230.e10. [CrossRef] [PubMed]
107. Caron, P.; Aymard, F.; Iacovoni, J.S.; Briois, S.; Canitrot, Y.; Bugler, B.; Massip, L.; Losada, A.; Legube, G. Cohesin protects genes against γH2AX Induced by DNA double-strand breaks. *PLoS Genet.* **2012**, *8*, e1002460-17. [CrossRef]
108. Natale, F.; Rapp, A.; Yu, W.; Maiser, A.; Harz, H.; Scholl, A.; Grulich, S.; Anton, T.; Hörl, D.; Chen, W.; et al. Identification of the elementary structural units of the DNA damage response. *Nat. Commun.* **2017**, *8*, 15760. [CrossRef]
109. Ochs, F.; Karemore, G.; Miron, E.; Brown, J.; Sedlackova, H.; Rask, M.-B.; Lampe, M.; Buckle, V.; Schermelleh, L.; Lukas, J.; et al. Stabilization of chromatin topology safeguards genome integrity. *Nature* **2019**, *574*, 571–574. [CrossRef]
110. Arnould, C.; Legube, G. The Secret Life of Chromosome Loops upon DNA Double Strand Break. *J. Mol. Biol.* **2019**, *432*, 724–736. [CrossRef]
111. Caron, P.; Pobega, E.; Polo, S.E. DNA Double-Strand Break Repair: All Roads Lead to HeterochROMAtin Marks. *Front. Genet.* **2021**, *12*, 730696. [CrossRef] [PubMed]
112. Sanders, J.T.; Freeman, T.F.; Xu, Y.; Golloshi, R.; Stallard, M.A.; Hill, A.M.; San Martin, R.; Balajee, A.S.; McCord, R.P. Radiation-induced DNA damage and repair effects on 3D genome organization. *Nat. Commun.* **2020**, *11*, 6178. [CrossRef] [PubMed]
113. Arnould, C.; Rocher, V.; Bader, A.S.; Lesage, E.; Puget, N.; Clouaire, T.; Mourad, R.; Noordermeer, D.; Bushell, M.; Legube, G. ATM-dependent formation of a novel chromatin compartment regulates the Response to DNA Double Strand Breaks and the biogenesis of translocations. *bioRxiv* **2021**.
114. Dion, V.; Kalck, V.; Horigome, C.; Towbin, B.D.; Gasser, S.M. Increased mobility of double-strand breaks requires Mec1, Rad9 and the homologous recombination machinery. *Nat. Cell Biol.* **2012**, *14*, 502–509. [CrossRef] [PubMed]
115. Miné-Hattab, J.; Rothstein, R. Increased chromosome mobility facilitates homology search during recombination. *Nat. Cell Biol.* **2012**, *14*, 510–517. [CrossRef]
116. Krawczyk, P.M.; Borovski, T.; Stap, J.; Cijsouw, T.; ten Cate, R.; Medema, J.P.; Kanaar, R.; Franken, N.A.P.; Aten, J.A. Chromatin mobility is increased at sites of DNA double-strand breaks. *J. Cell. Sci.* **2012**, *125*, 2127–2133. [CrossRef]
117. Miné-Hattab, J.; Chiolo, I. Complex Chromatin Motions for DNA Repair. *Front. Genet.* **2020**, *11*, 800. [CrossRef] [PubMed]
118. Seeber, A.; Gasser, S.M. Chromatin organization and dynamics in double-strand break repair. *Curr. Opin. Genet. Dev.* **2017**, *43*, 9–16. [CrossRef]
119. Hauer, M.H.; Seeber, A.; Singh, V.; Thierry, R.; Sack, R.; Amitai, A.; Kryzhanovska, M.; Eglinger, J.; Holcman, D.; Owen-Hughes, T.; et al. Histone degradation in response to DNA damage enhances chromatin dynamics and recombination rates. *Nat. Struct. Mol. Biol.* **2017**, *24*, 99–107. [CrossRef]
120. Dimitrova, N.; Chen, Y.-C.M.; Spector, D.L.; de Lange, T. 53BP1 promotes non-homologous end joining of telomeres by increasing chromatin mobility. *Nature* **2008**, *456*, 524–528. [CrossRef]
121. Nagai, S.; Dubrana, K.; Tsai-Pflugfelder, M.; Davidson, M.B.; Roberts, T.M.; Brown, G.W.; Varela, E.; Hediger, F.; Gasser, S.M.; Krogan, N.J. Functional targeting of DNA damage to a nuclear pore-associated SUMO-dependent ubiquitin ligase. *Science* **2008**, *322*, 597–602. [CrossRef] [PubMed]
122. Khadaroo, B.; Teixeira, M.T.; Luciano, P.; Eckert-Boulet, N.; Germann, S.M.; Simon, M.-N.; Gallina, I.; Abdallah, P.; Gilson, E.; Géli, V.; et al. The DNA damage response at eroded telomeres and tethering to the nuclear pore complex. *Nat. Cell Biol.* **2009**, *11*, 980–987. [CrossRef]
123. Su, X.A.; Dion, V.; Gasser, S.M.; Freudenreich, C.H. Regulation of recombination at yeast nuclear pores controls repair and triplet repeat stability. *Genes Dev.* **2015**, *29*, 1006–1017. [CrossRef] [PubMed]
124. Kramarz, K.; Schirmeisen, K.; Boucherit, V.; Ait Saada, A.; Lovo, C.; Palancade, B.; Freudenreich, C.; Lambert, S.A.E. The nuclear pore primes recombination-dependent DNA synthesis at arrested forks by promoting SUMO removal. *Nat. Commun.* **2020**, *11*, 5643. [CrossRef] [PubMed]

125. Seeber, A.; Hauer, M.H.; Gasser, S.M. Chromosome Dynamics in Response to DNA Damage. *Annu. Rev. Genet.* **2018**, *52*, 295–319. [CrossRef]
126. Jakob, B.; Splinter, J.; Conrad, S.; Voss, K.-O.; Zink, D.; Durante, M.; Loebrich, M.; Taucher-Scholz, G. DNA double-strand breaks in heterochromatin elicit fast repair protein recruitment, histone H2AX phosphorylation and relocation to euchromatin. *Nucleic Acids Res.* **2011**, *39*, 6489–6499. [CrossRef]
127. Birkenbihl, R.P.; Subramani, S. Cloning and Characterization of Rad21 an Essential Gene of Schizosaccharomyces-Pombe Involved in Dna Double-Strand-Break Repair. *Nucleic Acids Res.* **1992**, *20*, 6605–6611. [CrossRef]
128. Ünal, E.; Arbel-Eden, A.; Sattler, U.; Shroff, R.; Lichten, M.; Haber, J.E.; Koshland, D. DNA damage response pathway uses histone modification to assemble a double-strand break-specific cohesin domain. *Mol. Cell* **2004**, *16*, 991–1002. [CrossRef]
129. Strom, L.; Lindroos, H.B.; Shirahige, K.; Sjogren, C. Postreplicative recruitment of cohesin to double-strand breaks is required for DNA repair. *Mol. Cell* **2004**, *16*, 1003–1015. [CrossRef]
130. Potts, P.R.; Porteus, M.H.; Yu, H. Human SMC5/6 complex promotes sister chromatid homologous recombination by recruiting the SMC1/3 cohesin complex to double-strand breaks. *EMBO J.* **2006**, *25*, 3377–3388. [CrossRef]
131. Arnould, C.; Rocher, V.; Finoux, A.-L.; Clouaire, T.; Li, K.; Zhou, F.; Caron, P.; Mangeot, P.E.; Ricci, E.P.; Mourad, R.; et al. Loop extrusion as a mechanism for formation of DNA damage repair foci. *Nature* **2021**, *590*, 660–665. [CrossRef] [PubMed]
132. McAleenan, A.; Cordon-Preciado, V.; Clemente-Blanco, A.; Liu, I.-C.; Sen, N.; Leonard, J.; Jarmuz, A.; Aragon, L. SUMOylation of the α-kleisin subunit of cohesin is required for DNA damage-induced cohesion. *Curr. Biol.* **2012**, *22*, 1564–1575. [CrossRef] [PubMed]
133. Andrews, E.A.; Palecek, J.; Sergeant, J.; Taylor, E.; Lehmann, A.R.; Watts, F.Z. Nse2, a component of the Smc5-6 complex, is a SUMO ligase required for the response to DNA damage. *Mol. Cell. Biol.* **2005**, *25*, 185–196. [CrossRef] [PubMed]
134. Fousteri, M.I.; Lehmann, A.R. A novel SMC protein complex in Schizosaccharomyces pombe contains the Rad18 DNA repair protein. *EMBO J.* **2000**, *19*, 1691–1702. [CrossRef]
135. Venegas, A.B.; Natsume, T.; Kanemaki, M.; Hickson, I.D. Inducible Degradation of the Human SMC5/6 Complex Reveals an Essential Role Only during Interphase. *Cell Rep.* **2020**, *31*, 107533. [CrossRef]
136. Alt, A.; Dang, H.Q.; Wells, O.S.; Polo, L.M.; Smith, M.A.; McGregor, G.A.; Welte, T.; Lehmann, A.R.; Pearl, L.H.; Murray, J.M.; et al. Specialized interfaces of Smc5/6 control hinge stability and DNA association. *Nat. Commun.* **2017**, *8*, 14011–14014. [CrossRef] [PubMed]
137. De Piccoli, G.; Cortés-Ledesma, F.; Ira, G.; Torres-Rosell, J.; Uhle, S.; Farmer, S.; Hwang, J.-Y.; Machín, F.; Ceschia, A.; McAleenan, A.; et al. Smc5-Smc6 mediate DNA double-strand-break repair by promoting sister-chromatid recombination. *Nat. Cell Biol.* **2006**, *8*, 1032–1034. [CrossRef]
138. Betts Lindroos, H.; Ström, L.; Itoh, T.; Katou, Y.; Shirahige, K.; Sjögren, C. Chromosomal association of the Smc5/6 complex reveals that it functions in differently regulated pathways. *Mol. Cell* **2006**, *22*, 755–767. [CrossRef]
139. Leung, G.P.; Brown, J.A.R.; Glover, J.N.M.; Kobor, M.S. Rtt107 BRCT domains act as a targeting module in the DNA damage response. *DNA Repair Amst.* **2016**, *37*, 22–32. [CrossRef]
140. Horigome, C.; Bustard, D.E.; Marcomini, I.; Delgoshaie, N.; Tsai-Pflugfelder, M.; Cobb, J.A.; Gasser, S.M. PolySUMOylation by Siz2 and Mms21 triggers relocation of DNA breaks to nuclear pores through the Slx5/Slx8 STUbL. *Genes Dev.* **2016**, *30*, 931–945. [CrossRef]
141. Schär, P.; Fäsi, M.; Jessberger, R. SMC1 coordinates DNA double-strand break repair pathways. *Nucleic Acids Res.* **2004**, *32*, 3921–3929. [CrossRef] [PubMed]
142. Gelot, C.; Guirouilh-Barbat, J.; Lopez, B.S. The cohesin complex prevents the end-joining of distant DNA double-strand ends in S phase: Consequences on genome stability maintenance. *Nucleus* **2016**, *7*, 339–345. [CrossRef]
143. Shroff, R.; Arbel-Eden, A.; Pilch, D.; Ira, G.; Bonner, W.M.; Petrini, J.H.; Haber, J.E.; Lichten, M. Distribution and Dynamics of Chromatin Modification Induced by a Defined DNA Double-Strand Break. *Curr. Biol.* **2004**, *14*, 1703–1711. [CrossRef] [PubMed]
144. Lee, C.-S.; Lee, K.; Legube, G.; Haber, J.E. Dynamics of yeast histone H2A and H2B phosphorylation in response to a double-strand break. *Nat. Struct. Mol. Biol.* **2014**, *21*, 103–109. [CrossRef]
145. Berkovich, E.; Monnat, R.J.; Kastan, M.B. Roles of ATM and NBS1 in chromatin structure modulation and DNA double-strand break repair. *Nat. Cell Biol.* **2007**, *9*, 683–690. [CrossRef]
146. Iacovoni, J.S.; Caron, P.; Lassadi, I.; Nicolas, E.; Massip, L.; Trouche, D.; Legube, G. High-resolution profiling of gammaH2AX around DNA double strand breaks in the mammalian genome. *EMBO J.* **2010**, *29*, 1446–1457. [CrossRef]
147. Collins, P.L.; Purman, C.; Porter, S.I.; Nganga, V.; Saini, A.; Hayer, K.E.; Gurewitz, G.L.; Sleckman, B.P.; Bednarski, J.J.; Bassing, C.H.; et al. DNA double-strand breaks induce H2Ax phosphorylation domains in a contact-dependent manner. *Nat. Commun.* **2020**, *11*, 3158–3159. [CrossRef]
148. Piazza, A.; Bordelet, H.; Dumont, A.; Thierry, A.; Savocco, J.; Girard, F.; Koszul, R. Cohesin regulates homology search during recombinational DNA repair. *Nat. Cell Biol.* **2021**, *23*, 1176–1186. [CrossRef] [PubMed]
149. Peters, J.M. How DNA loop extrusion mediated by cohesin enables V(D)J recombination. *Curr. Opin. Cell Biol.* **2021**, *70*, 75–83. [CrossRef] [PubMed]
150. Ba, Z.; Lou, J.; Ye, A.Y.; Dai, H.Q.; Dring, E.W.; Lin, S.G.; Jain, S.; Kyritsis, N.; Kieffer-Kwon, K.-R.; Casellas, R.; et al. CTCF orchestrates long-range cohesin-driven V(D)J recombinational scanning. *Nature* **2020**, *586*, 305–310. [CrossRef]

151. Dai, H.Q.; Hu, H.; Lou, J.; Ye, A.Y.; Ba, Z.; Zhang, X.; Zhang, Y.; Zhao, L.; Yoon, H.S.; Chapdelaine-Williams, A.M.; et al. Loop extrusion mediates physiological Igh locus contraction for RAG scanning. *Nature* **2021**, *590*, 338–343. [CrossRef] [PubMed]
152. Hill, L.; Ebert, A.; Jaritz, M.; Wutz, G.; Nagasaka, K.; Tagoh, H.; Kostanova-Poliakova, D.; Schindler, K.; Sun, Q.; Bönelt, P.; et al. Wapl repression by Pax5 promotes V gene recombination by Igh loop extrusion. *Nature* **2020**, *584*, 142–147. [CrossRef] [PubMed]
153. Ström, L.; Karlsson, C.; Lindroos, H.B.; Wedahl, S.; Katou, Y.; Shirahige, K.; Sjögren, C. Postreplicative formation of cohesion is required for repair and induced by a single DNA break. *Science* **2007**, *317*, 242–245. [CrossRef]
154. Ünal, E.; Heidinger-Pauli, J.M.; Koshland, D. DNA double-strand breaks trigger genome-wide sister-chromatid cohesion through Eco1 (Ctf7). *Science* **2007**, *317*, 245–248. [CrossRef]
155. Almedawar, S.; Colomina, N.; Bermúdez-López, M.; Pociño-Merino, I.; Torres-Rosell, J. A SUMO-dependent step during establishment of sister chromatid cohesion. *Curr. Biol.* **2012**, *22*, 1576–1581. [CrossRef] [PubMed]
156. Heidinger-Pauli, J.M.; Ünal, E.; Guacci, V.; Koshland, D. The Kleisin Subunit of Cohesin Dictates Damage-Induced Cohesion. *Mol. Cell* **2008**, *31*, 47–56. [CrossRef]
157. Bekker-Jensen, S.; Lukas, C.; Kitagawa, R.; Melander, F.; Kastan, M.B.; Bartek, J.; Lukas, J. Spatial organization of the mammalian genome surveillance machinery in response to DNA strand breaks. *J. Cell Biol.* **2006**, *173*, 195–206. [CrossRef]
158. Watrin, E.; Peters, J.M. The cohesin complex is required for the DNA damage-induced G2/M checkpoint in mammalian cells. *EMBO J.* **2009**, *28*, 2625–2635. [CrossRef]
159. Solomon, D.A.; Kim, J.-S.; Waldman, T. Cohesin gene mutations in tumorigenesis: From discovery to clinical significance. *BMB Rep.* **2014**, *47*, 299–310. [CrossRef]

PLOS GENETICS

RESEARCH ARTICLE

Rad51 filaments assembled in the absence of the complex formed by the Rad51 paralogs Rad55 and Rad57 are outcompeted by translesion DNA polymerases on UV-induced ssDNA gaps

Laurent Maloisel*, Emilie Ma, Jamie Phipps, Alice Deshayes, Stefano Mattarocci, Stéphane Marcand, Karine Dubrana, Eric Coïc*

Université de Paris and Université Paris-Saclay, INSERM, CEA, Institut de Biologie François Jacob, UMR Stabilité Génétique Cellules Souches et Radiations, Fontenay-aux-Roses, France

* laurent.maloisel@cea.fr (LM); eric.coic@cea.fr (EC)

OPEN ACCESS

Citation: Maloisel L, Ma E, Phipps J, Deshayes A, Mattarocci S, Marcand S, et al. (2023) Rad51 filaments assembled in the absence of the complex formed by the Rad51 paralogs Rad55 and Rad57 are outcompeted by translesion DNA polymerases on UV-induced ssDNA gaps. PLoS Genet 19(2): e1010639. https://doi.org/10.1371/journal.pgen.1010639

Editor: Lorraine S. Symington, Columbia University, UNITED STATES

Received: March 17, 2022

Accepted: January 26, 2023

Published: February 7, 2023

Peer Review History: PLOS recognizes the benefits of transparency in the peer review process; therefore, we enable the publication of all of the content of peer review and author responses alongside final, published articles. The editorial history of this article is available here: https://doi.org/10.1371/journal.pgen.1010639

Abstract

The bypass of DNA lesions that block replicative polymerases during DNA replication relies on DNA damage tolerance pathways. The error-prone translesion synthesis (TLS) pathway depends on specialized DNA polymerases that incorporate nucleotides in front of base lesions, potentially inducing mutagenesis. Two error-free pathways can bypass the lesions: the template switching pathway, which uses the sister chromatid as a template, and the homologous recombination pathway (HR), which also can use the homologous chromosome as template. The balance between error-prone and error-free pathways controls the mutagenesis level. Therefore, it is crucial to precisely characterize factors that influence the pathway choice to better understand genetic stability at replication forks. In yeast, the complex formed by the Rad51 paralogs Rad55 and Rad57 promotes HR and template-switching at stalled replication forks. At DNA double-strand breaks (DSBs), this complex promotes Rad51 filament formation and stability, notably by counteracting the Srs2 anti-recombinase. To explore the role of the Rad55-Rad57 complex in error-free pathways, we monitored the genetic interactions between Rad55-Rad57, the translesion polymerases Polζ or Polη, and Srs2 following UV radiation that induces mostly single-strand DNA gaps. We found that the Rad55-Rad57 complex was involved in three ways. First, it protects Rad51 filaments from Srs2, as it does at DSBs. Second, it promotes Rad51 filament stability independently of Srs2. Finally, we observed that UV-induced HR is almost abolished in Rad55-Rad57 deficient cells, and is partially restored upon Polζ or Polη depletion. Hence, we propose that the Rad55-Rad57 complex is essential to promote Rad51 filament stability on single-strand DNA gaps, notably to counteract the error-prone TLS polymerases and mutagenesis.

Data Availability Statement: All relevant data are within the paper and its Supporting Information files.

Funding: This research was funded by Electricité de France (EDF), Commissariat à l'Energie Atomique et aux Energies Alternatives (CEA) Radiobiology call, Tandem Call CEA-PIC3i Institut Curie in Radiobiologie (to EC). The funders had no role in study design, data collection and analysis, decision to publish, or preparation of the manuscript.

Competing interests: The authors have declared that no competing interests exist.

Author summary

Processive and accurate DNA polymerases replicate genomic DNA during the S phase of each cell cycle. DNA base lesions on template DNA block these polymerases and result in an accumulation of single-stranded DNA gaps behind moving replication forks. These gaps are filled-in by error-prone and error-free pathways. In this work, we show that the complex made by the Rad51 paralogs Rad55 and Rad57 is essential for the error-free homologous recombination gap-filling pathway when DNA replication is stalled by UV-induced DNA lesions, but not for DNA double strand break repair. Interestingly, we found that homologous recombination is efficiently outcompeted by error-prone translesion DNA polymerases in Rad55-Rad57-deficient cells. We propose that the Rad55-Rad57 complex is essential for Rad51 filament stability at UV-induced DNA gaps to promote efficient error-free homologous recombination. Furthermore, our study in yeast predicts that inhibitors of error-prone DNA polymerases might selectively target cancer cells in which RAD51 paralogs are mutated.

Introduction

In all living organisms, genomic DNA undergoes chemical modifications or crosslinking with proteins. These damages greatly compromise DNA replication because they induce replication fork stalling. DNA damage tolerance mechanisms have evolved to ensure completion of genome replication [1], and rely on two main mechanisms: i) translesion synthesis (TLS) DNA polymerases and ii) the use of a homologous template, typically the newly synthesized sister chromatid. Specialized TLS polymerases efficiently insert nucleotides opposite and beyond lesions on DNA templates that block the replicative DNA polymerases [2]. They possibly extend blocked primer/template junctions at replication forks or at single-stranded DNA (ssDNA) gaps left behind the forks [3,4]. TLS polymerases are intrinsically error-prone and constitute a major source of DNA damage-induced mutagenesis [5,6]. Recombination-mediated pathways, such as the template switching and homologous recombination (HR) pathways, mediate damage bypass through the annealing of the damaged ssDNA gaps to the intact homologous template on the sister chromatid [7–9]. HR, also referred to as the salvage pathway, can use homologous chromosomes as intact donors rather than sister chromatids [10]. As TLS, template switching and HR compete for the same ssDNA substrates, they can partly compensate for each other [11–13]. However, template switching and HR are error-free lesion bypass mechanisms and counterbalance mutagenesis induced by TLS [14,15]. Thus, it is crucial to precisely characterize the factors that influence pathway choice to better understand genetic stability at replication forks.

The template switching pathway involves ubiquitin ligase and the Rad18/Rad6 pathway conjugating activities. In budding yeast, Rad6 and Rad18 induce PCNA mono-ubiquitination at its conserved K164 residue, whereas Rad5 and Mms2-Ubc13-dependent activities trigger its poly-ubiquitination at K164 [16,17] and the formation of X-shaped intermediates between sister chromatids when replication is challenged by DNA damages [8]. Interestingly, the formation of these X-shaped intermediates relies also on the HR factors Rad51 and Rad52 [7,18].

The HR pathway relies on the recombinase Rad51 that oligomerizes on ssDNA to form a right-handed helical nucleoprotein filament [19,20]. This filament performs homology search and catalyzes DNA joint formation between ssDNA and double-stranded DNA (dsDNA) homologous partners, thereby leading to strand exchange [21–23]. Eventually, repair DNA synthesis occurs from the damaged DNA invading ends on undamaged template homologous

DNA sequences [24]. Rad51 loading on RPA-coated ssDNA is a crucial step in HR and is mediated mainly by Rad52 in *Saccharomyces cerevisiae* and BRCA2 in metazoans [25–27]. Rad51 filament assembly also requires the activity of Rad51 paralogs (Rad55-Rad57 complex in *S. cerevisiae*; RAD51B, RAD51C, RAD51D, XRCC2, and XRCC3 in human cells; and the SHU complex in both [28]). Rad55 and Rad57 share 20% identity with the RecA/Rad51 ATPase core region [29,30]. However, they do not form filaments on ssDNA, and they do not exhibit strand exchange activity [31,32]. Electron microscopy images showed the association of gold-labeled Rad55 with Rad51 filaments assembled on ssDNA (Rad51-ssDNA) [32], and two-hybrid experiments revealed the interaction between Rad51 and Rad55 [33,34]. However, recent single-molecule studies suggest that the interaction between the Rad55-Rad57 complex and Rad51 filaments is transient and the Rad55-Rad57 complex dissociates during filament extension [35]. As similar findings were obtained in nematodes [36], it has been proposed that RAD51 paralogs behave as classical chaperones to temporarily assist Rad51 filament formation. More studies are required to clearly describe the precise role of each complex of Rad51 paralogs. In addition, each complex might play a specific role depending on the initial HR-inducing DNA lesion [37].

Rad55-Rad57 role in DNA double strand break (DSB) repair is considered accessory on the basis of the weaker sensitivity of *rad55* and *rad57* mutants to ionizing radiation and to site-directed DSBs compared with *rad51* mutants [38,39]. Interestingly, this sensitivity seems to depend on the Srs2 helicase activity because it is partially suppressed by *SRS2* ablation [32,39]. *In vitro* experiments have shown that the Srs2 translocase activity disrupts Rad51 filaments [40,41] and that the Rad55-Rad57 complex counteracts Srs2 to maintain Rad51 filaments on ssDNA [32,35]. Therefore, it has been proposed that Rad51 filament assembly and disassembly, which are mediated by the Rad55-Rad57 complex and Srs2 respectively, provide a regulatory mechanism to control HR initiation. However, *SRS2* deletion does not rescue spontaneous HR defects between direct repeats in the *rad55* and *rad57* mutants, indicating that the Rad55-Rad57 complex also acts independently of Srs2 [39].

To explain the different defects observed between spontaneous and DSB-induced HR, it was hypothesized that spontaneous HR between direct repeats is initiated by ssDNA gaps rather than DSBs [39]. Thus, the Rad55-Rad57 complex would play a more prominent role in HR when the initiating lesion is a ssDNA gap. In agreement, it has been observed that in cells lacking the TLS polymerases Pol ζ, *RAD55* ablation leads to a synergistic increase in DNA damage sensitivity [42–44].

Here, we explored Rad55-Rad57 role in Rad51 filament formation on ssDNA gaps and in the balance between HR and TLS in *S. cerevisiae*. For that purpose, we induced interhomolog HR in diploid strains by ionizing radiation (IR) or UV radiation. IR generates DSBs and ssDNA gaps [45], whereas UV generates mostly ssDNA gaps. UV-irradiated *S. cerevisiae* cells uncouple leading and lagging strand replication at irreparable UV lesions, thus generating long ssDNA regions on one side of the fork. Furthermore, small ssDNA gaps accumulate along replicated duplexes, likely resulting from repriming events downstream of the lesions on both leading and lagging strands. Translesion synthesis and homologous recombination counteract gap accumulation, without affecting fork progression [11]. Recently, RPA foci were used as a read-out of ssDNA gaps forming upon DNA replication through Methyl-methane sulfonate (MMS)- and UV-induced DNA damage [13]. They predominantly form far away from sites of ongoing replication, and they do not overlap with any of the repair centers associated with collapsed replication forks or DNA double-strand breaks. Instead, they represent sites of post-replicative DNA damage bypass involving translesion synthesis and homologous recombination. Therefore, we also used this mark to evaluate the cross-talk between TLS and HR.

We found that the Rad55-Rad57 complex is essential for UV-induced HR, but only accessory for IR-induced HR. Interestingly, this essential role is mainly Srs2-independent, and UV-induced HR in Rad55-Rad57-deficient cells can be restored by inactivation of a TLS polymerase (Polζ or Polη). Conversely, UV-induced HR cannot be restored upon inactivation of the template switch pathway in *MMS2* deficient cells. Overall, our results show that the Rad55-Rad57 complex is essential for Rad51 filament assembly on UV-induced ssDNA gaps. When this complex is absent, Rad51 filaments cannot prevent the recruitment of TLS polymerases and counterbalance mutagenesis.

Results

The Rad55-Rad57 heterodimer is essential for UV-induced homologous recombination

To investigate Rad55-Rad57 role in HR, we analyzed UV- and IR-induced interhomolog HR in wild type (WT) and *rad55*Δ isogenic diploid strains. The previous observation that *rad51* and *rad52* mutant cells are very sensitive to IR indicates that IR generates DSBs, whereas these mutants are much more resistant to UV radiation, indicating that DSBs are probably rarely induced [46,47]. Additionally, genetic evidence suggests that UV-induced HR is triggered by ssDNA gaps [48]. We measured interhomolog HR using two mutant alleles of *ARG4*: *arg4-RV*, a 2-bp deletion that ablates the *Eco*RV site at position +258, and *arg4-Bg*, a 4-bp insertion by fill-in of a *Bgl*II site at position +1,274 [49] (**Fig 1A**). These alleles do not revert [49] and only recombination in heteroallelic *arg4-RV/arg4-Bg* diploid cells results in the formation of a WT *ARG4* gene primarily by non-reciprocal transfer covering one mutation [50].

The *rad55*Δ diploid strain was not sensitive to UV radiation (**Fig 1B**), but remarkably, UV-induced recombinant [Arg^+] frequency was strongly reduced in the *rad55*Δ diploid strain compared with WT cells (10-fold at 120 J/m^2) (**Fig 1C**). These results are very similar to those previously obtained with *rad51*Δ mutants [46], suggesting that the Rad55-Rad57 complex is determinant in UV-induced HR. Conversely, *rad55*Δ diploid cells were sensitive to IR (**Fig 1D**), but γ-ray-induced HR frequencies were identical in *rad55*Δ and WT cells at high doses (400 Gy and 600 Gy) (**Fig 1E**). We observed the same phenotypes in the *rad57*Δ mutant (**S1A–S1D Fig**). Likewise, it was previously reported that spontaneous HR rates are identical in *rad57*Δ and WT cells [38,51], a result we confirmed here in *rad55*Δ cells (**Fig 1F**). These observations suggest that the Rad55-Rad57 complex plays a specific and essential role in UV-induced HR, probably at ssDNA gaps. This complex is also involved in the repair of IR-induced DSBs, as shown by the lower survival of *rad55*Δ mutant. However, it is not essential since the IR-induced HR frequencies are comparable to WT.

Resolution of UV-induced RPA foci is delayed in the *rad55*Δ mutant

To further examine the role of Rad55 in the management of ssDNA gaps induced by UV exposure, we monitored ssDNA by fluorescence microscopy using YFP-tagged Rfa1, the large subunit of the RPA complex [52]. It was indeed recently established that RPA foci formed upon UV-irradiation represent sites of post-replicative DNA damage bypass involving TLS and HR [13]. Exponentially growing cells were α-factor arrested in G1 and subjected or not to UV irradiation. In absence of irradiation, RPA foci were barely detectable in WT G1-arrested cells (**S1E Fig**). After UV-exposure, only a few G1-arrested WT cells displayed RPA foci (3.2% and 12.5% after 60 min and 240 min post-irradiation, respectively; **S1E Fig**). Unirradiated WT cells released into the cell cycle also exhibit few RPA foci (10% of the cells 60 min after release; **Fig 1H**). In marked contrast, 58% of WT irradiated cells displayed at least one RPA foci 60

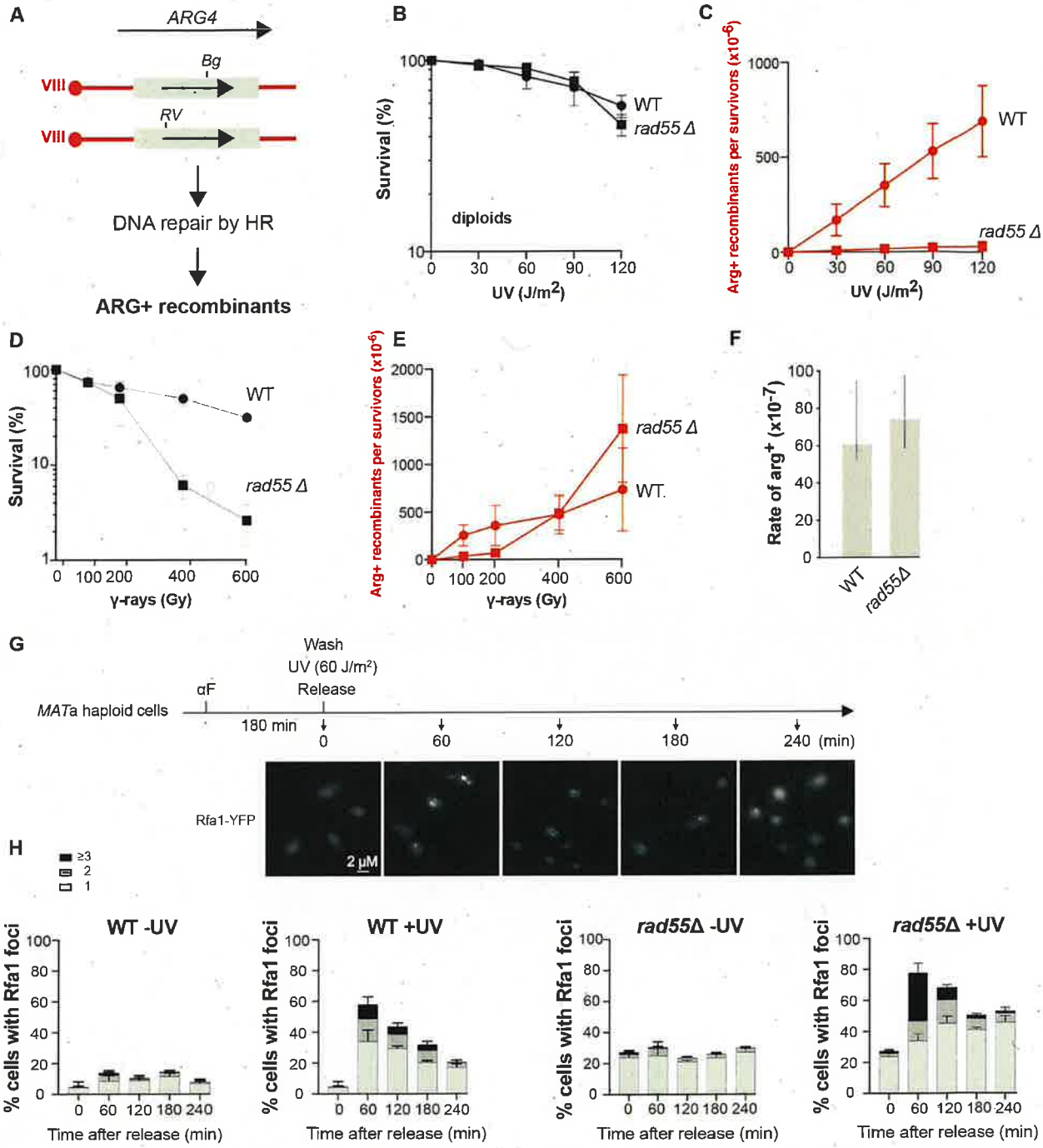

Fig 1. Rad55 plays a major role in UV-induced HR. (A) Schematic representation of the genetic system used. Frameshift mutations were introduced at the *Eco*RV site (RV, ±2 bp) or the *Bgl*II site (Bg, +4 bp). HR between the two *ARG4* mutant alleles can restore a WT *ARG4* allele associated with the [Arg+] phenotype. (B) Survival and (C) [Arg+] recombinant frequencies after UV exposure of WT and *rad55*Δ diploid cells. (D) Survival and (E) [Arg+] recombinant frequencies after γ irradiation of WT and *rad55*Δ diploid cells. (F) Spontaneous mitotic [Arg+] recombinant rates ([Arg+] x 10^{-7} /cell/generation) of WT and *rad55*Δ diploid strains. (G) Experimental scheme for microscopy analysis of RPA foci: Cells arrested in G1 phase with alpha-factor (αF) were exposed to UV before release into the cell cycle. Samples were collected for analysis every hour for four hours. Representative images of Rfa1-YFP cells are presented. Scale bars are 2 µm. (H) Quantification of Rfa1-YFP foci detected by fluorescence microscopy in WT and *rad55*Δ cells exposed or not to UV. Error bars indicate SDs from three independent experiments.

https://doi.org/10.1371/journal.pgen.1010639.g001

min after release in the cell cycle (Fig 1H). This confirms that UV-induced DNA damages induced in G1 leads to the formation of ssDNA gaps related to the encounter with DNA replication. Most of UV-induced RPA foci (70%) have been resolved 240 min after release (**Figs 1G and S1F**). This illustrates the efficient post-replicative DNA damage bypass in WT cells.

Surprisingly, a steady level of 20% of *rad55Δ* G1-arrested cells exhibits RPA foci (S1E Fig). This rate slowly increases after UV-exposure to reach 60% of G1-arrested cells at 240 min (S1E Fig). This newly described phenotype of *rad55Δ* cells is probably representative of an involvement of Rad55-Rad57 in the stabilization of repair intermediates of spontaneous and UV-induced DNA lesions in G1-arrested cells. 60 min after UV-exposure and release in the cell cycle, 80% of *rad55Δ* cells exhibit RPA foci (Fig 1H). Moreover, 31% of *rad55Δ* cells display three or more UV-induced RPA foci while this class is observed only in 10% of WT cells. In addition, contrary to WT, only 33% of RPA foci have been resolved 240 min post-irradiation. Finally, we observed an accumulation of *rad55Δ* cells in the second S phase 240 min after release from G1 arrest, probably related to the persistence of UV-induced gaps in absence of efficient HR (S1F Fig). Altogether, these results confirm that Rad55-Rad57 is important to manage ssDNA gaps forming upon UV-exposure.

In order to confirm that the different behavior of Rad55-Rad57 after UV- and IR-exposure is related to the difference in the lesions induced, we also observed RPA foci formation in WT and *rad55Δ* cells exposed to IR. To allow haploid cells to repair γ-induced DSBs by HR between sister chromatids, cells were irradiated 60 min after their release from the G1 arrest (S2A Fig). In WT and *rad55Δ* cells, we found the same proportion of cells displaying RPA foci after γ-rays exposure compared with UV, these foci being resolved with the same kinetics (S2B Fig). However, as already described in [13], 60 min after irradiation, 75% of the γ-irradiated cells with RPA foci display only one focus (S2B Fig), while this class represents 59% of UV-irradiated cells with RPA foci (Fig 1G). This difference could be attributed to the formation of a DSB repair center after γ-rays exposure while ssDNA gaps are not gathered after UV-irradiation. This difference is even more pronounced in the *rad55Δ* mutant. Indeed, 76% of γ-irradiated cells with RPA foci show only one focus while this class with a single focus represents 44% of UV-irradiated cells with RPA foci. These differences support our conclusion that Rad51 filament are assembled mainly on ssDNA gaps after UV exposure, while some events might be gathered in repair centers after γ-rays irradiation.

UV-induced DNA lesions are channeled towards the *REV3* error-prone DNA repair pathway in the *rad55Δ* mutant

Although UV-induced HR was almost abolished in *rad55Δ* cells, these cells were resistant to UV radiation. We hypothesized that in *rad55Δ* mutant cells, UV-induced ssDNA gaps at replication forks could be repaired by TLS instead of HR. The TLS polymerase Polζ is required to bypass UV-induced DNA lesions, as illustrated by the strong UV-sensitivity of haploid cells lacking the Rev3 catalytic subunit of Polζ (Fig 2A) [53]. Conversely, *rev3Δ* diploid cells were much more resistant to UV radiation (Fig 2B), possibly due to HR promoted by *MAT* heterozygosity [51,54–56]. In addition, Polζ, is responsible for almost all UV-induced mutagenesis in yeast cells [53,57], as shown by the absence of UV-induced mutagenesis observed in the Polζ essential component *rev3* mutant [53]. Therefore, *rad55Δ* cells should strongly rely on Polζ and on its catalytic subunit Rev3 for UV resistance, and that UV-induced mutagenesis should increase in *rad55Δ* cells, as previously shown for spontaneous mutagenesis [42]. In agreement with previous studies, we confirmed that UV sensitivity is much higher in the *rev3Δ rad55Δ* double mutant than in the *rev3Δ* single mutant in haploid cells [42–44] (Fig 2A) and also in diploid cells (Fig 2B). This UV sensitivity is comparable with those we previously observed in

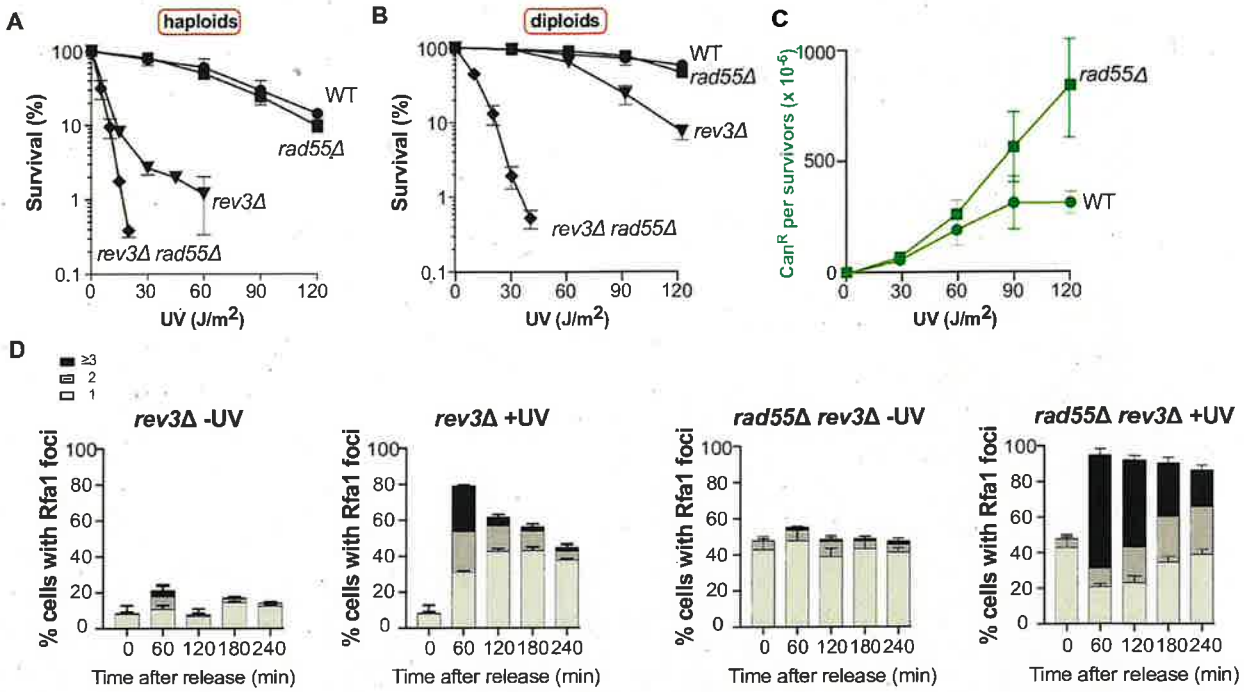

Fig 2. Channeling UV-induced DNA lesions into the *REV3*-dependent pathway in *rad55Δ* cells. (A) Survival of haploid cells following UV radiation. (B) Survival of diploid cells following UV radiation. (C) UV-induced mutagenesis in WT and *rad55Δ* cells determined by quantifying the Can^R mutant frequency for the indicated UV doses. (D) Quantification of Rfa1-YFP foci detected by fluorescence microscopy in *rev3Δ* and *rad55Δ rev3Δ* cells not irradiated or after UV exposure. Error bars indicate SDs from three independent experiments.

https://doi.org/10.1371/journal.pgen.1010639.g002

the *rev3Δ rad51Δ* double mutant [58], confirming the essential role of Rad55-Rad57 in UV-induced HR. Therefore, the high resistance to UV of Rad55-deficient cells relies on the TLS pathway that could compensate for HR deficiency in these cells. Consequently, we expected an increase of mutagenesis frequency in *rad55Δ* cells. In agreement with this hypothesis, the frequency of UV-induced canavanine-resistant cells [59] was two-fold higher in the *rad55Δ* mutant than in WT cells (Fig 2C). This observation supports the channeling of DNA lesions towards the error-prone Polζ-dependent pathway in *rad55Δ* cells.

Measurement of RPA foci in UV-irradiated cells confirmed that TLS can compensate for HR. While the number of RPA foci was about the same in the *rev3Δ* mutant and in the *rad55Δ* mutant (**Figs** 1G and 2D), the *rev3Δ rad55Δ* double mutant shows RPA foci in almost all cells with 64% of this population displaying at least three foci (Fig 2D). We also observed that *rev3Δ* mutants display an accumulation of cells in the second S phase 240 min after release from G1 arrest, while *rev3Δ rad55Δ* double mutant shows a block in the first G2 phase after the release (S3 Fig). The number of cells displaying RPA foci barely decreased with time in *rev3Δ rad55Δ* double mutant. However, the number of cells displaying at least three foci decreases strongly, which could represent repair events but also the disappearance of ssDNA gaps through degradation or breakage in the absence of repair. Considering the low survival of UV-irradiated *rev3Δ rad55Δ* cells, this more likely indicates that many ssDNA gaps formed during the first S phase after release cannot be repaired in absence of TLS and HR, leading to faulty mitosis. We also observed that the number of spontaneous RPA foci is 2-fold higher in the *rad55Δ rev3Δ* mutant compared with the *rad55Δ* mutant, indicating a large accumulation of ssDNA gaps

related to DNA replication independently of UV-exposure in this double-mutant (compare Figs 1G and 2D).

UV-induced DNA lesions are channeled to the HR pathway in cells lacking TLS polymerases

The finding that UV-induced DNA lesions can be channeled to the TLS pathway in *rad55Δ* cells suggested that such lesions could be managed by the HR pathway in TLS-deficient cells. In that case, TLS-deficient cells should display a hyper-recombinogenic phenotype. To test this hypothesis, we measured the frequencies of UV-induced HR in *rev3Δ* (Polζ mutant) and *rad30Δ* (Polη mutant) cells. As expected, HR frequency was strongly increased in *rev3Δ* cells and to a lower extent in the *rad30Δ* mutant (**Fig 3A and 3B**). However, UV sensitivity was similar in diploid cells harboring the *rev3Δ* or *rad30Δ* mutation (**Figs 2B and 3C**). We propose that in the *rad30Δ* mutant, UV-induced DNA lesions can be bypassed by both HR and Polζ, while Polη cannot always take over Polζ function in *rev3Δ* cells, resulting in higher HR frequency. Additionally, it is important to note that accordingly with the strong sensitivity of *rev3Δ* cells exposed to UV, HR cannot compensate for all UV-induced DNA lesions that are supported by the TLS pathway.

Translesion DNA polymerases prevent UV-induced HR in the *rad55Δ* mutant

We showed that UV-induced HR is strongly decreased in Rad55-Rad57 deficient cells. We also observed that the TLS and HR pathways compete for the same UV-induced ssDNA gaps, because mutagenesis was increased in *rad55Δ* mutants, and HR in *rev3Δ* mutants. Therefore, the recruitment of TLS polymerases at the lesion site might decrease HR in *rad55Δ* cells. We measured HR frequencies and observed a significantly increased frequency in the *rev3Δ rad55Δ* double mutant compared with *rad55Δ* cells (**Fig 4A**). This indicated that Polζ effectively impairs HR in the absence of the Rad55-Rad57 complex. We propose that the Rad55-Rad57 complex is important to stabilize Rad51 filaments on ssDNA gaps at the DNA lesion site, thus limiting the recruitment of TLS polymerases. Our results also suggest that in the absence of the Rad55-Rad57 complex, Rad51 filaments are functional enough to promote some HR events (**Fig 4A**), although this is not sufficient to improve UV resistance (**Fig 2**). We observed the same results when a Polη mutation (*rad30Δ*) was combined with *rad55Δ*

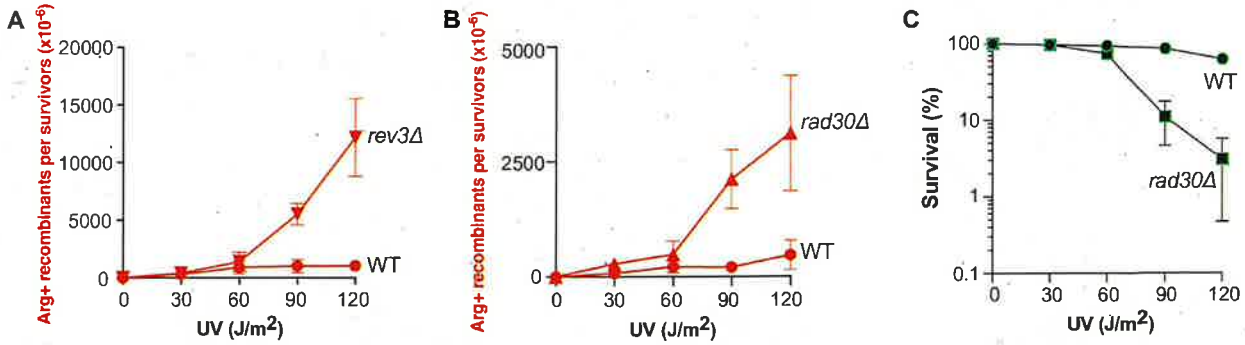

Fig 3. Channeling UV-induced DNA lesions into the HR pathway in TLS-deficient cells. (A) UV-induced [Arg+] recombinant frequencies in WT and *rev3Δ* diploid cells. (B) UV-induced [Arg+] recombinant frequencies in WT and *rad30Δ* diploid cells. (C) Survival of diploid *rad30Δ* cells after UV radiation.

https://doi.org/10.1371/journal.pgen.1010639.g003

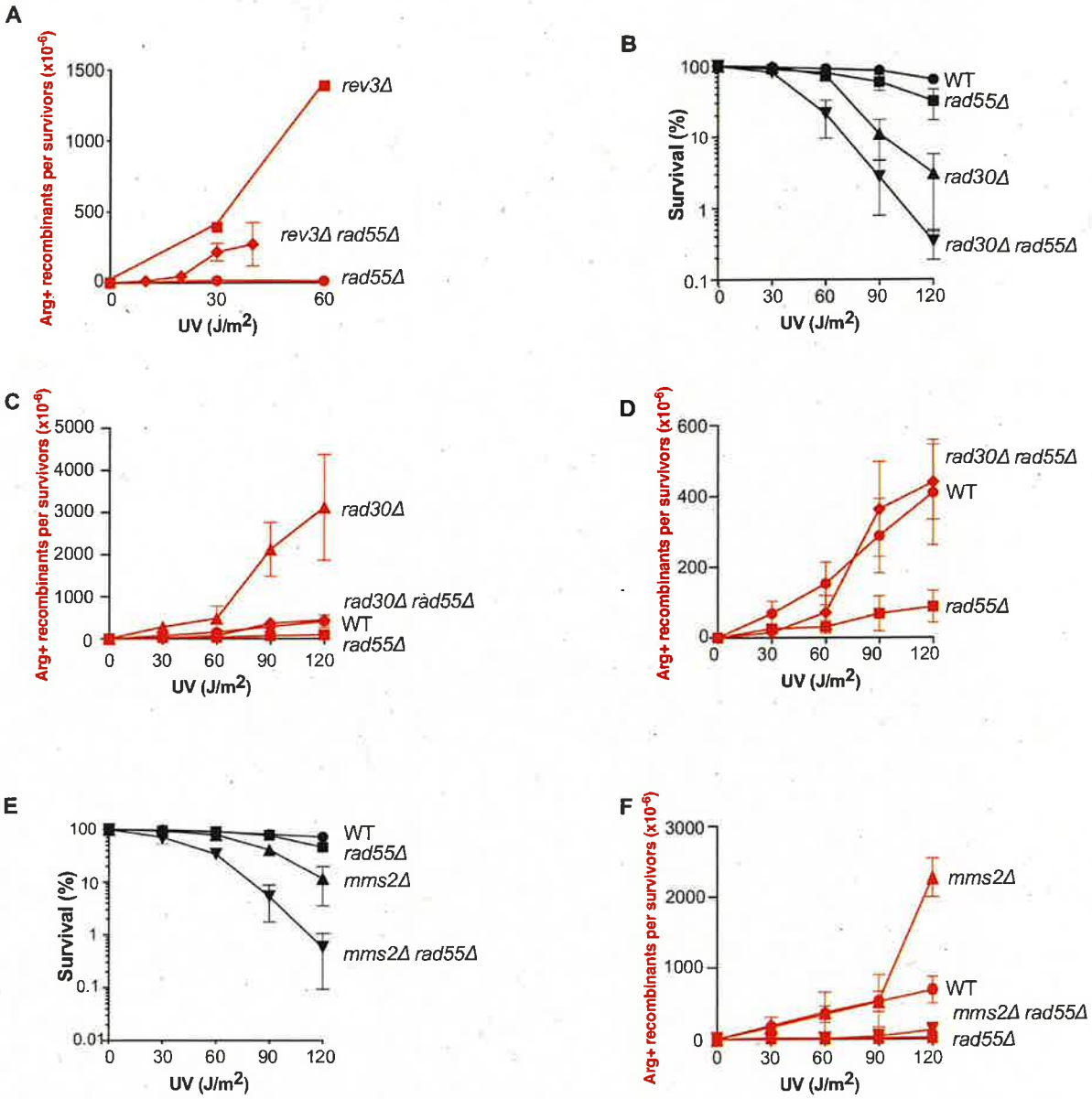

Fig 4. *RAD55*-independent UV-induced HR in TLS-deficient cells. (A) UV-induced [Arg+] recombinant frequencies in *rad55Δ rev3Δ* diploid cells. The very strong UV sensitivity displayed by the double mutant precluded the quantification of the UV-induced recombinant rate at UV doses higher than 40J/m^2. (B) Survival of *rad55Δ rad30Δ* diploid cells following UV radiation. (C) UV-induced [Arg+] recombinant frequencies in *rad55Δ* and *rad30Δ* diploids cells. (D) Close-up view of (C) to exclude the hyper-recombinogenic phenotype of *rad30Δ*. (E) *Rad55Δ mms2Δ* diploid cell-survival upon UV radiation. (F) UV-induced [Arg+] recombinant frequencies in *rad55Δ* and *mms2Δ* diploid cells.

https://doi.org/10.1371/journal.pgen.1010639.g004

(Fig 4B–4D). Thus, both Polζ and Polη contribute to the decrease of UV-induced HR in *rad55Δ* mutant cells.

Next, we asked whether UV-induced HR can be observed independently of the Rad55-Rad57 complex in cells deficient for the template switching pathway. Therefore, we measured the cell survival and recombination frequencies after UV radiation of cells in which

MMS2 was deleted. We found that the *rad55Δ mms2Δ* double mutant was more sensitive than the single mutants (Fig 4E), suggesting that some template switching events can occur independently of HR. Strikingly, the frequency of UV-induced recombinants was as low in the *rad55Δ mms2Δ* double mutant as in the *rad55Δ* mutant (Fig 4F). This suggests that the template switching pathway does not compete with HR between homologous chromosome and that TLS polymerases still prevent HR in the *rad55Δ mms2Δ* double mutant. On the other hand, the recombination frequency in the *mms2Δ* single mutant was increased, but only after exposure to the highest UV dose (120 J/m^2, Fig 4F).

The acute UV sensitivity of the *rad55Δ rev3Δ* double mutant is partially suppressed by *SRS2* deletion

As the Rad55-Rad57 complex limits Rad51 filament destabilization by Srs2 at DSBs [32,35], we asked whether Srs2 would be involved in the defective UV-induced HR associated with *rad55Δ* or *rad57Δ*. To address this question, we measured UV-induced HR frequencies in *rad55Δ srs2Δ* and *rad57Δ srs2Δ* double mutants. We found that they were similar to those observed in *rad55Δ* and *rad57Δ* single mutants (**Figs 5A and 5B, S4A, and S4B**). However, *rev3Δ rad55Δ srs2Δ* diploid cells were less sensitive to UV radiation than *rev3Δ rad55Δ* cells (Fig 5C). Thus, the Rad55-Rad57 complex is also involved in the protection of Rad51 filaments against Srs2 at ssDNA gaps formed after UV radiation, but this can only be seen in the absence of Polζ. When Polζ is active, the HR rate is probably too low in *rad55Δ* mutant cells to allow the detection of the effect of Rad51 displacement by Srs2.

Additionally, the level of resistance conferred by the deletion of *SRS2* in *rad55Δ rev3Δ* cells do not reach those of the *rev3Δ* single mutant (Fig 5C). This indicates that the Rad55-Rad57 complex plays a Srs2-independent role in UV-induced HR that is only revealed in *rev3Δ* mutants. We propose that the Rad55-Rad57 complex provides stability to Rad51 filaments independently of the protection against Srs2.

To sustain our conclusion, we analyzed UV-induced RPA foci in *srs2Δ* cells. The resolution of UV-induced RPA foci is delayed in *srs2Δ* cells compare to WT but in a lesser extent than in *rad55Δ* cells (**Figs 1G and 5E**). Moreover, the delay in UV-induced RPA foci resolution observed in the *rad55Δ* single mutant (**Figs 1G and S1F**) is the same than in the *rad55Δ srs2Δ* double mutant (**Figs 5F and S5**), suggesting that the antirecombinase activity of Srs2 does not account for the delay observed in the *rad55Δ* mutant. Similarly, the number of spontaneous and UV-induced RPA foci observed in *rev3Δ rad55Δ srs2Δ* haploid cells was the same as the number observed in the *rev3Δ rad55Δ* double mutant (**Fig 5F**). Moreover, the absence of Srs2 does not suppress the block in the first G2 phase after the release observed in the *rev3Δ rad55Δ* double mutant following UV irradiation (**S3 and S5 Figs**).

The Rad55-Rad57 complex is essential for the formation of UV-induced lethal recombination events

We confirmed that the *srs2Δ* diploid strain is very sensitive to UV radiation as reported before [60]; however, this sensitivity was completely suppressed in *rad55Δ srs2Δ* and *rad57Δ srs2Δ* mutant cells (**Figs 5D** and S4C). Previous genetic studies led to the concept of toxic Rad51-dependent recombination intermediates that accumulate in the absence of Srs2 [61–63]. Therefore, on the basis of the complete suppression of *srs2Δ*-associated UV sensitivity by *rad55Δ* and *rad57Δ*, we propose that the Rad55-Rad57 complex participates in the formation of UV-induced Rad51 filaments that are toxic for the cells in the absence of Srs2. In agreement with previous reports [60,64,65], we observed a strong UV-induced hyper-recombination

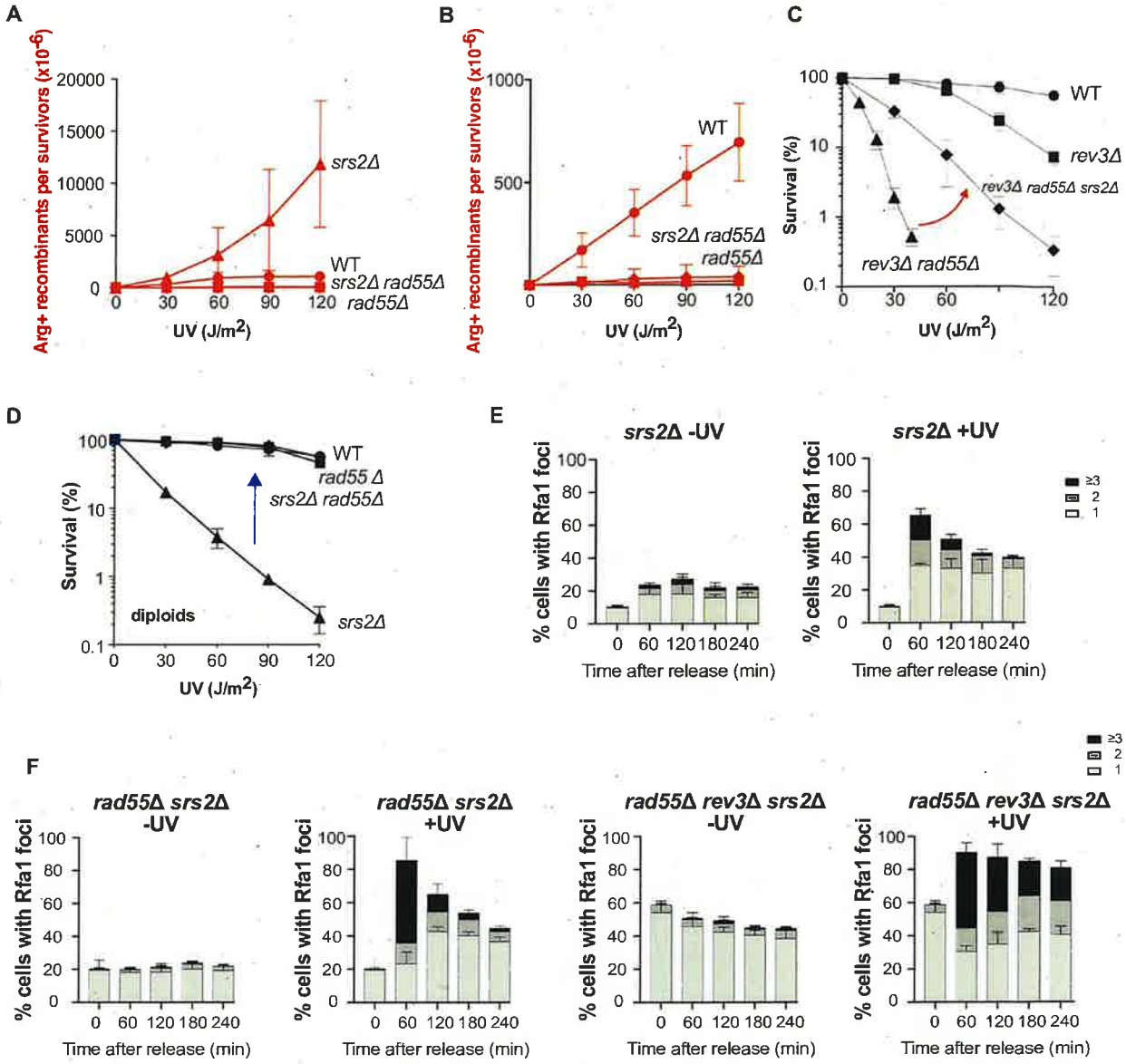

Fig 5. Srs2 role in the *rad55Δ* mutant exposed to UV radiation. (A) UV-induced [Arg+] recombinant frequencies in *rad55Δ srs2Δ* diploid cells. (B) Close-up view of (A) to exclude the hyper-recombinogenic phenotype of *srs2Δ*. (C) The acute UV sensitivity displayed by the *rad55Δ rev3Δ* mutant is partially suppressed by *SRS2* deletion. The red arrow between the *rev3Δ rad55Δ* and *rev3Δ rad55Δ srs2Δ* survival curves highlights the partial *srs2Δ* suppression. (D) Survival curves of diploid cells following UV radiation. The acute sensitivity to UV radiation of the diploid *srs2Δ* strain is suppressed by *rad55Δ* (blue arrow). (E) Quantification of Rfa1-YFP foci detected by fluorescence microscopy in *srs2Δ* cells not irradiated or after UV exposure. (F) Quantification of Rfa1-YFP foci detected by fluorescence microscopy in *rad55Δ srs2Δ* and *rad55Δ rev3Δ srs2Δ* cells not irradiated or after UV exposure. Error bars indicate SDs from three independent experiments.

https://doi.org/10.1371/journal.pgen.1010639.g005

phenotype in Srs2-deficient cells. This phenotype was completely suppressed by the concomitant deletion of Rad55 or Rad57 (**Figs** 5A and S4A).

The translesion DNA polymerases Polζ and Polη are not essential for DSB repair

The large impact of the *rad55Δ rev3Δ* double mutant on cell survival after UV radiation suggested that the Rad55-Rad57 complex and Polζ play an important and specific role in UV-induced DNA repair. Although the Rad55-Rad57 complex is not essential for DSB repair [39], we wanted to determine the potential role of TLS polymerases in DSB repair in *rad55Δ* cells. To this aim, we measured the repair of a DSB induced at the *MAT* locus upon expression of the HO endonuclease controlled by a galactose-inducible promoter. The DSB was repaired by HR using an ectopic *MAT***a**-inc sequence inserted in chromosome V [65,66] (**Fig 6A**). After DSB induction, survival was decreased by 3-fold in *rad55Δ* cells compared with WT cells (**Fig 6B**). Conversely, survival of the *rev3Δ*, *rad30Δ*, and *rev3Δ rad30Δ* mutants was not affected by DSB induction, and they did not change the sensitivity of the *rad55Δ* mutant. This indicates that the TLS polymerases are not required for DSB repair efficiency.

Discussion

The Rad55-Rad57 complex is essential for HR-mediated repair of UV-induced ssDNA gaps

Genetic studies provided evidence that ssDNA gaps are the major initiator of spontaneous and UV-induced HR in yeast [47,57]. In addition, electron microscopy and two-dimensional gel electrophoresis showed that UV-irradiated cells accumulate ssDNA gaps, likely resulting from re-priming events downstream of stalled replication forks at UV-induced DNA lesions [11]. UV-induced ssDNA gaps were also inferred from a physical assay [12] and from the study of RPA foci distribution relatively to sites of ongoing replication [13]. Interestingly, both studies reported that TLS and HR counteract ssDNA gap accumulation.

Here, we show that the complex formed by the Rad51 paralogs Rad55 and Rad57 is essential for UV-induced ssDNA gaps repair, while accessory at DSB sites. We observed a strong decrease of HR frequencies in the *rad55Δ* and *rad57Δ* mutants specifically after UV radiation. Moreover, we confirmed the synergistic increase of UV sensitivity upon depletion of both Rad55 and Polζ in haploid and diploid cells (**Fig 2A and 2B**). This was confirmed by the large

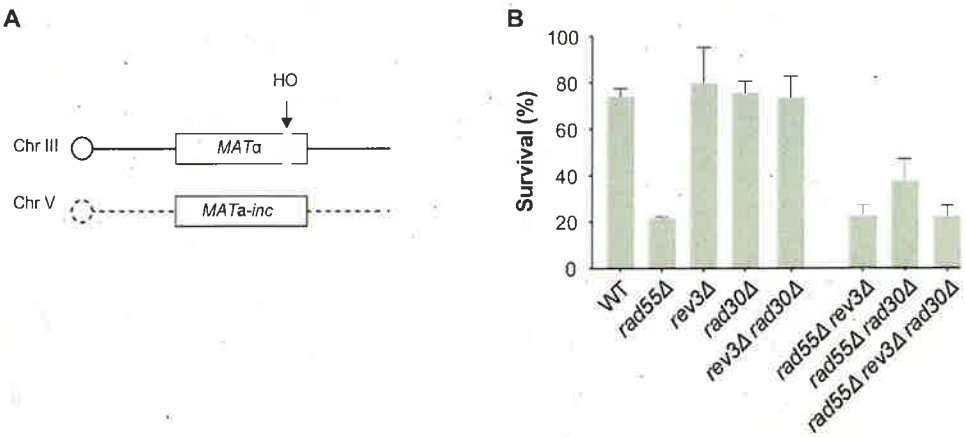

Fig 6. TLS DNA polymerases are not required for cell survival after a site-specific DSB. (A) Schematic representation of the system used to measure repair of a HO-induced DSB by gene conversion between ectopic copies of *MAT*. (B) Cell viability after DSB formation.

https://doi.org/10.1371/journal.pgen.1010639.g006

increase in the number of UV-induced RPA foci observed in the *rad55Δ rev3Δ* double mutant (Fig 2D). We did not observe this negative interaction after induction of a site-directed DSB (Fig 6). In addition, we found that UV-induced mutagenesis at the *CAN1* locus was increased in the *rad55Δ* mutant (Fig 2C), and that UV-induced HR was increased in Pol ζ and Pol η deficient cells (Fig 3A and 3B). Most importantly, we observed UV-induced HR in the absence of the Rad55-Rad57 complex only in cells deficient for TLS (Fig 4). These data suggest that the Rad55-Rad57 complex might stabilize Rad51 filaments on ssDNA gaps to prevent the recruitment of the TLS polymerases.

The Rad55-Rad57 complex plays three prominent roles in UV-induced HR

One of the best defined role of Rad55-Rad57 is the protection of Rad51 filaments from Srs2 at DSBs [32,35]. Here, we found that although the defect in UV-induced HR observed in *rad55Δ* cells was not suppressed by *SRS2* deletion (Fig 5A and 5B), the very high UV sensitivity of the *rad55Δ rev3Δ* double mutant was partially suppressed by *srs2Δ* (Fig 5C). This suggests that the Rad55-Rad57 complex protects Rad51 filaments against Srs2 also at UV-induced ssDNA gaps, although Esc2- and Elg1-dependent mechanisms also regulate negatively Srs2 at sites of stalled replication forks [67,68]. Additional studies are required to determine the interplay between these regulating factors.

The increased UV-sensitivity of the *rev3Δ rad55Δ srs2Δ* triple mutant compared with the *rev3Δ* single mutant (Fig 5C) clearly indicates that the Rad55-Rad57 complex plays a Srs2-independent role in UV-induced HR. We propose that the second role of this complex is to provide stability to Rad51 filaments, independently of the protection against Srs2. In agreement with this conclusion, we found that in *rad55Δ* or *rad57Δ* mutants, *srs2Δ*-associated UV-sensitivity was completely suppressed (Fig 5D **and** S4C). This indicates that in the absence of Srs2 activity, Rad51 stabilization by the Rad55-Rad57 complex would lead to lethal events, possibly initiated by ssDNA gaps that could block replication fork restart. On the basis of the results of single-molecule studies, it was proposed that the Rad55-Rad57 complex helps Rad51 filament formation by acting as a chaperone [35], in agreement with our observations.

Remarkably, UV-induced HR frequency increased in *rad55Δ* cells upon Polζ or Polη deletion (Fig 4). Therefore, the third role of the Rad55-Rad57 complex would be to allow HR to outcompete the TLS polymerases. Rad51 filament stabilization by the Rad55-Rad57 complex on ssDNA at the lesion site could prevent the recruitment of TLS polymerases by PCNA because of structural constraints. In the absence of Rad55-Rad57, unstable Rad51 filaments cannot prevent the loading of the TLS polymerases that inhibit HR and induce mutagenesis. TLS polymerase depletion in *rad55Δ* mutants would allow some HR events to occur, but the inherent instability of Rad51 filaments would make them rare and explain the low survival rate of *rev3Δ rad55Δ* mutant cells. Our results clearly highlight that UV-induced lesions can be channeled from HR to TLS and *vice versa*, when one pathway is inactivated. This provides further support to a model in which HR and TLS can share common substrates [12,13].

Model for the activity of the Rad55-Rad57 complex in ssDNA gap repair

Our genetic data suggest three different and essential functions for the Rad55-Rad57 complex in UV-induced interhomolog HR initiated at ssDNA gaps (Fig 7A). First, this complex is required for Rad51 filament formation and stabilization that are essential for efficient strand exchange at ssDNA gaps. The 5'ends of DSBs are resected to generate 3' ssDNA that can invade the homologous donor. Conversely, 3' ssDNA is not directly available at ssDNA gaps. Therefore, the Rad55-Rad57 complex may be required to form Rad51 filaments that can invade without 3' ssDNA extremities. Alternatively, the Rad55-Rad57 complex can be involved

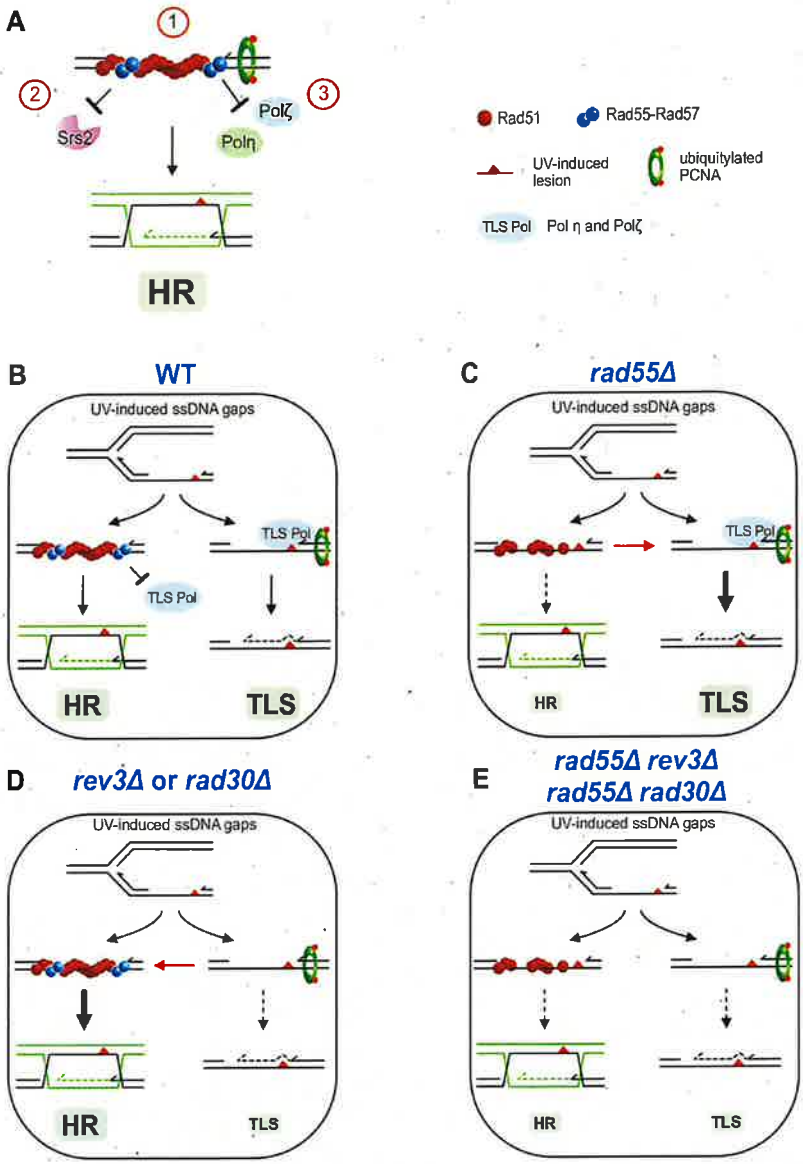

Fig 7. Model of Rad55-Rad57 roles in the repair of ssDNA gaps by HR behind replication forks. The figure shows an ssDNA gap generated after stalling of a replicative DNA polymerase at a UV-induced DNA lesion. This gap is a substrate for both the HR and TLS pathways. (**A**) The three roles of the Rad55-Rad57 complex in Rad51 filament formation on ssDNA gaps are highlighted: (1) formation of functional Rad51 filaments; (2) protection against Srs2 dismantling activity; (3) prevention of TLS polymerase recruitment at the primer/template junction. (**B**) In WT cells, Rad55-Rad57 heterodimers form and stabilize Rad51 filaments on ssDNA leading to HR, avoiding bypass by TLS. Rad51 filaments could prevent the recruitment of the TLS polymerases Polζ and Polη (collectively named TLS Pol) by covering the 3' extremity blocked at the DNA lesion. (**C**) In the *rad55Δ* mutant, inefficient and/or fewer Rad51 filaments are formed that cannot prevent the recruitment of the TLS polymerases. Therefore, more UV-induced DNA lesions are channeled towards the TLS pathway (bold arrow). (**D**) In the *rev3Δ* or in the *rad30Δ* mutant, the absence of Polζ or Polη allows channeling UV-induced DNA lesions towards the HR pathway (bold arrow). (**E**) In the *rad55Δ rev3Δ* and *rad55Δ rad30Δ* double mutants both the HR and the TLS pathways are impaired.

https://doi.org/10.1371/journal.pgen.1010639.g007

in the 3' end denaturation at the lesion site to generate a 3' ended ssDNA by recruitment of a DNA helicase. Second, the Rad55-Rad57 complex within Rad51 filaments counterbalances Srs2 activity through a mechanism that remains poorly understood [32,35]. Third, the Rad55-Rad57 complex could inhibit TLS polymerases by limiting their loading at the primer/template junction within ssDNA gaps, probably through the stabilization of Rad51 filaments (**Fig 7B-7E**). This competition might be crucial to control mutagenesis resulting from gap-filling by Polζ, but further studies will be required to understand how the access of HR and TLS are regulated at the site of lesions and to determine the nature of the lesions that can only be managed by TLS, as shown by the acute sensitivity of UV-irradiated *rev3Δ* mutant. Thus, in our model, Rad51 filaments formed with the Rad55-Rad57 complex preserve the genome stability through ssDNA gap repair by HR, but also through competition with TLS on common ssDNA gap substrates.

The interplay between HR and TLS in mammals

The interplay between error-prone and error-free lesion-bypass pathways is documented in *E. coli* and yeast (the present study, [13,14]), and it has been recently investigated in mammals. First of all, it was recently shown that BRCA-deficient tumors sensibility to cisplatin and synthetic lethality with PARP inhibitors were associated with a BRCA default in preventing replication-associated gaps rather than in preventing DSBs [69,70]. More specifically, HR can be triggered by PRIMPOL-dependent ssDNA gaps behind stalled replication forks [71]. Moreover, BRCA1- and BRCA2-defective breast cancer cells, display an increased somatic mutational load specific of TLS polymerases [72–75]. Accordingly, a recent study found that BRCA1/2-defective cancer cells rely much more on TLS for repair of PRIMPOL-dependent ssDNA gaps [76]. In addition, similarly to PARP1 or DNA polymerase Polθ inhibitors that are used to treat HR-deficient cancers [77–79], the small molecule JE-RH-06 disrupts the interaction between the TLS polymerases REV1 and Polζ and shows preferential cytotoxicity in BRCA1-deficient cancer cells [76,80]. Thus, it would be interesting to determine whether the association of cancer-associated RAD51 paralog mutations and TLS mutations leads to a synergic sensitivity to replication fork blocking lesions, as we observed in yeast in the *rad55Δ rev3Δ* double mutant. If an acute sensitivity is found, one might expect a cytotoxicity associated with TLS polymerase inhibitors in RAD51 paralog-deficient cancer cells.

Materials and methods

Yeast strains, plasmids and media

The *S. cerevisiae* strains used in the present study are isogenic derivatives of FF18733 (*his7-2, leu2-3,112, lys1-1, trp1-289, ura3-52*), JKM146 (*hml::ADE1 MATalpha hmr::ADE1, arg5,6::MATa-inc::HPH1, ade3::GAL::HO*) and W303 (*ADE2 leu2-3,112 his3-11,15 trp1-1, ura3-1*) and are listed in **S1 Table**. Yeast cells were incubated at 30˚C for all the experiments described. Gene deletions were performed by PCR-mediated one-step replacement [81,82]. Mutants were selected on YPD medium containing 300 mg/L geneticin (Sigma) or nourseothricin (clonAT; Werner BioAgents). All deletions were confirmed by PCR amplification of genomic DNA. All media were prepared as previously described [83].

Irradiation, cell survival assay, and measurement of DNA damage-induced HR frequency

Cells in stationary phase and in exponential growth phase were used for irradiation with UV and γ-rays, respectively. UV irradiation was performed using a 264 nm source. Yeast cells were irradiated with 30, 60, 90 and 120 J/m^2 (2 J/m^2/s dose rate). γ-irradiation was performed using

a GSR D1 irradiator (Gamma-Service Medical GmbH). It is a self-shielded irradiator with four sources of ^{137}Cesium. The total activity was 180.28 TBq in March 2014. As yeast cells resuspended in 1 mL of sterile H_2O were irradiated in 1.5ml plastic microtubes, dosimetry was performed using plastic microtubes with a cylindrical ionizing chamber 31010 (PTW, Freiburg, Germany) following the American Association of Physicists in Medicine recommendations [84]. This ionizing chamber has a cavity of 0.125 cm^3 calibrated with ^{137}Cesium in air kerma free in air and the reference number of our facility is 210382401. The polarity and the ion recombination were measured for this ^{137}Cesium source. Each measurement was corrected with the KTP factor to take into account the variations in temperature and atmospheric pressure. Yeast cells were irradiated at 100, 200, 400 and 600 Gy (single doses) and with a 12 Gy/min dose rate that takes the radioactive decrease into account.

Before (UV) or after (γ-rays) irradiation, cells were plated at the appropriate dilution on rich medium (YPD) to measure the survival rate, and on synthetic plates without arginine to quantify the number of HR events between *ARG4* heteroalleles. HR frequencies were determined by dividing the number of recombinant colonies growing on selective medium by the number of unselected colonies subjected to the same dose of irradiation. The values obtained were corrected by subtracting the number of recombinants on the non-irradiated plates. The mean percentage from at least three independent experiments is presented.

Measurement of spontaneous heteroallelic HR

Rates of spontaneous HR between two heteroalleles of *ARG4* were determined by fluctuation tests using the method of the median [85]. The reported rates were obtained from three independent experiments, each performed with nine independent 2-ml cultures started with less than 200 cells and incubated at 30°C for three days. The significance of the rates is indicated by the 95% confidence interval [85].

Measurement of UV-induced mutagenesis

UV-induced mutagenesis was measured with the *CAN1* forward-mutation assay [59]. UV-induced mutagenesis frequencies were obtained by dividing the number of colonies growing on synthetic plates without arginine and containing l-canavanine (Sigma, 30 mg/l) (*i.e.*, canavanine-resistant, Can^R, cells) by the number of cells that survived irradiation counted on rich media YPD. The number of Can^R colonies obtained after irradiation was corrected by subtracting the number of spontaneous Can^R colonies growing on non-irradiated plates.

Cell growth, synchronization and irradiation before microscopy

Cells were grown at 30°C in synthetic complete medium (Formedium). Before UV- and γ-irradiation, growing cells were synchronized in G1 using 17 mg/ml α-factor for 180 min. They were released from the G1 arrest by three consecutive washes with sterile H_2O. Cells were resuspended in 50 ml of sterile H_2O and UV-irradiated in a glass plate of diameter 190 mm. UV irradiation was performed using a 264 nm source. Yeast cells in water were irradiated with 60 J/m2 (2 J/m2/s dose rate) then resuspended in fresh complete medium. γ-irradiation was performed as described for survival studies. Cells were then resuspended in fresh complete medium. Time-course experiment were started with yeast cultures adjusted to OD_{600} 0.5.

Microscopy

Live-cell images were acquired using a wide-field inverted microscope (Leica DMI-6000B) equipped with Adaptive Focus Control to eliminate Z drift, a 100×/1.4 NA immersion

objective with a Prior NanoScanZ Nanopositioning Piezo Z Stage System, a CMOS camera (ORCA-Flash4.0; Hamamatsu) and a solid-state light source (SpectraX, Lumencore). The system is piloted by MetaMorph software (Molecular Device).

YFP images were acquired at indicated time points after alpha factor block release and UV or γ-rays irradiation; 19 focal steps of 0.20 μm were acquired with an exposure time of 100 ms using a solid-state 500-nm diode and a YFP filter (excitation 470–510 nm and dichroic 495 nm; Chroma Technology Corp.). A single bright-field image on one focal plane was acquired at each time point with an exposure of 50ms. All the images shown are z projections of z-stack images. Image analysis was achieved following processing with ImageJ software (National Institutes of Health), using scripts written in ImageJ macro language. Bright-field and maximum intensity projections of YFP images were merged, Rfa1-YPD foci were then quantified in 2D.

Measure of DNA content by flow cytometry

1 ml of cells were resuspended in 70% Ethanol and kept at 4˚C. Cells were centrifuged for 3 min at 7,000 RPM and washed once in PBS, resuspended in PBS with RNase A (0.5 mg/ml) for 2 hours at 50˚C. Cells were centrifugated and resuspended in PBS with iodure propidium (50 μg/ml) for one hour at room temperature. Cells were diluted 10-fold in PBS and cell aggregates were dissociated by sonication. DNA content analysis was performed using LSRII flow cytometer (BD Biosciences) and analyzed with the FlowJo software.

Survival following DSB formation

Cells were grown overnight in liquid culture medium containing lactate acid instead of glucose. Survival following HO-induced DSB was measured as the number of cells growing on galactose-containing medium divided by the number of colonies growing on YPD. The results shown are the mean values of at least 3 independent experiments.

Supporting information

S1 Fig. Rad57 plays a major role specifically in UV-induced HR. (A) Survival, and (B) [Arg+] recombinant frequencies in WT and *rad57Δ* diploid cells following UV radiation. (C) Survival and (D) [Arg+] recombinant frequencies in WT and *rad57Δ* diploid cells after γ irradiation. (E) Quantification of Rfa1-YFP foci in WT and *rad55Δ* cells not irradiated or after UV exposure in G1-arrested cells. Error bars indicate SDs from three independent experiments. (F) Representative images of Rfa1-YFP WT and *rad55Δ* cells released from G1 arrest and UV-irradiated or not. Bright-field (BF) images are merged with YFP images. Scale bars are 2 μm. FACS profiles for each corresponding time point are shown.
(TIF)

S2 Fig. γ-rays-induced RPA foci in WT and *rad55Δ* strains. (A) Experimental scheme: Cells arrested in G1 phase with alpha-factor (αF) were release into the cell cycle. After one hour from the release, cells were exposed to γ-rays. Samples were collected every hour for four hours. (B) Quantification of Rfa1-YFP foci in WT and *rad55Δ* cells not irradiated or after γ-rays irradiation. Error bars indicate SDs from three independent experiments.
(TIF)

S3 Fig. UV-induced RPA foci in the *rev3Δ* and *rad55Δ rev3Δ* strains. Representative images of Rfa1-YFP *rev3Δ* and *rad55Δ rev3Δ* cells after release from G1 arrest and UV irradiated or not. Bright-field (BF) images are merged with YFP images. Scale bars are 2 μm. FACS profiles for each corresponding time point are shown.
(TIF)

S4 Fig. Srs2 roles in the *rad57Δ* mutant exposed to UV radiation. (A) UV-induced [Arg+] recombinant frequencies in *rad57Δ srs2Δ* diploid cells. (B) Close-up view of (A) to exclude the hyper-recombinogenic phenotype of *srs2Δ*. (C) Survival curves of diploid cells following UV radiation. The acute sensitivity to UV radiation of the diploid *srs2Δ* strain is suppressed by *rad57Δ* (blue arrow).
(TIF)

S5 Fig. RPA foci in *rad55Δ rev3Δ srs2Δ* cells. Representative images of Rfa1-YFP *srs2Δ*, *rev3Δ srs2Δ* and *rad55Δ rev3Δ srs2Δ* cells after release from G1 arrest and UV irradiated or not. Bright-field (BF) images are merged with YFP images. Scale bars are 2 μm. FACS profiles for each corresponding time point are shown.
(TIF)

S1 Table. *Saccharomyces cerevisiae* strains.
(PDF)

Acknowledgments

We thank Jim Haber and Pablo Radicella, for critical and careful reading of the manuscript. We thank Véronique Ménard from the radiation facility of our institute for her help with the use of the GSRD1 irradiator. We also appreciate the help of Elisabetta Andermarcher with the English editing.

Author Contributions

Conceptualization: Laurent Maloisel, Eric Coïc.

Formal analysis: Laurent Maloisel.

Funding acquisition: Eric Coïc.

Investigation: Laurent Maloisel, Emilie Ma, Jamie Phipps, Alice Deshayes, Stefano Mattarocci, Eric Coïc.

Methodology: Laurent Maloisel, Emilie Ma, Alice Deshayes, Stéphane Marcand, Karine Dubrana, Eric Coïc.

Project administration: Eric Coïc.

Resources: Laurent Maloisel, Emilie Ma, Eric Coïc.

Software: Jamie Phipps.

Supervision: Stéphane Marcand, Karine Dubrana, Eric Coïc.

Validation: Laurent Maloisel, Emilie Ma, Alice Deshayes, Stefano Mattarocci, Eric Coïc.

Visualization: Laurent Maloisel.

Writing – original draft: Laurent Maloisel, Eric Coïc.

Writing – review & editing: Laurent Maloisel, Jamie Phipps, Stéphane Marcand, Karine Dubrana, Eric Coïc.

References

1. Branzei D, Psakhye I. DNA damage tolerance. Curr Opin Cell Biol. 2016; 40: 137–144. https://doi.org/10.1016/j.ceb.2016.03.015 PMID: 27060551

2. Zhao L, Todd Washington M. Translesion synthesis: Insights into the selection and switching of DNA polymerases. Genes. 2017. https://doi.org/10.3390/genes8010024 PMID: 28075396
3. Lehmann AR, Fuchs RP. Gaps and forks in DNA replication: Rediscovering old models. DNA Repair (Amst). 2006; 5: 1495–1498. https://doi.org/10.1016/j.dnarep.2006.07.002 PMID: 16956796
4. Hedglin M, Benkovic SJ. Eukaryotic Translesion DNA Synthesis on the Leading and Lagging Strands: Unique Detours around the Same Obstacle. Chemical Reviews. 2017. https://doi.org/10.1021/acs.chemrev.7b00046 PMID: 28497687
5. Waters LS, Minesinger BK, Wiltrout ME, D'Souza S, Woodruff R V, Walker GC. Eukaryotic translesion polymerases and their roles and regulation in DNA damage tolerance. Microbiol Mol Biol Rev. 2009; 73: 134–154. https://doi.org/10.1128/MMBR.00034-08 PMID: 19258535
6. Makarova A V, Stodola JL, Burgers PM. A four-subunit DNA polymerase ζ complex containing Pol δ accessory subunits is essential for PCNA-mediated mutagenesis. Nucleic Acids Res. 2012; 40: 11618–11626. https://doi.org/10.1093/nar/gks948 PMID: 23066099
7. Liberi G, Maffioletti G, Lucca C, Chiolo I, Baryshnikova A, Cotta-Ramusino C, et al. Rad51-dependent DNA structures accumulate at damaged replication forks in sgs1 mutants defective in the yeast ortholog of BLM RecQ helicase. Genes Dev. 2005; 19: 339–350. https://doi.org/10.1101/gad.322605 PMID: 15687257
8. Branzei D, Vanoli F, Foiani M. SUMOylation regulates Rad18-mediated template switch. Nature. 2008. pp. 915–920. https://doi.org/10.1038/nature07587 PMID: 19092928
9. Branzei D, Szakal B. DNA damage tolerance by recombination: Molecular pathways and DNA structures. DNA Repair (Amst). 2016; 44: 68–75. https://doi.org/10.1016/j.dnarep.2016.05.008 PMID: 27236213
10. Carr AM, Lambert S. Replication stress-induced genome instability: The dark side of replication maintenance by homologous recombination. Journal of Molecular Biology. 2013. pp. 4733–4744. https://doi.org/10.1016/j.jmb.2013.04.023 PMID: 23643490
11. Lopes M, Foiani M, Sogo JM. Multiple mechanisms control chromosome integrity after replication fork uncoupling and restart at irreparable UV lesions. Mol Cell. 2006; 21: 15–27. https://doi.org/10.1016/j.molcel.2005.11.015 PMID: 16387650
12. Ma W, Westmoreland JW, Resnick MA. Homologous recombination rescues ssDNA gaps generated by nucleotide excision repair and reduced translesion DNA synthesis in yeast G2 cells. Proc Natl Acad Sci U S A. 2013; 110. https://doi.org/10.1073/pnas.1301676110 PMID: 23858457
13. Wong RP, García-Rodríguez N, Zilio N, Hanulová M, Ulrich HD. Processing of DNA Polymerase-Blocking Lesions during Genome Replication Is Spatially and Temporally Segregated from Replication Forks. Mol Cell. 2020; 77: 3–16.e4. https://doi.org/10.1016/j.molcel.2019.09.015 PMID: 31607544
14. Fujii S, Isogawa A, Fuchs RP. Chronological switch from translesion synthesis to homology- Dependent gap repair in vivo. Toxicol Res. 2018; 34: 297–302. https://doi.org/10.5487/TR.2018.34.4.297 PMID: 30370004
15. Masłowska KH, Laureti L, Pagès V. iDamage: a method to integrate modified DNA into the yeast genome. Nucleic Acids Res. 2019; 47: e124. https://doi.org/10.1093/nar/gkz723 PMID: 31418026
16. Hoege C, Pfander B, Moldovan G-L, Pyrowolakis G, Jentsch S. RAD6-dependent DNA repair is linked to modification of PCNA by ubiquitin and SUMO. Nature. 2002; 419: 135–141. https://doi.org/10.1038/nature00991 PMID: 12226657
17. Torres-Ramos CA, Prakash S, Prakash L. Requirement of *RAD5* and *MMS2* for Postreplication Repair of UV-Damaged DNA in Saccharomyces cerevisiae. Mol Cell Biol. 2002; 22: 2419–2426. https://doi.org/10.1128/MCB.22.7.2419-2426.2002 PMID: 11884624
18. Vanoli F, Fumasoni M, Szakal B, Maloisel L, Branzei D. Replication and recombination factors contributing to recombination-dependent bypass of DNA lesions by template switch. PLoS Genet. 2010; 6: e1001205. https://doi.org/10.1371/journal.pgen.1001205 PMID: 21085632
19. Conway AB, Lynch TW, Zhang Y, Fortin GS, Fung CW, Symington LS, et al. Crystal structure of a Rad51 filament. Nat Struct Mol Biol. 2004; 11: 791–796. https://doi.org/10.1038/nsmb795 PMID: 15235592
20. Short JM, Liu Y, Chen S, Soni N, Madhusudhan MS, Shivji MKK, et al. High-resolution structure of the presynaptic RAD51 filament on single-stranded DNA by electron cryo-microscopy. Nucleic Acids Res. 2016; 44: 9017–9030. https://doi.org/10.1093/nar/gkw783 PMID: 27596592
21. San Filippo J, Sung P, Klein H. Mechanism of eukaryotic homologous recombination. Annu Rev Biochem. 2008; 77: 229–257. https://doi.org/10.1146/annurev.biochem.77.061306.125255 PMID: 18275380

22. Bell JC, Kowalczykowski SC. Mechanics and Single-Molecule Interrogation of DNA Recombination. Annu Rev Biochem. 2016; 85: 193–226. https://doi.org/10.1146/annurev-biochem-060614-034352 PMID: 27088880

23. Haber JE. DNA Repair: The Search for Homology. BioEssays. 2018. https://doi.org/10.1002/bies.201700229 PMID: 29603285

24. Mehta A, Haber JE. Sources of DNA double-strand breaks and models of recombinational DNA repair. Cold Spring Harb Perspect Biol. 2014; 6: a016428. https://doi.org/10.1101/cshperspect.a016428 PMID: 25104768

25. Sung P. Function of yeast Rad52 protein as a mediator between replication protein A and the Rad51 recombinase. J Biol Chem. 1997; 272: 28194–28197. https://doi.org/10.1074/jbc.272.45.28194 PMID: 9353267

26. Mortensen UH, Lisby M, Rothstein R. Rad52. Current Biology. 2009. https://doi.org/10.1016/j.cub.2009.06.001 PMID: 19706272

27. Carver A, Zhang X. Rad51 filament dynamics and its antagonistic modulators. Semin Cell Dev Biol. 2021; 113: 3–13. https://doi.org/10.1016/j.semcdb.2020.06.012 PMID: 32631783

28. Bonilla B, Hengel SR, Grundy MK, Bernstein KA. *RAD51* Gene Family Structure and Function. Annu Rev Genet. Annual Reviews; 2020; 54: 25–46. https://doi.org/10.1146/annurev-genet-021920-092410 PMID: 32663049

29. Kans JA, Mortimer RK. Nucleotide sequence of the *RAD57* gene of *Saccharomyces cerevisiae*. Gene. 1991; 105: 139–140. https://doi.org/10.1016/0378-1119(91)90527-i PMID: 1937004

30. Lovett ST. Sequence of the *RAD55* gene of *Saccharomyces cerevisiae*: similarity of *RAD55* to prokaryotic RecA and other RecA-like proteins. Gene. 1994; https://doi.org/10.1016/0378-1119(94)90362-x PMID: 8181742

31. Sung P. Yeast Rad55 and Rad57 proteins form a heterodimer that functions with replication protein A to promote DNA strand exchange by Rad51 recombinase. Genes Dev. 1997; 11: 1111–1121. https://doi.org/10.1101/gad.11.9.1111 PMID: 9159392

32. Liu J, Renault L, Veaute X, Fabre F, Stahlberg H, Heyer W-D. Rad51 paralogues Rad55–Rad57 balance the antirecombinase Srs2 in Rad51 filament formation. Nature. 2011; 479: 245–248. https://doi.org/10.1038/nature10522 PMID: 22020281

33. Hays SL, Firmenich AA, Berg P. Complex formation in yeast double-strand break repair: Participation of Rad51, Rad52, Rad55, and Rad57 proteins. Proc Natl Acad Sci U S A. 1995; 92: 6925–6929. https://doi.org/10.1073/pnas.92.15.6925 PMID: 7624345

34. Johnson RD, Symington LS. Functional differences and interactions among the putative RecA homologs Rad51, Rad55, and Rad57. Mol Cell Biol. 1995; 15: 4843–4850. https://doi.org/10.1128/MCB.15.9.4843 PMID: 7651402

35. Roy U, Kwon Y, Marie L, Symington L, Sung P, Lisby M, et al. The Rad51 paralog complex Rad55-Rad57 acts as a molecular chaperone during homologous recombination. Mol Cell. 2021; 81: 1043–1057.e8. https://doi.org/10.1016/j.molcel.2020.12.019 PMID: 33421364

36. Belan O, Barroso C, Kaczmarczyk A, Anand R, Federico S, O'Reilly N, et al. Single-molecule analysis reveals cooperative stimulation of Rad51 filament nucleation and growth by mediator proteins. Mol Cell. 2021; 81: 1058–1073.e7. https://doi.org/10.1016/j.molcel.2020.12.020 PMID: 33421363

37. Garcin EB, Gon S, Sullivan MR, Brunette GJ, de Cian A, Concordet JP, et al. Differential requirements for the RAD51 paralogs in genome repair and maintenance in human cells. PLoS Genet. 2019; 15: 1–29. https://doi.org/10.1371/journal.pgen.1008355 PMID: 31584931

38. Mozlin AM, Fung CW, Symington LS. Role of the *Saccharomyces cerevisiae* Rad51 paralogs in sister chromatid recombination. Genetics. 2008; 178: 113–125. https://doi.org/10.1534/genetics.107.082677 PMID: 18202362

39. Fung CW, Mozlin AM, Symington LS. Suppression of the double-strand-break-repair defect of the *Saccharomyces cerevisiae rad57* mutant. Genetics. 2009; 181: 1195–1206. https://doi.org/10.1534/genetics.109.100842 PMID: 19189942

40. Veaute X, Jeusset J, Soustelle C, Kowalczykowski SC, Le Cam E, Fabre F. The Srs2 helicase prevents recombination by disrupting Rad51 nucleoprotein filaments. Nature. 2003; 423: 309–312. https://doi.org/10.1038/nature01585 PMID: 12748645

41. Krejci L, Van Komen S, Li Y, Villemain J, Reddy MS, Klein H, et al. DNA helicase Srs2 disrupts the Rad51 presynaptic filament. Nature. 2003; 423: 305–309. https://doi.org/10.1038/nature01577 PMID: 12748644

42. Xu X, Ball L, Chen W, Tian X, Lambrecht A, Hanna M, et al. The yeast Shu complex utilizes homologous recombination machinery for error-free lesion bypass via physical interaction with a Rad51 paralogue. PLoS One. 2013; 8: 1–9. https://doi.org/10.1371/journal.pone.0081371 PMID: 24339919

43. Rattray AJ, Shafer BK, McGill CB, Strathern JN. The roles of *REV3* and *RAD57* in double-strand-break-repair-induced mutagenesis of *Saccharomyces cerevisiae*. Genetics. 2002; 162: 1063–1077. https://doi.org/10.1093/genetics/162.3.1063 PMID: 12454056

44. Ball LG, Zhang K, Cobb JA, Boone C, Xiao W. The yeast Shu complex couples error-free post-replication repair to homologous recombination. Mol Microbiol. 2009; 73: 89–102. https://doi.org/10.1111/j.1365-2958.2009.06748.x PMID: 19496932

45. Cadet J, Ravanat J-L, TavernaPorro M, Menoni H, Angelov D. Oxidatively generated complex DNA damage: Tandem and clustered lesions. Cancer Lett. 2012; 327: 5–15. https://doi.org/10.1016/j.canlet.2012.04.005 PMID: 22542631

46. Chanet R, Heude M, Adjiri a, Maloisel L, Fabre F. Semidominant mutations in the yeast Rad51 protein and their relationships with the Srs2 helicase. Mol Cell Biol. 1996; 16: 4782–9. Available: http://www.pubmedcentral.nih.gov/articlerender.fcgi?artid=231479&tool=pmcentrez&rendertype=abstract https://doi.org/10.1128/MCB.16.9.4782 PMID: 8756636

47. Game JC, Mortimer RK. A genetic study of X-ray sensitive mutants in yeast. Mutat Res—Fundam Mol Mech Mutagen. 1974; https://doi.org/10.1016/0027-5107(74)90176-6 PMID: 4606119

48. Lettier G, Feng Q, De Mayolo AA, Erdeniz N, Reid RJD, Lisby M, et al. The role of DNA double-strand breaks in spontaneous homologous recombination in *S. cerevisiae*. PLoS Genet. 2006; 2: 1773–1786. https://doi.org/10.1371/journal.pgen.0020194 PMID: 17096599

49. Coïc E, Gluck L, Fabre F. Evidence for short-patch mismatch repair in *Saccharomyces cerevisiae*. EMBO J. 2000; https://doi.org/10.1093/emboj/19.13.3408 PMID: 10880453

50. Petes TD, Malone RE, Symington LS. Recombination in Yeast. Cold Spring Harbor Monograph Archive. 1991; 21: 407–521

51. Friis J, Roman H. The effect of the mating-type alleles on intragenic recombination in yeast. Genetics. 1968; https://doi.org/10.1093/genetics/59.1.33 PMID: 5683638

52. Lisby M, Barlow JH, Burgess RC, Rothstein R. Choreography of the DNA damage response: Spatiotemporal relationships among checkpoint and repair proteins. Cell. 2004; 118: 699–713. https://doi.org/10.1016/j.cell.2004.08.015 PMID: 15369670

53. Lemontt JF. Pathways of ultraviolet mutability in *Saccharomyces cerevisiae*. I. Some properties of double mutants involving *uvs9* and *rev*. Mutat Res—Fundam Mol Mech Mutagen. 1971; https://doi.org/10.1016/0027-5107(71)90041-8 PMID: 4947374

54. Lovett ST, Mortimer RK. Characterization of null mutants of the *RAD55* gene of *Saccharomyces cerevisiae*: effects of temperature, osmotic strength and mating type. Genetics. 1987; https://doi.org/10.1093/genetics/116.4.547 PMID: 3305159

55. Heude M, Fabre F. a/α-control of DNA repair in the yeast *Saccharomyces cerevisiae*: Genetic and physiological aspects. Genetics. 1993;

56. Valencia-Burton M, Oki M, Johnson J, Seier TA, Kamakaka R, Haber JE. Different mating-type-regulated genes affect the DNA repair defects of *saccharomyces RAD51*, *RAD52* and *RAD55* mutants. Genetics. 2006; https://doi.org/10.1534/genetics.106.058685 PMID: 16782999

57. Quah SK, Von Borstel RC, Hastings PJ. The origin of spontaneous mutation in *Saccharomyces cerevisiae*. Genetics. 1980; https://doi.org/10.1093/genetics/96.4.819 PMID: 7021317

58. Tellier-Lebegue C, Dizet E, Ma E, Veaute X, Coïc E, Charbonnier J-B, et al. The translesion DNA polymerases Pol ζ and Rev1 are activated independently of PCNA ubiquitination upon UV radiation in mutants of DNA polymerase δ. PLoS Genet. 2017; 13. https://doi.org/10.1371/journal.pgen.1007119 PMID: 29281621

59. Whelan WL, Gocke E, Manney TR. The *CAN1* locus of *Saccharomyces cerevisiae*: Fine-structure analysis and forward mutation rates. Genetics. 1979; https://doi.org/10.1093/genetics/91.1.35 PMID: 372045

60. Aboussekhra A, Chanet R, Zgaga Z, Cassier-Chauvat C, Heude M, Fabre F. *RADH*, a gene of *Saccharomyces cerevisiae* encoding a putative DNA helicase involved in DNA repair. Characteristics of radH mutants and sequence of the gene. Nucleic Acids Res. 1989; https://doi.org/10.1093/nar/17.18.7211 PMID: 2552405

61. Gangloff S, Soustelle C, Fabre F. Homologous recombination is responsible for cell death in the absence of the Sgs1 and Srs2 helicases. Nat Genet. 2000; 25: 192–194. https://doi.org/10.1038/76055 PMID: 10835635

62. Klein HL. Mutations in recombinational repair and in checkpoint control genes suppress the lethal combination of *srs2Δ* with other DNA repair genes in *Saccharomycescerevisiae*. Genetics. 2001; 157: 557–565.

63. Fabre F, Chan A, Heyer WD, Gangloff S. Alternate pathways involving Sgs1/Top3, Mus81/ Mms4, and Srs2 prevent formation of toxic recombination intermediates from single-stranded gaps created by DNA

replication. Proc Natl Acad Sci U S A. 2002; 99: 16887–16892. https://doi.org/10.1073/pnas.252652399 PMID: 12475932

64. Rong L, Palladino F, Aguilera A, Klein HL. The hyper-gene conversion hpr5-1 mutation of *Saccharomyces cerevisiae* is an allele of the *SRS2/RADH* gene. Genetics. 1991; 127: 75 LP– 85. Available: http://www.genetics.org/content/127/1/75.abstract https://doi.org/10.1093/genetics/127.1.75 PMID: 1849857

65. Esta A, Ma E, Dupaigne P, Maloisel L, Guerois R, Le Cam E, et al. Rad52 sumoylation prevents the toxicity of unproductive Rad51 filaments independently of the anti-recombinase Srs2. PLoS Genet. 2013; 9: e1003833. https://doi.org/10.1371/journal.pgen.1003833 PMID: 24130504

66. Ira G, Malkova A, Liberi G, Foiani M, Haber JE. Srs2 and Sgs1-Top3 suppress crossovers during double-strand break repair in yeast. Cell. 2003; 115: 401–11. Available: http://www.ncbi.nlm.nih.gov/pubmed/14622595%0Ahttp://www.pubmedcentral.nih.gov/articlerender.fcgi?artid=PMC4493758 https://doi.org/10.1016/s0092-8674(03)00886-9 PMID: 14622595

67. Urulangodi M, Sebesta M, Menolfi D, Szakal B, Sollier J, Sisakova A, et al. Local regulation of the Srs2 helicase by the SUMO-like domain protein Esc2 promotes recombination at sites of stalled replication. Genes Dev. 2015; 29: 2067–2080. https://doi.org/10.1101/gad.265629.115 PMID: 26443850

68. Arbel M, Bronstein A, Sau S, Liefshitz B, Kupiec M. Access to pcna by srs2 and elg1 controls the choice between alternative repair pathways in *saccharomyces cerevisiae*. MBio. 2020; 11: 1–14. https://doi.org/10.1128/mBio.00705-20 PMID: 32371600

69. Panzarino NJ, Krais JJ, Cong K, Peng M, Mosqueda M, Nayak SU, et al. Replication Gaps Underlie BRCA Deficiency and Therapy Response. Cancer Res. 2021; 81: 1388–1397. https://doi.org/10.1158/0008-5472.CAN-20-1602 PMID: 33184108

70. Cong K, Peng M, Kousholt AN, Lee WTC, Lee S, Nayak S, et al. Replication gaps are a key determinant of PARP inhibitor synthetic lethality with BRCA deficiency. Mol Cell. 2021; 81: 3128–3144.e7. https://doi.org/10.1016/j.molcel.2021.06.011 PMID: 34216544

71. Piberger AL, Bowry A, Kelly RDW, Walker AK, González-Acosta D, Bailey LJ, et al. PrimPol-dependent single-stranded gap formation mediates homologous recombination at bulky DNA adducts. Nat Commun. 2020; https://doi.org/10.1038/s41467-020-19570-7 PMID: 33203852

72. Alexandrov LB, Nik-Zainal S, Wedge DC, Aparicio SAJR, Behjati S, Biankin A V., et al. Signatures of mutational processes in human cancer. Nature. 2013; 500: 415–421. https://doi.org/10.1038/nature12477 PMID: 23945592

73. Nik-Zainal S, Davies H, Staaf J, Ramakrishna M, Glodzik D, Zou X, et al. Landscape of somatic mutations in 560 breast cancer whole-genome sequences. Nature. 2016; 534: 47–54. https://doi.org/10.1038/nature17676 PMID: 27135926

74. Nolan E, Savas P, Policheni AN, Darcy PK, Vaillant F, Mintoff CP, et al. Combined immune checkpoint blockade as a therapeutic strategy for BRCA1-mutated breast cancer. Sci Transl Med. 2017; 9. https://doi.org/10.1126/scitranslmed.aal4922 PMID: 28592566

75. Wen WX, Leong CO. Association of BRCA1- And BRCA2-deficiency with mutation burden, expression of PD-L1/ PD-1, immune infiltrates, and T cell-inflamed signature in breast cancer. PLoS One. 2019; 14: 1–16. https://doi.org/10.1371/journal.pone.0215381 PMID: 31022191

76. Taglialatela A, Leuzzi G, Sannino V, Cuella-Martin R, Huang J-W, Wu-Baer F, et al. REV1-Polζ maintains the viability of homologous recombination-deficient cancer cells through mutagenic repair of PRIMPOL-dependent ssDNA gaps. Mol Cell. 2021; 81: 4008–4025.e7. https://doi.org/10.1016/j.molcel.2021.08.016 PMID: 34508659

77. Hurley D. In the Clinic. Neurol Today. 2017; 17: 22–23. https://doi.org/10.1097/01.nt.0000521902.81399.b2

78. Zhou J, Gelot C, Pantelidou C, Li A, Yücel H, Davis RE, et al. A first-in-class polymerase theta inhibitor selectively targets homologous-recombination-deficient tumors. Nat Cancer. 2021; 2: 598–610. https://doi.org/10.1038/s43018-021-00203-x PMID: 34179826

79. Zatreanu D, Robinson HMR, Alkhatib O, Boursier M, Finch H, Geo L, et al. Polθ inhibitors elicit BRCA-gene synthetic lethality and target PARP inhibitor resistance. Nat Commun. 2021; 12: 3636. https://doi.org/10.1038/s41467-021-23463-8 PMID: 34140467

80. Wojtaszek JL, Chatterjee N, Najeeb J, Ramos A, Lee M, Bian K, et al. A Small Molecule Targeting Mutagenic Translesion Synthesis Improves Chemotherapy. Cell. 2019; 178: 152–159.e11. https://doi.org/10.1016/j.cell.2019.05.028 PMID: 31178121

81. Baudin a, Ozier-Kalogeropoulos O, Denouel a, Lacroute F, Cullin C. A simple and efficient method for direct gene deletion in *Saccharomyces cerevisiae*. Nucleic Acids Res. 1993; 21: 3329–3330. https://doi.org/10.1093/nar/21.14.3329 PMID: 8341614

82. Longtine MS, McKenzie A, Demarini DJ, Shah NG, Wach A, Brachat A, et al. Additional modules for versatile and economical PCR-based gene deletion and modification in *Saccharomyces cerevisiae*. Yeast.

1998; 14: 953–61. https://doi.org/10.1002/(SICI)1097-0061(199807)14:10<953::AID-YEA293>3.0.CO;2-U PMID: 9717241

83. Sherman F. Getting started with yeast. Methods Enzymol. 2002; 350: 3–41. https://doi.org/10.1016/s0076-6879(02)50954-x PMID: 12073320

84. Ma CM, Coffey CW, DeWerd LA, Liu C, Nath R, Seltzer SM, et al. AAPM protocol for 40–300 kV x-ray beam dosimetry in radiotherapy and radiobiology. Med Phys. 2001; 28: 868–893. https://doi.org/10.1118/1.1374247 PMID: 11439485

85. Spell RM, Jinks-Robertson S. Determination of mitotic recombination rates by fluctuation analysis in *Saccharomyces cerevisiae*. Methods Mol Biol. 2004. https://doi.org/10.1385/1-59259-761-0:003 PMID: 14769952